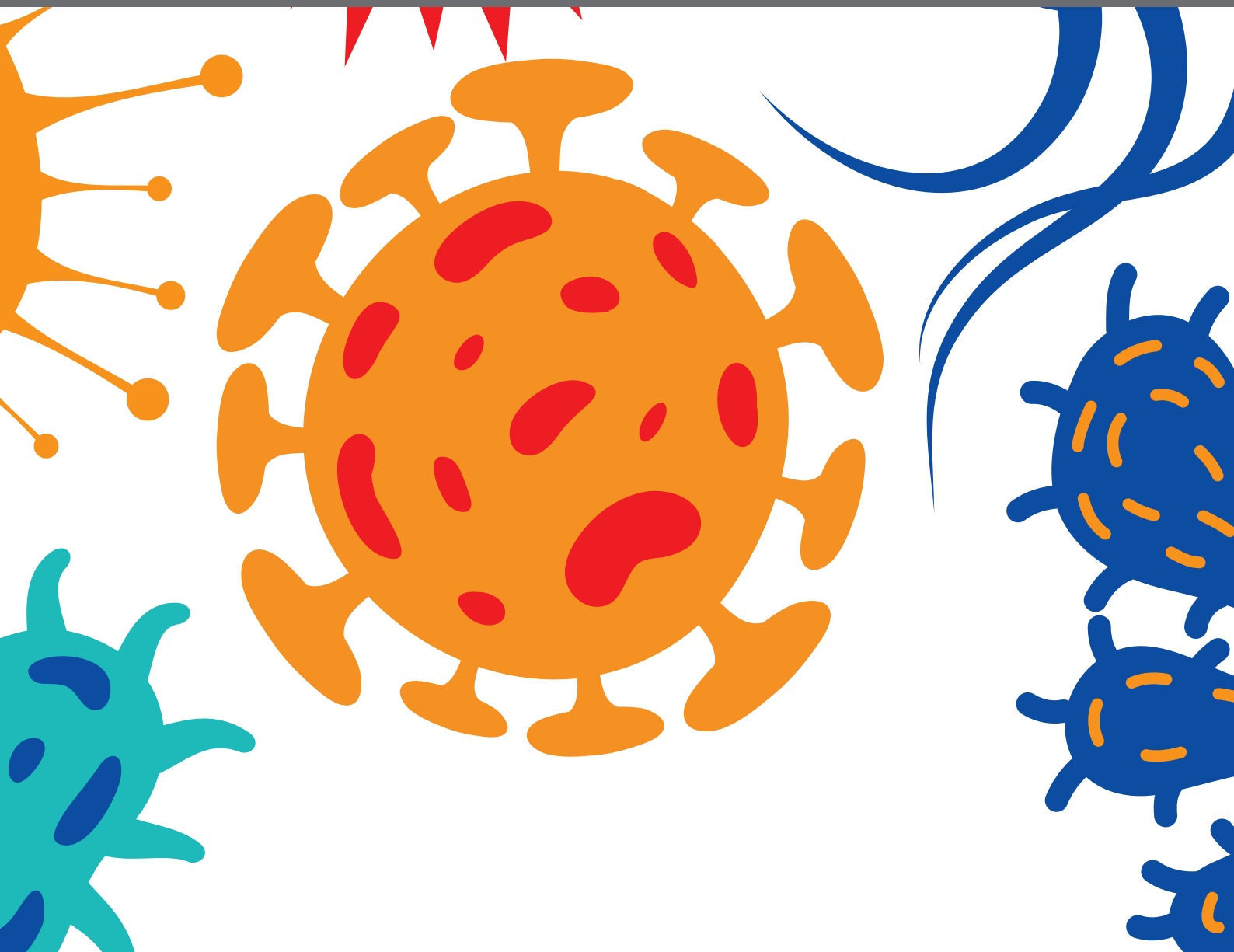




# PROTOZOAL INFECTIONS: TREATMENT AND CHALLENGES

EDITED BY: Vipin Kumar and Gaurav Bhargava

PUBLISHED IN: *Frontiers in Cellular and Infection Microbiology* and  
*Frontiers in Immunology*





# frontiers

## Frontiers eBook Copyright Statement

The copyright in the text of individual articles in this eBook is the property of their respective authors or their respective institutions or funders. The copyright in graphics and images within each article may be subject to copyright of other parties. In both cases this is subject to a license granted to Frontiers.

The compilation of articles constituting this eBook is the property of Frontiers.

Each article within this eBook, and the eBook itself, are published under the most recent version of the Creative Commons CC-BY licence.

The version current at the date of publication of this eBook is CC-BY 4.0. If the CC-BY licence is updated, the licence granted by Frontiers is automatically updated to the new version.

When exercising any right under the CC-BY licence, Frontiers must be attributed as the original publisher of the article or eBook, as applicable.

Authors have the responsibility of ensuring that any graphics or other materials which are the property of others may be included in the CC-BY licence, but this should be checked before relying on the CC-BY licence to reproduce those materials. Any copyright notices relating to those materials must be complied with.

Copyright and source acknowledgement notices may not be removed and must be displayed in any copy, derivative work or partial copy which includes the elements in question.

All copyright, and all rights therein, are protected by national and international copyright laws. The above represents a summary only. For further information please read Frontiers' Conditions for Website Use and Copyright Statement, and the applicable CC-BY licence.

ISSN 1664-8714

ISBN 978-2-83250-196-2

DOI 10.3389/978-2-83250-196-2

## About Frontiers

Frontiers is more than just an open-access publisher of scholarly articles: it is a pioneering approach to the world of academia, radically improving the way scholarly research is managed. The grand vision of Frontiers is a world where all people have an equal opportunity to seek, share and generate knowledge. Frontiers provides immediate and permanent online open access to all its publications, but this alone is not enough to realize our grand goals.

## Frontiers Journal Series

The Frontiers Journal Series is a multi-tier and interdisciplinary set of open-access, online journals, promising a paradigm shift from the current review, selection and dissemination processes in academic publishing. All Frontiers journals are driven by researchers for researchers; therefore, they constitute a service to the scholarly community. At the same time, the Frontiers Journal Series operates on a revolutionary invention, the tiered publishing system, initially addressing specific communities of scholars, and gradually climbing up to broader public understanding, thus serving the interests of the lay society, too.

## Dedication to Quality

Each Frontiers article is a landmark of the highest quality, thanks to genuinely collaborative interactions between authors and review editors, who include some of the world's best academicians. Research must be certified by peers before entering a stream of knowledge that may eventually reach the public - and shape society; therefore, Frontiers only applies the most rigorous and unbiased reviews.

Frontiers revolutionizes research publishing by freely delivering the most outstanding research, evaluated with no bias from both the academic and social point of view. By applying the most advanced information technologies, Frontiers is catapulting scholarly publishing into a new generation.

## What are Frontiers Research Topics?

Frontiers Research Topics are very popular trademarks of the Frontiers Journals Series: they are collections of at least ten articles, all centered on a particular subject. With their unique mix of varied contributions from Original Research to Review Articles, Frontiers Research Topics unify the most influential researchers, the latest key findings and historical advances in a hot research area! Find out more on how to host your own Frontiers Research Topic or contribute to one as an author by contacting the Frontiers Editorial Office: [frontiersin.org/about/contact](https://frontiersin.org/about/contact)

# PROTOZOAL INFECTIONS: TREATMENT AND CHALLENGES

Topic Editors:

**Vipan Kumar**, Guru Nanak Dev University, India

**Gaurav Bhargava**, I. K. Gujral Punjab Technical University, India

**Citation:** Kumar, V., Bhargava, G., eds. (2022). Protozoal Infections: Treatment and Challenges. Lausanne: Frontiers Media SA. doi: 10.3389/978-2-83250-196-2

# Table of Contents

- 04 Editorial: Protozoal Infections: Treatment and Challenges**  
Vipan Kumar and Gaurav Bhargava
- 07 Boromycin has Rapid-Onset Antibiotic Activity Against Asexual and Sexual Blood Stages of Plasmodium falciparum**  
Laís Pessanha de Carvalho, Sara Groeger-Otero, Andrea Kreidenweiss, Peter G. Kremsner, Benjamin Mordmüller and Jana Held
- 20 Novel Highlight in Malarial Drug Discovery: Aspartate Transcarbamoylase**  
Chao Wang, Arne Krüger, Xiaochen Du, Carsten Wrenger and Matthew R. Groves
- 29 Plasmodium falciparum-Specific Memory B-Cell and Antibody Responses Are Associated With Immunity in Children Living in an Endemic Area of Kenya**  
Peter Jahnmatz, Diana Nyabundi, Christopher Sundling, Linnea Widman, Jedidah Mwacharo, Jennifer Musyoki, Edward Otieno, Niklas Ahlborg, Philip Bejon, Francis M. Ndungu and Anna Färnert
- 41 Synthetic Red Blood Cell-Specific Glycolytic Intermediate 2,3-Diphosphoglycerate (2,3-DPG) Inhibits Plasmodium falciparum Development In Vitro**  
Inês Morais, Márcia M. Medeiros, Maria Carvalho, Judit Morello, Sara M. Teixeira, Suelma Maciel, Janice Nhantumbo, Ana Balau, Margarida T. G. Rosa, Fátima Nogueira, João Alexandre Rodrigues, Filomena A. Carvalho, Alexandra M. M. Antunes and Ana Paula Arez
- 55 Presence of Phylloquinone in the Intraerythrocytic Stages of Plasmodium falciparum**  
Rodrigo A. C. Sussmann, Heloisa B. Gabriel, Alejandro García Ríos, Danielle S. Menchaca Vega, Lydia F. Yamaguchi, Antonio Doménech-Carbó, Gerardo Cebrián-Torrejón, Emilia A. Kimura, Massuo J. Kato, Ignasi Bofill Verdaguer, Marcell Crispim and Alejandro M. Katzin
- 71 An Overview of Mucosa-Associated Protozoa: Challenges in Chemotherapy and Future Perspectives**  
Helena Lucia Carneiro Santos and Karina M. Rebello
- 86 Targeting the Plasmodium falciparum's Thymidylate Monophosphate Kinase for the Identification of Novel Antimalarial Natural Compounds**  
Kweku S. Enninful, Samuel K. Kwofie, Mark Tetteh-Tsifoanya, Amanda N. L. Lamptey, Georgina Djameh, Samuel Nyarko, Anita Ghansah and Michael D. Wilson
- 99 Homology Modeling, de Novo Design of Ligands, and Molecular Docking Identify Potential Inhibitors of Leishmania donovani 24-Sterol Methyltransferase**  
Patrick O. Sakyi, Emmanuel Broni, Richard K. Amewu, Whelton A. Miller III, Michael D. Wilson and Samuel Kojo Kwofie





## OPEN ACCESS

EDITED AND REVIEWED BY  
Max Maurin,  
Université Grenoble Alpes,  
France

\*CORRESPONDENCE  
Vipan Kumar  
vipan\_org@yahoo.com

SPECIALTY SECTION  
This article was submitted to  
Clinical Microbiology,  
a section of the journal  
Frontiers in Cellular and  
Infection Microbiology

RECEIVED 25 July 2022  
ACCEPTED 12 August 2022  
PUBLISHED 31 August 2022

CITATION  
Kumar V and Bhargava G (2022)  
Editorial: Protozoal infections:  
Treatment and challenges.  
*Front. Cell. Infect. Microbiol.*  
12:1002602.  
doi: 10.3389/fcimb.2022.1002602

COPYRIGHT  
© 2022 Kumar and Bhargava. This is an  
open-access article distributed under  
the terms of the [Creative Commons  
Attribution License \(CC BY\)](#). The use,  
distribution or reproduction in other  
forums is permitted, provided the  
original author(s) and the copyright  
owner(s) are credited and that the  
original publication in this journal is  
cited, in accordance with accepted  
academic practice. No use,  
distribution or reproduction is  
permitted which does not comply with  
these terms.

# Editorial: Protozoal infections: Treatment and challenges

Vipan Kumar<sup>1\*</sup> and Gaurav Bhargava<sup>2</sup>

<sup>1</sup>Department of Chemistry, Guru Nanak Dev University, Amritsar, India, <sup>2</sup>Department of Chemical Sciences, Inder Kumar Gujral (IKG) Punjab Technical University, Kapurthala, India

## KEYWORDS

neglected tropical diseases, malaria, anti-plasmodial, pyrimidine biosynthesis, kinase inhibitors, Anti-leishmanial

## Editorial on the Research Topic

### Protozoal infections: Treatment and challenges

Protozoal infections caused by *Plasmodium falciparum*, *Trypanosoma cruzi*, *Leishmania mexicana*, *Giardia lamblia*, and *Trichomonas vaginalis*, among others, are commonly referred to as Neglected Tropical Diseases (NTDs) because they receive little attention in terms of surveillance, prevention, and treatment. These group of infectious diseases are prevalent in 149 countries with tropical and subtropical environments and are closely linked with poverty. More than 1.5 billion people worldwide are afflicted by at least one NTD, with populations that lack access to sufficient sanitization, clean water, and healthcare as well as those who live close to infectious disease carriers being the most at risk. The tenth anniversary of the London Declaration on Neglected Tropical Diseases (NTDs) in 2022 marks a watershed moment in which governments, pharmaceutical companies, foundations, and non-governmental organisations (NGOs) pledged to work together to eradicate NTDs. The pandemic of COVID-19 has been a historic setback for the NTD agenda. It has harmed neglected populations disproportionately, not only increasing global poverty but also having a direct impact on NTD interventions. COVID-19 has frequently and severely impacted NTD services, causing disruptions in 44% of countries, according to a WHO survey. The papers published in this Research Topic are primarily concerned with alternative approaches for NTDs, particularly malaria and leishmaniasis (Special topic “Protozoal infections: Treatment and challenges”).

Jahnmatz et al. assessed cross-sectional pre-existing memory B-cells (MBCs) and antibody responses against six well-known *P. falciparum* antigens and measured their associations with previous infections and time to clinical malaria in Kenyan children. Children who exhibited three or more antigen-specific MBC or antibody responses at baseline had a reduced probability of contracting malaria during the next *P. falciparum* transmission season. They come to the conclusion that malaria protection is related with a wider range of merozoite antigen-specific MBC and antibody responses. According to Carvalho et al., boromycin has a highly effective anti-plasmodial effect against both the zoonotic *P. knowlesi* and *P. falciparum*. Unlike tetracyclines, boromycin quickly killed asexual stages of both Plasmodium species at low concentrations (1 nM), including

strains of *P. falciparum* that were multidrug resistant (Dd2, K1, 7G8). Additionally, low nanomolar concentrations of boromycin were effective against *P. falciparum* stage V gametocytes (IC<sub>50</sub>:  $8.5 \pm 3.6$  nM). The apicoplast was excluded as the primary target based on a mechanism of action investigation. Although significant ionophoric activity in potassium channels was observed, it was insufficient to fully account for the compound's antiplasmodial activities.

Malaria resistance has also been linked to pyruvate kinase deficiency in both population studies and experimental models. The diminution of ATP and the elevation of 2,3-biphosphoglycerate (2,3-BPG) concentration are two of the main pyruvate kinase deficient-cell disorders. [Morais et al.](#) investigated the effect of a synthetic form, 2,3-DPG, on the intraerythrocytic developmental cycle of *P. falciparum* *in vitro*. The findings demonstrated that 2,3-DPG exposure adversely affected parasite development, which in turn had an impact on parasite maturation. The pyrimidine biosynthesis pathway is critical for cell growth and proliferation. Since the malarial parasite lacks a functional pyrimidine salvage pathway, RNA and DNA synthesis is entirely dependent on *de novo* synthesis. The activity of the parasite transcarbamoylase has been identified as at least one of the targets of Torin2, a powerful but non-selective antimalarial. [Wang et al.](#) focused on an allosteric pocket that supports the catalytic pathways to provide a summary of the research on the *P. falciparum* ATCase structure. They performed a fragment-based screening to find hits using the crystal structures of the malarial aspartate transcarbamoylase.

[Sussman et al.](#) described the presence of phyloquinone (PK/ vitamin K1) in *P. falciparum* and talked about its possible origin. Exogenous PK attenuated the effects of atovaquone on parasitic growth and respiration, indicating that this metabolite can be transported from extracellular environment and that the mitochondrial electron transport system (ETS) of *P. falciparum* is capable of interacting with PK. This study emphasises the importance of PK in plasmodial metabolism, which will require further investigation in order to identify new antimalarial drug targets. Wilson and colleagues used the FAF-Drugs4 server to test 885 AfroDB-retrieved compounds, resulting in the discovery of 91 ADMET-acceptable compounds. ZINC13374323 and ZINC13365918 were chosen as potential lead compounds. ZINC13374323, also known as aurantiamide acetate, is a component of *A. annua* that acts as an inhibitor of *P. falciparum* thymidylate monophosphate kinase (*Pf*TMPK). The complex of *Pf*TMPK and ZINC13374323 has similar RMSD and RMSF to that of the protein in association with its native substrate, TMP, according to molecular dynamics simulations. *In vitro* testing revealed that aurantiamide acetate's IC<sub>50</sub> for anti-plasmodial activity was 69.33  $\mu$ M.

[Sakya et al.](#) used homology modelling to establish the structural model of *Leishmania donovani* 24-sterol methyltransferase (LdSMT) in order to find possible 24-SMT inhibitors through virtual screening, scaffold hopping, and *de-novo* fragment-based design. Six potential novel inhibitors were identified, with binding energies similar to 22,26-azasterol, the main inhibitor of LdSMT (7.6 kcal/mol). The binding mechanism determined that Tyr92 was necessary for binding, and estimates of the Poisson-Boltzmann surface area (MM-PBSA) and molecular dynamics simulations confirmed this. The review by [Santos and Rebello](#) mainly focused on the development of drug repositioning as a practical technique for the treatment of mucosal parasites while evaluating potential candidates that target protozoans which infect mucosal surfaces. When taken as a whole, these studies emphasise the significance of developing alternative strategies and drug repositioning for combating NTDs.

## Author contributions

The authors listed have made a substantial, direct, and intellectual contribution to the work and approved it for publication.

## Acknowledgments

All authors who contributed to the Research Topic "Protozoal Infections: Treatment and Challenges" are gratefully acknowledged by the editors. Each reviewer who has contributed and whose invaluable assistance is essential to the journal's success is acknowledged separately.

## Conflict of interest

The authors declare that the research was conducted in the absence of any commercial or financial relationships that could be construed as a potential conflict of interest.

## Publisher's note

All claims expressed in this article are solely those of the authors and do not necessarily represent those of their affiliated organizations, or those of the publisher, the editors and the reviewers. Any product that may be evaluated in this article, or claim that may be made by its manufacturer, is not guaranteed or endorsed by the publisher.

## Reference

Special topic “Protozoal infections: Treatment and challenges. Available at: <https://www.frontiersin.org/research-topics/22535/protozoal-infections-treatment-and-challenges> (Accessed July 25, 2022).



# Boromycin has Rapid-Onset Antibiotic Activity Against Asexual and Sexual Blood Stages of *Plasmodium falciparum*

Laís Pessanha de Carvalho<sup>1</sup>, Sara Groeger-Otero<sup>1</sup>, Andrea Kreidenweiss<sup>1,2,3</sup>, Peter G. Kremsner<sup>1,2,3</sup>, Benjamin Mordmüller<sup>1,2,3,4</sup> and Jana Held<sup>1,2,3\*</sup>

## OPEN ACCESS

### Edited by:

Vipin Kumar,  
Guru Nanak Dev University, India

### Reviewed by:

Arnish Chakraborty,  
TCG Lifesciences, India  
Raghu Raj,  
DAV College Amritsar, India

### \*Correspondence:

Jana Held  
janaheld@hotmail.de;  
jana.held@uni-tuebingen.de

### Specialty section:

This article was submitted to  
Clinical Microbiology,  
a section of the journal  
Frontiers in Cellular and  
Infection Microbiology

**Received:** 26 October 2021

**Accepted:** 27 December 2021

**Published:** 14 January 2022

### Citation:

de Carvalho LP,  
Groeger-Otero S, Kreidenweiss A,  
Kremsner PG, Mordmüller B  
and Held J (2022) Boromycin has  
Rapid-Onset Antibiotic Activity  
Against Asexual and Sexual Blood  
Stages of *Plasmodium falciparum*.  
Front. Cell. Infect. Microbiol. 11:802294.  
doi: 10.3389/fcimb.2021.802294

<sup>1</sup> Institute of Tropical Medicine, University of Tübingen, Tübingen, Germany, <sup>2</sup> Centre de Recherches Médicales de Lambaréné, Lambaréné, Gabon, <sup>3</sup> German Center for Infection Research (DZIF), partner site Tübingen, Tübingen, Germany, <sup>4</sup> Department of Medical Microbiology, Radboud University Medical Center, Nijmegen, Netherlands

Boromycin is a boron-containing macrolide antibiotic produced by *Streptomyces antibioticus* with potent activity against certain viruses, Gram-positive bacteria and protozoan parasites. Most antimalarial antibiotics affect plasmodial organelles of prokaryotic origin and have a relatively slow onset of action. They are used for malaria prophylaxis and for the treatment of malaria when combined to a fast-acting drug. Despite the success of artemisinin combination therapies, the current gold standard treatment, new alternatives are constantly needed due to the ability of malaria parasites to become resistant to almost all drugs that are in heavy clinical use. *In vitro* antiplasmodial activity screens of tetracyclines (omadacycline, sarecycline, methacycline, demeclocycline, lymecycline, meclocycline), macrolides (oleandomycin, boromycin, josamycin, troleandomycin), and control drugs (chloroquine, clindamycin, doxycycline, minocycline, eravacycline) revealed boromycin as highly potent against *Plasmodium falciparum* and the zoonotic *Plasmodium knowlesi*. In contrast to tetracyclines, boromycin rapidly killed asexual stages of both *Plasmodium* species already at low concentrations (~ 1 nM) including multidrug resistant *P. falciparum* strains (Dd2, K1, 7G8). In addition, boromycin was active against *P. falciparum* stage V gametocytes at a low nanomolar range (IC<sub>50</sub>: 8.5 ± 3.6 nM). Assessment of the mode of action excluded the apicoplast as the main target. Although there was an ionophoric activity on potassium channels, the effect was too low to explain the drug's antiplasmodial activity. Boromycin is a promising antimalarial candidate with activity against multiple life cycle stages of the parasite.

**Keywords:** antibiotics, *Plasmodium falciparum*, *Plasmodium knowlesi*, tetracyclines, delayed death effect, boromycin, macrolides

# 1 INTRODUCTION

Malaria remains one of the world's most serious public health problems, especially in tropical and subtropical areas, with approximately 241 million cases and 627,000 deaths in 2020 (World Health Organization, 2021). Intracellular parasites of the genus *Plasmodium* cause the disease, and among the six species that can infect humans *P. falciparum*, *P. vivax*, *P. malariae*, *P. ovale wallikeri*, *P. ovale curtisi*, and the zoonotic species *P. knowlesi* (Rutledge et al., 2017; Grignard et al., 2019), *P. falciparum* is the most virulent (World Health Organization, 2021). *P. knowlesi*, described originally as a simian parasite, was recognized in 2000 as a zoonotic species that can infect humans (White, 2008). Although *P. knowlesi* occurs mainly in Malaysia, counting 13,612 malaria cases between 2017 to 2020 (Hu et al., 2021), it can cause severe malaria in humans (Amir et al., 2018) and is phylogenetically closer to other human pathogenic *Plasmodium* species (*P. malariae*, *P. vivax*, and *P. ovale species*) than *P. falciparum* (Rutledge et al., 2017; van Schalkwyk et al., 2019).

*Plasmodium* parasites have a complex life cycle that includes mosquito and vertebrate hosts (Siciliano and Alano, 2015). Clinical symptoms of malaria appear during the replication of parasites in the erythrocytic cycle (lasting approximately 24 h for *P. knowlesi* and 48 h for *P. falciparum*) in the human host (van Biljon et al., 2018). These symptoms can develop into life-threatening complications such as severe anemia, liver and kidney failure and cerebral malaria if not treated properly (Milner et al., 2014). During each replication cycle, a small number of asexual parasites starts a different genetic program and develops into the transmissible sexual form, named gametocytes (Portugaliza et al., 2020). Gametocytes are non-dividing parasite stages with low metabolic activity whose immature stages are hidden in the bone marrow while the mature stage (stage V) circulates in the blood stream (Gardiner and Trenholme, 2015).

Currently, the mainstay *P. falciparum* malaria treatments are artemisinin-based combination therapies (ACT) (World Health Organization, 2021). Artemisinin and its derivatives are fast-acting and rapidly reduce the asexual parasite load but have a short half-life (2–4 h for artemisinin and <1 h for artesunate) (Benakis et al., 1997). They are combined to a slow-acting partner drug with longer half-life to clear remaining parasites, and to protect artemisinin against resistances. Nonetheless, reports of *P. falciparum* with delayed clearance after artesunate or ACT treatment are accumulating, especially from the Greater Mekong Region where resistances to the partner drugs are also present (Pluijm et al., 2019; WWARN K13 Genotype-Phenotype Study Group, 2019). More recently first reports of kelch13 mutated parasites with a slow clearance have also appeared from Africa (Balikagala et al., 2021). This poses a threat to the existing malaria treatment options (Straimer et al., 2015; Nsanzabana, 2019). In addition, the current ACT drugs are inactive against mature *P. falciparum* gametocytes (stage IV and V). In low transmission areas is recommended to give additionally a single dose of primaquine, except in children younger than six months, pregnant and breastfeeding women with infants younger than six months, to prevent transmission of

the parasite, but these recommendations are so far not strictly followed in all areas (World Health Organization, 2021).

The interest in using antibiotics for malaria treatment appeared due to the emergence of resistant parasites to the former mainstay drug chloroquine. Tetracyclines were the first antibiotics used to treat uncomplicated malaria, dating back to the 1950s (Imboden et al., 1950; Grande et al., 1956). Currently, doxycycline and the combination of sulfadoxine-pyrimethamine are used for malaria prevention of travelers and risk groups in malaria-endemic regions, respectively. In addition, clindamycin combined with quinine is used to treat pregnant women during the first trimester or combined with artesunate or quinine to treat uncomplicated malaria when an ACT is unavailable (World Health Organization, 2021).

Tetracyclines and macrolides, both naturally produced by *Streptomyces*, have shown promising antiplasmodial activities as reviewed before (Gaillard et al., 2015; Gaillard et al., 2016; de Carvalho et al., 2021). Most antibiotics with antiplasmodial activity target the apicoplast; a plastid-like organelle derived from endosymbiotic bacteria responsible for the biosynthesis of isoprenoid precursors (Yeh and DeRisi, 2011). Antibiotics can be fast or slow-acting drugs, depending on whether they target the treated parasites or act on their progeny, causing the so-called delayed death effect (Dahl and Rosenthal, 2007). Commonly, tetracyclines belong to the latter group (Gaillard et al., 2015; de Carvalho et al., 2021), and novel tetracyclines have shown superior antiplasmodial activity (e.g. eravacycline and tigecycline IC<sub>50</sub>s at 14 and 38 nM, respectively (Held et al., 2010; Koehne et al., 2021) versus doxycycline and tetracycline IC<sub>50</sub>s at 241 and 340 nM, respectively) (Koehne et al., 2021). Some macrolides such as ivermectin (Mendes et al., 2017; de Carvalho et al., 2019), borrelidin (Otoguro et al., 2003; Ishiyama et al., 2011), and kitasamycin (also called leucomycin) (Ekland et al., 2011) had a fast/first cycle *in vitro* growth inhibitory activity against *P. falciparum* (IC<sub>50</sub> values of ~ 100 nM, 1.8 nM and 50 nM, respectively). However, the molecular targets of these agents in *Plasmodium* species are not known.

This study aimed to identify antibiotics that are potent and fast acting against *P. falciparum*. Therefore, we evaluated the antiplasmodial effect of two recently marketed tetracyclines, named sarecycline, and omadacycline and some “old” tetracyclines in clinical use named demeclocycline, meclocycline, lymecycline, chlortetracycline and methacycline (Figure 1). In addition, the macrolides oleandomycin, troleandomycin, josamycin, and boromycin were evaluated (Figure 2). Tetracyclines with known antiplasmodial activity were used as controls. We identified boromycin to be a highly active and fast acting antibiotic. Boromycin is a polyether-macrolide antibiotic produced by *Streptomyces antibioticus* and was the first boron-containing compound found in nature (Dunitz et al., 1971). Previous studies showed a potent effect of boromycin against Gram-positive bacteria, HIV virus and protozoan parasites (Kohno et al., 1996; Moreira et al., 2016; Abenoja et al., 2021). Due to its low nanomolar activity in our screening, we further assessed its antiplasmodial profile also including transmission stages and investigated whether its

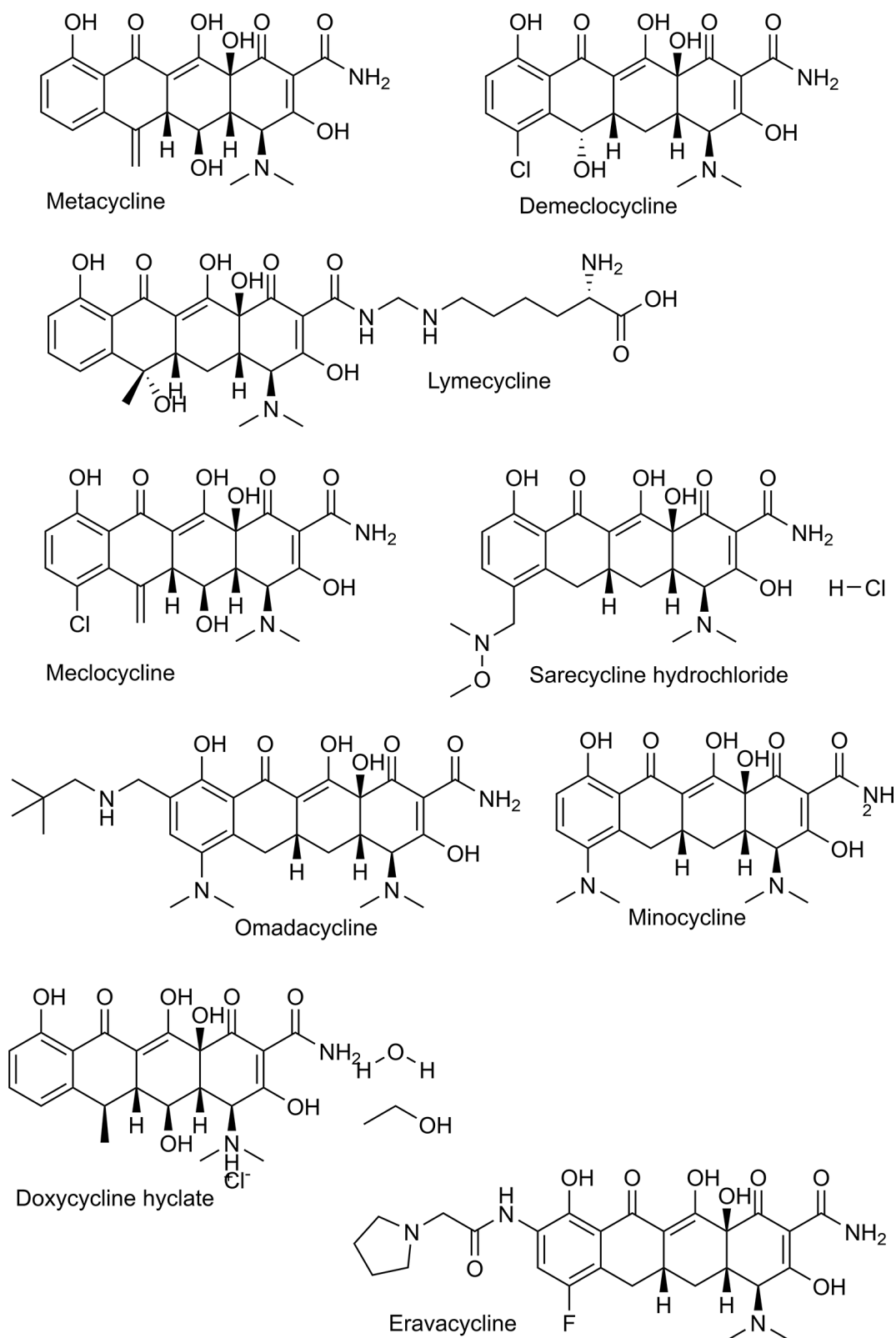


**FIGURE 1** | Chemical structures of tetracyclines tested in this study.

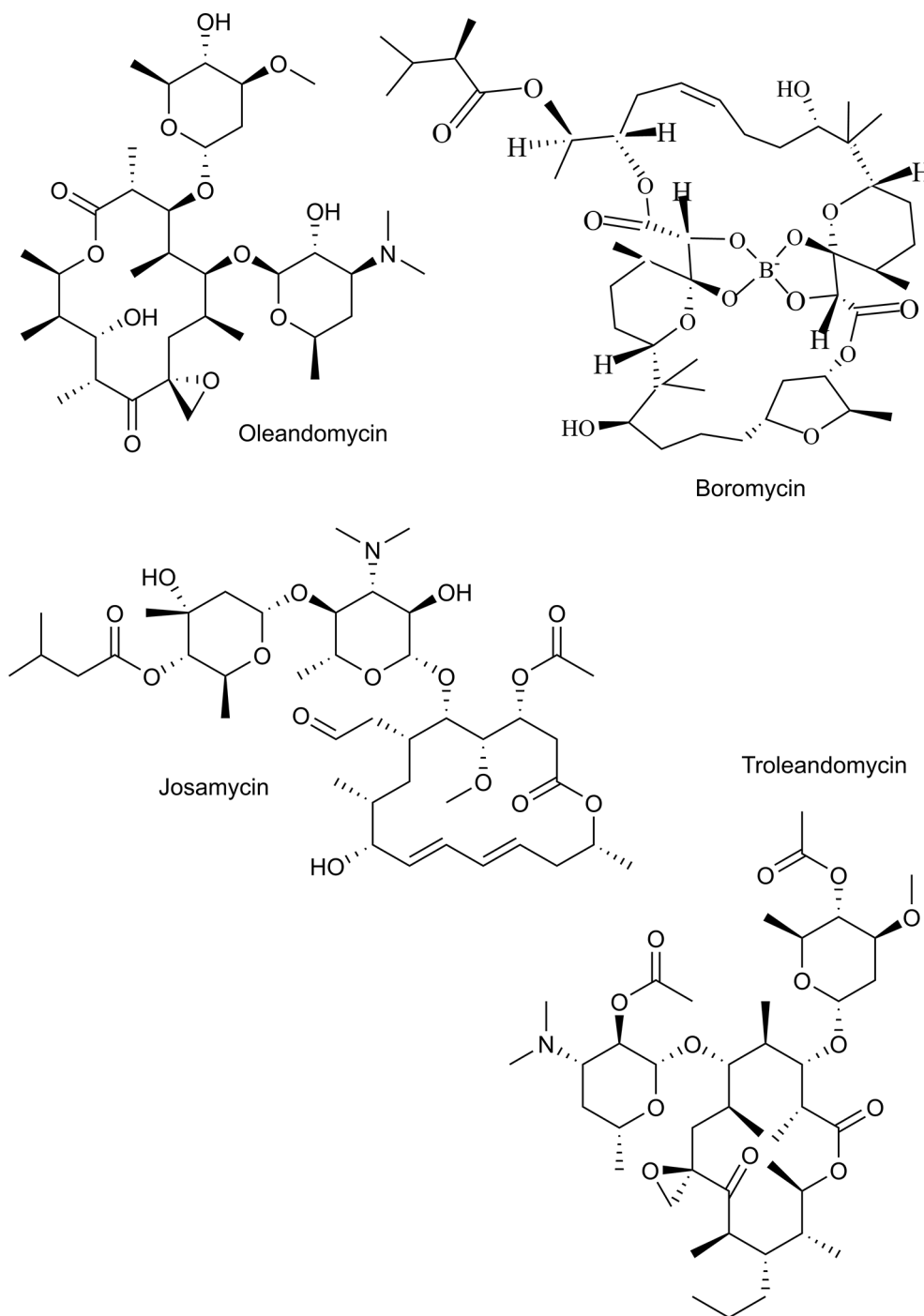


**FIGURE 2** | Chemical structures of macrolides tested in this study.

potential mode of action involves the apicoplast as described for antibiotics in general (Dahl and Rosenthal, 2007) or ionophoric activity on potassium channels as shown before for boromycin (Moreira et al., 2016). In addition, we evaluated its *in vitro* activity against another *Plasmodium* species (*P. knowlesi*).

## 2 MATERIALS AND METHODS

### 2.1 Chemicals

All tested drugs were first dissolved in their respective solvents and subsequently further diluted in complete culture medium to



have the desired final concentration (**Supplementary Table 1** and **Supplementary Information Figures 1, 2**).

## 2.2 Parasite *In Vitro* Culture

### 2.2.1 Plasmodium Asexual Stages

*P. falciparum* laboratory strains 3D7 (chloroquine-sensitive, provided by BEI resources, MRA-102), Dd2 (multidrug-resistant, provided by BEI resources, MRA-150), K1 (multidrug-resistant, provided by BEI resources, MRA-159), 7G8 (chloroquine resistant, provided by BEI resources, MRA-154) and NF-54 (chloroquine sensitive, provided by Sanaria, a vigorous gametocyte producer), and *P. knowlesi* laboratory strain A1-H.1 (kindly provided by Robert Moon of LSHTM, London, UK under a MTA by the Francis Crick institute) were cultivated *in vitro* as described before (Moon et al., 2013; de Carvalho et al., 2019). Briefly, the parasites were maintained in complete culture medium consisting of RPMI-1640 (Sigma-Aldrich) supplemented with 1M N-2-hydroxyethylpiperazine-N-2-ethane sulfonic acid (HEPES) solution (2.4% v/v) (Sigma-Aldrich), 200 mM L-glutamine (Gibco), 50 µg/ml gentamicin (Gibco), and 10% of AlbuMax II solution containing RPMI, HEPES, NaHCO<sub>3</sub>, D-Glucose, hypoxanthine and 50 g/l of AlbuMax II (0.5% wt/vol in culture medium) at 2.5% hematocrit. The cultures were maintained at 5% CO<sub>2</sub>, 5% O<sub>2</sub>, at 37°C, with a change of medium every two days. *P. falciparum* parasites were synchronized by magnetic column separation prior to the assays (Ribaut et al., 2008). *P. knowlesi* was cultivated as described for *P. falciparum*, with minor modifications. Parasites were cultivated in complete culture medium as detailed above supplemented with 5% human AB serum. Shortly before the growth inhibition assays, *P. knowlesi* were synchronized by density centrifugation with Nycodenz solution (Progen) to recover mature schizonts as described before (van Schalkwyk et al., 2017). The Nycodenz solution was prepared according to the manufacturer's instruction and kept protected from the light at 4°C and warmed before using.

The asexual growth inhibition assays were performed with 3D7 and A1-H.1, while NF-54 was used for gametocyte assays.

### 2.2.2 *P. falciparum* Sexual Stages

*P. falciparum* gametocyte culture was performed as described previously (de Carvalho et al., 2019) with minor modifications. The gametocyte culture was initiated with synchronized ring-stage NF54 parasites at 6% hematocrit and 0.3% parasitemia. Complete culture medium (as described above) was supplemented with 5% human serum and changed daily without parasite dilution for 14 days. The medium was doubled when parasitemia reached 5%, and 50-mM N-acetyl-d-glucosamine (MP Biomedicals GmbH) was added between day 11 and day 14 to remove asexual stages. On day 15, mature gametocytes were purified with a Nycodenz and magnetic column separation (MACS) to remove erythrocytes and concentrate the gametocyte population.

## 2.3 Growth Inhibition Assays With Asexual Parasites

Growth inhibition assays of asexual stages of *P. falciparum* were performed as described before (Noedl et al., 2005). Briefly, the

drugs (**Supplementary Table 1**) were distributed in a 3-fold serial dilution in 96-well plates. The highest concentration of the solvent (<0.1%) did not interfere with parasite growth. Synchronized ring-stage parasites were diluted to a parasitemia of 0.05% with O Rh+ erythrocytes in complete culture medium and seeded at a hematocrit of 1.5% in a total volume of 225 µl per well. Plates were subsequently incubated at 5% CO<sub>2</sub>, 5% O<sub>2</sub>, at 37°C before the plates were frozen and thawed three times. The growth inhibition of *P. falciparum* was measured through an enzyme-linked immunosorbent assay (ELISA) for histidine-rich protein 2 (HRP2) using a microplate reader (CLARIOstar BMG Labtech) (excitation filter: 450 nm).

Growth inhibition assays with *P. knowlesi* were performed as described previously with minor modifications (van Schalkwyk et al., 2019). Briefly, boromycin and chloroquine were distributed in a 3-fold serial dilution in 96-well plates. Synchronized ring-stage parasites were diluted to a parasitemia of 0.5% (a higher parasitemia compared to the HRP2 based assay is needed due to the differences in the limit of detection and therefore optimal assay conditions) with O Rh+ erythrocytes and subsequently seeded at a hematocrit of 2% and complete culture medium without human AB serum but double (20%) AlbuMax II solution in a total volume of 225 µl per well. The growth inhibition of *P. knowlesi* was measured with SYBR Green-I (ThermoFisher) using CLARIOstar (BMG Labtech) (490 nm excitation filter) as HRP2 is not present in this species. For comparison, growth inhibition of boromycin and chloroquine – treated *P. falciparum* was measured using the same methodology.

*P. falciparum* was incubated with the drugs for 3 and 6 days to assess the onset of activity. Both time points were assessed because many antibiotics target only the progeny of the treated parasites, causing a delayed death effect that is measured only after the second replication cycle (after 6 days). Chloroquine and clindamycin were used as positive controls for 3- and 6-day assays, respectively.

To observe the parasite morphology, *P. falciparum* strain 3D7 and Dd2 were incubated with boromycin at 1 nM and for comparison also 3D7 with chloroquine at 8 nM for 6 h for visual observation of drug effect by light microscopy. Thin blood smears were prepared, fixed in 100% methanol for 10 seconds, and stained with Giemsa (Merck) solution (5%) for 20 minutes. The slides were washed and observed under a Leica DMBL microscope, and pictures were taken using a ProgRes C10 camera and software (Jenoptik), at 100X magnification. Three biological replicates were prepared.

## 2.4 *In Vitro* Activity Against Mature Gametocytes of *P. falciparum*

Drug sensitivity assays against mature (stage V) *P. falciparum* gametocytes were performed as described previously (Lelièvre et al., 2012; de Carvalho et al., 2019). Briefly, the drugs were precoated in a 3-fold dilution in 96-well plates. The concentration of the solvent did not interfere with parasite growth. Epoxomicin and methylene blue (**Supplementary Table 1**) were used as positive control. Subsequently, the previously purified mature gametocytes were seeded to the



plates (50,000 gametocytes/well) and incubated at 37°C in 5% CO<sub>2</sub> and 5% O<sub>2</sub>. After 48 h, the ATP production was measured by the BacTiterGlo assay (Promega), according to the manufacturer's instructions. Finally, the results were quantified using a luminometer (LUmo; Autobio). In addition, to visually inspect the effect of boromycin on gametocytes thin blood smears of untreated and boromycin (8 nM) and epoxomicin (15 nM) - treated gametocytes (50,000 gametocytes/well), were prepared, fixed in 100% methanol for 10 seconds, and stained with Giemsa (Merck) solution (5%) for 20 minutes. The slides were washed and observed under a Leica DMBL microscope, and pictures were taken using a ProgRes C10 camera and software (Jenoptik), at 100X magnification.

## 2.5 Cytotoxicity Assay

HepG2 cells (obtained from ATCC; HB-8065), a human hepatocyte carcinoma cell line, were maintained in DMEM medium (Sigma-Aldrich) supplemented with 10% of inactivated foetal bovine serum (Sigma-Aldrich), 200 mM L-glutamine (Gibco), 12 mL of HEPES buffer (Gibco), and 50 µg/ml penicillin/streptomycin solution (Gibco). Trypsin (Gibco) was used to detach the cells when they reached a semi-confluent layer.

Cytotoxicity was evaluated using the neutral red assay as described previously (Mishra et al., 2021). Briefly, 300,000 cells were seeded in supplemented Dulbecco's Modified Eagle's Medium (DMEM) medium as described above to 96-well plates. After 24 hours, the cells were incubated with a twofold serial dilution of the respective drug diluted in supplemented DMEM medium for an additional 24 hours. The highest concentration of the solvent (<1%) did not interfere with cell viability. Subsequently, the drug-containing medium was replaced by a supplemented DMEM medium with 1.5% of neutral red, and the cells were incubated for an additional 3 h at 37°C. Cells were then washed with phosphate buffered saline (pH 7.2), and 100 µL of freshly prepared lysing buffer (50% methanol, 49% distilled water, and 1% acetic acid) were added to the plates. Subsequently, the cells were shaken for 10 min and the absorption was measured at a wavelength of 540 nm using CLARIOstar (BMG Labtech).

## 2.6 Isopentenyl Pyrophosphate Trilithium Salt (IPP) Rescue Assay

Growth inhibition assays were prepared as described in section *Parasite In Vitro Culture* with modifications to assess the specificity of boromycin for the inhibition of the isoprenoid precursor biosynthetic pathway (MEP/DOXP/non-mevalonate pathway) found in the apicoplast (Uddin et al., 2018). Briefly, the parasites (*P. falciparum* strain 3D7) were incubated with boromycin and clindamycin (positive control) and supplemented with IPP (Sigma) at 200 µM for 6 days as described before (Uddin et al., 2018). Since biosynthesis of isoprenoid precursors is the only required function of the apicoplast, supplementation with IPP can rescue treated parasites if the apicoplast is the main target of the drug (Uddin et al., 2018). The assay was done with and without IPP

supplementation on the same plate and results were directly compared.

## 2.7 Ionophoric Activity Assay

Previously, boromycin was described to act as a potassium ionophore in *Bacillus subtilis* and *Mycobacterium tuberculosis* (Pache and Zaehner, 1969a; Moreira et al., 2016). So herein, growth inhibition assays complemented with KCl or MgCl<sub>2</sub> (negative control) were performed to evaluate if this is also the case in *P. falciparum*. To define a subtoxic concentration of MgCl<sub>2</sub> and KCl for *P. falciparum* a standard growth inhibition assays with serial dilutions of these compounds were performed as described in section *Parasite In Vitro Culture*. The concentration of 220 µg/mL was chosen as no signs of toxicity were seen and first inhibitory effects were observed with 440 µg/mL (**Supplementary Figure 1**). Subsequently, a growth inhibition assay was prepared with a 2-fold dilution of boromycin with the addition of the sub-toxic concentration of either MgCl<sub>2</sub> (Sigma) or KCl (Sigma) to all wells. The assay was run in parallel to a standard growth inhibition assay of boromycin without supplementation of MgCl<sub>2</sub> or KCl as control, and the obtained IC<sub>50</sub>s were compared.

## 2.8 Analysis

All assays were performed at least three times in duplicates. Individual IC<sub>50</sub> values were determined by nonlinear regression analysis of log concentration-response curves, using the drc v3.0-1 package (Ritz and Streibig, 2005) of R v4.1.2 (R Core Team, 2014). Mean IC<sub>50</sub> values and standard deviations (SDs) were calculated for each growth inhibition assay using Excel. The chemical structures of the drugs were drawn using ChemDraw 19.0. The graphical presentations and statistical analyses (unpaired t-test) were done with GraphPad Prism v8.

## 3 RESULTS

### 3.1 Activity of Antibiotics Against Asexual Stages of *P. falciparum* and *P. knowlesi*

*P. falciparum* was exposed to 15 antibiotics (tetracyclines, macrolides) and chloroquine (control drug) for 3 and for 6 days. This allowed to assess the drug's inhibitory effect on the first and second parasite replication cycle, respectively (see results in **Table 1**), that indicates a fast or slow onset of antiplasmodial activity of the antibiotics.

None of the tetracyclines evaluated in this study showed a pronounced activity (in the nanomolar range) in the 3-day assay against *P. falciparum*, but had some delayed activity after 6 days of drug exposure (**Table 1**). Chlortetracycline, methacycline and lymecycline were still poorly active after 6 days. The first-time tested drugs against *P. falciparum* demeclocycline, sarecycline, omadacycline and the already previously tested drugs/controls doxycycline, minocycline, and eravacycline were active in the nanomolar range against both species after 6 days (**Table 1**). Boromycin was highly active against *P. falciparum* at an IC<sub>50</sub> of 1.0 nM after 3 days of incubation (**Table 1**). To further characterize its antiplasmodial activity, boromycin was also

**TABLE 1 |** Activity of antibiotics against *P. falciparum* strain 3D7 after 3 and 6 days of incubation and *P. knowlesi* strain A1-H.1 after 3 days.

Classe	Drug	Plasmodium falciparum (3D7) and P. knowlesi (A1-H.1) (IC <sub>50</sub> in nM)			Fold differences between 3 and 6 days
		3 day-assay		6 day-assay	
		3D7	A1-H.1	3D7	
<b>Tetracyclines</b>	Chlortetracycline	> 18000		> 18000	NA
	Methacycline	> 18000		3719 ± 3134	NA
	Lymecycline	> 18000		1124 ± 247	NA
	Demeclocycline	> 18000		410.1 ± 165	NA
	Meclocycline	> 18000		291.7 ± 41	NA
	Sarecycline	13378.9 ± 1053		244.1 ± 136	59
	Omadacycline	8443 ± 618		247.8 ± 109	34
<b>Macrolides</b>	Oleandomycin	8186 ± 3851		> 18000	NA
	Troleandomycin	> 18000		> 18000	NA
	Josamycin	> 18000		387.8 ± 185	NA
	Boromycin	0.9 ± 0.1	1.3 ± 0.2*	1.0 ± 0.7	0
<b>Controls</b>	Minocycline	9393 ± 4354		83.5 ± 25	113
	Eravacycline	2514 ± 550		5.1 ± 1.1	502
	Clindamycin	> 18000		5.9 ± 3.4	NA
	Doxycycline	9579 ± 2756		385.7 ± 292	24
	Chloroquine	8.4 ± 4.9	21.1 ± 11*	10.4 ± 4.8	0

\*Measured by SYBR Green-I.

All experiments have been done at least 3 times in duplicate.

assessed against *P. knowlesi* and its pronounced activity was confirmed there (Table 1).

## 3.2 Cytotoxicity of Boromycin Against Human Cells

Boromycin was cytotoxic at millimolar concentrations against human HepG2 cells with a selectivity index (SI) higher than 200,000. (Table 2). Chloroquine was used as comparator and was more cytotoxic than boromycin.

## 3.3 Characterization of the Antiplasmodial Activity of Boromycin

### 3.3.1 Activity of Boromycin Against Asexual Stages of *P. falciparum* Chloroquine-Resistant Strains

Different drug resistant strains of *P. falciparum* (Dd2, K1 and 7G8) were incubated with boromycin for 3 days to assess the potential of cross-resistance. Results were comparable to activities against 3D7 with IC<sub>50</sub> values in the picomolar range, and no cross-resistance to boromycin by these parasite lines was seen (Table 3). When investigating the morphological effect of the drug treatment on the parasite, untreated *P. falciparum* parasites of the strain 3D7 (Figure 3A) showed the usual ring shape, while boromycin-treated ring-stages (Figure 3B), as well as trophozoites and schizonts (– Supplementary Figure 2) showed the same pyknotic appearance after boromycin

incubation at 1 nM for 6 h. In addition, the same fast effect and morphological changes were also induced in the chloroquine resistant strain Dd2 (Figure 3C).

### 3.3.2 Activity of Boromycin Against Mature Gametocytes

Mature *P. falciparum* gametocytes (stage IV and V) were incubated with a serial dilution of boromycin for 48 h. Afterwards, ATP production was quantified to evaluate the gametocytocidal effect (Figure 4A). The results revealed that boromycin was highly active (IC<sub>50</sub> at 8.5 ± 3.6 nM), similarly active as the positive comparator epoxomicin (15.2 ± 3.4 nM) and more active than methylene blue (284 ± 35 nM). When observed microscopically, untreated gametocytes displayed their usual elongated shape with rounded edges (Figure 4A), but both boromycin (Figures 4B, C) and epoxomicin – treated (Figures 4C, D) parasites showed thinner body and edges, and intracellular disorganization. The length was not affected in epoxomicin-treated gametocytes, resulting in a needle-like shape, while boromycin-treated gametocytes presented a smaller appearance.

### 3.3.3 Activity of Boromycin on the Apicoplast

*P. falciparum* parasites were incubated with boromycin supplemented with IPP for 6 days to assess whether boromycin targets the apicoplast as described for many antibiotics;

**TABLE 2 |** Cytotoxicity of boromycin and the comparator chloroquine against HepG2 cells and calculated selectivity index.

	IC <sub>50</sub> (μM) in HepG2 cells	SI 3D7*	SI A1-H.1*
<b>Boromycin</b>	1250.5 ± 230	1,388,000	211,864
<b>Chloroquine</b>	153.4 ± 52.9	18,214	10,551

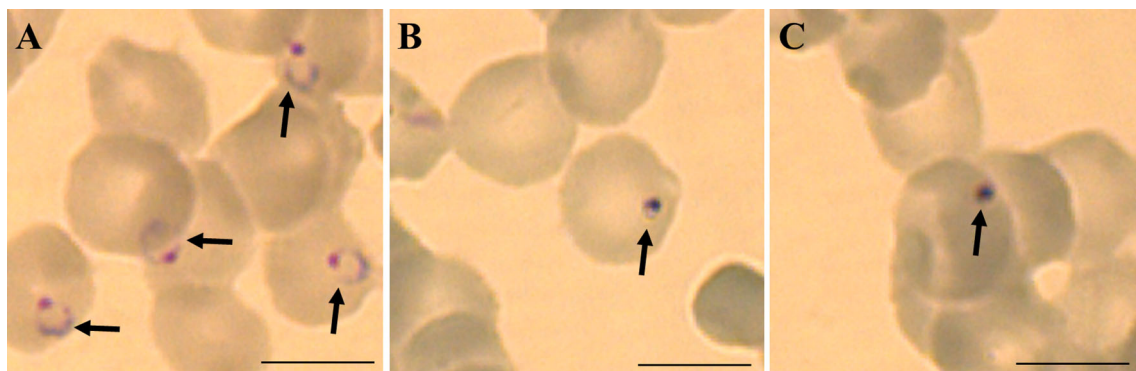
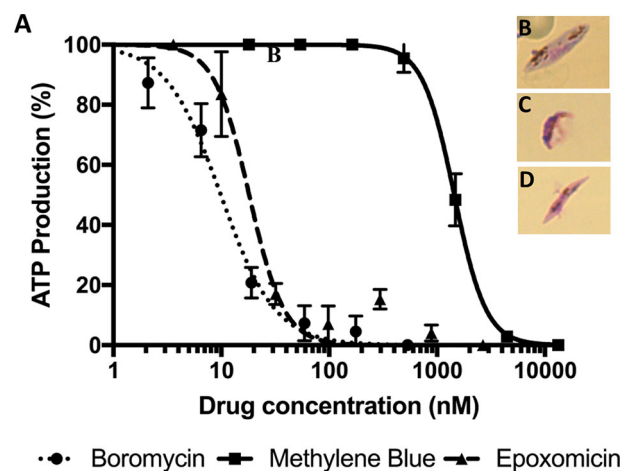
\*IC<sub>50</sub> 3-day assays; SI: selectivity index calculated by IC<sub>50</sub> HepG2/IC<sub>50</sub> Plasmodium species.

All experiments have been done at least 3 times in duplicate.

**TABLE 3** | Antiplasmodial activity of boromycin against different *P. falciparum* chloroquine-resistant strains in comparison to 3D7 after 3 days of incubation.

	Plasmodium falciparum strains (IC <sub>50</sub> in nM)			
	3D7	Dd2	K1	7G8
<b>Boromycin</b>	0.9 ± 0.1	0.6 ± 0.4	0.7 ± 0.1	0.4 ± 0.07
<b>Chloroquine</b>	8.4 ± 4.9	302 ± 119	401.4 ± 28.3	303.6 ± 18.2

All experiments have been done at least 3 times in duplicate.

**FIGURE 3** | Representative micrographies of *P. falciparum* infected erythrocytes stained with Giemsa: **(A)** untreated ring stage parasites after 6 hours, **(B)** parasites strain 3D7 treated with 1 nM of boromycin for 6 h and **(C)** parasites strain Dd2 treated with 1 nM of boromycin for 6 h. Arrows: parasites. Scale bar: 10 μm.**FIGURE 4** | Activity of boromycin, and the positive controls epoxomicin and methylene blue against mature (stage IV-V) *P. falciparum* gametocytes treated for 48 h. **(A)** Boromycin showed a more potent activity than methylene blue and similar activity to epoxomicin. **(B)** Untreated mature gametocytes. **(C)** Boromycin-treated gametocytes and **(D)** epoxomicin-treated parasites. All experiments were done at least 3 times in duplicate.

clindamycin was used as positive control. At the same time a standard growth inhibition assay without IPP was carried out as a comparator. As expected, clindamycin-treated parasites could be rescued by the supplementation with IPP, but the IC<sub>50</sub> values for boromycin remained similar at low nanomolar concentrations for both conditions (Table 4), suggesting that this drug effect cannot be rescued by IPP and has a different target from the apicoplast (Figure 5).

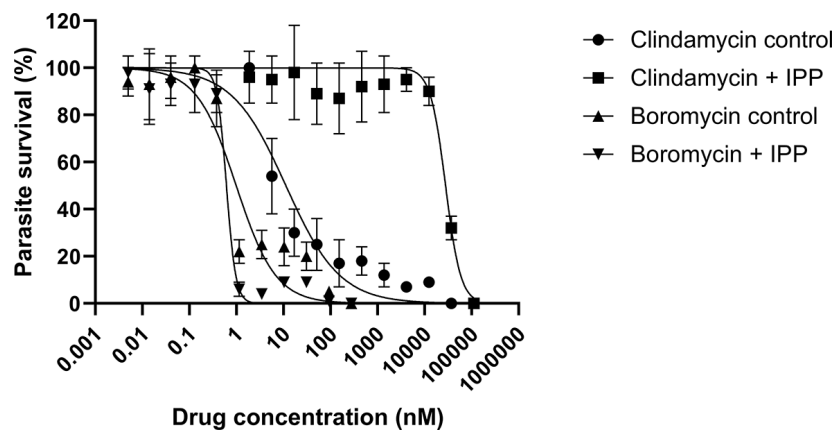
### 3.3.4 Ionophoric Activity of Boromycin

*P. falciparum* parasites were incubated with a serial dilution of boromycin, and chloroquine (control) with or without supplementation of 220 μg/mL of MgCl<sub>2</sub> or KCl, for 3 days to assess whether boromycin has the ionophoric activity on *P. falciparum* as described for *Mycobacterium* and *Bacillus subtilis* (Abenoja et al., 2021) (Table 5). Boromycin and chloroquine displayed the expected IC<sub>50</sub> value, the supplementation of KCl at

**TABLE 4** | IC<sub>50</sub> values obtained with isopentenyl pyrophosphate trilithium salt (IPP) rescue assay in comparison to standard drug assays against *P. falciparum* strain 3D7.

	IC <sub>50</sub> (nM)		P value (unpaired t-test)
	control	IPP supplementation	
<b>Clindamycin</b>	6.9 ± 1.3	>18000	0.02
<b>Boromycin</b>	0.9 ± 0.1	1.4 ± 0.8	0.717

All experiments have been done at least 3 times in duplicate.

**FIGURE 5** | Survival curves of isopentenyl pyrophosphate trilithium salt (IPP) rescue assays. Parasites of the *P. falciparum* strain 3D7 were treated with boromycin or clindamycin (positive control) with or without IPP supplementation and incubated for 6 days. Boromycin-treated parasites were not rescued by IPP, indicating that the apicoplast is not the main target. Experiments were done at least 3 times in duplicate.**TABLE 5** | Activity of boromycin and the control drug chloroquine against the *P. falciparum* strain 3D7 in the presence/absence of KCl (220 µg/ml) and MgCl<sub>2</sub> (220 µg/ml).

IC <sub>50</sub> (in nM)			
	control	KCl supplemented	MgCl <sub>2</sub> supplemented
<b>Boromycin</b>	0.7 ± 0.1	2.1 ± 0.2	0.2 ± 0
<b>Chloroquine</b>	12 ± 0.8	11.6 ± 1.4	2.2 ± 0

All experiments have been done at least 3 times in duplicate.

220 µg/mL increased IC<sub>50</sub> of boromycin by 3-fold, while no difference was observed for chloroquine. On the other hand, the incubation with boromycin or chloroquine in the presence of MgCl<sub>2</sub> led to a 3-5-fold decrease in the respective IC<sub>50</sub>s.

## 4 DISCUSSION

Antibiotics for malaria treatment have been investigated since the middle of the last century, with tetracyclines playing a central role. In recent years, macrolides have also been particularly studied as antimalarials (Gaillard et al., 2015; Gaillard et al., 2016a; Gaillard et al., 2016b). Although the delayed death effect caused by most antibiotics limits their use as first-line chemotherapy, some antibiotics such as doxycycline,

clindamycin, and the combination sulfadoxine-pyrimethamine (that does not display the delayed activity) are recommended as prophylaxis or treatment in certain populations (World Health Organization, 2021). The need for new alternative therapies, along with the limited investments in drug discovery to treat malaria, make drug repurposing a worthy alternative. Herein, the *in vitro* antiplasmodial activity of tetracyclines and macrolides not previously tested against Plasmodia along with comparator drugs were evaluated against blood-stages of *P. falciparum* revealing boromycin, as a potent antiplasmodial drug with a fast/first cycle activity that we assessed further.

All tested active tetracyclines showed a delayed death effect against *P. falciparum* (strain 3D7). The newly licensed tetracyclines omadacycline (licensed for treatment of bacterial pneumonia and acute skin infections) (Nuzya, 2021) and sarecycline (licensed for treatment of acne) (United States



Food and Drug Administration, 2021) showed comparable activity to doxycycline. None of the newly tested tetracyclines achieved the activity of the next generation tetracyclines tigecycline (Held et al., 2010) and eravacycline (Koehne et al., 2021) that suggested that modifications at the C9 position on the D ring that circumvents the ribosomal protection resistance mechanism found in bacteria could be beneficial for the activity against Plasmodia. However, the structurally similar omadacycline did not show this improved activity. In a similar way, differences in activities for these three antibiotics were also seen for rickettsia species (Quade et al., 2021). The delayed death effect was also shown by the macrolide josamycin suggesting that the apicoplast could be the target of this drug. The tetracyclines chlortetracycline, methacycline, lymecycline, and the macrolides troleandomycin and oleandomycin were only poorly active with  $IC_{50}$  in the micromolar range. Whereas the macrolide boromycin showed a fast onset of activity at a single-digit nanomolar concentration against both *Plasmodium* species.

*P. falciparum* is undoubtedly responsible for most of the malaria burden, especially for most of the malaria deaths, which justifies to mainly tailor treatments to this malaria species. However, there are five additional *Plasmodium* species responsible for malaria in humans and when elimination of malaria is the aim, all these species must be targeted. Until recently, *P. falciparum* was the only option for drug screening *in vitro* because the other human malaria parasites could not be kept in continuous *in vitro* culture (Mehlotra et al., 2017; van Schalkwyk et al., 2019). However, now *P. knowlesi* has been adapted for *in vitro* culture and its inclusion in drug screenings could give additional information on antiplasmodial activities of compounds as it is phylogenetically closer to the other human *Plasmodium* species (Rutledge et al., 2017; van Schalkwyk et al., 2019). Even though previous studies have claimed that most antiplasmodial compounds are equipotent against *P. falciparum* and *P. knowlesi* (Moon et al., 2013; Fatih et al., 2013), recent studies have reported different susceptibility profiles (van Schalkwyk et al., 2021) especially for some novel drugs in development. *P. knowlesi* was described as less susceptible to inhibitors of the dihydrofolate reductase, dihydroorotate dehydrogenase (van Schalkwyk et al., 2017), and ATP4 (van Schalkwyk et al., 2019). Herein, we also observed that boromycin was very potent against both species, *P. knowlesi* was slightly less vulnerable than *P. falciparum*, with a 4.5-fold higher  $IC_{50}$ .

The most promising antibiotic from our screening was the macrolide boromycin. Boromycin was isolated from a *Streptomyces antibioticus* found in a soil sample from Ivory coast and was first described in 1967 (Hütter et al., 1967; Pache and Zaehner, 1969b). It has a potent effect against Gram-positive bacteria *in vitro* (Moreira et al., 2016), and it was shown to be active against HIV (Kohn et al., 1996), *Babesia* (Hütter et al., 1967) and some other pathogens (de Carvalho et al., 2019). Its antiplasmodial activity was already once described in a patent filed in the US in 1973 where its activity in the malaria models of *P. berghei* in mice (ED<sub>50</sub>: 2.2 mg/kg) and *P. gallinaceum* in birds (ED<sub>50</sub>: ~ 7 mg/kg) is given (Prelog et al., 1973). Additionally, its *in vitro* activity against *P.*

*falciparum* strain K1 (chloroquine – resistant) and FCR3 (chloroquine – sensitive) was described to be 39 and 40 nM, respectively (Tsutsui et al., 2010). In the same study, only a low selectivity index against MRC-5 cells (~12) was described, but a 97.9% parasite reduction was observed when *P. berghei* – infected mice were treated *p.o.* at 10 mg/kg according to Peter's test. However, no description of the evaluation of its gametocytocidal activity and stage specific effect could be identified by us.

In our investigation, boromycin showed a high activity and a fast onset of action, a desired property of antimalarials to quickly reduce parasite load and avoid the disease progression to the severe form. It also showed an excellent selectivity index against HepG2 cells. This favorable toxicity profile was also confirmed previously (Moreira et al., 2016), and the LD<sub>50</sub> in mice is given as 180 mg/kg<sup>-1</sup> (Klingel, 1980). These results encouraged a more detailed investigation of the antiplasmodial activity of boromycin.

Boromycin's *in vitro* activity against laboratory strains showed potent activity as it was active at low nanomolar and even at picomolar concentrations. No cross-resistance with the tested chloroquine/multi-resistant strains (Dd2, 7G8, and K1) was seen as the  $IC_{50}$  values were in same range as for the drug sensitive strain 3D7, suggesting that is not affected by the common resistance mechanisms (Ding et al., 2012). Morphologically, ring stage parasites showed a pyknotic appearance after 6 h treatment with boromycin at 1 nM, suggesting that it leads to a rapid death. We additionally evaluated the activity of boromycin against mature gametocytes and could see a very potent activity superior to the positive control methylene blue, similarly active as the proteasome inhibitor epoxomicin. Drugs with transmission-blocking activity are of special interest and would be a great asset for controlling and eliminating malaria (Sinden, 2017; Wadi et al., 2019). Currently, primaquine is the only approved drug active against gametocytes (Lin et al., 2017) but its use is restricted mainly due to its haemolysis-inducing effect in patients with glucose-6-phosphate dehydrogenase deficiency (Recht et al., 2018), and additionally it has to be metabolized by a liver enzyme (CYP2D6) to be active. Drugs with multi-stage activities and novel modes of action are especially desired for the next generation of antimalarials (Ding et al., 2012).

The apicoplast is described as the main target of antibiotics that exert the delayed death effect (Dahl and Rosenthal, 2007; Eklund et al., 2011) and the fast-acting antibiotic fosmidomycin (Uddin et al., 2018). Apicoplast-free parasites can survive and proliferate when the medium is supplemented with IPP (Yeh and DeRisi, 2011), but this did not rescue the boromycin-treated parasites in our assay; therefore, we could rule out the apicoplast as a main target.

The ionophoric activity of boromycin, especially for K<sup>+</sup> channels, was firstly described in *Bacillus subtilis* in addition to the impairment of protein, RNA, and DNA synthesis (Pache and Zaehner, 1969a). This ionophoric activity was later confirmed in *Mycobacterium bovis*, where a rapid loss of membrane potential, reduction of intracellular ATP, and leakage of cytoplasmic proteins were induced (Moreira et al., 2016) and the external

addition of a high concentration of KCl (20 mg/mL) decreased boromycin activity from 50% to 10%. To assess whether boromycin acts as a potassium ionophore also in *P. falciparum*, parasites were simultaneously incubated with boromycin together with the highest non-toxic concentration (220 µg/mL) of KCl or MgCl<sub>2</sub> (negative control). We could not incubate *Plasmodium* parasites at a similar high ion concentration as in the *Mycobacterium* experiments, as this concentration was toxic to the parasites. We identified a three-fold IC<sub>50</sub> increase with the addition of KCl. However, it is most probably not the primary mode of action, as the activity remained in the low nanomolar range. On the other hand, the boromycin IC<sub>50</sub> decreased with addition of MgCl<sub>2</sub>, this was also seen for chloroquine, an effect that was described before (Hess et al., 1995). Recently, boromycin was shown to decrease intracellular multiplication of both *Toxoplasma gondii* and *Cryptosporidium parvum* (Abenoja et al., 2021), but the potential target in these parasites was not further investigated.

In conclusion, we presented the antiplasmodial activity of different tetracycline and macrolide antibiotics against *P. falciparum*. The tetracyclines tested here did not show higher *in vitro* activities than previously tested tetracyclines and all displayed a slow/second cycle onset of action. The macrolide boromycin showed the most noticeable results as a fast-acting drug against both *Plasmodium* species and *P. falciparum* mature gametocytes. These results, along with the historical antiparasitic effects of boromycin, suggest that boromycin deserves a deeper investigation as an alternative therapy for diseases caused by apicomplexan parasites, including Plasmodia.

## REFERENCES

- Abenoja, J., Cotto-Rosario, A., and O'Connor, R. (2021). Boromycin has Potent Anti-Toxoplasma and Anti-Cryptosporidium Activity. *Antimicrob. Agents Chemother.* 65, e01278–e01220. doi: 10.1128/AAC.01278-20
- Amir, A., Cheong, F. W., de Silva, J. R., Liew, J. W. K., and Lau, Y. L. (2018). Plasmodium Knowlesi Malaria: Current Research Perspectives. *Infect. Drug Resist.* 11, 1145–1155. doi: 10.2147/IDR.S148664
- Balikagala, B., Fukuda, N., Ikeda, M., Katuro, O. T., Tachibana, S.-I., Yamauchi, M., et al. (2021). Evidence of Artemisinin-Resistance Malaria in Africa. *NEJM* 385, 1163–1171. doi: 10.1056/NEJMoa2101746
- Benakis, A., Paris, M., Loutan, L., Plessas, C. T., and Plessas, S. T. (1997). Pharmacokinetics of Artemisinin and Artesunate After Oral Administration in Healthy Volunteers. *Am. J. Trop. Med. Hyg.* 56, 17–23. doi: 10.4269/ajtmh.1997.56.17
- Dahl, E. L., and Rosenthal, P. J. (2007). Multiple Antibiotics Exert Delayed Effects Against the Plasmodium Falciparum Apicoplast. *Antimicrob. Agents Chemother.* 51, 3485–3490. doi: 10.1128/AAC.00527-07
- de Carvalho, L. P., Kreidenweiss, A., and Held, J. (2021). Drug Repurposing: A Review of Old and New Antibiotics for the Treatment of Malaria: Identifying Antibiotics With a Fast Onset of Antiplasmodial Action. *Molecules* 26, 2304. doi: 10.3390/molecules26082304
- de Carvalho, L. P., Sandri, T. L., de Melo, E. J. T., Fendel, R., Kremsner, P. G., Mordmüller, B., et al. (2019). Ivermectin Impairs the Development of Sexual and Asexual Stages of Plasmodium Falciparum In Vitro. *Antimicrob. Agents Chemother.* 63, e00085–e00019. doi: 10.1128/AAC.00085-19
- Ding, X. C., Ubben, D., and Wells, T. N. C. (2012). A Framework for Assessing the Risk of Resistance for Anti-Malarials in Development. *Malar. J.* 11, 292–303. doi: 10.1186/1475-2875-11-292
- Dunitz, J. D., Hawley, D. M., Mikol, D., White, D. N. J., Berlin, Y., Marusic, R., et al. (1971). Structure of Boromycin. *Helv. Chim. Acta* 54, 1709–1713. doi: 10.1002/hlca.19710540624

## DATA AVAILABILITY STATEMENT

The original contributions presented in the study are included in the article/**Supplementary Material**. Further inquiries can be directed to the corresponding author.

## AUTHOR CONTRIBUTIONS

JH and LPC designed the study, experiments were performed by SG-O. JH, LPC, and SG-O analyzed the data, all authors contributed to interpretation of the data. The first draft of the manuscript was written by LPC. All authors commented and contributed to the article and approved the final version of the manuscript.

## ACKNOWLEDGMENTS

We acknowledge support by Open Access Publishing Fund of University of Tübingen.

## SUPPLEMENTARY MATERIAL

The Supplementary Material for this article can be found online at: <https://www.frontiersin.org/articles/10.3389/fcimb.2021.802294/full#supplementary-material>

- Ekland, E. H., Schneider, J., and Fidock, D. A. (2011). Identifying Apicoplast-Targeting Antimalarials Using High-Throughput Compatible Approaches. *FASEB J.* 25, 3583–3593. doi: 10.1096/fj.11-187401
- Fatih, F. A., Staines, H. M., Siner, A., Ahmed, M. A., Woon, L. C., Pasini, E. M., et al. (2013). Susceptibility of Human Plasmodium Knowlesi Infections to Anti-Malarials. *Malar. J.* 12, 1–7. doi: 10.1186/1475-2875-12-425
- Gaillard, T., Dormoi, J., Madamet, M., and Pradines, B. (2016a). Macrolides and Associated Antibiotics Based on Similar Mechanism of Action Like Lincosamides in Malaria. *Malar. J.* 15, 1–11. doi: 10.1186/s12936-016-1114-z
- Gaillard, T., Madamet, M., and Pradines, B. (2015). Tetracyclines in Malaria. *Malar. J.* 14, 445. doi: 10.1186/s12936-015-0980-0
- Gaillard, T., Madamet, M., Tsombeng, F. F., Dormoi, J., and Pradines, B. (2016b). Antibiotics in Malaria Therapy: Which Antibiotics Except Tetracyclines and Macrolides may be Used Against Malaria? *Malar. J.* 556, 1–10. doi: 10.1186/s12936-016-1613-y
- Gardiner, D. L., and Trenholme, K. R. (2015). Plasmodium Falciparum Gametocytes: Playing Hide and Seek. *Ann. Transl. Med.* 3, 45. doi: 10.3978/j.issn.2305-5839.2015.01.23
- Grande, E. N., Sanchez, A. R., and Sanchez, F. R. (1956). The Treatment of Malaria With Tetracycline. *Antibiot. Med. Clin. Ther.* 3, 193–196.
- Grignard, L., Shah, S., Chua, T. H., William, T., Drakeley, C. J., and Fornace, K. M. (2019). Natural Human Infections With Plasmodium Cynomolgi and Other Malaria Species in an Elimination Setting in Sabah, Malaysia. *J. Inf. Dis.* 220, 1946–1949. doi: 10.1093/infdis/jiz397
- Held, J., Zanger, P., Issifou, S., Kremsner, P. G., and Mordmüller, B. (2010). In Vitro Activity of Tigecycline in Plasmodium Falciparum Culture-Adapted Strains and Clinical Isolates From Gabon. *Int. J. Antimicrob. Agents* 35, 587–589. doi: 10.1016/j.ijantimicag.2010.02.003
- Hess, F. I., Kilian, A., Söllner, W., Nothdurft, H. D., Pröll, S., and Löscher, T. (1995). Plasmodium Falciparum and Plasmodium Berghei: Effect of

- Magnesium on the Development of Parasitemia. *Exp. Parasitol.* 80, 186–193. doi: 10.1006/expr.1995.1023
- Hu, T. H., Rosli, N., Mohamad, D. S. A., Kadir, K. A., Ching, Z. H., Chai, Y. H., et al. (2021). A Comparison of the Clinical, Laboratory and Epidemiological Features of Two Divergent Subpopulations of *Plasmodium Knowlesi*. *Sci. Rep.* 11, 20117. doi: 10.1038/s41598-021-99644-8
- Hütter, R., Keller-Schien, W., Knüsel, F., Prelog, V., Rodgers, G. C. Jr., Suter, P., et al. (1967). Stoffwechselprodukte Von Mikroorganismen. 57. Mitteilung. Boromycin. *Helv. Chim. Acta* 50, 1533–1539. doi: 10.1002/hlca.19670500612
- Imboden, C. A., Cooper, W. C., Coatney, G. R., and Jeffrey, G. M. (1950). Studies in Human Malaria. XXIX. Trials of Aureomycin, Chloramphenicol, Penicillin, and Dihydrostreptomycin Against the Chesson Strain of *Plasmodium Vivax*. *J. Natl. Malar. Soc.* 9, 377–380.
- Ishiyama, A., Iwatsuki, M., Namatame, M., Nishihara-Tsukashima, A., Sunazuka, T., Takahashi, Y., et al. (2011). Borrelidin, a Potent Antimalarial: Stage-Specific Inhibition Profile of Synchronized Cultures of *Plasmodium Falciparum*. *J. Antibiot.* 64, 381–384. doi: 10.1038/ja.2011.6
- Klingel, W. (1980). *Bor in Biologie, Medizin Und Pharmazie: Physiologische Wirkungen Und Anwendung Von Borverbindungen* (Braunschweig: Springer-Verlag), 902.
- Koehne, E., Kreidenweiss, A., Adegbite, B. R., Manego, R. Z., McCall, M. B. B., Mombo-Ngoma, G., et al. (2021). *In Vitro* Activity of Eravacycline, a Novel Synthetic Halogenated Tetracycline, Against the Malaria Parasite *Plasmodium Falciparum*. *J. Glob. Antimicrob. Resist.* 24, 93–97. doi: 10.1016/j.jgar.2020.11.024
- Kohno, J., Kawahata, T., Otake, T., Morimoto, M., Mori, H., Ueba, N., et al. (1996). Boromycin, an Anti-HIV Antibiotic. *Biosci. Biotechnol. Biochem.* 60, 1036–1037. doi: 10.1271/bbb.60.1036
- Lelièvre, J., Almela, M. J., Lozano, S., Miguel, C., Franco, V., Leroy, D., et al. (2012). Activity of Clinically Relevant Antimalarial Drugs on *Plasmodium Falciparum* Mature Gametocytes in an ATP Bioluminescence “Transmission Blocking” Assay. *PLoS One* 7, 1–8. doi: 10.1371/journal.pone.0035019
- Lin, J. T., Lon, C., Spring, M. D., Sok, S., Chann, S., Ittiverakul, M., et al. (2017). Single Dose Primaquine to Reduce Gametocyte Carriage and *Plasmodium Falciparum* Transmission in Cambodia: An Open-Label Randomized Trial. *PLoS One* 12, e0168702. doi: 10.1371/journal.pone.0168702
- Mehlota, R. K., Blankenship, D., Howes, R. E., Rakotomanga, T. A., Ramiranirina, B., Ramboarina, S., et al. (2017). Long-Term *In Vitro* Culture of *Plasmodium Vivax* Isolates From Madagascar Maintained in Saimiri Boliviensis Blood. *Malar. J.* 16, 1–13. doi: 10.1186/s12936-017-2090-7
- Mendes, A. M., Albuquerque, I. S., Machado, M., Pissarra, J., Meireles, P., and Prudêncio, M. (2017). Inhibition of *Plasmodium* Liver Infection by Ivermectin. *Antimicrob. Agents Chemother.* 61, 1–8. doi: 10.1128/AAC.02005-16
- Milner, D. A. Jr., Whitten, R. O., Kamiza, S., Carr, R., Liomba, G., Dzamalala, C., et al. (2014). The Systemic Pathology of Cerebral Malaria in African Children. *Front. Cell Infect. Microbiol.* 4, 1–13. doi: 10.3389/fcimb.2014.00104
- Mishra, S. J., Liu, W., Beebe, K., Banerjee, M., Kent, C. N., Munthali, V., et al. (2021). The Development of Hsp90 $\beta$ -Selective Inhibitors to Overcome Detriments Associated With Pan-Hsp90 Inhibition. *J. Med. Chem.* 11, 1545–1557. doi: 10.1021/acs.jmedchem.0c01700
- Moon, R. W., Hall, J., Rangkuti, F., Ho, Y. S., Almond, N., Mitchell, G. H., et al. (2013). Adaptation of the Genetically Tractable Malaria Pathogen *Plasmodium Knowlesi* to Continuous Culture in Human Erythrocytes. *Proc. Natl. Acad. Sci. U. S. A.* 110, 531–536. doi: 10.1073/pnas.1216457110
- Moreira, W., Aziz, D. B., and Dick, T. (2016). Boromycin Kills Mycobacterial Persists Without Detectable Resistance. *Front. Microbiol.* 7, 199. doi: 10.3389/fmicb.2016.00199
- Noedl, H., Bronnert, J., Yingyuen, K., Attlmayr, B., Kollaritsch, H., and Fukuda, M. (2005). Simple Histidine-Rich Protein 2 Double-Site Sandwich Enzyme-Linked Immunosorbent Assay for Use in Malaria Drug Sensitivity Testing. *Antimicrob. Agents Chemother.* 49, 5–8. doi: 10.1128/AAC.49.8.3575-3577.2005
- Nsanjabana, C. (2019). Resistance to Artemisinin Combination Therapies (ACTs): Do Not Forget the Partner Drug! *Trop. Med. Infect. Dis.* 4, 26. doi: 10.3390/tropicalmed4010026
- Nuzrya. Available at: <https://www.nuzrya.com/hcp/> (Accessed October 15, 2021).
- Otoguro, K., Ui, H., Ishiyama, A., Kobayashi, M., Togashi, H., Takahashi, Y., et al. (2003). *In Vitro* and *In Vivo* Antimalarial Activities of a Non-Glycosidic 18-Membered Macrolide Antibiotic, Borrelidin, Against Drug-Resistant Strains of *Plasmodia*. *J. Antibiot.* 56, 727–729. doi: 10.7164/antibiotics.56.727
- Pache, W., and Zaehner, H. (1969a). Metabolic Products of Microorganisms. *Arch. für. Mikrobiol.* 67, 156–165. doi: 10.1007/BF00409681
- Pache, W., and Zaehner, H. (1969b). Stoffwechselprodukte Von Mikroorganismen. *Arch. Mikrobiol.* 288, 281–288. doi: 10.1007/BF00412060
- Pluijm, R. W., Imwong, M., Chau, N. H., Hoa, N. T., Thuy-Nhien, N. T., Thanh, N. V., et al. (2019). Determinants of Dihydroartemisinin-Piperaquine Treatment Failure in *Plasmodium Falciparum* Malaria in Cambodia, Thailand, and Vietnam: A Prospective Clinical, Pharmacological, and Genetic Study. *Lancet Inf. Dis.* 19, 952–961. doi: 10.1016/S1473-3099(19)30391-3
- Portugaliza, H. P., Miyazaki, S., Geurten, F. J. A., Pell, C., Rosanas-Urgell, A., Janse, C. J., et al. (2020). Artemisinin Exposure at the Ring or Trophozoite Stage Impacts *Plasmodium Falciparum* Sexual Conversion Differently. *Elife* 9, e60058. doi: 10.7554/eLife.60058
- Prelog, V., Zaehner, H., and Bickel, H. (1973). U.S. Patent No 584,215 (Ardslay, New York: Ciba-Geigy Corporation).
- Quade, B. R., Ramirez-Hernández, A., and Blanton, L. S. (2021). *In Vitro* Susceptibility of Rickettsia Species to Eravacycline, Omadacycline, and Tigecycline. *Antimicrob. Agents Chemother.* 65, e0066521. doi: 10.1128/AAC.00665-21
- R Core Team. (2014). *R: A Language and Environment for Statistical Computing* (Vienna, Austria: R Foundation for Statistical Computing). Available at: <http://www.R-project.org>.
- Recht, J., Ashley, E. A., and White, N. J. (2018). Use of Primaquine and Glucose-6-Phosphate Dehydrogenase Deficiency Testing: Divergent Policies and Practices in Malaria Endemic Countries. *PLoS Negl. Trop. Dis.* 12, e0006230. doi: 10.1371/journal.pntd.0006230
- Ribaut, C., Berry, A., Chevalley, S., Reybier, K., Morlais, I., Parzy, D., et al. (2008). Concentration and Purification by Magnetic Separation of the Erythrocytic Stages of All Human *Plasmodium* Species. *Malar. J.* 7, 1–5. doi: 10.1186/1475-2875-7-45
- Ritz, C., and Streibig, J. C. (2005). Bioassay Analysis Using R. *J. Stat. Softw.* 12, 1–22. doi: 10.18637/jss.v012.i05
- Rutledge, G. G., Böhm, U., Sanders, M., Reid, A. J., Cotton, J. A., Maiga-Ascofare, O., et al. (2017). *Plasmodium Malariae* and *P. Ovale* Genomes Provide Insights Into Malaria Parasite Evolution. *Nature* 542, 101–104. doi: 10.1038/nature21038
- Siciliano, G., and Alano, P. (2015). Enlightening the Malaria Parasite Life Cycle: Bioluminescent *Plasmodium* in Fundamental and Applied Research. *Front. Microbiol.* 6, 1–8. doi: 10.3389/fmicb.2015.00391
- Sinden, R. E. (2017). Developing Transmission-Blocking Strategies for Malaria Control. *PLoS Pathog.* 13, 1–12. doi: 10.1371/journal.ppat.1006336
- Straimer, J., Gnädig, N. F., Witkowski, B., Amaratunga, C., Duru, V., Ramadani, A. P., et al. (2015). K13-Propeller Mutations Confer Artemisinin Resistance in *Plasmodium Falciparum* Clinical Isolates. *Science* 347, 428–431. doi: 10.1126/science.1260867
- Tsutsui, A., Furuya, Y., Hirose, T., Kim, R., Masuma, R., Matsumoto, A., et al. (2010). Boromycin Derivatives: Synthesis and Antimalarial Activity *In Vitro* and *In Vivo*. *Heterocycles* 82, 289–295. doi: 10.3987/COM-10-S(E)55
- Uddin, T., McFadden, G. I., and Goodman, C. D. (2018). Validation of Putative Apicoplast-Targeting Drugs Using a Chemical Supplementation Assay in Cultured Human Malaria. *Antimicrob. Agents Chemother.* 62, e01161–e01117. doi: 10.1128/AAC.01161-17
- United States Food and Drug Administration *Drug Trials Snapshot: Seysara*. Available at: <https://www.fda.gov/drugs/drug-approvals-and-datab> (Accessed October 15, 2021).
- van Bijljon, R., Niemand, J., van Wyk, R., Clark, K., Verlinden, B., Abrie, C., et al. (2018). Inducing Controlled Cell Cycle Arrest and Re-Entry During Asexual Proliferation of *Plasmodium Falciparum* Malaria Parasites. *Sci. Rep.* 8, 1–14. doi: 10.1038/s41598-018-34964-w
- van Schalkwyk, D. A., Blasco, B., Davina, N. R., Liew, J. W. K., Amir, A., Lau, Y. L., et al. (2019). *Plasmodium Knowlesi* Exhibits Distinct *In Vitro* Drug Susceptibility Profiles From Those of *Plasmodium Falciparum*. *Int. J. Parasitol. Drugs Drug Resist.* 9, 93–99. doi: 10.1016/j.ijddr.2019.02.004
- van Schalkwyk, D. A., Moon, R. W., Blasco, B., and Sutherland, C. J. (2017). Comparison of the Susceptibility of *Plasmodium Knowlesi* and *Plasmodium*

- Falciparum to Antimalarial Agents. *J. Antimicrob. Chemother.* 72, 3051–3058. doi: 10.1093/jac/dkx279
- van Schalkwyk, D. A., Moon, R. W., Duffey, M., Leroy, D., and Sutherland, C. J. (2021). *Ex Vivo* Susceptibility to New Antimalarial Agents Differs Among Human-Infecting Plasmodium Species. *Int. J. Parasitol. Drugs Drug Resist.* 17, 5–11. doi: 10.1016/j.ijpddr.2021.07.002
- Wadi, I., Nath, M., Anvikar, A. R., Singh, P., and Sinha, A. (2019). Recent Advances in Transmission-Blocking Drugs for Malaria Elimination. *Future Med. Chem.* 11, 3047–3088. doi: 10.4155/fmc-2019-0225
- White, N. J. (2008). Plasmodium Knowlesi: The Fifth Human Malaria Parasite. *Clin. Infect. Dis.* 15, 172–173. doi: 10.1086/524889
- World Health Organization. *Guidelines for Malaria*. Available at: <https://www.who.int/publications/i/item/guidelines-for-malaria> (Accessed December 10, 2021).
- World Health Organization. (2021). *World Malaria Report*. Available at: <https://www.who.int/teams/global-malaria-programme/reports/world-malaria-report-2021> (Accessed December 22, 2021).
- WWARN K13 Genotype-Phenotype Study Group. (2019). Association of Mutation in the Plasmodium Falciparum Kelch13 Gene (Pf3D7\_1343700) With Parasite Clearance Rates After Artemisinin-Based Treatments – A WWARN Individual Patient Data Meta-Analysis. *BMC Med.* 17, 1. doi: 10.1186/s12916-018-1207-3
- Yeh, E., and DeRisi, J. L. (2011). Chemical Rescue of Malaria Parasites Lacking an Apicoplast Defines Organelle Function in Blood-Stage Plasmodium Falciparum. *PLoS Biol.* 9, e1001138. doi: 10.1371/journal.pbio.1001138

**Conflict of Interest:** The authors declare that the research was conducted in the absence of any commercial or financial relationships that could be construed as a potential conflict of interest.

**Publisher's Note:** All claims expressed in this article are solely those of the authors and do not necessarily represent those of their affiliated organizations, or those of the publisher, the editors and the reviewers. Any product that may be evaluated in this article, or claim that may be made by its manufacturer, is not guaranteed or endorsed by the publisher.

Copyright © 2022 de Carvalho, Groeger-Otero, Kreidenweiss, Kremsner, Mordmüller and Held. This is an open-access article distributed under the terms of the Creative Commons Attribution License (CC BY). The use, distribution or reproduction in other forums is permitted, provided the original author(s) and the copyright owner(s) are credited and that the original publication in this journal is cited, in accordance with accepted academic practice. No use, distribution or reproduction is permitted which does not comply with these terms.





# Novel Highlight in Malarial Drug Discovery: Aspartate Transcarbamoylase

Chao Wang<sup>1</sup>, Arne Krüger<sup>2</sup>, Xiaochen Du<sup>1</sup>, Carsten Wrenger<sup>2\*</sup> and Matthew R. Groves<sup>1\*</sup>

<sup>1</sup> Department of Drug Design, Groningen Research Institute of Pharmacy, University of Groningen, Groningen, Netherlands,

<sup>2</sup> Unit for Drug Discovery, Department of Parasitology, Institute of Biomedical Sciences, University of São Paulo, São Paulo, Brazil

## OPEN ACCESS

### Edited by:

Vipan Kumar,  
Guru Nanak Dev University, India

### Reviewed by:

Palak Patel,  
National Institute of Allergy and  
Infectious Diseases (NIH),  
United States

### \*Correspondence:

Matthew R. Groves  
m.r.groves@rug.nl  
Carsten Wrenger  
cwrenger@icb.usp.br

### Specialty section:

This article was submitted to  
Clinical Microbiology,  
a section of the journal  
Frontiers in Cellular and  
Infection Microbiology

**Received:** 22 December 2021

**Accepted:** 15 February 2022

**Published:** 04 March 2022

### Citation:

Wang C, Krüger A, Du X, Wrenger C  
and Groves MR (2022) Novel Highlight  
in Malarial Drug Discovery: Aspartate  
Transcarbamoylase.  
Front. Cell. Infect. Microbiol. 12:841833.  
doi: 10.3389/fcimb.2022.841833

Malaria remains one of the most prominent and dangerous tropical diseases. While artemisinin and analogs have been used as first-line drugs for the past decades, due to the high mutational rate and rapid adaptation to the environment of the parasite, it remains urgent to develop new antimalarials. The pyrimidine biosynthesis pathway plays an important role in cell growth and proliferation. Unlike human host cells, the malarial parasite lacks a functional pyrimidine salvage pathway, meaning that RNA and DNA synthesis is highly dependent on the *de novo* synthesis pathway. Thus, direct or indirect blockage of the pyrimidine biosynthesis pathway can be lethal to the parasite. Aspartate transcarbamoylase (ATCase), catalyzes the second step of the pyrimidine biosynthesis pathway, the condensation of L-aspartate and carbamoyl phosphate to form N-carbamoyl aspartate and inorganic phosphate, and has been demonstrated to be a promising target both for anti-malaria and anti-cancer drug development. This is highlighted by the discovery that at least one of the targets of Torin2 – a potent, yet unselective, antimalarial – is the activity of the parasite transcarbamoylase. Additionally, the recent discovery of an allosteric pocket of the human homology raises the intriguing possibility of species selective ATCase inhibitors. We recently exploited the available crystal structures of the malarial aspartate transcarbamoylase to perform a fragment-based screening to identify hits. In this review, we summarize studies on the structure of *Plasmodium falciparum* ATCase by focusing on an allosteric pocket that supports the catalytic mechanisms.

**Keywords:** aspartate transcarbamoylase, allosteric pocket, pyrimidine biosynthesis, anti-malarials, *Plasmodium falciparum*, X-ray structure

## INTRODUCTION

Malaria is an infectious disease that remains a clear and present threat to human health. It has been estimated that the disease is responsible for more than half a million deaths annually. In 2016, nearly half of the world's population was at risk of malaria and according to the latest World Malaria Report 2021 (WHO, 2021), there were an estimated 241 million cases of malaria in 2020 in 85 malaria endemic countries, increasing from 227 million in 2019, and malaria deaths increased by

12% compared with 2019, to an estimated 627 000. Children under 5 years accounted for the majority of malaria deaths in areas of high malaria transmission (77% in 2020). To date there are more than 200 known species of the genus *Plasmodium*, but just five of them cause human malaria, comprising *P. vivax*, *P. ovale*, *P. malariae*, *P. knowlesi* and *P. falciparum* (Majori, 2012), the most virulent malaria parasite. A potent vaccine is currently not available and therefore disease control depends mostly on drugs (Greenwood et al., 2008). Malaria is presently undergoing resurgence and the control of *P. falciparum* has become a major challenge in global health. Due to the high mutational rate of the parasite and its resulting rapid adaptation to environmental changes, both drug resistance and the geographic distribution of the disease are increasing (Piel et al., 2010). The inevitable emergence of antimalarial drug resistance (López et al., 2010) forces continuous efforts towards the discovery and development of new antimalarial drugs. There is therefore an urgent need for novel chemotherapeutic targets. Highly attractive avenues for the antimalarial drug discovery are metabolic pathways. The pyrimidine-biosynthesis pathway of *Plasmodium falciparum* is a promising target for antimalarial drug discovery as we reported previously (Lunev et al., 2016; Lunev et al., 2018). Active proliferation during the intraerythrocytic stage of *P. falciparum* requires a supply of purines and pyrimidines for parasite growth to support the production of DNA and parasite replication. As the malarial parasite lacks a purine biosynthetic pathway (De Koning et al., 2005; Hyde, 2007), as well as a functional pyrimidine-import pathway (Reyes et al., 1982; Rathod and Reyes, 1983; Gardner et al., 2002), the parasite relies solely on the *de novo* synthesis pathway to produce pyrimidines, and therefore the *de novo* pyrimidine biosynthesis pathway has been demonstrated to be a promising target for antimalarial drug discovery (Downie et al., 2008; Vaidya and Mather, 2009; Rodrigues et al., 2010; Belen Cassera et al., 2011).

The *de novo* synthesis of pyrimidines process in general contains six sequential enzymatic steps (Figure 1) in *P. falciparum* and starts with the Carbamoyl phosphate synthetase II (CPS II) which is responsible for the formation of carbamoyl phosphate in the cytosol from bicarbonate, glutamine and ATP (Müller et al., 2010; Müller et al., 2010). The Aspartate transcarbamoylase (PF3D7\_1344800, ATCase), the second enzyme in the pathway, catalyzes the condensation of aspartate and carbamoyl phosphate to form N-carbamoyl-L-aspartate and inorganic phosphate. The third step is the intramolecular condensation catalyzed by dihydroorotase (DHOase) to the product dihydroorotate. Then dihydroorotate dehydrogenase oxidizes dihydroorotate to orotate. Subsequently orotate and 5-phosphoribosyl-1-pyrophosphate (PRPP) are combined to produce orotidine-5'-monophosphate (OMP) by orotate phosphoribosyl transferase (OPRTase), the final product, molecular uridine monophosphate (UMP), is yielded by decarboxylation of OMP catalyzed by OMP decarboxylase (O'Donovan and Neuhaud, 1970; Jones, 1980).

In the following review, we summarize the current knowledge of the PfATCase, by highlighting the potential of an allosteric pocket and describing how these structures provide insights into

the ATCase catalytic mode of action. We will also review current studies on drug discovery against other ATCases, not solely against the human malaria parasite by Torin 2 (Bosch et al., 2020).

## ASPARTATE TRANSCARBAMOYLASE STRUCTURE AND IMPACT ON MECHANISM

Aspartate transcarbamoylase catalyzes the second step in *de novo* pyrimidine biosynthesis, where the condensation of L-aspartate (L-Asp) and carbamoyl phosphate (CP) to form N-carbamoyl aspartate (CA) and phosphate (Pi) (Figure 2A). The *Escherichia coli* aspartate transcarbamoylase holoenzyme represents the canonical form and is composed of six catalytic and six regulator subunits in which three regulatory pairs coordinate two catalytic trimers (G., 1964; Gerhart and Schachman, 1965; Weber, 1968; Ke et al., 1984; Stevens et al., 1990). The *E. coli* enzyme has been extensively studied and is now a textbook example that regulates pyrimidine biosynthesis pathway through its catalytic and regulatory mechanisms and has been fully characterized by Lipscomb and Kantrowitz (2012). The *E. coli* ATCase is inhibited by the final products of the pyrimidine biosynthesis pathway (CTP) and by a combination of CTP and UTP. The catalytic reaction by the canonical ATCase is sequential (Wang et al., 2005); CP binds first inducing a conformational changes and creating a binding site for L-aspartate. Similarly, N-carbamoyl aspartate leaves the active site before phosphate.

The *P. falciparum* ATCase is a homotrimer with three active sites in which each of the three active sites is formed at adjacent oligomeric interface (Figure 3A), following the canonical example. Each catalytic site is composed of two functional domains - the aspartate domain, which is mainly responsible for the binding of the substrate L-aspartate, and the carbamoyl phosphate domain, which is mainly responsible for the binding of the substrate carbamoyl phosphate. Apart from the catalytic site, the *E. coli* ATCase also contains regulatory sites, which are targets for the binding of the allosteric effectors - ATP and CTP (Lipscomb and Kantrowitz, 2012). These regulatory sites on the *E. coli* ATCase, are located approximately 60 Å from the closest active site. However, no homologs of the ATCase allosteric chain have been reported in the plasmodial genome.

## STRUCTURE OF PLASMODIUM FALCIPARUM ATCASE

PfATCase is a 43.3 kDa polypeptide with 375 amino acids. In previous studies we determined the crystal structure of truncate aspartate transcarbamoylase from *P. falciparum* (Lunev et al., 2016). Superposition of the PfATCase structure with catalytic chain of *E. coli* ATCase (PDB code: 1ZA1) and huATCase (PDB code: 5G1O) (Figures 3B–D), showed a high degree of homology

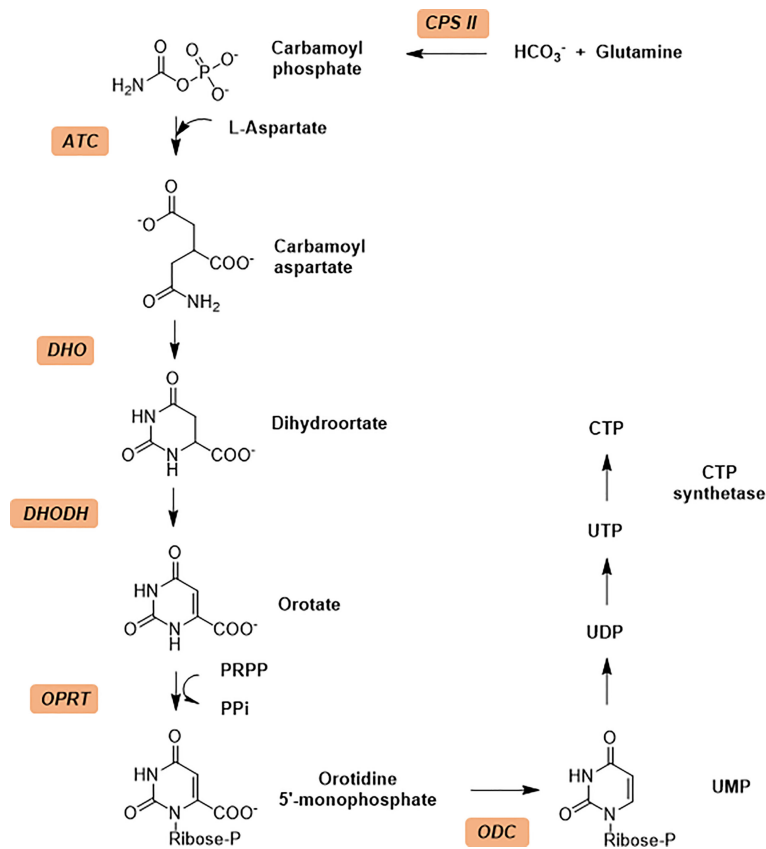


**FIGURE 1** | The *de novo* pyrimidine biosynthesis pathway. Enzymes in *de novo* pathway are italicized and colored with light orange. Enzymes: CPS II, carbamoyl phosphate synthetase II; ATCase, aspartate transcarbamoylase; DHO, dihydroorotase; DHODH, dihydroorotate dehydrogenase; OPRT, orotate phosphoribosyl transferase; ODC, orotidine 5'-monophosphate decarboxylase.

with the catalytic domain of *E. coli* ATCase and huATCase. Similarly to *E. coli* ATCase, PfATCase is a homo-trimer in which each of the three active site is formed at the oligomeric interface. Each active site comprises residues from two adjacent subunits in the trimer with a high degree of evolutionary conservation.

## THE STRUCTURAL CHANGES OF ATCASE BETWEEN T STATE AND R STATE

As reported the active site of ATCase exists in two distinct states, which are known as the T state and R state. These two states differ in substrate affinity and activity, with the T state, active site present in an open conformation with lower affinity and lower activity for substrate than the R state (Lipscomb and Kantrowitz, 2012; Ruiz-Ramos et al., 2016). We have recently elucidated several structures (Lunev et al., 2016; Lunev et al., 2018) of the plasmodial ATCase (PfATCase) which provide insight into the conformational changes present in the transition between T and R states in the plasmodial enzyme. While the parasite lacks an ATCase regulatory element, an understanding of this transition may allow for the discovery of drugs that can provide a similar

allosteric inhibition impact to that shown by the CTP feedback inhibition of the human and *E. coli* enzymes.

The structures reported by ourselves and others (Lipscomb and Kantrowitz, 2012; Lunev et al., 2016; Ruiz-Ramos et al., 2016) show that the conformation of ATCase can be induced from the T state to the R state when both aspartate and carbamoyl phosphate are present at the active site as well as *N*-phosphonacetyl-L-aspartate (PALA **Figure 2A**) – an analog of the transition state of the reaction catalyzed by ATCase. Additionally, the enzyme can also change from T state to R state by binding carbamoyl phosphate (CP) and succinate, an analog of aspartate.

## INHIBITORS AGAINST ATCASE

### N-(Phosphonacetyl)-L-Aspartate (PALA)

N-(phosphonacetyl)-L-aspartate (PALA) has been the most potent ATCase inhibitor of ATCase for the past 48 years (Swyryd et al., 1974). PALA is an analog of the transition state of reaction catalyzed by aspartate transcarbamoylase and it combines the structural features of two natural substrates

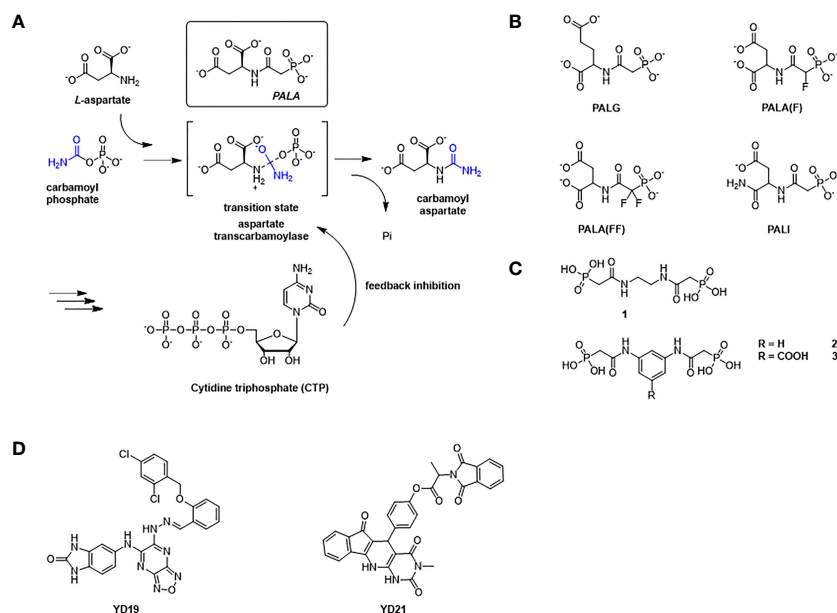


**FIGURE 2 |** The reaction catalyzed by ATCase and feedback regulation mechanism in *de novo* pyrimidine biosynthesis pathway, and inhibitors against ATCase. **(A)** Aspartate Transcarbamoylase (ATCase) combines L-aspartate and carbamoyl phosphate into carbamoyl aspartate through an enzyme stabilized transition state and inhibition feedback by CTP. The ATC inhibitor PALA closely resembles this transition state intermediate. CTP (a product of the pyrimidine biosynthesis pathway) provides feedback inhibition of ATC activity. **(B)** Structures of PALA analogues as *E. coli* ATCase inhibitors. **(C)** Structures of T-state inhibitors against *E. coli* ATCase that prevent the allosteric transition. **(D)** Structures of allosteric inhibitors of *huATCase* (Lei et al., 2020).

(Figure 2A), CP and ASP. The inhibition of PALA against ATCase is competitive with respect to carbamoyl phosphate (CP) and noncompetitive with respect to aspartate (Hoogenraad, 1974; Roberts et al., 1976). From human cell lines and patient tissue samples, PALA was found to bind around 1000 times more tightly than CP, displaying a  $K_d$  of 0.69  $\mu\text{M}$  (Moore et al., 1982; Baillon et al., 1983). Unfortunately, while PALA is a strong *in vitro* inhibitor of the *E. coli* and human ATC enzymes it is a poor inhibitor of the malarial homolog *in vitro* (Bosch et al., 2020). However, the potential exists that PALA could be developed as an active site inhibitor of the malarial ATCase, as the transition state is identical in all species.

## PALA Analogues

Inspired by success of PALA as a potent inhibitor of ATCase, several groups tried to improve the inhibition ability of PALA for ATCase (Figure 2B and Table 1). Kafarski et al. (Kafarski et al., 1985) designed a series of phosphate analogues of PALA, as well as the synthesis of other N-(phosphonoacetyl) amino phosphonic acids to evaluate their anticancer activity in human tumor cell lines. However, replacing the  $\alpha$ - or  $\beta$ -carboxylic groups in the aspartate moiety by a phosphate group resulted in the total loss of inhibition activity in human KB cell lines. In 2004, Grison et al. (Grison et al., 2004) synthesized N-phosphonoacetyl-L-glutamate (PALG), replacing the aspartate of PALA with glutamate, as the side chain of glutamate is larger than aspartate, they hypothesized that PALG would bind to the open T state and prevent the closure of the two substrate binding domains, thus stabilizing it in the

low affinity, low activity T state. The results showed that PALG failed to inhibit *E. coli* ATCase at concentration of 1 mM. Grison et al. also synthesized other analogues of PALA by introducing one [PALA (F)] or two fluorine [PALA (FF)] atoms in the  $\alpha$ -position of the phosphorus atom. Unfortunately, PALA(F) inhibited *E. coli* ATCase to only 45% at concentration of 5mM while PALA(FF) show no inhibitory activity towards *E. coli* ATCase. PALA (P) is a bisubstrate analogue, incorporating an element to mimic the leaving phosphate group, that also showed no inhibitory effect on native *E. coli* ATCase. As PALA is highly negatively charged, it is possible that it is difficult for PALA to be transported across lipid bilayers to the enzyme active site (Kempe et al., 1976). Based on this hypothesis, Eldo et al. (Eldo et al., 2006) synthesized the  $\alpha$ -amide derivative of PALA, termed PALI, which would reduce the negative charge of the analogue and at the same time enhance the its lipophilicity. The  $K_d$  of PALI against *E. coli* ATCase was 2  $\mu\text{M}$ , while PALA is reported as 0.69  $\mu\text{M}$ .

## T State ATCase Inhibitors

To generate a class of inhibitors of ATCase targeted at T state of the enzyme, Heng et al. (Heng et al., 2006) synthesized a series of compounds (Figure 2C) that were composed of two phosphonacetamide groups linked together based on co-crystal structure of *E. coli* ATCase-CP complex in its T-structure state. The X-ray structure determination of these enzyme-inhibitor complexes showed that these compounds bind to the T state, preventing the conversion of the enzyme to the R state, thereby trapping the enzyme in the low-activity, low affinity T state.



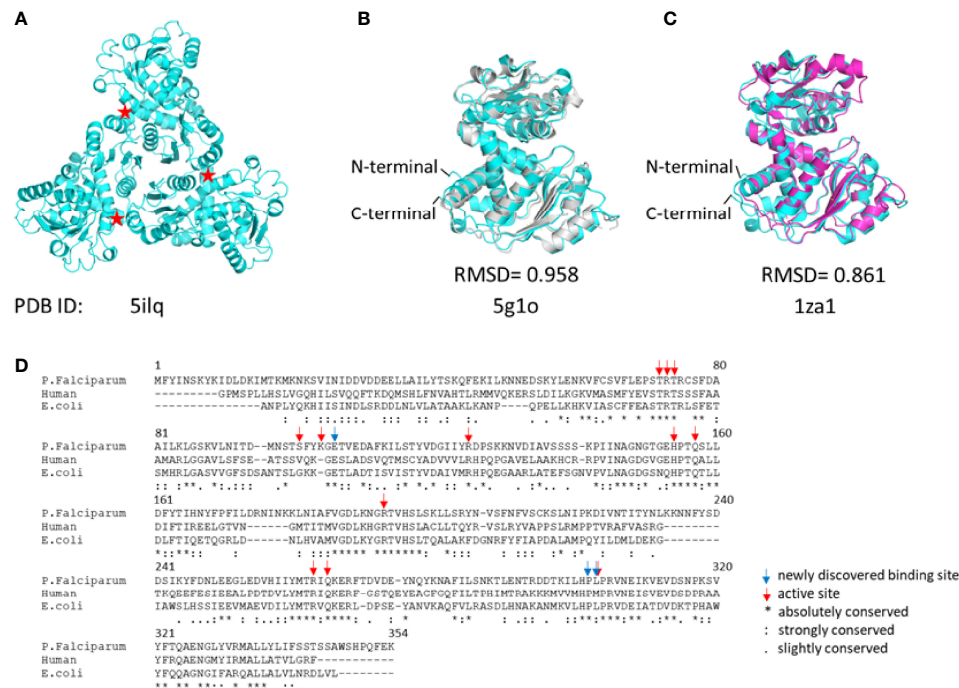


**FIGURE 3** | The structure of *Pf*ATCase compare to *hu*ATCase and catalytic subunit of *E.coli* ATCase. **(A)** A ribbon diagram of the crystal structure of the truncated *Pf*ATCase indicating an overall trimeric assembly (Lunev et al., 2016), three active sites formed at the oligomeric interfaces are labeled with stars. **(B)** structural alignment of the monomeric *Pf*ATCase structure (blue, PDB code: 5L1Q) with human ATCase (grey, PDB code: 5G1O) and the catalytic chain of *E.coli* ATCase (magenta, PDB code: 1ZA1) **(C)**. The structural alignments were carried out with Pymol (Schrodinger and DeLano, 2020). **(D)** multiple protein sequence alignment of the human, *P. falciparum* and *E. coli* ATCases using *Tcofee* (Armougom et al., 2006; Di Tommaso et al., 2011).

However, the  $K_i$  values for inhibition of ATCase with respect to CP by compounds 1, 2, 3 were 2160, 420, 250  $\mu\text{M}$ , respectively. Compound 1 is a relatively weaker inhibitor compared to compounds 2 and 3.

## Allosteric Inhibitors of Human ATCase

Recently Zhen et al. applied a computational approach to the discovery of inhibitors of the human ATCase (Lei et al., 2020). Based on a large-scale docking experiment the authors identified a series of compounds that were predicted to bind to a previously undetermined allosteric site of the human ATCase. compounds YD19 and YD21 (**Figure 2D**) showed good inhibitory effect on cancer cell lines. Xenograph results showed both YD19 and YD21 inhibited xenograft Hela tumor growth similar to 5FU, one of the most commonly used anti-cancer drugs, as a positive control. These results clearly showed the potential for the discovery of an allosteric pocket for *P. falciparum*.

## Identification of Hits for PfATCase

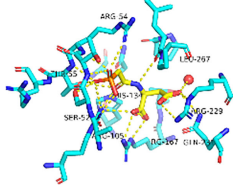
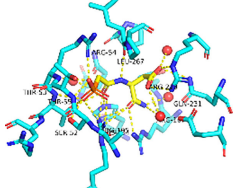
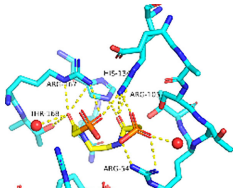
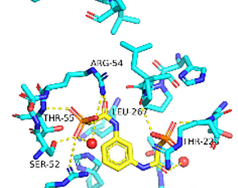
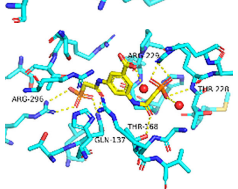
To identify the initial hits for *Pf*ATCase, we performed a Differential Scanning Fluorimetry (DSF) based screening against our in-house small fragment library (Lunev et al., 2018). 2,3-naphthalenediol showed a significant increase in the thermal stability of *Pf*ATCase, indicating it binds and stabilizes the enzyme *in vitro*. Further, we performed Microscale Thermophoresis (MST) assay to confirm hit binding ability against *Pf*ATCase,

with the dissociation constant (Kd) of binding measured as  $19.9 \pm 4.7 \mu\text{M}$ . To cross-validate 2, 3-naphthalenediol inhibitory activity against *PfATCase*, we performed an enzyme assay *in vitro*, in which 2, 3-naphthalenediol demonstrated inhibition of *PfATCase* with an  $\text{IC}_{50}$  of  $5.5 \pm 0.9 \mu\text{M}$ . The X-ray crystal structure of 2, 3-naphthalenediol in complex with *PfATCase* was solved at a resolution of  $2.0 \text{ \AA}$ . The *PfATCase*-2, 3-naphthalenediol complex crystal structure has been deposited under accession code 6FBA.

## MECHANISM OF ALLOSTERIC INHIBITION OF PFATCASE BY 2,3-NAPHTHALENEDIOL

Previously, we determined the high-resolution of X-ray crystal structure of the 2, 3-naphthalenediol-*Pf*ATCase complex (**Figure 4A**). 2, 3-naphthalenediol was identified buried in cavity between two adjacent monomers, which is close to the traditional substrates binding site (**Figure 4B**) and is accommodated in a hydrophobic region buried under the 128-142 loop. Analysis the binding site of 2, 3-naphthalenediol reveals the hydroxyl groups of 2, 3-naphthalenediol forms polar contact with the side chain of Glu140 and a water bridge with Pro333 and Leu334's carbonyl main chain oxygens (**Figure 4C**). The structural alignment of the 2, 3-naphthalenediol-*Pf*ATCase complex structure with apo-*Pf*ATCase structure did not significantly affect the structure of

**TABLE 1** | A table summarizing the ATCase inhibitors described in this review.

		Compound code	PDB ID	Activity assay	Compound structure/binding mode
ATCase inhibitors	R state inhibitors	PALA	1D09	$K_i = 27$ nM (against <i>E. coli</i> ATCase)	
		PALG	NA	$IC_{50} > 5$ mM (against <i>E. coli</i> ATCase)	NA
		PALA(F)	NA	$IC_{50} > 5$ mM (against <i>E. coli</i> ATCase)	NA
		PALA(FF)	NA	No inhibition against <i>E. coli</i> ATCase	NA
		PALI	2H3E	$K_D = 2$ $\mu$ M (against <i>E. coli</i> ATCase)	
	T state inhibitors	1	2FZC	$K_i = 2160$ $\mu$ M (against <i>E. coli</i> ATCase)	
		2	2FZG	$K_i = 420$ $\mu$ M (against <i>E. coli</i> ATCase)	
		3	2FZK	$K_i = 250$ $\mu$ M (against <i>E. coli</i> ATCase)	
	Allosteric inhibitors	YD19	NA	$K_D = 12.63$ $\mu$ M (against human ATCase)	NA
		YD21	NA	$K_D = 8.93$ $\mu$ M (against <i>E. coli</i> ATCase) $K_D = 18.08$ $\mu$ M (against human ATCase) $K_D = 14.06$ $\mu$ M (against <i>E. coli</i> ATCase)	NA

\*NA means not available.

*Pf*ATCase compared to un-ligand crystal structure. Which strongly suggests that the 2, 3-naphthalenediol-*Pf*ATCase complex (PDB ID: 6FBA) is still in T state. In addition, both the X-ray and DSF results determined that 2, 3-naphthalenediol can stabilize the *Pf*ATCase.

Furthermore, the comparison of *Pf*ATCase complexed with 2, 3-naphthalenediol, citrate-liganded crystal structures (PDB ID: 5ILN) suggest an allosteric mode of inhibition, as 2, 3-naphthalenediol binds in a cavity between adjacent subunits of the trimer. The 128-142 loop of the citrate-bound *Pf*ATCase loop showed a significant shift compared to 2, 3-naphthalenediol-bound structure (11.2 Å between the alpha-carbons of Thr134 in the two structures) (**Figure 4D**), indicating

that 2, 3-naphthalenediol could hold *Pf*ATCase in its low affinity, low activity T-state, preventing the 128-142 loop pushing the Asp domain and CP domain towards each other to form the carbamoyl aspartate and phosphate.

The superposition of the *Pf*ATCase with human ATCase and catalytic subunit of *E. coli* ATCase showed high level of sequence and secondary structure conservation (**Figures 3B–D**). *Tcoffee* (Armougom et al., 2006; Di Tommaso et al., 2011) analysis against human ATCase and the catalytic subunit of *E. coli* ATCase showed that of 12 active site residues 9 (75%) were absolutely conserved, and the residues which we found to have polar contact with 2, 3-naphthalenediol showed 2 of 3 (66.7%) are absolutely conserved.

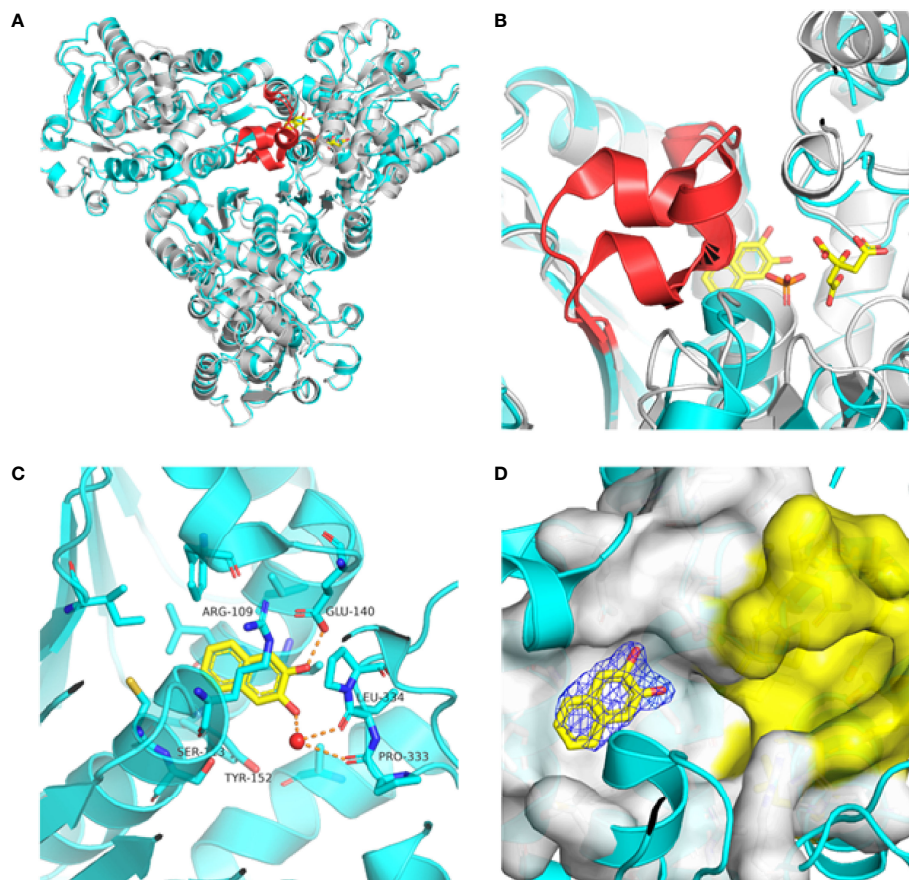


**FIGURE 4** | Crystal structure of the 2,3-naphthalenediol-PfATCase complex. **(A)** structural alignment of the 2,3-naphthalenediol-bound PfATCase [PDB ID: 6FBA; blue (Lunev et al., 2018)] with citrate-bound PfATCase [PDB ID: 5ILN; grey (Lunev et al., 2018)], RMSD=0.478 Å, providing a structural model of PfATCase in the T-state compared with the R-state. The location of the active site is shown for orientation. The conformational change in the loop128-142 in both cases is highlighted in red. **(B)** shows the structural rearrangements of 2,3-naphthalenediol binding site, the traditional active site is highlighted in yellow for orientation, 2Fo-Fc electron density of 2,3-naphthalenediol is shown in blue mesh at a contour of 1.0σ. **(C)** shows the binding site of 2,3-naphthalenediol and the polar contacts between 2,3-naphthalenediol and surrounding residues. **(D)** magnified view of the newly discovered allosteric binding site and active binding site. The structural alignments were carried out with Pymol (Schrödinger and DeLano, 2020).

## CONCLUSION

Malaria is an infectious disease that remains a clear and present threat to human health. Though several anti-malarial medications are available, the spread of multidrug-resistant severely limits their efficacy. There is pressing need for academic research to discover new targets and drugs for the treatment of severe malaria. For intracellular proliferation, *P. falciparum* requires biosynthesis of pyrimidines for parasite growth to support the production of DNA and parasite replication. ATCase supports the second step of the *de novo* biosynthesis pathway and, as the malaria parasite lacks a functional pyrimidine-import pathway, the *de novo* pyrimidine biosynthesis pathway has been demonstrated to be a major target for antimalarial drug development. While PALA has been long available as a strong ATCase inhibitor, it represents a suboptimal starting point for the development of an anti-malarial for several reasons. Firstly, PALA has been shown to be relatively poor

inhibitor of the plasmodial ATCase (Bosch et al., 2020). Secondly, while PALA is a strong *in vitro* inhibitor of canonical ATCases it appears to be limited in development towards a selective inhibitor as it is a mimic of the enzyme transition state. This transition state is likely to be absolutely conserved across species, suggesting that inhibitors of the transition state of the plasmodial homolog may show significant side effects through their inhibition of the human homologs. Finally, the transition state intermediate mimicked by PALA is by nature rather highly charged, which possibly accounts for its relatively poor performance in cell-based assays, as this high charge state is not compatible with efficient transfer across cell membranes. A situation that would be made more challenging when considering the additional membranes that must be traversed to access the parasite ATCase. A potential mechanism to address these limitations and leverage the sensitivity of the parasite to inhibition of *de novo* pyrimidine biosynthesis is to identify allosteric sites of inhibition. Such sites

would allow for more selectivity between species and would not be constrained by the limitations imposed by the heavily charged transition state. Our studies have focused on the structure of PfATCase, and identified an allosteric pocket through the determination of a co-crystal structure of PfATCase with 2,3-naphthalenediol. By comparing the crystal structure of the 2,3-naphthalenediol:ATCase complex structure as an exemplary of the low-affinity low-activity T-state with a high-affinity high activity R-state represented by the structure of PfATCase in complex with citrate, there exists the intriguing potential for the development of an allosteric inhibitor of PfATCase represented by the 2,3-naphthalenediol binding site. The further understanding of the mechanism of inhibition of 2,3-naphthalenediol would provide an opportunity for further drug development. Such a compound would strengthen the case of PfATCase as a drug target and would be an invaluable addition to the antimalarial “toolbox”.

## REFERENCES

- Armougom, F., Moretti, S., Poirot, O., Audic, S., Dumas, P., Schaeli, B., et al. (2006). Expresso: Automatic Incorporation of Structural Information in Multiple Sequence Alignments Using 3D-Coffee. *Nucleic Acids Res.* 34, W604–W608. doi: 10.1093/nar/gkl092
- Baillon, J., Guichard, M., Malaise, E. P., and Hervé, G. (1983). Kinetic Parameters of Aspartate Transcarbamylase in Human Normal and Tumoral Cell Lines. *Cancer Res.* 43, 2277–2282. doi: 0008-5472/83/0043-0000\$02.00
- Belen Cassera, M., Zhang, Y., Hazleton, K. Z., and Schramm, V. L. (2011). Purine and Pyrimidine Pathways as Targets in Plasmodium Falciparum. *Curr. Topics Med Chem.* 11, 2103–2115. doi: 10.2174/156802611796575948
- Bosch, S. S., Lunev, S., Batista, F. A., Linzke, M., Kronenberger, T., Domling, A. S., et al. (2020). Molecular Target Validation of Aspartate Transcarbamoylase From Plasmodium Falciparum by Torin 2. *ACS Infect. Dis.* 6, 986–999. doi: 10.1021/acsinfectdis.9b00411
- De Koning, H. P., Bridges, D. J., and Burchmore, R. J. (2005). Purine and Pyrimidine Transport in Pathogenic Protozoa: From Biology to Therapy. *FEMS Microbiol. Rev.* 29, 987–1020. doi: 10.1016/j.femsre.2005.03.004
- Di Tommaso, P., Moretti, S., Xenarios, I., Orobitg, M., Montanyola, A., Chang, J.-M., et al. (2011). T-Coffee: A Web Server for the Multiple Sequence Alignment of Protein and RNA Sequences Using Structural Information and Homology Extension. *Nucleic Acids Res.* 39, W13–W17. doi: 10.1093/nar/gkr245
- Downie, M. J., Kirk, K., and Mamoun, C. B. (2008). Purine Salvage Pathways in the Intraerythrocytic Malaria Parasite Plasmodium Falciparum. *Eukaryotic Cell* 7, 1231–1237. doi: 10.1128/EC.00159-08
- Eldo, J., Cardia, J. P., O'Day, E. M., Xia, J., Tsuruta, H., and Kantrowitz, E. R. (2006). N-Phosphonoacetyl-L-Isoasparagine a Potent and Specific Inhibitor of Escherichia C Oli Aspartate Transcarbamoylase. *J. Med Chem.* 49, 5932–5938. doi: 10.1021/jm0607294
- G., J. C. (1964). Subunits for Control and Catalysis in Aspartate Transcarbamylase, *Brookhaven Symposia in Biology* 17, 222–231.
- Gardner, M. J., Hall, N., Fung, E., White, O., Berriman, M., Hyman, R. W., et al. (2002). Genome Sequence of the Human Malaria Parasite Plasmodium Falciparum. *Nature* 419, 498–511. doi: 10.1038/nature01097
- Gerhart, J. C., and Schachman, H. K. (1965). Distinct Subunits for the Regulation and Catalytic Activity of Aspartate Transcarbamylase. *Biochemistry* 4, 1054–1062. doi: 10.1021/bi00882a012
- Greenwood, B. M., Fidock, D. A., Kyle, D. E., Kappe, S. H., Alonso, P. L., Collins, F. H., et al. (2008). Malaria: Progress, Perils, and Prospects for Eradication. *J. Clin. Invest.* 118, 1266–1276. doi: 10.1172/JCI33996
- Grison, C., Coutrot, P., Comoy, C., Balas, L., Jolie, S., Lavecchia, G., et al. (2004). Design, Synthesis and Activity of Bisubstrate, Transition-State Analogues and Competitive Inhibitors of Aspartate Transcarbamylase. *Eur. J. Med Chem.* 39, 333–344. doi: 10.1016/j.ejmech.2004.01.006

## AUTHOR CONTRIBUTIONS

All authors listed have made a substantial, direct, and intellectual contribution to the work, and approved it for publication.

## ACKNOWLEDGMENTS

This work was supported by the Fundação de Apoio à Pesquisa do Estado de São Paulo (FAPESP), grants 2015/26722-8 (CW) and 2018/08820-0 (AK). CW is recipient of the productivity fellowship and obtain financial support from Conselho Nacional de Desenvolvimento Científico e Tecnológico (CNPq), 301524/2019-0 and 428389/2018-0, respectively. The Universities of Groningen (RUG) and São Paulo (USP) host the international doctoral double degree programme MALAR-ASP.

- Heng, S., Stieglitz, K. A., Eldo, J., Xia, J., Cardia, J. P., and Kantrowitz, E. R. (2006). T-State Inhibitors of E. Coli Aspartate Transcarbamoylase That Prevent the Allosteric Transition. *Biochemistry* 45, 10062–10071. doi: 10.1021/bi0601095
- Hoogenraad, N. J. (1974). Reaction Mechanism of Aspartate Transcarbamylase From Mouse Spleen. *Arch. Biochem. Biophysics* 161, 76–82. doi: 10.1016/0003-9861(74)90236-7
- Hyde, J. E. (2007). Drug-Resistant Malaria— an Insight. *FEBS J.* 274, 4688–4698. doi: 10.1111/j.1742-4658.2007.05999.x
- Jones, M. E. (1980). Pyrimidine Nucleotide Biosynthesis in Animals: Genes, Enzymes, and Regulation of UMP Biosynthesis. *Annu. Rev. Biochem.* 49, 253–279. doi: 10.1146/annurev.bi.49.070180.001345
- Kafarski, P., Lejczak, B., Mastalerz, P., Dus, D., and Radzikowski, C. (1985). N-(Phosphonoacetyl) Amino Phosphonates. Phosphonate Analogs of N-(Phosphonoacetyl)-L-Aspartic Acid (PALA). *J. Med Chem.* 28, 1555–1558. doi: 10.1021/jm00149a002
- Ke, H.-M., Honzatko, R. B., and Lipscomb, W. N. (1984). Structure of Unligated Aspartate Carbamoyltransferase of Escherichia Coli at 2.6-Å Resolution. *Proc. Natl. Acad. Sci.* 81, 4037–4040. doi: 10.1073/pnas.81.13.4037
- Kempe, T. D., Swyryd, E. A., Bruist, M., and Stark, G. R. (1976). Stable Mutants of Mammalian Cells That Overproduce the First Three Enzymes of Pyrimidine Nucleotide Biosynthesis. *Cell* 9, 541–550. doi: 10.1016/0092-8674(76)90036-2
- Lei, Z., Wang, B., Lu, Z., Wang, N., Tan, H., Zheng, J., et al. (2020). New Regulatory Mechanism-Based Inhibitors of Aspartate Transcarbamoylase for Potential Anticancer Drug Development. *FEBS J.* 287, 3579–3599. doi: 10.1111/febs.15220
- Lipscomb, W. N., and Kantrowitz, E. R. (2012). Structure and Mechanisms of Escherichia Coli Aspartate Transcarbamoylase. *Accounts Chem. Res.* 45, 444–453. doi: 10.1021/ar200166p
- López, C., Saravia, C., Gomez, A., Hoebeke, J., and Patarroyo, M. A. (2010). Mechanisms of Genetically-Based Resistance to Malaria. *Gene* 467, 1–12. doi: 10.1016/j.gene.2010.07.008
- Lunev, S., Bosch, S. S., Batista, F. A., Wang, C., Li, J., Linzke, M., et al. (2018). Identification of a Non-Competitive Inhibitor of Plasmodium Falciparum Aspartate Transcarbamoylase. *Biochem. Biophys. Res. Commun.* 497, 835–842. doi: 10.1016/j.bbrc.2018.02.112
- Lunev, S., Bosch, S. S., Batista, F. D. A., Wrenger, C., and Groves, M. R. (2016). Crystal Structure of Truncated Aspartate Transcarbamoylase From Plasmodium Falciparum. *Acta Crystallographica Section F: Struct. Biol. Commun.* 72, 523–533. doi: 10.1107/S2053230X16008475
- Majori, G. (2012). Short History of Malaria and its Eradication in Italy With Short Notes on the Fight Against the Infection in the Mediterranean Basin. *Mediterranean J. Hematol. Infect. Dis.* 4(1). doi: 10.4084/MJHID.2012.016
- Moore, E. C., Friedman, J., Valdivieso, M., Plunkett, W., Marti, J. R., Russ, J., et al. (1982). Aspartate Carbamoyltransferase Activity, Drug Concentrations, and Pyrimidine Nucleotides in Tissue From Patients Treated With N-



- (Phosphonacetyl)-L-Aspartate. *Biochem. Pharmacol.* 31, 3317–3321. doi: 10.1016/0006-2952(82)90567-6
- Müller, I. B., Hyde, J. E., and Wrenger, C. (2010). Vitamin B Metabolism in *Plasmodium falciparum* as a Source of Drug Targets. *Trends Parasitol.* 26, 35–43. doi: 10.1016/j.pt.2009.10.006
- Müller, I. B., Knöckel, J., Eschbach, M. L., Bergmann, B., Walter, R. D., and Wrenger, C. (2010). Secretion of an Acid Phosphatase Provides a Possible Mechanism to Acquire Host Nutrients by *Plasmodium falciparum*. *Cell. Microbiol.* 12, 677–691. doi: 10.1111/j.1462-5822.2010.01426.x
- O'Donovan, G. A., and Neuhaud, J. (1970). Pyrimidine Metabolism in Microorganisms. *Bacteriol. Rev.* 34, 278–343. doi: 10.1128/br.34.3.278-343.1970
- Piel, F. B., Patil, A. P., Howes, R. E., Nyangiri, O. A., Gething, P. W., Williams, T. N., et al. (2010). Global Distribution of the Sickle Cell Gene and Geographical Confirmation of the Malaria Hypothesis. *Nat. Commun.* 1, 1–7. doi: 10.1038/ncomms1104
- Rathod, P. K., and Reyes, P. (1983). Orotidylate-Metabolizing Enzymes of the Human Malarial Parasite, *Plasmodium falciparum*, Differ From Host Cell Enzymes. *J. Biol. Chem.* 258, 2852–2855. doi: 10.1016/S0021-9258(18)32795-9
- Reyes, P., Rathod, P. K., Sanchez, D. J., Mrema, J. E., Rieckmann, K. H., and Heidrich, H.-G. (1982). Enzymes of Purine and Pyrimidine Metabolism From the Human Malaria Parasite, *Plasmodium falciparum*. *Mol. Biochem. Parasitol.* 5, 275–290. doi: 10.1016/0166-6851(82)90035-4
- Roberts, M., Opella, S., Schaffer, M., Phillips, H., and Stark, G. (1976). Evidence From <sup>13</sup>C NMR for Protonation of Carbamyl-P and N-(Phosphonacetyl)-L-Aspartate in the Active Site of Aspartate Transcarbamylase. *J. Biol. Chem.* 251, 5976–5985. doi: 10.1016/S0021-9258(17)33047-8
- Rodrigues, T., Lopes, F., and Moreira, R. (2010). Inhibitors of the Mitochondrial Electron Transport Chain and *De Novo* Pyrimidine Biosynthesis as Antimalarials: The Present Status. *Curr. Med. Chem.* 17, 929–956. doi: 10.2174/092986710790820660
- Ruiz-Ramos, A., Velázquez-Campoy, A., Grande-García, A., Moreno-Morcillo, M., and Ramón-Maiques, S. (2016). Structure and Functional Characterization of Human Aspartate Transcarbamoylase, the Target of the Anti-Tumoral Drug PALA. *Structure* 24, 1081–1094. doi: 10.1016/j.str.2016.05.001
- Schrödinger, L., and DeLano, W. (2020) *PyMOL*. Available at: <http://www.pymol.org/pymol>.
- Stevens, R. C., Gouaux, J. E., and Lipscomb, W. N. (1990). Structural Consequences of Effector Binding to the T State of Aspartate Carbamoyltransferase: Crystal Structures of the Unligated and ATP-And CTP-Complexed Enzymes at 2.6-Å. *ANG Resolution Biochem.* 29, 7691–7701. doi: 10.1021/bi00485a019
- Swyryd, E. A., Seaver, S. S., and Stark, G. R. (1974). N-(Phosphonacetyl)-L-Aspartate, a Potent Transition State Analog Inhibitor of Aspartate Transcarbamylase, Blocks Proliferation of Mammalian Cells in Culture. *J. Biol. Chem.* 249, 6945–6950. doi: 10.1016/S0021-9258(19)42149-2
- Vaidya, A. B., and Mather, M. W. (2009). Mitochondrial Evolution and Functions in Malaria Parasites. *Annu. Rev. Microbiol.* 63, 249–267. doi: 10.1146/annurev.micro.091208.073424
- Wang, J., Stieglitz, K. A., Cardia, J. P., and Kantrowitz, E. R. (2005). Structural Basis for Ordered Substrate Binding and Cooperativity in Aspartate Transcarbamoylase. *Proc. Natl. Acad. Sci.* 102, 8881–8886. doi: 10.1073/pnas.0503742102
- Weber, K. (1968). New Structural Model of *E. coli* Aspartate Transcarbamylase and the Amino-Acid Sequence of the Regulatory Polypeptide Chain. *Nature* 218, 1116–1119. doi: 10.1038/2181116a0
- World Health Organization (WHO). (2021). *World Malaria Report 2021* (Geneva: World Health Organization).

**Conflict of Interest:** The authors declare that the research was conducted in the absence of any commercial or financial relationships that could be construed as a potential conflict of interest.

**Publisher's Note:** All claims expressed in this article are solely those of the authors and do not necessarily represent those of their affiliated organizations, or those of the publisher, the editors and the reviewers. Any product that may be evaluated in this article, or claim that may be made by its manufacturer, is not guaranteed or endorsed by the publisher.

Copyright © 2022 Wang, Krüger, Du, Wrenger and Groves. This is an open-access article distributed under the terms of the Creative Commons Attribution License (CC BY). The use, distribution or reproduction in other forums is permitted, provided the original author(s) and the copyright owner(s) are credited and that the original publication in this journal is cited, in accordance with accepted academic practice. No use, distribution or reproduction is permitted which does not comply with these terms.



## OPEN ACCESS

## Edited by:

Leonardo Jose de Moura Carvalho,  
Oswaldo Cruz Foundation (Fiocruz),  
Brazil

## Reviewed by:

Lisa Ioannidis,  
Walter and Eliza Hall Institute of  
Medical Research, Australia  
Issiaka SOULAMA,  
Research Institute for Health Sciences  
(IRSS), Burkina Faso

## \*Correspondence:

Francis M. Ndungu  
FNdungu@kemri-wellcome.org  
Anna Färnert  
anna.farnert@ki.se  
Peter Jahnmatz  
peter.jahnmatz@ki.se

†These authors have contributed  
equally to this work

## Specialty section:

This article was submitted to  
Parasite Immunology,  
a section of the journal  
Frontiers in Immunology

Received: 21 October 2021

Accepted: 16 February 2022

Published: 09 March 2022

## Citation:

Jahnmatz P, Nyabundi D, Sundling C,  
Widman L, Mwacharo J, Musyoki J,  
Otieno E, Ahlborg N, Bejon P,  
Ndungu FM and Färnert A (2022)  
*Plasmodium falciparum*-Specific  
Memory B-Cell and Antibody  
Responses Are Associated With  
Immunity in Children Living in an  
Endemic Area of Kenya.  
Front. Immunol. 13:799306.  
doi: 10.3389/fimmu.2022.799306

# *Plasmodium falciparum*-Specific Memory B-Cell and Antibody Responses Are Associated With Immunity in Children Living in an Endemic Area of Kenya

Peter Jahnmatz<sup>1,2\*</sup>, Diana Nyabundi<sup>3</sup>, Christopher Sundling<sup>1,4</sup>, Linnea Widman<sup>5</sup>,  
Jedidah Mwacharo<sup>3</sup>, Jennifer Musyoki<sup>3</sup>, Edward Otieno<sup>3</sup>, Niklas Ahlborg<sup>2,6</sup>, Philip Bejon<sup>3</sup>,  
Francis M. Ndungu<sup>3,1,7\*†</sup> and Anna Färnert<sup>1,4\*†</sup>

<sup>1</sup> Division of Infectious Diseases, Department of Medicine Solna and Center for Molecular Medicine, Karolinska Institutet, Stockholm, Sweden, <sup>2</sup> Mabtech AB, Nacka Strand, Sweden, <sup>3</sup> KEMRI - Wellcome Research Programme/Centre for Geographical Medicine Research (Coast), Kilifi, Kenya, <sup>4</sup> Department of Infectious Diseases, Karolinska University Hospital, Stockholm, Sweden, <sup>5</sup> Division of Biostatistics, Institute of Environmental Medicine, Karolinska Institutet, Stockholm, Sweden, <sup>6</sup> Department of Molecular Biosciences, The Wenner-Gren Institute, Stockholm University, Stockholm, Sweden, <sup>7</sup> Centre for Tropical Medicine and Global Health, University of Oxford, Oxford, United Kingdom

Identifying the mechanism of naturally acquired immunity against *Plasmodium falciparum* malaria could contribute to the design of effective malaria vaccines. Using a recently developed multiplexed FluoroSpot assay, we assessed cross-sectional pre-existing memory B-cells (MBCs) and antibody responses against six well known *P. falciparum* antigens (MSP-1<sub>19</sub>, MSP-2 (3D7), MSP-2 (FC27), MSP-3, AMA-1 and CSP) and measured their associations with previous infections and time to clinical malaria in the ensuing malaria season in Kenyan children. These children were under active weekly surveillance for malaria as part of a long-term longitudinal malaria immunology cohort study, where they are recruited from birth. After performing Cox regression analysis, we found that children with a breadth of three or more antigen-specific MBC or antibody responses at the baseline had a reduced risk for malaria in the ensuing *P. falciparum* transmission season. Specifically, MBC responses against AMA-1, MSP-2 (3D7) and MSP-3, as well as antibody responses to MSP-2 (3D7) and MSP-3 were prospectively associated with a reduced risk for malaria. The magnitude or breadth of MBC responses were however not correlated with the cumulative number of malaria episodes since birth. We conclude that increased breadth for merozoite antigen-specific MBC and antibody responses is associated with protection against malaria.

**Keywords:** *P. falciparum* malaria, recombinant antigens, memory B-cells, antibodies, FluoroSpot

## INTRODUCTION

*Plasmodium falciparum* malaria is a leading cause of death in Sub-Saharan Africa, especially in children. Globally, over 241 million malaria cases and 627,000 related deaths were reported in 2020 (1, 2). Children living in high endemic areas are at particular risk of life threatening malaria before gradually acquiring immunity, which requires repeated exposure (3). The lead malaria vaccine, RTS,S, is insufficiently protective and a more effective vaccine is needed (4, 5). In order to develop such a vaccine, a better understanding of the biological processes leading to natural acquired immunity is needed.

Protection against the most severe forms of malaria is achieved more rapidly than against uncomplicated malaria, with immunity against uncomplicated malaria developing gradually after repeated parasite exposures in children living in endemic areas (6, 7). However, this clinical immunity has been shown to decline in the absence of continuous exposure, resulting in a loss of protection against re-infections (8).

Antibodies specific for different parasite antigens have been identified as important components of naturally acquired immunity (9–11), although the mechanisms of this antibody-based immunity are not completely understood. Antibodies have been found to bind to the surface antigens on the parasite, thereby blocking its invasion of hepatocytes and red blood cells, activating complement-associated lysis of merozoites, inhibiting parasite egress from schizonts, and mediating parasite opsonophagocytosis *in vitro* (12–17). Plasma levels of antibodies to various *P. falciparum* antigens have been associated with protection, and are also used to assess exposure and changing transmission patterns, in immunoepidemiological studies (18–21). However, antibody responses against *P. falciparum* antigens have been found to be short-lived (19), especially in young children living in endemic areas (22), and may also be highly transient during malaria seasons (8, 19, 23). Development of naturally acquired immunity against *P. falciparum* is further constrained by the extensive genetic diversity, including antigenic variation and polymorphisms displayed by many of the parasite antigens (24, 25).

As a complement to studies on antibody responses, increased focus has been directed towards circulating antigen-specific memory B-cells (MBCs). Although MBCs by themselves are unlikely to neutralize infectious agents, they are critical for maintaining anamnestic antibody driven immunity, whereby they rapidly proliferate and differentiate into antibody secreting cells in response to antigen re-stimulation (26). In humans, these quiescent MBCs have been shown to be located in both secondary lymphoid organs and in blood (27).

Circulating malaria specific MBCs can be long-lived even in the absence of re-exposure to parasites, whilst antibodies may decay to below detectable levels over time (28, 29). Thus, studies investigating the role of antigen-specific antibody responses in immunity could provide complementary information by including parallel analysis of antigen-specific MBCs. This has not always been possible for a majority of immunoepidemiological studies as the methods for quantifying antigen-specific MBCs are highly demanding due to the large volumes of blood required for

peripheral blood mononuclear cell (PBMC) isolation. Moreover, the methods involved have been laborious as only one antigen could be tested at a time in ELISpot assays. These limitations are especially apparent in studies involving small volumes of blood from young children in malaria endemic areas, who also happen to be the most important group to study as they are the most affected by malaria. To solve this problem, we recently developed and validated a novel reversed B-cell FluoroSpot assay with the capacity to simultaneously detect MBCs against multiple parasite antigens from the same sample in the same well (30).

Here, we have used this multiplexed FluoroSpot assay to measure the frequencies of MBCs specific for six well known *P. falciparum* antigens [merozoite surface protein 1 (19) (MSP-1<sub>19</sub>), MSP-2 (3D7), MSP-2 (FC27), MSP-3, apical membrane antigen 1 (AMA-1) and circumsporozoite protein (CSP)] in children living in an endemic region of Kenya. Circulating antibody responses to these antigens have previously been identified as possible markers of immunity against malaria (25, 31–34). We compared antigen-specific MBCs against their cognate circulating antibodies in their ability to predict immunity to malaria, as well as previous exposure.

## MATERIALS AND METHODS

### Study Area

The study cohort involved children from two regions, Junju and Ngerenya, within Kilifi County, Kenya. The regions are located within 20 km of each other and are separated by the Kilifi Indian Ocean Creek. However, they experience different levels of malaria transmission, most of which occurs during two distinct annual rainy seasons: June–August, and November–December (35). While *P. falciparum* transmission in Ngerenya had declined to extremely low levels by the time of this study, malaria transmission in Junju remained relatively stable with a prevalence of asymptomatic *P. falciparum* infections at 25–30% among children (36).

### Study Population

Children in the Ngerenya and Junju cohorts have been under active weekly surveillance for malaria since 1998 and 2005, respectively. In both cases, children are recruited at birth and remain under surveillance until their 15<sup>th</sup> birthday. The weekly visit by field workers involves testing for malaria in cases where the child is febrile. Treatment is given based on a *P. falciparum* rapid diagnostic test (RDT; CareStart™ Malaria Test, AccessBio, NJ, USA) and blood smears for microscopy. All children with RDT positive tests are treated with artemether/lumefantrine (Coartem®, Novartis, Basel, Switzerland). All positive RDT results are confirmed by microscopy. For the purpose of this study, the definition of a clinical malaria episode was set as having an axillary body temperature of  $\geq 37.5^{\circ}\text{C}$  combined with a *P. falciparum* parasite density of  $\geq 2500$  parasites per microliter of blood (37). Active surveillance is still ongoing in Junju but was discontinued in favor of passive surveillance in 2015 for Ngerenya children due to extremely low levels of malaria

transmission (38). An annual cross-sectional survey is held in March in both cohorts, where venous blood samples, anthropometric and parasitological data are collected for immunology studies. Blood samples are processed into PBMC and plasma, which are stored in liquid nitrogen and  $-80^{\circ}\text{C}$ , respectively, until use.

For this study, we used samples collected in the cross-sectional survey of March 2016 (**Figure 1**). In Junju, children (1-12 years) were still under active weekly surveillance for fever and detection of malaria parasites through home visits (compliance 94.9%, range 33.3-100%) and annual cross-sectional surveys (compliance 98.1%, range 88.7-100%). In contrast, the Ngerenya children (1-6 years) included in this study as malaria naïve controls for antigen-specific immune responses were born after the complete control of malaria in the area. We also confirmed that the Ngerenya children were all negative for asymptomatic *P. falciparum* infections by both PCR and microscopy from all the previous cross-sectional surveys, and that they had no recorded malaria episodes since birth, as determined from the passive surveillance.

## Sample Collection and Parasite Detection

In March 2016, prior to the main rainy season, 5 ml of venous blood were drawn from each child by venesection into heparinized tubes. PBMC and plasma samples were processed and stored in liquid nitrogen and  $-80^{\circ}\text{C}$ , respectively, until use. Examination for malaria parasites was performed at all annual surveys by microscopy with thick and thin blood smear stained with 10% Giemsa and 1x1000 magnification (39, 40). In addition, samples were examined for malaria parasites by *Plasmodium* species-specific real-time PCR as previously described (41).

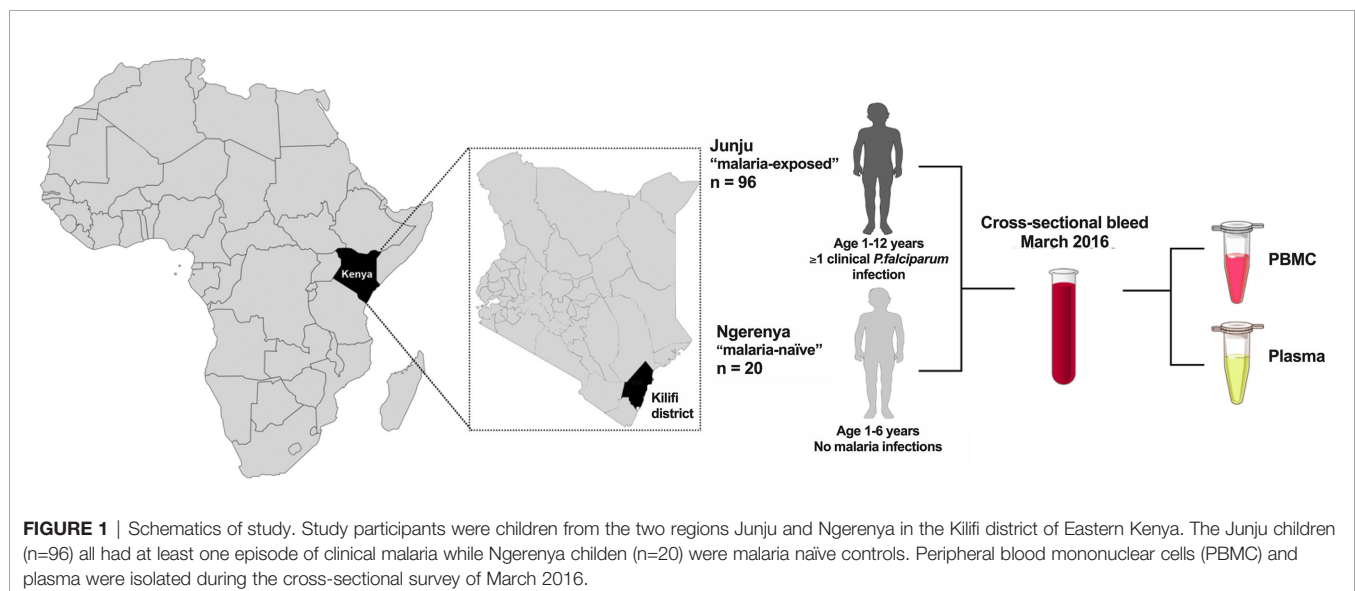
## Antigen Preparation

*P. falciparum* merozoite antigens MSP-1<sub>19</sub>, MSP-2 (3D7), MSP-2 (FC27), MSP-3 and AMA-1 were expressed recombinantly in a

mammalian expression system for use in the FluoroSpot and peptide tag ELISA assays, respectively, as described elsewhere (30). CSP was expressed, based on Uniprot accession number P19597, using the same method as the merozoite antigens. The merozoite antigens were tagged with the following peptide tags as described previously (42): MSP-1<sub>19</sub> with BAM; MSP-2 (3D7) with GAL; MSP-2 (FC27) with Twin-Strep-tag® (IBA LifeSciences, Goettingen, Germany); MSP-3 with WASP, AMA-1 with Twin-Strep-tag®; and the newly expressed CSP was tagged with the peptide tag WASP.

## Reversed B-Cell FluoroSpot Assay

The reversed B-cell FluoroSpot was multiplexed with three antigens simultaneously in two separate wells combining MSP-1<sub>19</sub>, MSP-3 and AMA-1 in one well, and MSP-2 (3D7), MSP-2 (FC27) and CSP in another (**Figure 2**). Briefly, plates (Merck Millipore, Burlington, MA, USA) were precoated with a monoclonal antibody (mAb) anti-human IgG (mAb MT91/145 from Mabtech) and blocked in culture medium. Thereafter, 250,000 cells that previously had been cultured for 5 days at  $37^{\circ}\text{C}$  and 5%  $\text{CO}_2$  in the presence of  $1\text{ }\mu\text{g/mL}$  R848 and 10 ng/ml of recombinant IL-2 (both from Mabtech), were added to the wells used for the multiplex MBC antigen-specific analysis; and 25,000 cells to wells used for MBC total IgG analysis. Cells were then cultivated in these wells for 20-24 hours in  $37^{\circ}\text{C}$  and 5%  $\text{CO}_2$ . Plates were washed, followed by addition of combinations of supernatants containing the respective tagged parasite antigens diluted in PBS and 0.1% BSA (Sigma-Aldrich, Saint Louis, MO, USA) (PBS/BSA) and incubated at room temperature (RT) for 1 hr. Irrelevant control antigens (cow-, horse-, dog- or woodchuck IFN- $\gamma$  tagged with the same peptide tags as the parasite antigens) were added in separate wells. After another wash, fluorophore-conjugated anti-tag antibodies or fluorophore-conjugated Strep-Tactin®XT (IBA LifeSciences) were added to wells and incubated for 1 hr at RT in PBS/BSA supplemented with filtered human plasma diluted 1:100. For the





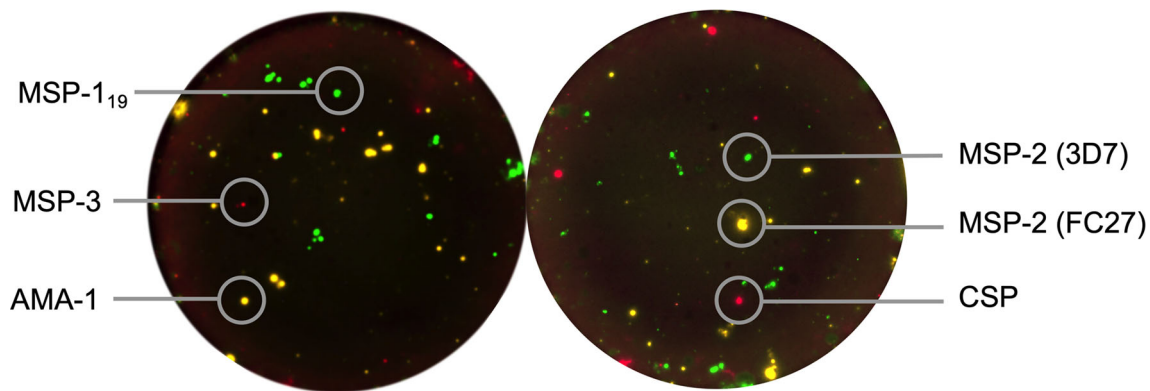


**FIGURE 2** | Reversed B-cell FluoroSpot readout with *Plasmodium falciparum* antigens. Computerized overlay of images from a FluoroSpot readout with a donor responding to all parasite antigens. To the left, green spots represent spot-forming units (SFU) from memory B cells (MBC) specific against *P. falciparum* MSP-1<sub>19</sub>, yellow; AMA-1 and red; MSP-3. To the right, green spots represent SFU from MBC specific against MSP-2 (3D7), yellow; MSP-2 (FC27) and red; CSP.

total IgG analysis, a biotinylated anti-human IgG (mAb MT78/145-biotin from Mabtech) followed by fluorescently conjugated streptavidin (SA) were added instead. After a last wash, Fluorescent enhancer (Mabtech) was added to the plates and incubated for 10 minutes at RT before plate underdrains were removed, and plates were dried in the dark at RT. The FluoroSpot plates were analysed using the Mabtech IRIS<sup>TM</sup> reader system equipped with Apex<sup>TM</sup> software version 1.1.7. Definition of assay disqualification was applied to samples with <1000 total IgG spot forming units (SFU) per 250,000 cells. Magnitudes of MBC responses were expressed as proportions of antigen-specific IgG spots per total IgG spots (%MBC/total IgG) and SFU per 10<sup>6</sup> PBMCs after subtracting reactivity to negative control antigens (i.e., the respective peptide tags used in the expression and purification of the *P. falciparum* recombinant proteins). The frequency of MBCs to the expression tag control antigen was low for all antigens (median 3, range 0–24 SFU/10<sup>6</sup> PBMCs, **Supplementary Figure 1**). Threshold for MBC positivity was then set to ≥20 SFU per 10<sup>6</sup> PBMCs corresponding to ≥5 SFU per well with 250,000 PBMCs to account for artefact spots in the assay.

### Peptide Tag-Based ELISA

Plasma samples were analysed by ELISA for detection of circulating IgG antibodies against *P. falciparum* MSP-1<sub>19</sub>, MSP-2 (3D7), MSP-2 (FC27), MSP-3, AMA-1 and CSP as well as a negative control antigen (horse IFN-γ) as previously described (30). Briefly, ELISA plates were coated with Strep-Tactin<sup>®</sup>XT (IBA LifeScience) at a concentration of 1 μg/mL in PBS and incubated overnight. The following day, additional binding sites were blocked by the addition of 100 μL of PBS supplemented with 0.1% Tween 20, 0.1% BSA (both from Sigma-Aldrich) (incubation buffer), and incubated for 1 hr at RT. Plates were then washed in PBS supplemented with 0.1% Tween 20 (Sigma) followed by addition of Twin-Strep<sup>®</sup> tagged variants of the *P. falciparum* antigen diluted 1:5 in incubation buffer. Plates were then incubated for 1 hr at RT. After another

wash, human plasma samples diluted to 1:2000 in incubation buffer was added to plates and incubated for 1 hr in RT. Plasma antibodies having bound the respective antigen were detected by addition of horse-radish peroxidase conjugated anti-human IgG mAb (Mabtech AB) at a concentration of 0.5 μg/mL followed by subsequent addition of TMB substrate to develop signal. The reaction was stopped by addition of ELISA Stop solution (Mabtech AB) and the plates were read in a Synergy HTX Absorbance reader and analysed using Gen5 software (both from Bio Tek, Winooski, VT, USA). Mean OD values are presented as antibody levels.

### Statistical Analyses

Statistical analyses were performed using STATA MP version (16.0), and GraphPad Prism (version 8.3) (GraphPad Software, La Jolla, CA). Mann-Whitney test was used to compare IgG spots (%MBC/total IgG), spot forming units (SFU)/10<sup>6</sup> PBMCs and antibody levels between two age groups (1–6 and 7–12 years old) within the children in Junju (defined as malaria-exposed) and children in Ngerenya (defined as malaria-naïve) aged 1–6 years. Spearman correlation was used to determine the association between logarithmically transformed MBC and antibody responses, as well as to determine the association of MBC and antibody responses with age, number of clinical malaria episodes since birth and parasite density at baseline in separate multivariate analysis. A Cox-regression model was used to investigate the risk of subsequent clinical malaria after baseline (date of sample collection in March 2016) until one year later, and similarly for time since last malaria episode until baseline. The models were performed by either subgrouping individuals considered positive or negative for MBC and antibody responses against an antigen or performed with number of SFU/10<sup>6</sup> PBMC. In addition, the risk analyses were also performed with the levels of MBC responses as continuous values. Proportional hazards were tested using Schoenfeld's residuals. The *p*-values below 0.05 and hazard ratio (HR) with 95% CI not crossing 1 were considered significant.

## RESULTS

### Heterogeneity in the Magnitude of MBC Responses to Different *P. falciparum* Antigens

Among the 316 children participating the Junju-cohort March 2016 cross sectional survey, 96 children, aged 1-12 years were selected for the analyses of antigen-specific antibody and MBC responses. Children in the Juju cohort were selected based on their prior exposure status: having a history of at least one clinical episode of *P. falciparum* malaria since birth. None of them had symptoms of clinical malaria either at the time, or within 15 days before and after sampling. However, 16 of the 96 (16%) children had asymptomatic *P. falciparum* infection detected by PCR at sampling. In addition, 20 children from the Ngerenya cohort, aged 1-6 years, who had no recorded malaria episode during their lifetime, or detection of asymptomatic parasites in either the current, or in any of the preceding annual surveys (since birth) were included as a malaria naïve comparison group (Table 1). Hereafter, children from Junju are referred to as “malaria-exposed” and children from Ngerenya as “malaria-naïve”.

The magnitude of the MBC responses differed between antigens and between the two comparison groups (Figure 3A). Frequencies of antigen-specific MBCs among malaria-exposed children exceeded the malaria-naïve controls for all antigens except for MSP-2 (FC27) and CSP, where these responses were at background levels. In the malaria-exposed children, median frequency of MBCs specific to MSP-1<sub>19</sub> was 4 SFU/10<sup>6</sup> PBMCs (range 0-192), median 4 (range 0-240) for MSP-2 (3D7), median 0 (range 0-96) for MSP-2 (FC27), median 4 (range 0-204) for MSP-3, median 4 (range 0-344) for AMA-1 and median 0 (range 0-28) for CSP (Figure 3A).

Cross-reactivity (i.e., co-positioned spots in the multiplex FluoroSpot assay) was not observed between the two allelic forms of MSP-2 (3D7 and FC27), when assessing spots counted using different wavelength-specific filters. Data from six malaria-exposed children were excluded from the analysis due to assay disqualification i.e., <1000 total IgG spot-forming units (SFU) per 250,000 cells in the FluoroSpot assay. Furthermore, MSP-1<sub>19</sub> and CSP MBC data from 28 children were excluded from the analysis owing to technical challenges and could not be repeated due to limitations in PBMC numbers.

### *P. falciparum*-Specific MBC and Antibody Levels Increase With Age

The proportions of malaria-exposed children qualifying as MBC positive were 19/90 (21%) for AMA-1, 17/90 (19%) for MSP-3, 13/90 (14%) for MSP-2 (3D7), 7/90 (8%) for MSP-2 (FC27), 10/62 (16%) for MSP-1<sub>19</sub>, and 3/62 (5%) for CSP. None of the responding children had MBC responses to all antigens tested, 3 children (3.3%) responded to four antigens, 9 children (10%) responded to three antigens, 7 children responded to two antigens (7.8%), 16 children (17.7%) responded to one antigen, and 55 children (61.1%) were negative to all the antigens. All the malaria-naïve children were negative against all the antigens tested.

The median frequencies of MBCs for MSP-2 (3D7), MSP-3 and AMA-1 were higher in children aged 7-12 years compared to 1-6-year old's (Mann-Whitney test  $p=0.007$ ,  $0.022$  and  $0.022$ , respectively) (Figure 3B). Similarly, frequencies of MBCs for all antigens except for CSP were positively correlated with age (Spearman correlation coefficient  $r_s$   $-0.273$   $p=0.031$  for MSP-1<sub>19</sub>,  $r_s$   $0.318$   $p=0.002$  for MSP-2 (3D7),  $r_s$   $0.298$   $p=0.004$  for MSP-2 (FC27),  $r_s$   $0.213$   $p=0.044$  for MSP-3 and  $r_s$   $0.284$   $p=0.006$  for AMA-1). Furthermore, the breadth of MBC responses was also weakly correlated with age ( $r_s$   $0.258$   $p=0.014$ ) (Table 2).

Median antibody OD levels were higher for MSP-2 (3D7) (Mann-Whitney test  $p=0.001$ ), MSP-3 (Mann-Whitney test  $p=0.006$ ) and for AMA-1 (Mann-Whitney test  $p=0.009$ ) in children aged 7-12 compared to 1-6 year old's among malaria-exposed children (Figure 3C). Antibody levels were positively correlated with age for MSP-2 (3D7) (Spearman correlation coefficient  $r_s$   $0.239$ ,  $p=0.025$ ) and MSP-3 ( $r_s$   $0.23$ ,  $p=0.031$ ) (Table 2). Breadth of antibody responses was also weakly correlated with age ( $r_s$   $0.244$ ,  $p=0.023$ ) (Table 2), and the median breadth of antibody responses was higher in children aged 7-12 years compared to 1-6 years (median 1 compared to 0.5, Mann-Whitney U-test  $p=0.011$ ) (Figure 3D).

### Correlations Between Frequencies of Antigen-Specific MBCs and Antibody Levels

Frequencies of MBCs were positively but weakly correlated with antibody levels for MSP-2 (3D7) (Spearman correlation coefficient  $r_s$   $0.221$   $p=0.038$ ), MSP-2 (FC27) ( $r_s$   $0.347$   $p \leq 0.001$ ), MSP-3 ( $r_s$   $0.274$   $p=0.09$ ) and AMA-1 ( $r_s$   $0.420$   $p \leq 0.001$ ). However, this was not the case for MSP-1<sub>19</sub>, and neither was it for CSP (Supplementary Figure 2).

TABLE 1 | Characteristics of study participants from the Junju and Ngerenya cohorts.

	Junju (malaria-exposed)	Ngerenya (malaria-naïve)
Number of children	96	20
Female, n (%)	46 (48)	8 (40)
Age, years, median (range)	6 (1-12)	4 (1-6)
<i>P. falciparum</i> parasites detected by PCR at sample collection, n (%)	16 (18)	0
Number of clinical malaria episodes since birth, median (range)	8 (1-28)	0
Days since last clinical malaria episode before sample collection, median (range)	94 (34-2764)	0 (0-0)
Participants with a clinical <i>P. falciparum</i> infection during follow up, n (%)	83 (86)	0

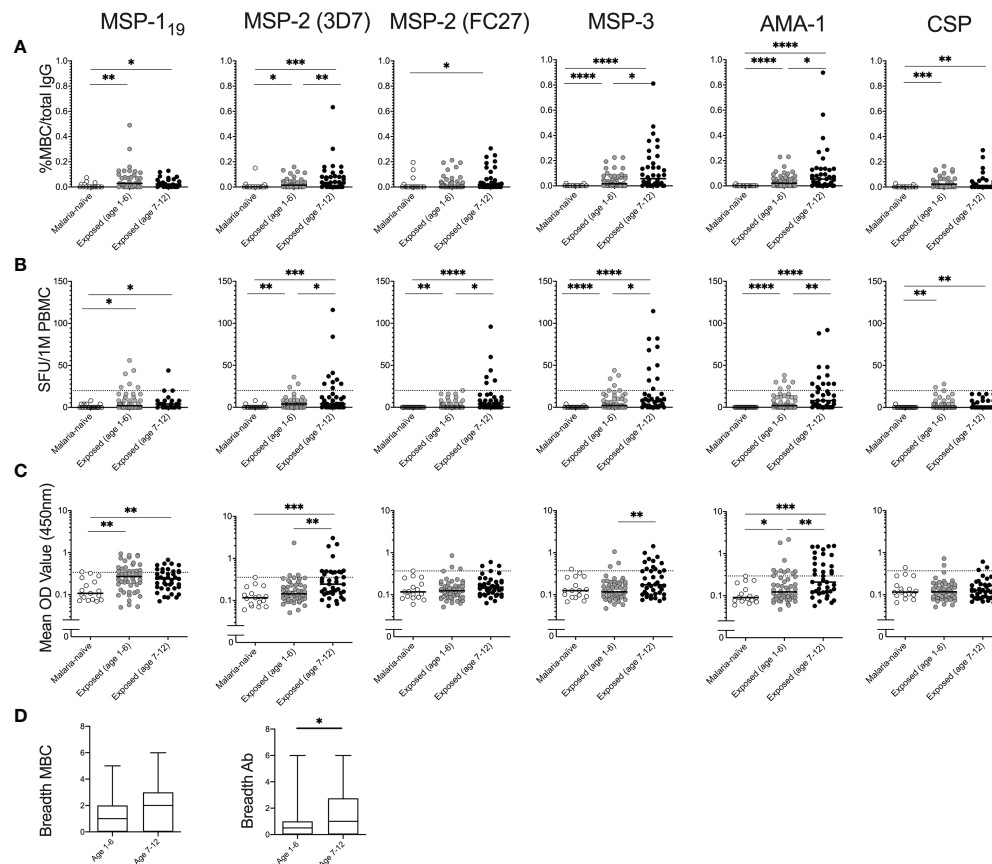


**FIGURE 3 |** Magnitude of memory B-cell (MBC) and antibody responses to *Plasmodium falciparum* antigens in children with and without history of parasite exposure. Magnitude of MBC responses to parasite antigens measured by B-cell FluoroSpot in exposed children of different age groups (Junju) as well as malaria naïve controls (Ngerenya) displayed as (A) proportion of MBC per total IgG producing cells, or (B) Spot-forming units (SFU) per million peripheral blood mononuclear cells (PBMC). Dotted line indicate threshold for positivity. (C) Antibody responses to *P. falciparum* antigens measured by ELISA. Dotted line indicate threshold for positivity. (D) Breadth of MBC and antibody responses of malaria-exposed children of different age groups as measured by FluoroSpot and ELISA respectively. The breadth of the response was defined as the number of antigens against which an individual had reactivity above threshold. Differences between groups were evaluated by Mann-Whitney test. \* $p < 0.05$ , \*\* $p < 0.01$ , \*\*\* $p < 0.001$ , \*\*\*\* $p < 0.0001$ .

## Correlation of the Breadth of MBC and Antibody Responses With Cumulative Number of Clinical Malaria Episodes Since Birth

The frequency of MBCs did not correlate with the cumulative number of clinical malaria episodes since birth for any of the antigens tested (Table 2). However, antibody levels against MSP-1<sub>19</sub> were negatively correlated with the cumulative number of clinical malaria episodes since birth ( $r_s -0.307$   $p=0.003$ ). The point estimates for antibody levels to the other antigens as well as their breadth showed a negative but non-significant correlation with the number of clinical episodes since birth (Table 2).

## Correlation of Antigen-Specific MBCs and Antibody Responses With the Time Since the Last Clinical Episode

Number of days since previous clinical episode of *P. falciparum* malaria was not correlated with the frequency of MBCs for any of

the antigens tested. However, antibody levels against AMA-1 were weakly negatively correlated with number of days since malaria episode ( $r_s -0.213$ ,  $p=0.044$ ) (Table 2). Furthermore, the number of days since last clinical malaria episode was not correlated with breadth of neither frequency of MBCs nor antibody levels (Table 2).

## Correlation of Antigen-Specific MBC and Antibody Responses With Contemporaneous Asymptomatic *P. falciparum* Parasitemia

At the time of sample collection in March 2016, 16 (17.7%) of the 90 malaria-exposed children (5 aged 1-6 years, and 11 aged 7-12 years) with MBC data had asymptomatic *P. falciparum* parasitemia detected by microscopy and PCR. Parasite positivity at baseline was positively correlated with frequencies of MBCs and levels of antibodies against MSP-2, MSP-3 and AMA-1, as well as breadth of MBC responses (Table 2). Lastly, frequencies of MBCs of parasite positive children were higher in

**TABLE 2 |** Correlation of MBC and antibody responses with age, cumulative number of clinical infections since birth and parasite positivity at sample collection.

	Age		Number of clinical <i>P.falciparum</i> episodes since birth to sample collection		Parasite positivity at sample collection		Days since last previous clinical <i>P.falciparum</i> infection	
	Coefficient	p	Coefficient	p	Coefficient	p	Coefficient	p
MBC MSP-1 <sub>19</sub>	<b>-0.273</b>	<b>0.031</b>	-0.194	0.131	-0.148	0.250	0.071	0.071
MSP-2 (3D7)	<b>0.318</b>	<b>0.002</b>	0.045	0.674	<b>0.274</b>	<b>0.009</b>	-0.126	0.235
MSP-2 (FC27)	<b>0.298</b>	<b>0.004</b>	0.043	0.688	<b>0.289</b>	<b>0.006</b>	-0.161	0.129
MSP-3	<b>0.213</b>	<b>0.044</b>	-0.125	0.239	<b>0.300</b>	<b>0.004</b>	-0.179	0.089
AMA-1	<b>0.284</b>	<b>0.006</b>	-0.064	0.550	<b>0.459</b>	<b>&lt;0.001</b>	-0.087	0.411
CSP	-0.036	0.779	0.001	0.963	0.046	0.721	-0.045	0.726
Ab MSP-1 <sub>19</sub>	-0.143	0.177	<b>-0.307</b>	<b>0.003</b>	0.027	0.796	0.001	0.993
MSP-2 (3D7)	<b>0.281</b>	<b>0.007</b>	-0.051	0.631	<b>0.342</b>	<b>&lt;0.001</b>	-0.178	0.093
MSP-2 (FC27)	0.095	0.371	-0.147	0.166	0.144	0.176	-0.04	0.722
MSP-3	<b>0.212</b>	<b>0.045</b>	-0.149	0.161	<b>0.218</b>	<b>0.038</b>	-0.092	0.382
AMA-1	<b>0.208</b>	<b>0.049</b>	-0.030	0.779	<b>0.355</b>	<b>&lt;0.001</b>	<b>-0.213</b>	<b>0.044</b>
CSP	0.043	0.688	-0.087	0.414	-0.038	0.718	0.006	0.955
Breadth <sup>a</sup> MBC	<b>0.258</b>	<b>0.014</b>	-0.074	0.488	<b>0.359</b>	<b>&lt;0.001</b>	-0.156	0.141
Ab	<b>0.248</b>	<b>0.018</b>	-0.131	0.216	<b>0.332</b>	<b>&lt;0.001</b>	-0.171	0.108
Total IgG	0.124	0.239	0.036	0.737	0.053	0.689	0.117	0.273

Spearman's correlation coefficient indicating the association with immune responses and age, number of clinical episodes of malaria, parasite positivity by PCR at baseline.

<sup>a</sup>Breadth was defined as number of antigens (0-6) an individual had above threshold (20 spot-forming units for memory B cell responses or mean reactivity of malaria-naïve children + 2 SD). Values presented in bold represent a correlation with a p value below 0.05 and thereby considered to be statistically significant.

children aged 7-12 years compared to children aged 1-6 years (Supplementary Figure 3).

### Association of Breadth and Magnitude of Baseline Antigen-Specific MBC and Antibody Responses With the Prospective Risk of Clinical Malaria

Since the MBC and antibody levels were measured from samples collected in March, towards the end of a 4-month dry season when malaria transmission is very low, we assessed the prospective risk of subsequent clinical malaria associated with MBC and antibody positivity during the ensuing malaria transmission season starting from May. Time to a clinical episode of malaria from baseline in children with and without MBC and antibody responses, respectively, is visualized in Figure 4. The risk of malaria was further assessed in Cox regression models, in the first unadjusted models, the risk of malaria was reduced for individuals that were MBC positive for MSP-2-3D7 (HR 0.18, 95% CI 0.04-0.75,  $p=0.019$ ), MSP-3 (HR 0.17, 95% CI 0.05-0.54,  $p=0.003$ ) and AMA-1 (HR 0.41, 95% CI 0.17-0.97,  $p=0.044$ ) (Table 3). Similarly, antibody positivity for MSP-2 (3D7) (HR 0.36, 95% CI 0.15-0.86,  $p=0.021$ ) and MSP-3 (HR 0.36, 95% CI 0.14-0.92,  $p=0.033$ ) were associated with a reduced risk of malaria (Table 3). After adjusting for age, the risk of malaria was reduced for individuals that were MBC positive for MSP-2 (3D7) (HR 0.17, 95% CI 0.04-0.73,  $p=0.017$ ), and MSP-3 (HR 0.15, 95% CI 0.04-0.50,  $p=0.002$ ). Also, after adjusting for parasite positivity the risk of malaria was only reduced for individuals that were MBC positive for MSP-3 (HR 0.21, 95% CI 0.06-0.69,  $p=0.01$ ). Finally, after adjusting for both age and parasite positivity, the risk of malaria was reduced for individuals that were MBC positive for MSP-2 (3D7) (HR 0.22, 95% CI 0.05-0.98,  $p=0.047$ ), and MSP-3 (HR 0.19, 95% CI 0.05-0.63,  $p=0.007$ ).

In a separate univariate analysis within age groups, point estimates for MBC positive responses indicated reduced risk of malaria in older children (7-12 years), with significant associations for MSP-3 (HR 0.08 95% CI 0.01-0.64  $p=0.017$ ) (Supplementary Table 1). In contrast, the point estimates for MBC responses against CSP were increased but not significantly in younger children (Supplementary Table 1). For antibodies, the risk of clinical episode of malaria was significantly reduced in children aged 7-12 who were antibody positive for MSP-2 (3D7) (HR 0.37 95% CI 0.11-0.99  $p=0.035$ ) and MSP-3 (HR 0.33 95% CI 0.13-0.84  $p=0.021$ ) (Supplementary Table 1). A stratified analysis of the association between risk of malaria with MBC or antibody positivity in parasite positive versus negative children could not be tested due to small sample size.

The breadth of antigen-specific MBC responses was associated with a reduced risk of malaria in children positive for 3 or more antigens in both the unadjusted analysis and after adjusting for age (Table 3, Figure 5). Similarly, when the analysis was split by age, there was a delay to the first clinical episode after baseline (HR 0.20, 95% CI 0.04-0.89,  $p=0.034$ ) for children aged 7-12 and with a breadth of MBC responses exceeding 3 antigens (Supplementary Table 1). For antibodies, a breadth of  $\geq 3$  antigens were associated with a reduced risk of subsequent malaria in all children (HR 0.20, 95% CI 0.06-0.67,  $p=0.009$ ) (Table 3) as well as children aged 7-12 years (HR 0.15, 95% CI 0.03-0.72,  $p=0.018$ ) (Supplementary Table 1).

Lastly, we repeated the above analyses with the magnitudes of MBCs (number of antigen-specific SFU per  $10^6$  PBMC) instead of MBC positivity, and the results were similar with the outcomes of the models based on MBC positivity. Similar to the Cox analysis based on MBC positivity (Table 3), magnitude of MBC responses to MSP-2 (3D7), MSP-3 and AMA-1 were associated with a reduced risk of subsequent malaria (Supplementary Table 2).



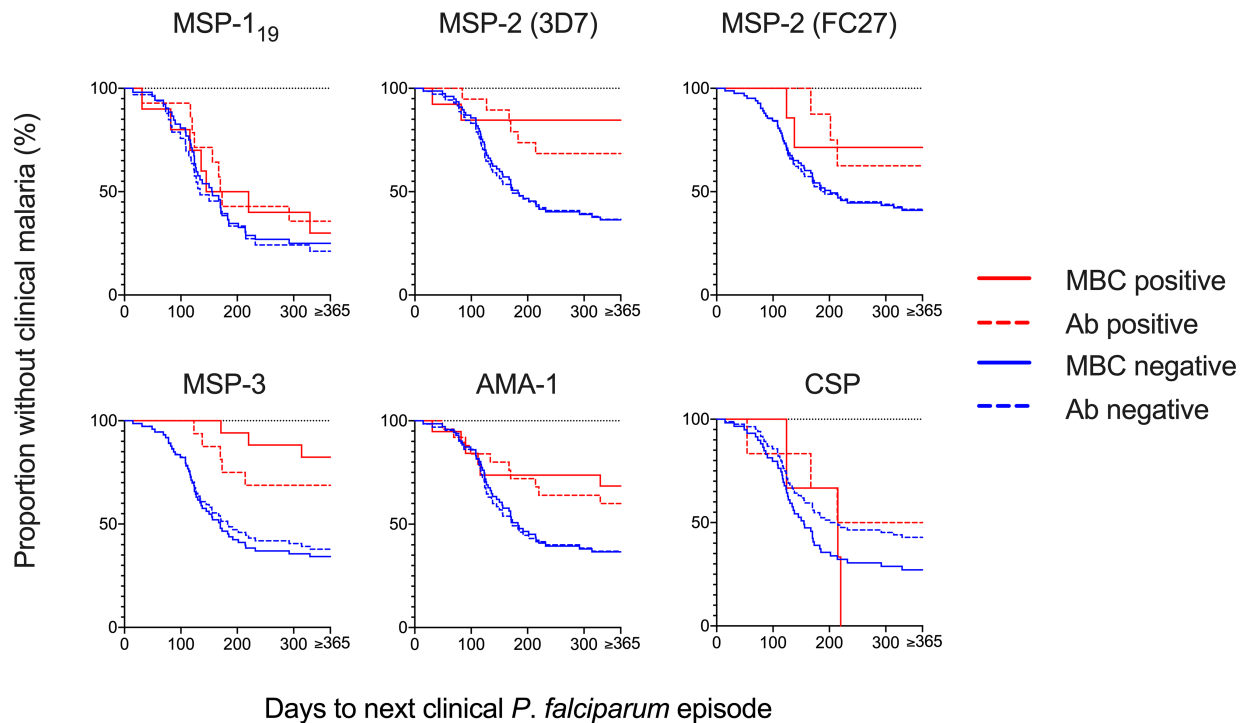


**FIGURE 4** | Risk of a clinical episode of malaria in relation to memory B-cell (MBC) and antibody positivity at baseline. The Kaplan-Meier curves present the proportion of malaria-exposed children (Junju) without a clinical episode, based on MBC positivity (solid line) and antibody positivity (dashed line) at baseline. The blue lines represent positive children and red lines the negative children, respectively. Positivity was defined as a reactivity above threshold. Unadjusted and adjusted Cox regression analyses of the risk of malaria are presented in **Table 3**.

**TABLE 3** | Memory B cell and antibody responses to *P. falciparum* antigens and risk of subsequent clinical malaria in malaria-exposed children (Junju).

Covariate	HR	95% CI	HRadj <sup>a</sup> age	95% CI	HRadj <sup>b</sup> parasites	95% CI	HRadj <sup>c</sup> age/parasite	95% CI
<b>MBC MSP-1<sub>19</sub></b>	0.83	(0.37-1.87)	0.91	(0.40-2.11)	0.75	(0.33-1.71)	0.85	(0.37-1.96)
<b>MSP-2 (3D7)</b>	<b>0.18</b>	<b>(0.04-0.75)</b>	<b>0.17</b>	<b>(0.04-0.73)</b>	0.24	(0.05-1.03)	<b>0.22</b>	<b>(0.05-0.98)</b>
<b>MSP-2 (FC27)</b>	0.38	(0.09-1.58)	0.39	(0.09-1.71)	0.46	(0.11-1.91)	0.43	(0.1-1.09)
<b>MSP-3</b>	<b>0.17</b>	<b>(0.05-0.54)</b>	<b>0.15</b>	<b>(0.04-0.50)</b>	<b>0.21</b>	<b>(0.06-0.69)</b>	<b>0.19</b>	<b>(0.05-0.63)</b>
<b>AMA-1</b>	<b>0.41</b>	<b>(0.17-0.97)</b>	0.41	(0.16-1.00)	0.63	(0.25-1.61)	0.62	(0.23-1.62)
<b>CSP</b>	1.1	(0.34-3.61)	1.21	(0.37-3.98)	1.02	(0.31-3.33)	1.13	(0.34-3.71)
<b>Ab MSP-1<sub>19</sub></b>	0.61	(0.33-1.13)	0.60	(0.32-1.11)	0.64	(0.34-1.19)	0.64	(0.34-1.19)
<b>MSP-2 (3D7)</b>	<b>0.36</b>	<b>(0.15-0.86)</b>	<b>0.36</b>	<b>(0.15-0.87)</b>	0.48	(0.19-1.16)	0.46	(0.18-1.13)
<b>MSP-2 (FC27)</b>	0.47	(0.14-1.50)	0.47	(0.15-1.50)	0.43	(0.13-1.38)	0.43	(0.13-1.38)
<b>MSP-3</b>	<b>0.36</b>	<b>(0.14-0.92)</b>	<b>0.36</b>	<b>(0.14-0.93)</b>	0.50	(0.19-1.32)	0.48	(0.17-1.29)
<b>AMA-1</b>	0.51	(0.25-1.01)	0.51	(0.24-1.05)	0.66	(0.32-1.37)	0.65	(0.31-1.37)
<b>CSP</b>	0.79	(0.24-2.55)	0.78	(0.24-2.52)	0.79	(0.24-2.54)	0.79	(0.24-2.55)
<b>MBC Breadth<sup>d</sup> 0</b>	1.00	ref	1.00	ref	1.0	ref	1.0	ref
<b>1</b>	0.58	(0.27-1.24)	0.56	(0.25-1.21)	0.57	(0.26-1.23)	0.55	(0.26-1.20)
<b>2</b>	0.47	(0.14-1.53)	0.47	(0.14-1.54)	0.55	(0.17-1.82)	0.57	(0.17-1.90)
<b>≥3</b>	<b>0.26</b>	<b>(0.08-0.86)</b>	<b>0.24</b>	<b>(0.07-0.84)</b>	0.39	(0.11-1.33)	0.34	(0.09-1.27)
<b>Ab Breadth<sup>d</sup> 0</b>	1.00	ref	1.0	ref	1.0	ref	1.0	ref
<b>1</b>	0.74	(0.44-1.23)	0.73	(0.39-1.35)	0.86	(0.46-1.06)	0.85	(0.45-1.59)
<b>2</b>	0.46	(0.17-1.19)	0.43	(0.16-1.17)	0.59	(0.22-1.58)	0.57	(0.21-1.54)
<b>≥3</b>	<b>0.20</b>	<b>(0.06-0.67)</b>	<b>0.19</b>	<b>(0.05-0.65)</b>	<b>0.26</b>	<b>(0.08-0.90)</b>	<b>0.24</b>	<b>(0.07-0.84)</b>

<sup>a</sup>Adjusted for age at sample collection.

<sup>b</sup>Adjusted for asymptomatic parasitaemia at sample collection.

<sup>c</sup>Adjusted for age at sample collection and for asymptomatic parasitaemia at sample collection.

<sup>d</sup>Breadth was defined as number of antigens (0-6) an individual had above threshold (≥20 spot-forming units for memory B cell responses or mean reactivity of malaria-naïve children + 2 SD for antibody responses).

Values presented in bold represent a hazard ratio (HR) with 95% CI not crossing 1 and a p value below 0.05 therefore considered to be statistically significant.

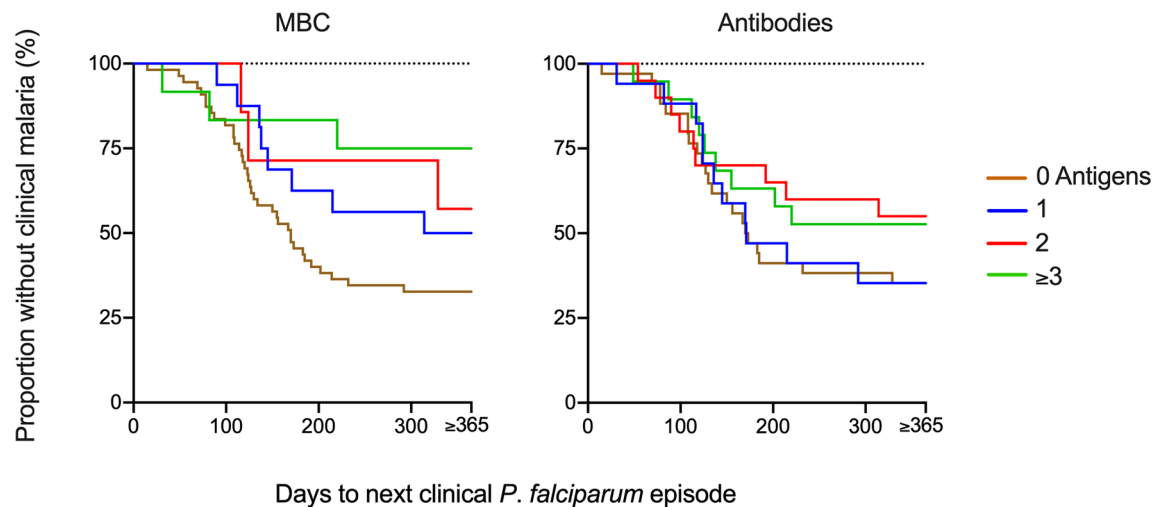


**FIGURE 5** | Risk of infection based on breadth of memory B-cell (MBC) and antibody responses at baseline. The breadth of the response was defined as the number of antigens against which a child had reactivity above threshold. The Kaplan-Meier curves present the proportion of malaria-exposed children (Junju) without clinical malaria and time to next malaria episode with regard to the breadth of MBC or antibody responses. The brown line represents a breadth of zero antigens; blue 1 antigen, red 2 antigens, and green line  $\geq 3$  antigens. Unadjusted and adjusted Cox regression analyses of the risk of malaria are presented in **Table 3** and **Supplementary Table 1**.

## DISCUSSION

We assessed MBC and antibody responses specific for six well characterized *P. falciparum* antigens with risk of malaria in children living in an endemic area in Kenya. Our results indicate that levels for some of the merozoite MBC and antibody specificities were associated with a reduced risk of malaria. However, these associations were confounded by age and parasite positivity (at sampling) individually, and sometimes by both age and asymptomatic parasitemia. Importantly, a breadth of three or more antigens for either MBCs or antibodies remained protective even after controlling for age. Similarly, MBC positivity towards MSP-2 and MSP-3 remained protective after controlling for age and parasite positivity.

While the protective role of antibodies against *P. falciparum* antigens have been rigorously investigated (9, 43–45), the potential role of circulating MBCs in immunity remain understudied. Since MBCs need approximately 5–7 days to differentiate into antibody-secreting cells, their direct role in preventing new infections is unlikely. However, MBC could modulate the outcome of new infections by reducing their ability to induce malaria symptoms or reducing disease severity by rapidly differentiating into antibody secreting cells, upon reinfection. It is also likely that MBCs provide protection indirectly by frequently proliferating and differentiating into antibody secreting cells that keep replenishing *P. falciparum* specific bone marrow resident long-lived plasma cells that could maintain circulating antibodies at protective levels (46). That older children have both higher levels of MBCs and antibodies compared with younger ones, is consistent with our observation.

We found associations between MBC positivity for AMA-1, MSP-2 and MSP-3 and antibody positivity for MSP-2 (3D7) and

MSP-3, as well as breadth of responses, with reduced risk of clinical *P. falciparum* malaria. However, some of these associations disappeared upon adjusting for age and/or asymptomatic parasitemia.

We also found that the number of antigen-specific MBCs varied between the tested antigens and was overall most pronounced for MSP-2 and MSP-3. In contrast, using the same FluoroSpot method including four antigens in adult Swedish travelers returning from the tropics with acute malaria, MBC responses were most pronounced for MSP-1<sub>19</sub> and AMA-1 (30). This demonstrates that MBC responses can vary with study settings and illustrates the importance of including multiple antigens for the analysis within the same experiments. In our previous studies in travelers, it has also been shown that Africans with a history of exposure to *P. falciparum* did not respond to reinfection with higher frequencies of antigen-specific MBCs compared with first time-infected individuals, supporting our findings that a high parasite exposure is not necessarily correlated with increased number of parasite antigen-specific MBC in circulation (29, 30).

This study had some limitations. Despite the substantial number of children for this type of study, the statistical analyses including subgroup and multivariate analyses were restricted by relatively small sample sizes. For instance, the low number of children with asymptomatic parasitemia prevented us to properly perform statistical analysis of this group.

In addition, the children from Ngerenya village, included as a malaria-naïve controls, were relatively younger than the Junju children. Furthermore, malaria exposure among the control children was determined by passive surveillance and annual cross-sectional surveys, and although we define them as malaria-naïve, we cannot completely exclude the possibility of

some limited exposure. Regarding the FluoroSpot methodology, reactivity to irrelevant tag antigens was low in general, and no cross-reactivity was detected between antigens, displaying the robustness of the assay.

In summary, we identified associations between levels and breadth of some antigen-specific MBC and antibody responses and reduced risk for malaria in children living in an endemic area. Antigen-specific MBC and antibody responses to merozoite antigens were associated with age and concurrent asymptomatic infections but not with the cumulative number of malaria episodes since birth. This would suggest that accumulated age, which would inevitably correlate with increased exposure, is more important for building the sufficient breadth for immunity compared to cumulative number of clinical episodes of malaria. Further studies will be needed to understand immunological memory in immunity to malaria.

## DATA AVAILABILITY STATEMENT

The original contributions presented in the study are included in the article/**Supplementary Material**. Further inquiries can be directed to the corresponding authors.

## ETHICS STATEMENT

The studies involving human participants were reviewed and approved by The Kenyan Medical Research Institute National Ethics Committee (KEMRI SERU Protocol, No. 3149. Written informed consent to participate in this study was provided by the participants' legal guardian/next of kin.

## REFERENCES

- World Malaria Report 2021. Geneva: World Health Organization; 2021. Licence: CC BY-NC-SA 3.0 IGO.
- Snow RW, Sartorius B, Kyalo D, Maina J, Amratia P, Mundia CW, et al. The Prevalence of Plasmodium Falciparum in Sub-Saharan Africa Since 1900. *Nature* (2017) 7677(550):515–8. doi: 10.1038/nature24059
- Crompton PD, Moebius J, Portugal S, Waisberg M, Hart G, Garver LS, et al. Malaria Immunity in Man and Mosquito: Insights Into Unsolved Mysteries of a Deadly Infectious Disease. *Annu Rev Immunol* (2014) 32:157–87. doi: 10.1146/annurev-immunol-032713-120220
- Olotu A, Fegan G, Wambua J, Nyangweso G, Leach A, Lievens M, et al. Seven-Year Efficacy of RTS,S/AS01 Malaria Vaccine Among Young African Children. *N Engl J Med* (2016) 374(26):2519–29. doi: 10.1056/NEJMoa1515257
- Rts SCTP, Agnandji ST, Lell B, Fernandes JF, Abossolo BP, Methogo BG, et al. A Phase 3 Trial of RTS,S/AS01 Malaria Vaccine in African Infants. *N Engl J Med* (2012) 367(24):2284–95. doi: 10.1056/NEJMoa1208394
- Gupta S, Snow RW, Donnelly CA, Marsh K, Newbold C. Immunity to Non-Cerebral Severe Malaria Is Acquired After One or Two Infections. *Nat Med* (1999) 5(3):340–3. doi: 10.1038/6560
- Murungi LM, Sonden K, Llewellyn D, Rono J, Guleid F, Williams AR, et al. Targets and Mechanisms Associated With Protection From Severe Plasmodium Falciparum Malaria in Kenyan Children. *Infect Immun* (2016) 84(4):950–63. doi: 10.1128/IAI.01120-15

## AUTHOR CONTRIBUTIONS

PJ designed and performed the study; analyzed and interpreted the data; and prepared the manuscript. DN assisted in sample collection, interpretation of the data, and data analysis. CS assisted in the design of the study, assisted with interpretation of data; supervised the study and revised the manuscript. LW assisted with statistical analysis of data. JMw, JMu, and EO assisted in sample collection and patient handling. NA assisted in interpretation of the data and revised the manuscript. PB assisted in the design of the study, assisted with interpretation of data and revised the manuscript. AF and FN designed the study, supervised the study implementation, analyzed the data, and revised the manuscript. All authors contributed to the article and approved the submitted version.

## FUNDING

This work was funded by The Swedish Foundation for Strategic Research (Industrial Doctoral grant ID14-0070), the Swedish Research Council (Development Research project grant 2018-04468) and Karolinska Institutet Travel Grant (2018-02525). FMN is supported by an MRC/UKRI African Research Leadership Award (MR/P020321/1), and Senior Fellowship from EDCTP (TMA2016SF).

## SUPPLEMENTARY MATERIAL

The Supplementary Material for this article can be found online at: <https://www.frontiersin.org/articles/10.3389/fimmu.2022.799306/full#supplementary-material>

- Mugenyi CK, Elliott SR, Yap XZ, Feng G, Boeuf P, Fegan G, et al. Declining Malaria Transmission Differentially Impacts the Maintenance of Humoral Immunity to Plasmodium Falciparum in Children. *J Infect Dis* (2017) 216(7):887–98. doi: 10.1093/infdis/jix370
- Osier FH, Fegan G, Polley SD, Murungi L, Verra F, Tetteh KK, et al. Breadth and Magnitude of Antibody Responses to Multiple Plasmodium Falciparum Merozoite Antigens Are Associated With Protection From Clinical Malaria. *Infect Immun* (2008) 76(5):2240–8. doi: 10.1128/IAI.01585-07
- Fowkes FJ, Richards JS, Simpson JA, Beeson JG. The Relationship Between Anti-Merozoite Antibodies and Incidence of Plasmodium Falciparum Malaria: A Systematic Review and Meta-Analysis. *PloS Med* (2010) 7(1):e1000218. doi: 10.1371/journal.pmed.1000218
- Bongfen SE, Ntsama PM, Offner S, Smith T, Felger I, Tanner M, et al. The N-Terminal Domain of Plasmodium Falciparum Circumsporozoite Protein Represents a Target of Protective Immunity. *Vaccine* (2009) 27(2):328–35. doi: 10.1016/j.vaccine.2008.09.097
- Nahrendorf W, Scholzen A, Bijker EM, Teirlinck AC, Bastiaens GJ, Schats R, et al. Memory B-Cell and Antibody Responses Induced by Plasmodium Falciparum Sporozoite Immunization. *J Infect Dis* (2014) 210(12):1981–90. doi: 10.1093/infdis/jiu354
- Weiss GE, Traore B, Kayentao K, Ongoiba A, Doumbo S, Doumtable D, et al. The Plasmodium Falciparum-Specific Human Memory B Cell Compartment Expands Gradually With Repeated Malaria Infections. *PloS Pathog* (2010) 6(5):e1000912. doi: 10.1371/journal.ppat.1000912

14. Cohen S, Mc GI, Carrington S. Gamma-Globulin and Acquired Immunity to Human Malaria. *Nature* (1961) 192(480):733–7. doi: 10.1038/192733a0
15. Boyle MJ, Reiling L, Feng G, Langer C, Osier FH, Aspelting-Jones H, et al. Human Antibodies Fix Complement to Inhibit Plasmodium Falciparum Invasion of Erythrocytes and Are Associated With Protection Against Malaria. *Immunity* (2015) 42(3):580–90. doi: 10.1016/j.immuni.2015.02.012
16. Raj DK, Nixon CP, Nixon CE, Dvorin JD, DiPetrillo CG, Pond-Tor S, et al. Antibodies to PfSEA-1 Block Parasite Egress From RBCs and Protect Against Malaria Infection. *Science* (2014) 344(6186):871–7. doi: 10.1126/science.1254417
17. Dups JN, Pepper M, Cockburn IA. Antibody and B Cell Responses to Plasmodium Sporozoites. *Front Microbiol* (2014) 5:625. doi: 10.3389/fmicb.2014.00625
18. Woehlbier U, Epp C, Hackett F, Blackman MJ, Bujard H. Antibodies Against Multiple Merozoite Surface Antigens of the Human Malaria Parasite Plasmodium Falciparum Inhibit Parasite Maturation and Red Blood Cell Invasion. *Malar J* (2010) 9(-):77. doi: 10.1186/1475-2875-9-77
19. Yman V, White MT, Asghar M, Sundling C, Sonden K, Draper SJ, et al. Antibody Responses to Merozoite Antigens After Natural Plasmodium Falciparum Infection: Kinetics and Longevity in Absence of Re-Exposure. *BMC Med* (2019) 17(1):17–22. doi: 10.1186/s12916-019-1255-3
20. Triller G, Scally SW, Costa G, Pissarev M, Kreschel C, Bosch A, et al. Natural Parasite Exposure Induces Protective Human Anti-Malarial Antibodies. *Immunity* (2017) 47(6):1197–209.e10. doi: 10.1016/j.immuni.2017.11.007
21. Hsiang MS, Hwang J, Kunene S, Drakeley C, Kandula D, Novotny J, et al. Surveillance for Malaria Elimination in Swaziland: A National Cross-Sectional Study Using Pooled PCR and Serology. *PLoS One* (2012) 7(1):e29550. doi: 10.1371/journal.pone.0029550
22. Kinyanjui SM, Conway DJ, Lanar DE, Marsh K. IgG Antibody Responses to Plasmodium Falciparum Merozoite Antigens in Kenyan Children Have a Short Half-Life. *Malaria J* (2007) 6:82. doi: 10.1186/1475-2875-6-82
23. White MT, Griffin JT, Akpogheneta O, Conway DJ, Koram KA, Riley EM, et al. Dynamics of the Antibody Response to Plasmodium Falciparum Infection in African Children. *J Infect Dis* (2014) 210(7):1115–22. doi: 10.1093/infdis/jiu219
24. Takala SL, Plowe CV. Genetic Diversity and Malaria Vaccine Design, Testing and Efficacy: Preventing and Overcoming ‘Vaccine Resistant Malaria’. *Parasite Immunol* (2009) 31(9):560–73. doi: 10.1111/j.1365-3024.2009.01138.x
25. Soulama I, Bigoga JD, Ndiaye M, Bougouma EC, Quagrainie J, Casimiro PN, et al. Genetic Diversity of Polymorphic Vaccine Candidate Antigens (Apical Membrane Antigen-1, Merozoite Surface Protein-3, and Erythrocyte Binding Antigen-175) in Plasmodium Falciparum Isolates From Western and Central Africa. *Am J Trop Med Hyg* (2011) 84(2):276–84. doi: 10.4269/ajtmh.2011.10-0365
26. Nutt SL, Hodgkin PD, Tarlinton DM, Corcoran LM. The Generation of Antibody-Secreting Plasma Cells. *Nat Rev Immunol* (2015) 15(3):160–71. doi: 10.1038/nri3795
27. Kurosaki T, Kometani K, Ise W. Memory B Cells. *Nat Rev Immunol* (2015) 15(3):149–59. doi: 10.1038/nri3802
28. Wipasa J, Suphavilai C, Okell LC, Cook J, Corran PH, Thaikla K, et al. Long-Lived Antibody and B Cell Memory Responses to the Human Malaria Parasites, Plasmodium Falciparum and Plasmodium Vivax. *PLoS Pathog* (2010) 6(2):e1000770. doi: 10.1371/journal.ppat.1000770
29. Ndungu FM, Lundblom K, Rono J, Illingworth J, Eriksson S, Farnert A. Long-Lived Plasmodium Falciparum Specific Memory B Cells in Naturally Exposed Swedish Travelers. *Eur J Immunol* (2013) 43(11):2919–29. doi: 10.1002/eji.201343630
30. Jahnmatz P, Sundling C, Yman V, Widman L, Asghar M, Sonden K, et al. Memory B-Cell Responses Against Merozoite Antigens After Acute Plasmodium Falciparum Malaria, Assessed Over One Year Using a Novel Multiplexed FluoroSpot Assay. *Front Immunol* (2021) 11:3788. doi: 10.3389/fimmu.2020.619398
31. Ferreira MU, Hartl DL. Plasmodium Falciparum: Worldwide Sequence Diversity and Evolution of the Malaria Vaccine Candidate Merozoite Surface Protein-2 (MSP-2). *Exp Parasitol* (2007) 115(1):32–40. doi: 10.1016/j.exppara.2006.05.003
32. Ayieko C, Maue AC, Jura WG, Noland GS, Ayodo G, Rochford R, et al. Changes in B Cell Populations and Merozoite Surface Protein-1-Specific Memory B Cell Responses After Prolonged Absence of Detectable P. Falciparum Infection. *PLoS One* (2013) 8(6):e67230. doi: 10.1371/journal.pone.0067230
33. Daou M, Kouriba B, Ouedraogo N, Diarra I, Arama C, Keita Y, et al. Protection of Malian Children From Clinical Malaria Is Associated With Recognition of Multiple Antigens. *Malaria J* (2015) 14:56. doi: 10.1186/s12936-015-0567-9
34. Blank A, Furler K, Jaschke A, Mikus G, Lehmann M, Husing J, et al. Immunization With Full-Length Plasmodium Falciparum Merozoite Surface Protein 1 Is Safe and Elicits Functional Cytophilic Antibodies in a Randomized First-in-Human Trial. *NPJ Vaccines* (2020) 5(1):10. doi: 10.1038/s41541-020-0160-2
35. Hay SI, Snow RW, Rogers DJ. Predicting Malaria Seasons in Kenya Using Multitemporal Meteorological Satellite Sensor Data. *Trans R Soc Trop Med Hyg* (1998) 92(1):12–20. doi: 10.1016/S0035-9203(98)90936-1
36. Walker M, Winskill P, Basanez MG, Mwangangi JM, Mbogo C, Beier JC, et al. Temporal and Micro-Spatial Heterogeneity in the Distribution of Anopheles Vectors of Malaria Along the Kenyan Coast. *Parasit Vectors* (2013) 6:311. doi: 10.1186/1756-3305-6-311
37. Bejon P, Williams TN, Liljander A, Noor AM, Wambua J, Ogada E, et al. Stable and Unstable Malaria Hotspots in Longitudinal Cohort Studies in Kenya. *PLoS Med* (2010) 7(7):e1000304. doi: 10.1371/journal.pmed.1000304
38. O'Meara WP, Mwangi TW, Williams TN, McKenzie FE, Snow RW, Donnelly CA, et al. Relationship Between Exposure, Clinical Malaria, and Age in an Area of Changing Transmission Intensity. *Am J Trop Med Hyg* (2008) 79(2):185–91. doi: 10.4269/ajtmh.2008.79.185
39. Mogeni P, Williams TN, Fegan G, Nyundo C, Bauni E, Mwai K, et al. Age, Spatial, and Temporal Variations in Hospital Admissions With Malaria in Kilifi County, Kenya: A 25-Year Longitudinal Observational Study. *PLoS Med* (2016) 13(6):e1002047. doi: 10.1371/journal.pmed.1002047
40. Njuguna P, Maitland K, Nyaguara A, Mwanga D, Mogeni P, Mturi N, et al. Observational Study: 27 Years of Severe Malaria Surveillance in Kilifi, Kenya. *BMC Med* (2019) 17(1):124. doi: 10.1186/s12916-019-1359-9
41. Rougemont M, Van Saanen M, Sahli R, Hinrikson HP, Bille J, Jatón K. Detection of Four Plasmodium Species in Blood From Humans by 18S rRNA Gene Subunit-Based and Species-Specific Real-Time PCR Assays. *J Clin Microbiol* (2004) 42(12):5636–43. doi: 10.1128/JCM.42.12.5636-5643.2004
42. Jahnmatz P, Bengtsson T, Zuber B, Farnert A, Ahlborg N. An Antigen-Specific, Four-Color, B-Cell FluoroSpot Assay Utilizing Tagged Antigens for Detection. *J Immunol Methods* (2016) 433:23–30. doi: 10.1016/j.jim.2016.02.020
43. Polley SD, Conway DJ, Cavanagh DR, McBride JS, Lowe BS, Williams TN, et al. High Levels of Serum Antibodies to Merozoite Surface Protein 2 of Plasmodium Falciparum Are Associated With Reduced Risk of Clinical Malaria in Coastal Kenya. *Vaccine* (2006) 24(19):4233–46. doi: 10.1016/j.vaccine.2005.06.030
44. Osier FHA, Murungi LM, Fegan G, Tuju J, Tetteh KK, Bull PC, et al. Allele-Specific Antibodies to Plasmodium Falciparum Merozoite Surface Protein-2 and Protection Against Clinical Malaria. *Parasite Immunol* (2010) 32(3):193–201. doi: 10.1111/j.1365-3024.2009.01178.x
45. Adamou R, Dechavanne C, Sadissou I, d'Almeida T, Bouraima A, Sonon P, et al. Plasmodium Falciparum Merozoite Surface Antigen-Specific Cytophilic IgG and Control of Malaria Infection in a Beninese Birth Cohort. *Malar J* (2019) 18(1):194. doi: 10.1186/s12936-019-2831-x
46. Portugal S, Pierce SK, Crompton PD. Young Lives Lost as B Cells Falter: What We Are Learning About Antibody Responses in Malaria. *J Immunol* (2013) 190(7):3039–46. doi: 10.4049/jimmunol.1203067

**Conflict of Interest:** PJ and NA are employed by Mabtech AB, Sweden.

The remaining authors declare that the research was conducted in the absence of any commercial or financial relationships that could be construed as a potential conflict of interest.

Several of the reagents and the FluoroSpot reader systems used in this study are produced by Mabtech. Mabtech has no influence on the content of this study or interpretation of results.

**Publisher's Note:** All claims expressed in this article are solely those of the authors and do not necessarily represent those of their affiliated organizations, or those of

the publisher, the editors and the reviewers. Any product that may be evaluated in this article, or claim that may be made by its manufacturer, is not guaranteed or endorsed by the publisher.

Copyright © 2022 Jahnmatz, Nyabundi, Sundling, Widman, Mwacharo, Musyoki, Otieno, Ahlborg, Bejon, Ndungu and Färnert. This is an open-access

article distributed under the terms of the Creative Commons Attribution License (CC BY). The use, distribution or reproduction in other forums is permitted, provided the original author(s) and the copyright owner(s) are credited and that the original publication in this journal is cited, in accordance with accepted academic practice. No use, distribution or reproduction is permitted which does not comply with these terms.





# Synthetic Red Blood Cell-Specific Glycolytic Intermediate 2,3-Diphosphoglycerate (2,3-DPG) Inhibits *Plasmodium falciparum* Development *In Vitro*

## OPEN ACCESS

### Edited by:

Abhai K. Tripathi,  
Johns Hopkins University,  
United States

### Reviewed by:

Slavica Pavlovic Djuranovic,  
Washington University in St. Louis,  
United States  
Annie Shu-Ping Yang,  
Radboud University Nijmegen Medical  
Centre, Netherlands

### \*Correspondence:

Ana Paula Arez  
aparez@ihmt.unl.pt

<sup>†</sup>These authors have contributed  
equally to this work and share  
first authorship

### Specialty section:

This article was submitted to  
Parasite and Host,  
a section of the journal  
Frontiers in Cellular and  
Infection Microbiology

**Received:** 21 December 2021

**Accepted:** 21 January 2022

**Published:** 15 March 2022

### Citation:

Morais I, Medeiros MM, Carvalho M,  
Morello J, Teixeira SM, Maciel S,  
Nhantumbo J, Balau A, Rosa MTG,  
Nogueira F, Rodrigues JA,  
Carvalho FA, Antunes AMM and  
Arez AP (2022) Synthetic Red Blood  
Cell-Specific Glycolytic Intermediate  
2,3-Diphosphoglycerate (2,3-DPG)  
Inhibits *Plasmodium falciparum*  
Development *In Vitro*.  
Front. Cell. Infect. Microbiol. 12:840968.  
doi: 10.3389/fcimb.2022.840968

Inês Morais<sup>1†</sup>, Márcia M. Medeiros<sup>1†</sup>, Maria Carvalho<sup>1†</sup>, Judit Morello<sup>2</sup>, Sara M. Teixeira<sup>3</sup>, Suelma Maciel<sup>1</sup>, Janice Nhantumbo<sup>1</sup>, Ana Balau<sup>1</sup>, Margarida T. G. Rosa<sup>1</sup>, Fátima Nogueira<sup>1</sup>, João Alexandre Rodrigues<sup>4</sup>, Filomena A. Carvalho<sup>5</sup>, Alexandra M. M. Antunes<sup>3</sup> and Ana Paula Arez<sup>1\*</sup>

<sup>1</sup> Global Health and Tropical Medicine (GHTM), Instituto de Higiene e Medicina Tropical (IHMT), Universidade NOVA de Lisboa (UNL), Lisbon, Portugal, <sup>2</sup> CEDOC, NOVA Medical School, Universidade NOVA de Lisboa, Lisbon, Portugal,

<sup>3</sup> Centro de Química Estrutural, Instituto Superior Técnico, Universidade de Lisboa, Lisbon, Portugal, <sup>4</sup> Clarify Analytical, Évora, Portugal, <sup>5</sup> Instituto de Medicina Molecular, Faculdade de Medicina, Universidade de Lisboa, Lisbon, Portugal

Mechanisms of malaria parasite interaction with its host red blood cell may provide potential targets for new antimalarial approaches. Pyruvate kinase deficiency has been associated with resistance to malaria in both experimental models and population studies. Two of the major pyruvate kinase deficient-cell disorders are the decrease in ATP and the increase in 2,3-biphosphoglycerate (2,3-BPG) concentration. High levels of this metabolite, only present in mammalian red blood cell, has an inhibitory effect on glycolysis and we hypothesized that its accumulation may also be harmful to the parasite and be involved in the mechanism of protection provided by that enzymopathy. We examined the effect of a synthetic form, 2,3-DPG, on the *Plasmodium falciparum* intraerythrocytic developmental cycle *in vitro*. Results showed an impairment of parasite growth with a direct effect on parasite maturation as significant lower progeny emerged from parasites that were submitted to 2,3-DPG. Further, adding the compound to the culture medium did not result in any effect on the host cell, but instead the metabolic profile of an infected cell became closer to that of a non-infected cell.

**Keywords:** malaria, host-parasite interactions, red blood cell, 2,3-BPG, 2,3-DPG, glycolysis, pyruvate kinase deficiency

## 1 INTRODUCTION

Nowadays, together with COVID-19, malaria is a major public and global health problem, which accounted for 241 million cases and 627 000 deaths in 2020 (World Health Organization, 2021). A significant progress has been made in reducing the malaria burden but a stagnation in the reduction rate has been observed in most recent years in the most historically high-burden malaria countries. Further, this effect is now intensified by a high risk of 19 000 additional deaths in sub-Saharan Africa

due to disruptions of national control programs associated with COVID-19 pandemics (World Health Organization, 2020).

Malaria has been one of the strongest selective forces on the human genome, selecting host variants and cellular mechanisms that are determinant for parasite survival, influence pathogenesis and may protect against infection or disease severity (Kariuki and Williams, 2020). The understanding of these mechanisms of parasite dependency on host factors mainly related to the red blood cell (RBC), as well as differences between the biochemistry of host and parasite metabolic pathways may provide potential targets for new approaches.

Pyruvate kinase deficiency (PKD), the most frequent inherited abnormality in RBC glycolysis, is caused by loss-of-function mutations in the *pkfr* gene leading to hemolytic anemia. PKD was associated with resistance to malaria (Min-Oo et al., 2003; Laroque et al., 2017) and babesiosis (Oka et al., 2008) in rodent models and in *in vitro* cultures of *P. falciparum* using human PK-deficient RBC (Ayi et al., 2008; Durand and Coetzer, 2008). This association has been corroborated by population studies (Alves et al., 2010; Machado et al., 2010; Machado et al., 2012). Ayi et al. (2008) suggested that the protective mechanism provided by this erythrocyte enzymopathy may involve a reduction of RBC invasion in case of homozygous subjects and a higher macrophage clearance of ring stage infected RBCs for both heterozygous and homozygous individuals. However, the precise biological and biochemical mechanisms underlying the putative protection of PKD are still unknown.

Pyruvate kinase (PK) catalyzes the conversion of phosphoenolpyruvate to pyruvate, transferring the phosphate group from phosphoenolpyruvate to an ADP molecule producing ATP. Three major cell abnormalities due to PKD are the decrease in ATP and pyruvate production and an increase in 2,3-biphosphoglycerate (2,3-BPG) concentration (Wijk and van Solinge, 2005).

2,3-BPG, the master allosteric regulator of oxygen affinity to hemoglobin, is synthesized on the Rapoport-Luebering shunt, only present in mammalian RBC, by the multifunctional enzyme biphosphoglycerate mutase (BPGM). The increase in 2,3-BPG synthesis found in PKD results in the decrease in ATP synthesis, since an higher activity of the Rapoport-Luebering shunt bypasses the synthesis of ATP catalyzed by phosphoglycerate kinase (PGK) (Wijk and van Solinge, 2005). Also, 2,3-BPG is linked to the conversion of NADH to NAD<sup>+</sup> by glyceraldehyde-3-phosphate dehydrogenase and in high levels has an inhibitory effect on the glycolytic pathway upstream, precisely the phosphorylation of glucose by hexokinase (Min-Oo and Gros, 2005), and on another metabolic pathway, the pentose phosphate shunt (PPP) (Tomoda et al., 1983).

The metabolic derangements resulting from low intracellular ATP and pyruvate levels lead to the dysfunction of Na<sup>+</sup>/K<sup>+</sup> pump in RBC membrane, inability to maintain the electrochemical gradient and membrane integrity, and inefficient methemoglobin reduction. The failure on restoring two molecules of NAD<sup>+</sup> upstream, and accumulation of 2,3-BPG may create an unsuitable intracellular environment for parasite development and may be involved in the mechanism of

protection against *Plasmodium* infection. Ayi et al. (2009) mimicked ATP depletion phenotype of PKD targeting the RBC enolase, a glycolytic enzyme upstream to PK step, and achieved protection against RBC invasion by *P. falciparum* *in vitro*. However, a potential role for 2,3-BPG in that protection, which potentially also had increased due to enolase inhibition, was not addressed, and remains unsolved. Further, *Plasmodium falciparum* does not possess BPGM and does not synthesize 2,3-BPG, thus we conjecture that not only this metabolite does not play a role in parasite survival, but on the contrary, it may even be harmful to it.

Here, we examined the effect of 2,3-BPG on the *P. falciparum* intraerythrocytic developmental cycle. To this end, we used 2,3 diphosphoglycerate (2,3-DPG), a synthetic form of 2,3-BPG, used in hematology and transfusion medicine as a reference compound in analysis of RBC glycolytic cycle metabolites, to test whether concentrations of 2,3-BPG above the physiological range inhibits *P. falciparum* development *in vitro*. Next, we compared the inhibitory effect of 2,3-DPG with that of ATP depletion with an enolase inhibitor (sodium fluoride, NaF), which has been previously used to emulate PKD *in vitro*. Finally, we compared the metabolic profiles of infected and non-infected RBCs treated versus not treated with 2,3-DPG.

## 2 MATERIALS AND METHODS

### 2.1 Blood Donors

Healthy RBCs (type 0) were obtained from adult volunteer donors. Total venous blood was collected into EDTA tubes and immediately washed four times with PBS pH 7.0 to remove plasma and buffy coat. RBCs were left at 50% hematocrit in complete RPMI culture medium [cRPMI, (1.044% (w/v) RPMI 1640 medium (RPMI) (Biowest) supplemented with 0.59% (w/v) HEPES (Sigma-Aldrich), 0.005% (w/v) hypoxanthine (Sigma-Aldrich), 0.5% (w/v) AlbuMAXII (Gibco, Thermo Fisher Scientific) and 0.2% (w/v) of sodium bicarbonate (Merck), buffered to pH 7.0 to 7.2] and stored at 4°C no longer than three weeks to assure no major changes of ATP and 2,3-BPG levels (Capps and Jensen, 1983).

To rule out blood variants that could bias the effect on parasite growth, an aliquot of whole blood was used to perform molecular diagnosis of the most common polymorphisms in Portugal of HBB [A>T mutation on codon 6, exon 1, chr 11 (Waterfall and Cobb, 2001)], *pkfr* [1456C>T mutation on exon 11, chr 1 (Manco and Abade, 2001)] and *g6pd* [Med mutation, 563C>T mutation on exon 6, chr X, (Tishkoff et al., 2001)] genes.

### 2.2 *Plasmodium falciparum* In Vitro Cultures

Chloroquine (CQ)-sensitive 3D7 *P. falciparum* parasites (BEI Resources MRA-102) were cultivated at standard conditions (5% hematocrit, at 37°C in wet atmosphere with 5% CO<sub>2</sub>), with daily cRPMI changes according to an adapted protocol from the one developed by Trager and Jensen (1976). Parasite growth was

monitored daily by estimating parasite density (percentage of infected-RBCs/total RBCs) in 20% Giemsa-stained (Giemsa's azur-eosin-methylene blue, Sigma-Aldrich) thin blood smears.

## 2.3 Effect of High Concentrations of 2,3-DPG on Human Cells

According to the oxygen-hemoglobin dissociation curve (Bohr's effect), that describes the shift in the oxygen dissociation curve to hemoglobin due to changes in the concentration of carbon dioxide, environmental pH and 2,3-BPG concentrations (Hamilton et al., 2004), the physiological concentration range of 2,3-BPG in healthy RBCs varies between 3.6 and 5mM and may increase until 8mM at high altitudes. Based on this range, prior to assays with parasites we tested the potential toxicity for the human cells, of concentrations of synthetic 2,3-Diphospho-D-glyceric acid pentasodium salt (2,3-DPG, Sigma-Aldrich) above the physiological range of the endogenous metabolite. Healthy RBCs and human hepatocellular carcinoma cells [HEPG2 cells (ATCC® HB-8065™)] were used.

### 2.3.1 Red Blood Cells

RBCs were incubated in triplicate in a 96 well U-bottom microplate for 0, 30, 60 and 90 minutes with 2,3-DPG in 0.9% NaCl according to a two-fold serial dilution (ranging from 16 to 0.25mM), following an adapted protocol from de Freitas et al. (2008) and Evans et al. (2013). To exclude possible confounders due to 2,3-DPG addition such as increase in sodium concentration or changes in pH value, solutions of 1.36% and 0.9% (w/v) NaCl (corresponding to sodium concentrations found in the final concentrations of 16mM and 0.25mM 2,3-DPG solutions, respectively), and solutions of 0.9% NaCl in 0.05M Tris Buffer Saline (TBS) (pH 6.5 and 8.5, corresponding to the pH of the 16mM and 0.25mM solutions, respectively) were used as negative controls. A 20% of Triton X-100 solution in 0.9% NaCl was used as a positive control for RBC lysis. After centrifugation, supernatant was recovered, and absorbance (Abs) was measured at a 450nm wavelength in a luminometer plate reader (Triad TM Series Multimode Detector Dynex Technologies). The percentage of hemolysis was calculated as follows: % Hemolysis = (Sample Abs - Negative Control Abs) / (Positive Control Abs - Negative Control Abs) × 100.

### 2.3.2 HEPG2 Cells

HEPG2 cells were cultivated in T75 culture flasks in cell culture medium [RPMI 1640 medium + GlutaMAX™ (Gibco)], supplemented with 10% (v/v) fetal bovine serum (Sigma-Aldrich) and 1% (v/v) Penicillin/Streptomycin (Sigma-Aldrich) until reaching a confluence of ≥ 75%. After that, HEPG2 cells were detached by trypsinization using Trypsin (Sigma-Aldrich) and Hank's Balanced Salt solution (HBSS without Ca<sup>2+</sup>, Mg<sup>2+</sup>, Sigma-Aldrich), according to manufacturer's orientations. Then, 1 × 10<sup>5</sup> cells/well were incubated in triplicate in a 96 well flat-bottom microplate with the two-fold serial dilution of 2,3-DPG previously described added to the cell culture medium, for 48 hours. Untreated HEPG2 cells were used as negative controls. Cell viability was assessed after addition of 3-(4,5-Dimethyl-2-thiazolyl)-2,5-diphenyl-2H-tetrazolium bromide, MTT,

Methylthiazolyl-diphenyl-tetrazolium bromide (M2128 Sigma-Aldrich), following the protocol described in Santos et al. (2015). MTT in culture medium was also added in triplicate to cell-free wells (blank). Absorbance was measured at a 595nm wavelength in the same luminometer plate reader as above. The percentage of cell viability in relation to untreated cells were calculated as follows: % Cell Viability = [(Sample Abs - Blank Abs) / (Control Abs - Blank Abs)] × 100. Absorbance greater than the control indicates cell proliferation and absorbance below the control indicates cell death or inhibition of proliferation. A dose-response analysis was performed to determine the half maximal inhibitory concentration (IC<sub>50</sub>) of 2,3-DPG against HEPG2 cells in three independent experiments.

## 2.4 Effect of High Concentrations of 2,3-DPG on Malaria Parasite Development

### 2.4.1 Dose Response Analysis

Prior to all assays, parasite cultures were synchronized by sorbitol treatment with a 5% (w/v) D-sorbitol solution (Sigma-Aldrich) (Radfar et al., 2009) to increase the proportion of ring stages up to 12 hours after invasion.

Based on the physiological range of 2,3-BPG concentration in RBCs, a dose-response analysis was performed to determine the half maximal inhibitory concentration (IC<sub>50</sub>) of 2,3-DPG against 3D7 *P. falciparum* parasite. Solutions of 2,3-DPG 1.33M were prepared in ultrapure water, from which intermediate dilutions were done with cRPMI. RBCs *ex-vivo* infected initially with synchronized parasite forms at ring stage were put in triplicate in a 96-well flat-bottom microplate culture with cRPMI adjusted to 3% hematocrit and 1% parasite density (at hour 0) in the presence of the two-fold serial dilution of 2,3-DPG (16 – 0.25mM). Infected RBCs incubated without the compound were used as control. SYBR Green (Thermo Fisher Scientific) (0.001% v/v in PBS) was added to each well prepared for each time point (12, 24, 36, 48, 60, 72, 84 and 96 hours of incubation), and plates were incubated again for 1 hour under standard culture conditions. After centrifugation, supernatant was discarded, and cells were resuspended in 1× PBS. Fluorescence (Relative Fluorescence Units, RFU) was measured on the fluorimeter plate reader (excitation 485nm and emission 535nm). IC<sub>50</sub> was determined by plotting parasite density against RFU and analyzed by nonlinear regression (log [inhibitor] vs normalized response) using GraphPad Prism version 8 for Windows (GraphPad Software) (Machado et al., 2016).

### 2.4.2 Antimalarial Activity of 2,3-DPG

Three biological replicates of synchronized *P. falciparum* cultures maintained as described above, were allowed to grow for one cycle (48h) under daily changed culture media with or without the addition of 2,3-DPG at 8mM (at 0h and 24h). Thin blood smears were daily made to monitor the progress of parasite density (the experiment was repeated three times in a total of eighteen cultures).

Further, during the assays, thin blood smears were daily made to monitor the progress of cultures submitted to different conditions and each blood smear was observed by light



microscopy for mature schizonts (at segmented stage), in which it was possible to clearly count the number of resulting merozoites from nuclear division. In total, 10 microscopy fields with approximately 200 cells each in each of 6 smears, from infected treated and untreated RBCs, were blindly examined by two researchers.

### 2.4.3 Invasion and Maturation Assay and Measurement of ATP Content

To test the effect of 2,3-DPG supplementation on invasion and maturation capacity of the parasite, we kept synchronized cultures with 0.5% of schizont density in 5% hematocrit under standard conditions for two growth cycles (96h). Giemsa-stained thin blood smears were daily prepared to determine the densities of early parasite forms (ring) and of mature parasite forms (late trophozoite plus schizont). RBCs invasion and parasite development inside RBCs, i.e. maturation, were assessed at 24 and 72 hours, and at 48 and 96 hours, respectively.

To exclude a possible 2,3-DPG confounder effect on parasite invasion and/or maturation, such as primary 2,3-DPG effect on RBC ATP content, RBCs were incubated with 8mM 2,3-DPG for 24 hours and then put on *in vitro* culture conditions. ATP content and invasion and maturation levels were compared with the daily addition of 2,3-DPG to culture medium of infected and non-infected RBCs (iRBC and niRBC, respectively).

The ATP depleted phenotype of PKD was induced by blocking RBC glycolytic enzyme enolase (Zerez and Tanaka, 1987), through the treatment of RBCs for 24 hours with two different concentrations (4mM and 8mM in cRPMI) of sodium fluoride (NaF), similar to the described by Ayi et al. (2009). RBCs were incubated with NaF for 24 hours, then washed and put in newly prepared cRPMI and ATP level was daily measured, for 96 hours. The maintenance of PKD phenotype for 96 hours after NaF withdrawal was confirmed in a previous experiment, by daily ATP level measurements, using the ATP cell viability luciferase assay kit (Sigma-Aldrich), according to manufacturer's orientation (data not shown). The amount of light emitted was measured as previously described and ATP (pmol) was quantified through a linear regression calibration equation performed with known ATP concentrations. Since the amount of ATP depleted with 2mM and 4mM NaF was slightly lower than that described by Ayi et al. (2009), we chose to work with 4mM and 8mM NaF. Incubation occurred before infection to assure no effect on parasite enolase (Pal Bhowmick et al., 2009).

In summary, five experimental groups were simultaneously analyzed in the invasion/maturation assay: 1) RBCs incubated for 24 hours with 2,3-DPG 8mM prior to infection and then, put in culture conditions (iRBC DPGt), 2) infected RBCs incubated with 2,3-DPG 8mM added every 24 hours to culture medium after infection (iRBC DPGadd), 3) and 4) two different infected NaF-inducible PKD RBCs described above (iRBC NaF4 and iRBC NaF8 respectively), and 5) a control group with infected RBCs in cRPMI alone (iRBC C).

ATP depletion inside RBCs due to 2,3-DPG and NaF treatment was assessed by ATP level measurements in the five experimental groups and respective non-infected controls added

for each condition (niRBC DPGt, niRBCadd, niRBC NaF4, niRBC NaF8 and niRBC C). Measures were done at the time-points conventionally named -24h (at the end of non-infected RBC incubation with NaF, 2,3-DPG or cRPMI alone for 24h), -10h (removal of compounds by washing with cRPMI), at 0h (onset of invasion and maturation assays) and every 24 hours afterwards for 96 hours. Measurements were done using the same kit as above and performed in triplicate, both in infected-RBCs and in paired control non-infected RBCs, kept exactly under the same conditions as described above.

### 2.4.4 Egress Assay

An egress assay was designed to evaluate the effect of 2,3-DPG on the parasite ability to egress from an infected and 2,3-DPG treated RBC and start a new cycle by reinvasion untreated RBCs.

Initial ring-stage synchronized *P. falciparum* cultures were allowed to grow for a full cycle, being then divided into four new cultures with a 5% hematocrit and 1% ring stage parasites. 2,3-DPG 8mM was added to the culture medium of two of these experimental groups and all four were incubated at standard conditions with daily media change. At approximately 44 hours of the parasite life cycle, schizonts from one culture treated with 2,3-DPG and from an untreated one were recovered through magnetic separation using LD columns attached to a QuadroMACS separator (Miltenyi Biotec), while other two cultures were allowed to grow under normal conditions. After magnetic separation, at approximately 48 hours (mature schizonts stage), three similar 96 well flat-bottom microplates were then prepared as follows: 1) 100µL triplicates of recovered schizonts from the two enriched cultures were added to untreated RBCs (niRBCs C) to a final 3% hematocrit and 1% schizont density and 2) 100µL triplicates from non-enriched cultures were cultivated at the same 3% hematocrit.

Plates were incubated for parasite reinvasion at standard conditions and parasite densities were read by flow cytometry (Cytoflex, Beckman Coulter) at approximately 48 hours of the current parasite life cycle and then at 1.5, 3, and 24 hours of the following cycle, i.e., after invasion. For each plate reading, after incubation, SYBR Green solution (0.001% v/v in PBS) as described above was added to each cell. The plate was incubated again for 45 minutes in standard conditions, centrifuged the supernatant was discarded, and the cells were resuspended in 100µL of 1X PBS. Hematocrits were diluted to 0.3% in new wells. Three independent assays were performed. Approximately 100,000 RBCs were analyzed, and parasite density was calculated using FlowJo V10 software (Tree Star Inc.).

## 2.5 Untargeted Metabolomics Analysis

Synchronized *P. falciparum* cultures at ring-stage forms of 12 hours post-invasion and cultures of non-infected RBCs submitted to the same synchronization procedure using 5% sorbitol, as described above were cultivated in cRPMI supplemented or not with 2,3-DPG 8mM for 30 hours. Four biological replicates to each experimental condition corresponding to non-infected and infected-*P. falciparum* RBCs, treated or untreated with 2,3-DPG were used.

Although the RBC is a simple anucleate cell with well-characterized metabolic pathways and 2,3-BPG targets and effects inside RBC are known, an untargeted metabolomics analysis was performed as a first approach to provide an unbiased analysis and the possibility of expose new targets or biomarkers of 2,3-DPG treatment on parasites.

### 2.5.1 Extraction of Metabolites

Metabolites were extracted from each biological replicate according to a protocol developed by MacRae et al. (2013) with little adjustments. Briefly, after 30 hours of *in vitro* culture non-infected and infected-RBCs, treated with 2,3-DPG or untreated, were quickly quenched from 37°C to 12°C through immersing Falcon tubes containing the cultures for few seconds, in a solution of metallic beads in absolute ethanol kept overnight at -80°C. After that, all the downstream procedures were performed at 4°C. Infected treated or untreated RBCs were subsequently submitted to a magnetic separation procedure to deplete non-infected RBCs and assure metabolite extraction from an enriched material comprised with more than 95% of infected RBCs by mature forms. Thus,  $3.05 \times 10^7$  RBCs per biological replicate were submitted to extraction in 1.5 mL Eppendorf microtubes. A solution with chloroform and methanol (2:1 v/v) was added into each microtube and then immersed in water/ice solution in an ultrasound cleaning bath (Model 3000512, Voltage 220V, Current 0.2A, Power 50W, JP Selecta) and submitted to three series of eight minutes of high frequency sound waves (40kHz) interpolated by 12 minutes of resting, for one hour. The liquid content was removed from each microtube and concentrated in new ones using a concentrator device (5301 speed-vac Eppendorf) at 250Xg and room temperature. Then, pellets were resuspended in a solution with methanol and water (2:1 v/v) and submitted to a new round of high frequency sound waves as described above. The liquid content was removed and added to the dried material inside the previous microtubes, and a new round of concentration was performed. Finally, a solution with chloroform, methanol, and water (1:3:3 v/v/v) was added to the dried material in each microtube, then vortexed rigorously and centrifuged for 5 minutes at 0°C at 20817Xg. The upper phase containing polar metabolites was separated from the lower phase containing apolar metabolites, both phases were concentrated in separated tubes in the speed-vac and stored at -80°C until high performance liquid chromatography coupled to mass spectrometry (HPLC/MS) analysis.

### 2.5.2 High Performance Liquid Chromatography Coupled to Mass Spectrometry (HPLC/MS)

Samples were analyzed by liquid chromatography (Ultimate 3000 RSLC nano system, Thermo Fisher Scientific) interfaced with a Bruker Impact II quadrupole time-of-flight mass spectrometer equipped with an electrospray source (Bruker Daltonics, Bremen). Chromatographic separation was performed on a column Kinetex Polar C18, 2.6µm, 100Å, and 100 × 2.1mm (Phenomenex) at 45°C. The gradient was as follows: 1 min 5% phase B, then in 5 min to 50% phase B, next in 4 min to 100% phase B, held for 8 min at 100% phase B, subsequently in 1 min to 0% phase B and held for 6 min at 0% phase B. Internal calibration was achieved with a sodium formate

solution introduced to the ion source via a 20µL loop at the beginning of each analysis using a six-port valve. Calibration was then performed using high-precision calibration mode (HPC). The Mass Spectrometer was operated in positive ionization mode on the full scan mode and data was acquired in the mass range from m/z 50 to 1000 with a spectra rate of 1 Hz. The capillary was set at 4500 V, the End Plate offset at 500 V, the Nebulizer gas (N2) at 4 Bar and the Dry gas (N2) at 8 L/min at 200°C. To evaluate the performance of the instrument, quality control pools (QCpool, n=3; made by pooling 5µl of upper and lower extracted phases) were injected every 7 to 10 samples.

### 2.5.3 Data Extraction

LC-MS files (31 samples, one infected treated sample from upper phase was lost during the LC-MS process, 3 QCpools and 4 water samples) were converted to mzXML files using the ProteoWizard MSConvert software (Chambers et al., 2012). LC-MS data was then preprocessed using XCMS (R package xcms 3.6.2) (Smith et al., 2006; Tautenhahn et al., 2008; Benton et al., 2010) and consisted of peak picking, retention time alignment, peak matching and gap filling. Peak picking was performed with the centwave algorithm and the following parameters: ppm=15, peakwidth = 10-40 s, snthresh = 10, prefilter = 3, 10,000 and noise=1000. Retention time alignment was performed against the average of the QCpools with a m/z width = 0.01. Peak grouping was performed with the following parameters: bandwidth = 5, m/z width = 0.01, minimum fraction = 0.5. Gap filling was performed with a fixed retention time deviation = 10 s. A total of 356 features (peaks with specific retention time and m/z values) were extracted with their corresponding m/z, retention time and peak area.

In order to reduce the number of features, two filters were applied. The first filter excluded all ions that appeared in water samples with an average area > 10,000. The second filter excluded all ions with a coefficient of variability >= 30% in the QC pools. After applying these filters, the list was reduced to 90 features. Data was normalized by total area.

### 2.5.4 Metabolite Identification

After statistical analysis, MS and MS/MS data of ions of interest were manually searched against metabolomics databases (HMDB and Metlin). SIRIUS metabolomics search tool was also used (Dührkop et al., 2019).

## 2.6 Statistical Analysis

Statistical analysis was performed using GraphPad Prism version 8 for Windows (GraphPad Software). Kolmogorov-Smirnov test was used to assess data normality and non-parametric Mann-Whitney U test, or unpaired Student's t test was used for comparisons on continuous values between two-independent groups, as appropriate.

Intergroup comparisons were conducted for the merozoite count assay, through the application of unpaired Student's t test between treated and untreated sample groups.

For metabolomics statistical analyses, LC-MS data was centered, and unit-variance scaled. Metabolic differences between non-infected and infected-*P. falciparum* RBCs, both treated and



untreated, were assessed using multivariate analysis based on principal component analyses (PCA) and partial-least squares discriminant analyses (PLS-DA) using SIMCA software (MKS Umetrics, Sweden Umetrics, version 16.0.1). Venn diagrams were built in R environment (<https://cran.r-project.org/bin/windows/base/old/3.6.1>) using the “VennDiagram” package.

For all tests, statistical significance level was set at  $<0.05$ , unless otherwise stated.

## 2.7 Ethics Statement

This study followed the European and national directives. All blood donors were clearly informed that participation in the study was voluntary and confidential and were made aware of the objectives of the work. Each participant signed an informed consent form before blood collection and a numerical code was assigned to each donor to maintain confidentiality. The Ethical Committee of IHMT approved the protocol (as part of project PTDC\_BIA-CEL\_28456\_2017, *Parecer* 16.18).

## 3 RESULTS

### 3.1 2,3-DPG Has Little Effect on Human Cells

No hemolysis was observed due to the direct effect of 2,3-DPG for any of the doses added to the culture medium comprised in the range of two-fold serial dilutions from 16mM to 0.25mM or to an indirect effect of sodium concentration or changes in pH value of the solutions for 90 minutes of incubation as opposed to the positive control. This observation was confirmed during all the subsequent experiments where no hemolysis occurred with this same range of serial dilutions of 2,3-DPG concentrations administrated up to 96 hours with daily media renewal to in *in vitro* cultures of infected or non-infected red blood cells (data not shown).

On cytotoxicity assay, HEPG2 viability started to decrease from the 2,3-DPG dose of 4mM and less than 10% of viable cells were observed with the 16mM dose. The IC<sub>50</sub>, the minimum concentration of 2,3-DPG able to inhibit the cellular growth or reduce the cell viability in 50%, was 6.40mM (95% CI of IC<sub>50</sub> 5.16-7.78). Results of three independent experiments are summarized in **Supplementary Figure S1**.

### 3.2 Effect of 2,3-DPG Addition on Parasite Development

#### 3.2.1 2,3-DPG Showed Antimalarial Activity Causing a Significant Decrease of Parasite Densities

IC<sub>50</sub> values determined at time points of 24h, 36h, 48h, 60h, 72h and 96h are presented in **Table 1** and **Supplementary Figure S2** (it was not possible to determine the values at 12h and 84h). As a concentration of 8mM would be well tolerated by the RBCs

(physiological concentration at high altitudes) and had some effect on the parasite (IC<sub>50</sub>), we considered this dose for all the following assays.

We observed that the addition of 2,3-DPG 8mM into culture medium impairs the parasite growth as shown in **Figure 1**. For the three independent experiments, which have started with initial parasite density of 1%, results show that, under normal conditions, there is an exponential increase in density levels from approximately 30h to 48h/0h, corresponding to the parasites egress from the host cell and invasion of new RBCs to start a new asexual cycle. On the opposite, when parasites have grown in the presence of 2,3-DPG for 48 hours, parasite density levels decreased at the same time point, suggesting that parasites are able to mature but cannot normally progress into a new cycle.

#### 3.2.2 2,3-DPG Impacts Parasite Development But Does Not Deplete ATP

**Figure 2** summarizes data of parasite densities from three independent experiments where the effect of the addition of 2,3-DPG (prior infection or daily added) and of PKD phenotype induction, on parasite invasion (at 24h – first cycle, and at 72h – second cycle) and maturation (at 48h – first cycle, and at 96h – second cycle) was assessed.

Parasite densities over two parasite cycles were significantly lower than the control group when RBCs were previously treated with NaF 4mM and 8mM (NaF4 and NaF8, respectively) or when culture medium was daily supplemented with 2,3-DPG 8mM (DPGadd). Parasite densities started to differ at 24 hours and become more notorious at 48 and 72 hours (predominance of schizont and ring stages, respectively). On the opposite, when RBCs were previously treated with 2,3-DPG 8mM for 24 hours before being infected (DPGt), similar parasite densities to the control group were observed.

ATP concentration inside RBCs was measured in the different experimental groups both in infected-RBCs and paired non-infected controls at the time of incubation and removal of 2,3-DPG and NaF (-24 hours and -10 hours, respectively), at the onset of invasion and maturation assay (0 hours) and every 24 hours onwards for 96 hours (**Figure 3**). A depletion of ATP was only observed when RBCs were previously incubated with NaF being the concentration slightly higher in the infected cells. 2,3-DPG addition, either previously to infection or daily to the culture medium, caused no effect on the ATP levels in the cells, independently of infection.

#### 3.2.3 2,3-DPG Does Not Hinder Parasite Egress But Reduces Progeny Number

Although no hemolysis had been observed or ATP depletion as a result of 2,3-DPG addition, we cannot exclude an adverse effect on the RBC membrane, which could prevent parasite progression into a new cycle. Therefore, the ability of parasites that have grown in the presence of 2,3-DPG 8mM added daily to culture medium to egress

**TABLE 1** | IC<sub>50</sub> values after 24, 36, 48, 60, 72 and 96 hours of incubation of 3D7 *P. falciparum* parasites with 2,3-DPG.

Time point (hour)	24	36	48	60	72	96
IC <sub>50</sub> (mM) ± SD	3.42 ± 1.48	6.21 ± 0.80	8.56 ± 0.33	8.18 ± 0.80	5.61 ± 0.59	10.17 ± 1.95

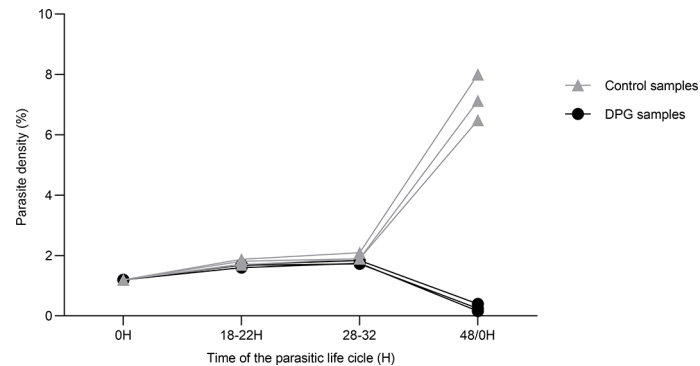


**FIGURE 1** | 2,3-DPG caused a significant decrease of parasite densities. Total parasite density of 3D7 *P. falciparum* parasites during one cycle of growth (48h) in the absence (light triangles) and presence (dark dots) of 2,3-DPG 8mM. This graph was chosen as representative of three independent experiments performed in triplicate.

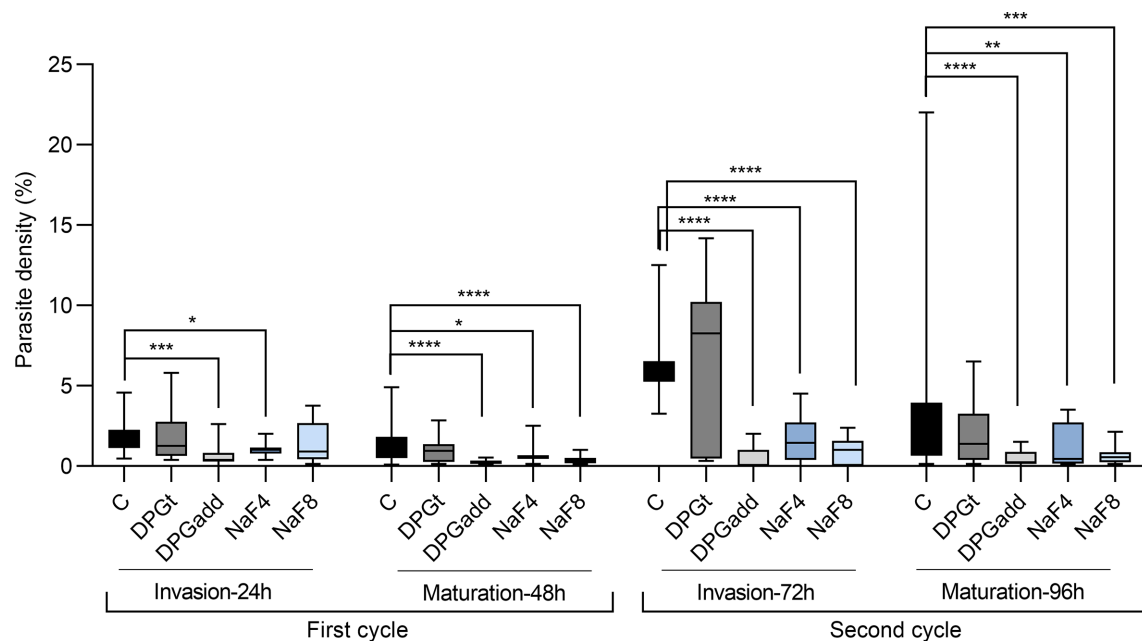


**FIGURE 2** | Impact on parasite development. Parasite densities measured in 3D7 *P. falciparum* parasites during invasion and maturation assays for two growth cycles (96h). Invasion of erythrocytes was assessed at 24 hours (1st cycle) and 72 hours (2nd cycle), and maturation was assessed at 48 hours (1st cycle) and 96 hours (2nd cycle). Data are summarized from three independent experiments. C - control group with parasites growing in cRPMI alone, DPGt - RBCs incubated for 24 hours with 2,3-DPG 8mM prior to infection, DPGadd - 2,3-DPG 8mM added every 24 hours to culture medium, NaF4 and NaF8 - inducible-PKD RBC groups, incubated with NaF 4mM and 8mM, respectively (\* $p < 0.05$ , \*\* $p < 0.01$ , \*\*\* $p < 0.001$ , \*\*\*\* $p < 0.0001$ ; lines inside boxes represent median values and error bars the minimum and maximum values for each box).

from RBCs and start a new intraerythrocytic cycle by reinventing untreated cells (niRBCs C) was assessed through an egress assay. Both enriched (schizont stage) and non-enriched parasites, from treated and untreated cultures, were allowed to pursue the developmental cycle in untreated RBCs.

As previously shown, parasite densities were higher in untreated cultures than in cultures treated with 2,3-DPG 8mM for 48 hours, which was more evident in non-enriched cultures

(Untreated Normal *versus* DPG Normal, **Supplementary Figure S3**). Nonetheless, a similar parasite growth rate in the new cycle in untreated cells was observed in all four groups, regardless of the previous treatment with 2,3-DPG.

As the egress or invasion of new cells did not seem compromised, we analyzed by light microscopy, whether the number of resulting merozoites from parasite segmentation process (schizogony) could have been altered due to effect of

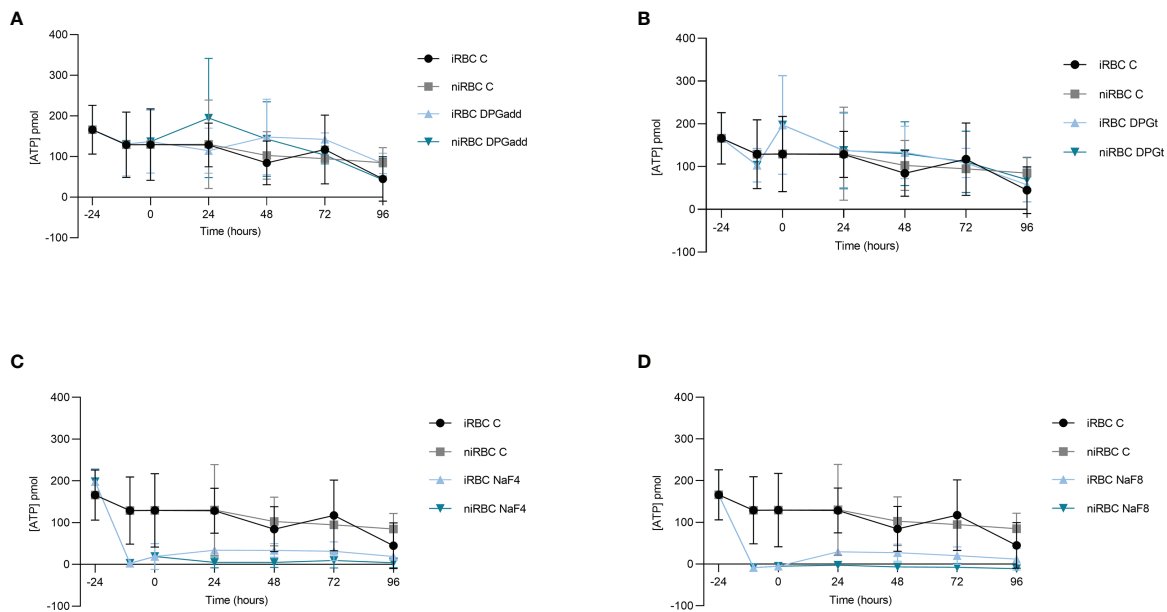


**FIGURE 3 |** 2,3-DPG does not deplete ATP. ATP content inside RBCs under different experimental conditions tested during the invasion and maturation assay. **(A)** 2,3-DPG 8mM added every 24 hours to culture medium, infected (iRBC DPGadd) and non-infected (niRBC DPGadd), **(B)** RBCs incubated for 24 hours with 2,3-DPG 8mM prior to infection, infected (iRBC DPGt) and non-infected (niRBC DPGt), **(C)** inducible-PKD RBC incubated with NaF 4mM, infected (iRBC NaF4) and non-infected (niRBC NaF4); **(D)** inducible-PKD RBC incubated with NaF 8mM, infected (iRBC NaF8) and non-infected (niRBC NaF8). Untreated RBCs, infected (iRBC C) and non-infected (niRBC C) control groups were included in all experiments. Error bars represent the standard deviation in each timepoint.

2,3-DPG treatment, impacting the parasite multiplication and increase of parasite densities, by counting the number of merozoites present within intact, late-stage schizonts from both 2,3-DPG treated and untreated RBCs ( $n=132$  each). **Figure 4** shows a scatter plot where each point represents the number of merozoites within a single schizont that either developed in the presence or absence of 2,3-DPG, showing a significant difference between samples ( $p$  value  $< 0.0001$ ). Schizonts that developed in the presence of the compound ultimately resulted in a lower number of merozoites (mean = 14.51; SD = 3.08) than those that have grown in normal culture medium (mean = 20.65, SD = 5.17). The same trend was obtained with the inducible-PKD groups, but the low parasite densities precluded a similar analysis.

### 3.3 2,3-DPG Makes the Metabolic Profile of an Infected Cell More Similar to That of a Non-Infected Cell

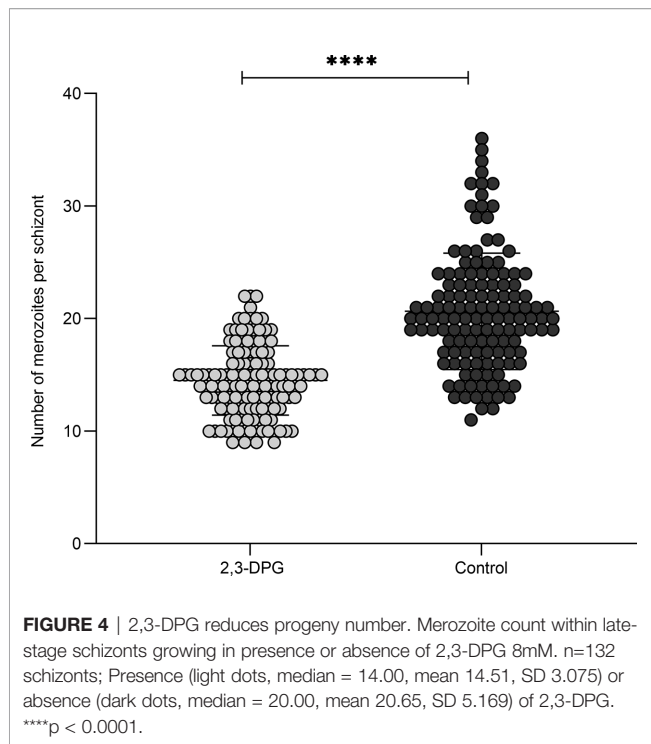
PCA was performed with all samples and QCpools to identify which of the factors (sample phase, infection, or treatment) had the most important influence on the metabolic profile. The first two components explained 47% and 24% of the variance of the data, respectively. Sample phase was the most relevant factor, as there was a clear separation between lower and upper phases (**Supplementary Figure S4**). In addition, the variability of the samples was much higher than the variability of the QCpools, confirming the LC-MS analysis performance.

PCA were performed for all upper and lower phase samples separately. The first and second components of the models

explained 41% and 17% of the variance of the lower phase data and 43% and 19% of the variance of the upper phase data. Infection had a clear influence in the metabolic profile, independently of the phase (**Figures 5A, C**). Influence of 2,3-DPG exposure was less clear (**Figures 5B, D**). However, treated infected erythrocytes appeared closer to non-infected erythrocytes, mainly in the upper phase samples (**Figure 5B**).

In order to better evaluate the influence of 2,3-DPG, PCA were performed in infected (**Figures 6A, C**) and non-infected samples (**Figures 6B, D**), separately, for each phase. Influence of 2,3-DPG was only observed in infected samples for both upper and lower phases (**Figures 6A, C**, respectively).

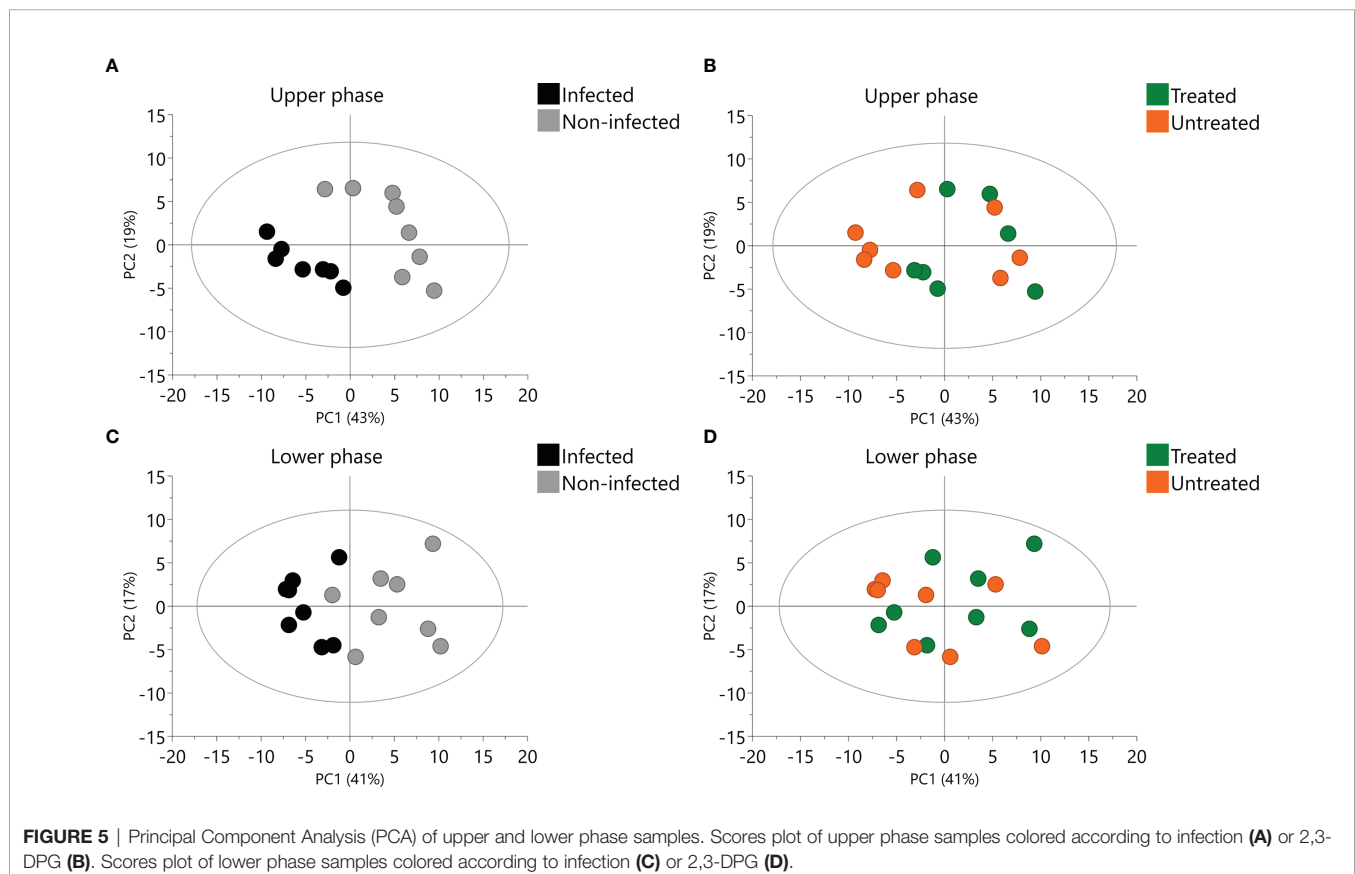
Since the aim of the untargeted metabolomics analyses was to evaluate the metabolites that were affected by 2,3-DPG in infected RBCs, the first approach was to build PLS-DA models between treated and untreated RBCs. However, no statistically significant models were obtained either considering all samples or only infected or non-infected samples for both upper and lower phases. One of the possible causes of no statistical significance might be the reduced number of infected treated samples ( $n=3$  for the upper phase). Taking this in consideration together with the proximity of infected treated RBCs to non-infected RBCs observed in the PCA (**Figure 5B**), we built a PLS-DA model to compare infected treated samples and non-infected samples (treated and untreated) versus infected untreated samples ( $p = 0.005$ ,  $R^2(X) = 0.43$ ,  $R^2(Y) = 0.66$ ,  $Q^2(Y) = 0.58$ ; upper phase samples). We also built a PLS-DA model comparing only non-infected samples (treated and untreated) versus infected untreated samples ( $p = 0.002$ ,  $R^2(X) =$



0.71,  $R^2(Y) = 0.99$ ,  $Q^2(Y) = 0.96$ ; upper phase samples). By comparing the most relevant features (peaks with a specific retention time and  $m/z$  value) of both models, we can disclose those features that are specific for the effects of 2,3-DPG on infected cells. The most relevant metabolites for each model were defined as those having a Variable Importance on the Projection (VIP) value  $> 1$  and a correlation coefficient  $p(\text{corr})$  value  $> |0.6|$ . A total of 31 features were obtained in each model, from which 27 were common and 4 were specific for each model (see Venn-Diagram in **Supplementary Figure S5**). The four features that were specific for the PLS-DA model comparing infected treated and non-infected (treated and untreated) samples *versus* infected untreated samples can be considered as being specific for the effects of 2,3-DPG on infected cells, since they are not relevant in the PLS-DA model that compares non-infected samples (treated and untreated) *versus* infected untreated samples. Whereas we could not identify any of the four features, their  $m/z$  ratios are presented in the **Supplementary Figure S5**.

## 4 DISCUSSION

With a complex life cycle, the malaria parasite has interacted with the human host for thousands of years, and this coevolution has shaped both parasites and humans. Malaria has been one of



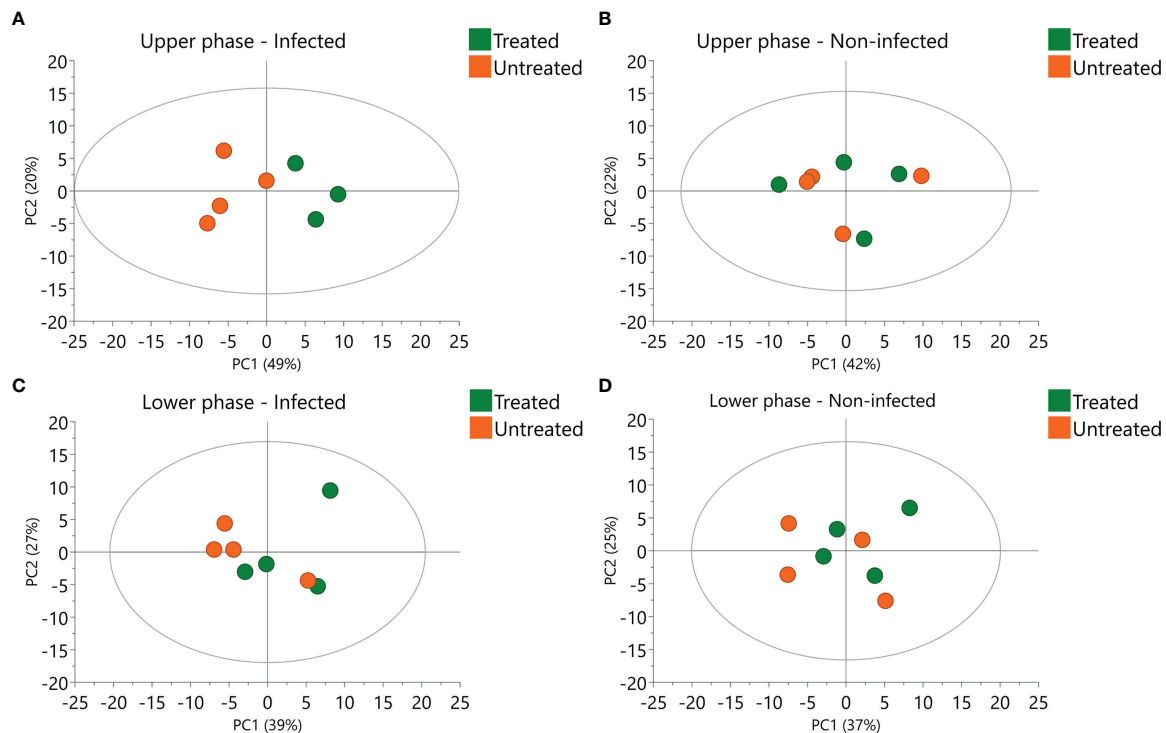


**FIGURE 6** | Principal Component Analysis (PCA) of infected and non-infected samples. Scores plot of infected (A) and non-infected (B) upper phase samples colored according to 2,3-DPG. Scores plot of infected (C) and non-infected (D) lower phase samples colored according to 2,3-DPG.

the strongest selective forces on the human genome and has selected many human genetic variants that would hardly be maintained in human populations due to their impact on human health. Nevertheless, these variants, most of them related to erythrocyte specific structural proteins or enzymes, may reach high frequencies in malaria endemic areas as they provide some protection against malaria disease (Kwiatkowski, 2005).

Among erythrocyte enzymopathies, the association between G6PD deficiency and protection against malaria is the best described (Mbanefo et al., 2017). The second most frequent erythrocyte enzymopathy worldwide is PK deficiency, but only a few studies addressed the frequency of PK-deficiency in malaria endemic areas and its possible association to malaria protection (Alves et al., 2010; Machado et al., 2010; Berghout et al., 2012; Machado et al., 2012; Bruggen et al., 2015). Still, as RBCs do not have nucleus and cannot produce new proteins to replace old or depleted ones, any limitation in the erythrocyte metabolic pathways may carry consequences to the cell integrity and may interfere with parasite development. Some evidence gathered from experimental models shows that this is the case of PK deficiency. The present study aimed to further explore the mechanisms involved in this interaction, focusing on the role of 2,3-BPG in PK deficiency-mediated protection against malaria parasites.

The malaria parasite *P. falciparum* relies on glycolysis for the generation of energy and holds a complete set of glycolytic enzymes, except BPGM, that seems to differ biochemically and structurally from their host counterparts (Roth, 1990). The rate of

glycolysis in *P. falciparum*-infected erythrocytes is significant, using glucose and generating lactate at 20 to 100 times the rate observed in non-infected cells (Mehta et al., 2005; Schalkwyk et al., 2008). Pyruvate kinase activity is a rate-limiting step of RBC glycolysis (Roy et al., 2021), and a relative increase in its activity rises RBC ATP at the expense of 2,3-BPG. Under normal circumstances, the parasite seems to be able to operate its own PK isozyme into the host red cells and an increase in RBC ATP and a decrease in 2,3-BPG are observed in infected cells, which results from a PK activity with parasite origin (Oelshlegel et al., 1975; Dubey et al., 2003), also suggesting that the enormous glucose flux into the infected RBCs is almost totally for parasite use. However, when host PK activity sharply decreases, 2,3-BPG content rises, and we questioned whether it could have harmful consequences for the parasite. We analyzed an induced PK-deficiency phenotype (through enolase inhibition and confirmed by the depletion of ATP) and the effect on the parasite if 2,3-BPG itself (synthetic form 2,3-DPG) would be administered in the extracellular medium.

Present results show that at the end of an intraerythrocytic developmental cycle, when 2,3-DPG 8mM was daily added into culture medium, there was a sharp reduction in parasite densities and parasites were not able to normally progress to a new cycle. We analyzed this impairment of parasite growth through invasion and maturation assays, and we observed that parasite densities were significantly lower than the control group and this effect is equally visible both on invasion and maturation. Same result is obtained with the PK-deficiency induced phenotype,



which suggests a similar effect and a role for the 2,3-DPG. However, this mechanism seems not to be related with the intracellular level of ATP as an ATP depletion, which is also a consequence of PK-deficiency and may also be damaging for the parasite (Min-Oo et al., 2003; Ayi et al., 2009), was only observed in the PK-deficiency induced phenotype, being the concentration slightly higher in the infected cells which may be due to the ATP production by the parasite (Jacobasch et al., 1990).

The cycles of growth that result in parasite proliferation depend both on the ability of the parasite to access and complete invasion of susceptible cells as well as to mature and generate new merozoites to egress from the host cell. The egress from RBCs and the normal progression for a new intraerythrocytic developmental cycle was confirmed, being the sharp reduction on parasite densities due to a direct effect on parasite maturation as significant lower progeny emerged from parasites that were submitted to 2,3-DPG. Parasite may adapt its multiplication and regulation of progeny number as a result of nutrient exhaustion or type or stress factors (Mancio-Silva et al., 2017; Simon et al., 2021), and also may be influenced by intrinsic or extrinsic host factors as mimicked in the present study.

Several glycolytic enzymes from human erythrocytes such as hexokinase, phosphofructokinase, pyruvate kinase, and phosphoglycerate kinase are inhibited by unbound 2,3-bisphosphoglycerate, as a regulatory effect on glycolytic pathway (Ponce et al., 1971). As previously stated, *Plasmodium* parasite has a complete set of glycolytic enzymes. The addition of 2-halo derivatives of D-glucose results in the rapid acidification of the parasite cytosol, inhibition of glucose phosphorylation by hexokinase, and a marked reduction in the ATP levels within the parasite having an effect on the parasite proliferation (van Schalkwyk et al., 2008). The synthetic compound 2,3-DPG may be acting as an inhibitor of parasite key enzymes of glycolysis such as hexokinase, phosphofructokinase, pyruvate kinase, and phosphoglycerate kinase (Roth et al., 1988). As we did not observe any impact on ATP production in infected RBCs, maybe there would be another target of 2,3-DPG on the parasite. The results obtained with our PLS-DA model comparing infected (treated) and non-infected (treated and untreated) samples versus infected untreated samples for polar metabolites (upper phase samples) suggest new targets and we cannot exclude novel and undescribed parasite metabolites as 2,3-DPG targets. The analysis of the parasite's metabolic capabilities is likely to unveil these presumable effects.

The addition of 2,3-DPG seemed to not affect the host cell as no change on ATP levels were observed, independently of infection, and no effect on parasite was obtained when only RBCs were treated prior to infection. The effect only on the parasite was also suggested by the closer metabolic profile of infected and treated RBC to the one from non-infected cells, as observed with the untargeted metabolomics analysis. 2,3-DPG treatment appeared not only not to affect the RBC, but to reverse the metabolic profile of the infected cell and make it closer to the non-infected. Unfortunately, metabolomics analysis was not conclusive to determine which metabolites could be differentially present in infected treated RBCs that could restore the metabolic

profile to the one of non-infected RBCs. A future approach with biological replicates with higher parasite density and complemented with targeted analyses addressing the four polar metabolites seen in the present study will contribute to elucidate the impact of 2,3-DPG on metabolic profile of infected RBCs.

The targeted action of 2,3-DPG on parasite rather than on host cell may be due to the differences between the membrane of the infected and non-infected erythrocytes as the parasite metabolic activity results in an increased permeability of the infected erythrocyte membrane (Mehta et al., 2006; Desai, 2014; Counihan et al., 2021), which may facilitate the 2,3-DPG entrance into the cell. However, since increased amounts of intracellular 2,3-BPG affect the mechanical stability of RBC membrane, an effect on host cell cannot be excluded and needs further analyses.

Targeting host glycolysis as an antimalarial strategy is a promising approach and has been attempted in a few studies. Jezewski et al. (2021) observed that enolase inhibition increased erythrocyte susceptibility to oxidative damage and induces rapid and premature erythrocyte senescence, rather than direct hemolysis, also affecting parasite development. However, an inhibitory effect also on parasite enolase was not unequivocally ruled out, so the interaction mechanism was not clearly established. Xu et al. (2020) reported that mice suffering from BPGM deficiency, the enzyme responsible for the synthesis of 2,3-BPG, show severely reduced 2,3-BPG levels and protection against severe malaria-induced anemia and intensity of neuroinflammation on experimental cerebral malaria. The authors suggest that the reduced 2,3-BPG levels results in increased O<sub>2</sub>-bound hemoglobin, decreased oxygen delivery to tissues and compensatory erythropoiesis, which leads to protection against anemia. This augmented erythropoiesis response to mounting parasitemia and RBC destruction would provide more efficient replacement of infected RBCs. Further, the authors observed a 5% decrease in the proportion of *Plasmodium* late-stage parasites in deficient RBCs and suggest that intracellular environment may be less permissive to replication and maturation of the malarial parasite. This would be contrary to our observations, but authors cannot exclude that RBCs infected with mature parasite forms are being more efficiently replaced in the process of superior erythropoiesis.

Oppositely, Roth et al. (1988) have grown *P. falciparum* parasites in RBCs lacking BPGM, where 2,3-BPG metabolite was barely detectable and parasite growth was entirely normal. Mehta et al. (2005) demonstrated a downregulation of the glucose utilization rate in the majority of non-infected RBCs by the infected ones, suggesting a selective inhibition of non-infected RBCs' phosphofructokinase due to a decrease in pH as a result of production of lactic acid by the infected cells. Authors suggest that reduced glucose utilization would result in lower ATP production in erythrocytes and lower 2,3-BPG levels with subsequent lower oxygen supply to the tissues, contributing to an overall lethargic state for the patient.

A better understanding of the above mechanisms may provide potential targets for new approaches such as development of host directed therapies (HDT), which could

potentially be designed to mimic the protective effects exhibited by naturally occurring RBC disorders (Zumla et al., 2016), allowing a better management of complicated and uncomplicated malaria patients. Despite this not being a therapeutic study, the observations that glycolysis, namely the possible action of an increased amount of the 2,3-BPG metabolite, may be important for this goal. Its action on the reduction of the intraerythrocytic multiplication of *P. falciparum* may help to delay the development of life-threatening parasite densities until parasite clearing immunity or the effect of a co-delivered traditional antimalarial are achieved, transcending multidrug resistance. However, the mechanism underlying this effect remains unclear and further work will be carried out in order to fully disclose the impact on the parasite and overcome the major limitations of the present study, namely an unequivocal quantification of the amount of 2,3-DPG inside the cell and the inconclusive results of the pilot metabolomics analysis of infected and non-infected cells submitted to the action of the compound since it was not possible to identify the extracted metabolites nor to detect the compound inside the cell.

## DATA AVAILABILITY STATEMENT

The original contributions presented in the study are included in the article/**Supplementary Material**. Further inquiries can be directed to the corresponding author.

## ETHICS STATEMENT

The studies involving human participants were reviewed and approved by Ethical Committee of Institute of Hygiene and Tropical Medicine, University NOVA of Lisboa, Lisbon, Portugal. The patients/participants provided their written informed consent to participate in this study.

## REFERENCES

- Alves, J., Machado, P., Silva, J., Gonçalves, N., Ribeiro, L., Faustino, P., et al. (2010). Analysis of Malaria Associated Genetic Traits in Cabo Verde, a Melting Pot of European and Sub Saharan Settlers. *Blood Cells Mol. Dis.* 44 (1), 62–68. doi: 10.1016/j.bcmd.2009.09.008
- Ayi, K., Liles, W. C., Gros, P., and Kain, K. C. (2009). Adenosine Triphosphate Depletion of Erythrocytes Simulates the Phenotype Associated With Pyruvate Kinase Deficiency and Confers Protection Against Plasmodium Falciparum In Vitro. *J. Infect. Dis.* 200 (8), 1289–1995. doi: 10.1086/605843
- Ayi, K., Min-Oo, G., Serghides, L., Crockett, M., Kirby-Allen, M., Quirt, I., et al. (2008). Pyruvate Kinase Deficiency and Malaria. *N Engl. J. Med.* 358 (17), 1805–1810. doi: 10.1056/NEJMoa072464
- Berghout, J., Higgins, S., Loucoubar, C., Sakuntabhai, A., Kain, K. C., and Gros, P. (2012). Genetic Diversity in Human Erythrocyte Pyruvate Kinase. *Genes Immun.* 13 (1), 98–102. doi: 10.1038/gene.2011.54
- Bruggen, R.v., Gualtieri, C., Iliescu, A., Cheepsunthorn, C. L., Mungkalasut, P., Trape, J.-F., et al. (2015). Modulation of Malaria Phenotypes by Pyruvate Kinase (PKLR) Variants in a Thai Population Edited by Alistair G. Craig. *PLoS One* 10 (12), e0144555. doi: 10.1371/journal.pone.0144555

## AUTHOR CONTRIBUTIONS

All authors have read and agreed to the published version of the manuscript. Conceptualization: APA. Methodology: JM, SMT, FN, JAR, and FAC. Formal analysis: IM, MMM, MC, JM, SMT, AMMA, and APA. Funding acquisition: APA and FAC. Investigation: IM, MMM, MC, SMT, JN, AB, and MTGR. Project administration: APA. Supervision: APA. Writing—original draft: IM, MMM, MC, JM, and APA. Writing—review and editing: MTGR and AMMA. All authors contributed to the article and approved the submitted version.

## FUNDING

This research was funded by Fundação para a Ciência e Tecnologia (<https://www.fct.pt/index.phtml.en>), projects PTDC\_BIA-CEL\_28456\_2017 and GHTM - UID/04413/2020 (<https://ghmt.ihmt.unl.pt/>). The funders had no role in study design, data collection and analysis, decision to publish, or preparation of the manuscript.

## ACKNOWLEDGMENTS

We would like to thank all blood donors and Ana Reis, from Instituto de Higiene e Medicina Tropical (Portugal) for collecting blood samples. We also would like to thank Marcelo Urbano Ferreira for the critical review of the manuscript.

## SUPPLEMENTARY MATERIAL

The Supplementary Material for this article can be found online at: <https://www.frontiersin.org/articles/10.3389/fcimb.2022.840968/full#supplementary-material>

- Capps, T. C., and Jensen, J. B. (1983). Storage Requirements for Erythrocytes Used to Culture Plasmodium Falciparum. *J. Parasitol.* 69 (1), 1585. doi: 10.2307/3281291
- Chambers, M. C., Maclean, B., Burke, R., Amodei, D., Ruderman, D. L., Neumann, S., et al. (2012). A Cross-Platform Toolkit for Mass Spectrometry and Proteomics. *Nat. Biotechnol.* 30 (10), 918–920. doi: 10.1038/nbt.2377
- Counihan, N. A., Modak, J. K., and de Koning-Ward, T. F. (2021). How Malaria Parasites Acquire Nutrients From Their Host. *Front. Cell Dev. Biol.* 9 (March), 649184. doi: 10.3389/fcell.2021.649184
- Desai, S. A. (2014). Why do Malaria Parasites Increase Host Erythrocyte Permeability? *Trends Parasitol.* 30 (3), 151–159. doi: 10.1016/j.pt.2014.01.003
- Dubey, M. L., Hegde, R., Ganguly, N. K., and Mahajan, R. C. (2003). “Decreased Level of 2,3-Diphosphoglycerate and Alteration of Structural Integrity in Erythrocytes Infected With Plasmodium Falciparum In Vitro,” in *Vascular Biochemistry*. Eds. P. Zahradka, J. Wigle and G. N. Pierce (Boston, MA: Springer US), 137–141. Available at: [https://doi.org/10.1007/978-1-4615-0298-2\\_20](https://doi.org/10.1007/978-1-4615-0298-2_20).
- Dührkop, K., Fleischauer, M., Ludwig, M., Aksenov, A. A., Melnik, A. V., Meusel, M., et al. (2019). SIRIUS 4: A Rapid Tool for Turning Tandem Mass Spectra Into Metabolite Structure Information. *Nat. Methods* 16 (4), 299–3025. doi: 10.1038/s41592-019-0344-8

- Durand, P. M., and Coetzer, T. L. (2008). Pyruvate Kinase Deficiency Protects Against Malaria in Humans. *Haematologica* 93 (6), 939–940. doi: 10.3324/haematol.12450
- Evans, B. C., Nelson, C. E., Yu, S. S., Beavers, K. R., Kim, A. J., Li, H., et al. (2013). *Ex Vivo* Red Blood Cell Hemolysis Assay for the Evaluation of PH-Responsive Endosomolytic Agents for Cytosolic Delivery of Biomacromolecular Drugs. *J. Visualized Experiments: JoVE* 73 (March), e50166. doi: 10.3791/50166
- Freitas, M.V.de, Netto, R.de C.M., da Costa Huss, J. C., de Souza, T. M. T., Costa, J. O., Firmino, C. B., et al. (2008). Influence of Aqueous Crude Extracts of Medicinal Plants on the Osmotic Stability of Human Erythrocytes. *Toxicol. Vitro* 22 (1), 219–245. doi: 10.1016/j.tiv.2007.07.010
- Hamilton, C., Steinlechner, B., Gruber, E., Simon, P., and Wollenek, G. (2004). The Oxygen Dissociation Curve: Quantifying the Shift. *Perfusion* 19 (3), 141–445. doi: 10.1191/0267659104pf7340a
- Jacobasch, G., Buckwitz, D., Gerth, C., and Thamm, R. (1990). Regulation of the Energy Metabolism of Plasmodium Berghei. *Biomed. Biochim. Acta* 49 (2–3), S289–S294.
- Jezewski, A. J., Lin, Y.-H., Reisz, J. A., Culp-Hill, R., Barekatain, Y., Yan, V. C., et al. (2021). Targeting Host Glycolysis as a Strategy for Antimalarial Development. *Front. Cell. Infect. Microbiol.* 11, 730413. doi: 10.3389/fcimb.2021.730413
- Kariuki, S. N., and Williams, T. N. (2020). Human Genetics and Malaria Resistance. *Hum. Genet.* 139 (6–7), 801–811. doi: 10.1007/s00439-020-02142-6
- Kwiatkowski, D. P. (2005). How Malaria Has Affected the Human Genome and What Human Genetics Can Teach Us About Malaria. *Am. J. Hum. Genet.* 77 (2), 171–192. doi: 10.1086/432519
- Laroque, A., Min-Oo, G., Tam, M., Ponka, P., Stevenson, M. M., and Gros, P. (2017). The Mouse Char10 Locus Regulates Severity of Pyruvate Kinase Deficiency and Susceptibility to Malaria. *PLoS One* 12 (5), e01778185. doi: 10.1371/journal.pone.0177818
- Machado, P., Manco, L., Gomes, C., Mendes, C., Fernandes, N., Salomé, G., et al. (2012). Pyruvate Kinase Deficiency in Sub-Saharan Africa: Identification of a Highly Frequent Missense Mutation (G829A;Glu277Lys) and Association With Malaria. *PLoS One* 7 (10), e47071. doi: 10.1371/journal.pone.0047071
- Machado, M., Murtinheira, F., Lobo, E., and Nogueira, F. (2016). Whole-Cell SYBR Green I Assay for Antimalarial Activity Assessment. *Ann. Clin. Med. Microbiol.* 2 (1), 1010. Available at: <https://www.jscimedcentral.com/MedicalMicrobiology/medicalmicrobiology-2-1010.pdf>.
- Machado, P., Pereira, R., Rocha, A. M., Manco, L., Fernandes, N., Miranda, J., et al. (2010). Malaria: Looking for Selection Signatures in the Human PKLR Gene Region. *Br. J. Haematol.* 149 (5), 775–784. doi: 10.1111/j.1365-2141.2010.08165.x
- MacRae, J. I., Dixon, M. W. A., Dearnley, M. K., Chua, H. H., Chambers, J. M., Kenny, S., et al. (2013). Mitochondrial Metabolism of Sexual and Asexual Blood Stages of the Malaria Parasite Plasmodium Falciparum. *BMC Biol.* 11 (1), 675. doi: 10.1186/1741-7007-11-67
- Mancio-Silva, L., Slavic, K., Grilo Ruivo, M. T., Grosso, A. R., Modrzynska, K. K., Vera, I. M., et al. (2017). Nutrient Sensing Modulates Malaria Parasite Virulence. *Nature* 547 (7662), 213–216. doi: 10.1038/nature23009
- Manco, L., and Abade, A. (2001). Pyruvate Kinase Deficiency: Prevalence of the 1456C→T Mutation in the Portuguese Population. *Clin. Genet.* 60 (6), 472–473. doi: 10.1034/j.1399-0004.2001.600612.x
- Mbanefo, E. C., Ahmed, A. M., Titouna, A., Elmarazy, A., Huyen Trang, N. T., Phuoc Long, N., et al. (2017). Association of Glucose-6-Phosphate Dehydrogenase Deficiency and Malaria: A Systematic Review and Meta-Analysis. *Sci. Rep.* 7 (1), 45963. doi: 10.1038/srep45963
- Mehta, M., Sonawar, H. M., and Sharma, S. (2005). Malaria Parasite-Infected Erythrocytes Inhibit Glucose Utilization in Uninfected Red Cells. *FEBS Lett.* 579 (27), 6151–6158. doi: 10.1016/j.febslet.2005.09.088
- Mehta, M., Sonawar, H. M., and Sharma, S. (2006). Glycolysis in Plasmodium Falciparum Results in Modulation of Host Enzyme Activities. *J. Vector Borne Dis.* 43(3), 95–103.
- Min-Oo, G., Fortin, A., Tam, M.-F., Nantel, A., Stevenson, M. M., and Gros, P. (2003). Pyruvate Kinase Deficiency in Mice Protects Against Malaria. *Nat. Genet.* 35 (4), 357–625. doi: 10.1038/ng1260
- Min-Oo, G., and Gros, P. (2005). Erythrocyte Variants and the Nature of Their Malaria Protective Effect. *Cell Microbiol.* 7 (6), 753–763. doi: 10.1111/j.1462-5822.2005.00524.x
- Oelshlegel, F. J., Sander, B. J., and Brewer, G. J. (1975). Pyruvate Kinase in Malaria Host-Parasite Interaction. *Nature* 255 (5506), 345–347. doi: 10.1038/255345a0
- Oka, H., Tabara, A., Fujisawa, K., Jinnai, M., Nakajima, R., Arai, S., et al. (2008). Babesia Rodhaini: The Protective Effect of Pyruvate Kinase Deficiency in Mice. *Exp. Parasitol.* 120 (3), 290–945. doi: 10.1016/j.exppara.2008.08.008
- Pal Bhowmick, I., Kumar, N., Sharma, S., Coppens, I., and Jarori, G. K. (2009). Plasmodium Falciparum Enolase: Stage-Specific Expression and Sub-Cellular Localization. *Malaria J.* 8 (1), 1795. doi: 10.1186/1475-2875-8-179
- Benton, H. P., Want, E. J., and Ebbels, T. M. D. (2010). Correction of Mass Calibration Gaps in Liquid Chromatography–Mass Spectrometry Metabolomics Data. *Bioinformatics* 26 (19), 2488–2895. doi: 10.1093/bioinformatics/btq441
- Ponce, J., Roth, S., and Harkness, D. R. (1971). Kinetic Studies on the Inhibition of Glycolytic Kinases of Human Erythrocytes by 2,3-Diphosphoglyceric Acid. *Biochim. Biophys. Acta (BBA) - Enzymol.* 250 (1), 63–74. doi: 10.1016/0005-2744(71)90120-3
- Radfar, A., Méndez, D., Moneriz, C., Linares, M., Marín-García, P., Puyet, A., et al. (2009). Synchronous Culture of Plasmodium Falciparum at High Parasitemia Levels. *Nat. Protoc.* 4 (12), 1899–19155. doi: 10.1038/nprot.2009.198
- Roth, E. (1990). Plasmodium Falciparum Carbohydrate Metabolism: A Connection Between Host Cell and Parasite. *Blood Cells* 16 (2–3), 453–460discussion 461–466.
- Roth, E.Jr, Joulin, V., Miwa, S., Yoshida, A., Akatsuka, J., Cohen-Solal, M., et al. (1988). The Use of Enzymopathic Human Red Cells in the Study of Malarial Parasite Glucose Metabolism. *Blood* 71 (5), 1408–1413. doi: 10.1182/blood.V71.5.1408.1408
- Roy, M. K., Cendali, F., Ooyama, G., Gamboni, F., Morton, H., and D'Alessandro, A. (2021). Red Blood Cell Metabolism in Pyruvate Kinase Deficient Patients. *Front. Physiol.* 12 (October), 735543. doi: 10.3389/fphys.2021.735543
- Santos, S. A., Lukens, A. K., Coelho, L., Nogueira, F., Wirth, D. F., Mazitschek, R., et al. (2015). Exploring the 3-Piperidin-4-Yl-1H-Indole Scaffold as a Novel Antimalarial Chemotype. *Eur. J. Med. Chem.* 102 (September), 320–333. doi: 10.1016/j.ejmech.2015.07.047
- Schalkwyk, D.A.v., Priebe, W., and Saliba, K. J. (2008). The Inhibitory Effect of 2-Halo Derivatives of D-Glucose on Glycolysis and on the Proliferation of the Human Malaria Parasite Plasmodium Falciparum. *J. Pharmacol. Exp. Ther.* 327 (2), 511–175. doi: 10.1124/jpet.108.141929
- Simon, C. S., Stürmer, V. S., and Guizetti, J. (2021). How Many Is Enough? - Challenges of Multinucleated Cell Division in Malaria Parasites. *Front. Cell. Infect. Microbiol.* 11 (May), 658616. doi: 10.3389/fcimb.2021.658616
- Smith, C. A., Want, E., O'Maille, G., Abagyan, R., and Siuzdak, G. (2006). XCMS: Processing Mass Spectrometry Data for Metabolite Profiling Using Nonlinear Peak Alignment, Matching, and Identification. *Analytical Chem.* 78 (3), 779–875. doi: 10.1021/ac051437y
- Tautenhahn, R., Böttcher, C., and Neumann, S. (2008). Highly Sensitive Feature Detection for High Resolution LC/MS. *BMC Bioinf.* 9 (1), 5045. doi: 10.1186/1471-2105-9-504
- Tishkoff, S. A., Varkonyi, R., Cahinhan, N., Abbes, S., Argyropoulos, G., Destro-Bisol, G., et al. (2001). Haplotype Diversity and Linkage Disequilibrium at Human G6PD: Recent Origin of Alleles That Confer Malarial Resistance. *Science* 293 (5529), 455–462. doi: 10.1126/science.1061573
- Tomoda, A., Lachant, N. A., Noble, N. A., and Tanaka, K. R. (1983). Inhibition of the Pentose Phosphate Shunt by 2,3-Diphosphoglycerate in Erythrocyte Pyruvate Kinase Deficiency. *Br. J. Haematol.* 54 (3), 475–845. doi: 10.1111/j.1365-2141.1983.tb02122.x
- Trager, W., and Jensen, J. B. (1976). Human Malaria Parasites in Continuous Culture. *Sci. (New York N.Y.)* 193 (4254), 673–675. doi: 10.1126/science.781840
- Waterfall, C. M., and Cobb, B. D. (2001). Single Tube Genotyping of Sickle Cell Anaemia Using PCR-Based SNP Analysis. *Nucleic Acids Res.* 29 (23), e1195. doi: 10.1093/nar/29.23.e119
- Wijk, R.v., and van Solinge, W. W. (2005). The Energy-Less Red Blood Cell Is Lost: Erythrocyte Enzyme Abnormalities of Glycolysis. *Blood* 106 (13), 4034–4425. doi: 10.1182/blood-2005-04-1622
- World Health Organization (2020). *World Malaria Report 2020: 20 Years of Global Progress and Challenges* (Geneva: World Health Organization). Available at: <https://apps.who.int/iris/handle/10665/337660>.
- World Health Organization (2021). *World Malaria Report 2021* (Geneva: World Health Organization). Available at: <https://apps.who.int/iris/handle/10665/350147>.
- Xu, G., van Bruggen, R., Gualtieri, C. O., Moradin, N., Fois, A., Vallerand, D., et al. (2020). Bisphosphoglycerate Mutase Deficiency Protects Against Cerebral Malaria and Severe Malaria-Induced Anemia. *Cell Rep.* 32 (12), 108170. doi: 10.1016/j.celrep.2020.108170

Zerez, C. R., and Tanaka, K. R. (1987). Impaired Nicotinamide Adenine Dinucleotide Synthesis in Pyruvate Kinase- Deficient Human Erythrocytes: A Mechanism for Decreased Total NAD Content and a Possible Secondary Cause of Hemolysis. *Blood* 69 (4), 999–1005. doi: 10.1182/blood.V69.4.999.999

Zumla, A., Rao, M., Wallis, R. S., Kaufmann, S. H. E., Rustomjee, R., Mwaba, P., et al. (2016). Host-Directed Therapies for Infectious Diseases: Current Status, Recent Progress, and Future Prospects. *Lancet Infect. Dis.* 16 (4), e47–e63. doi: 10.1016/S1473-3099(16)00078-5

**Conflict of Interest:** Author JAR was employed by company Clarify Analytical.

The remaining authors declare that the research was conducted in the absence of any commercial or financial relationships that could be construed as a potential conflict of interest.

**Publisher's Note:** All claims expressed in this article are solely those of the authors and do not necessarily represent those of their affiliated organizations, or those of the publisher, the editors and the reviewers. Any product that may be evaluated in this article, or claim that may be made by its manufacturer, is not guaranteed or endorsed by the publisher.

Copyright © 2022 Morais, Medeiros, Carvalho, Morello, Teixeira, Maciel, Nhantumbo, Balau, Rosa, Nogueira, Rodrigues, Carvalho, Antunes and Arez. This is an open-access article distributed under the terms of the Creative Commons Attribution License (CC BY). The use, distribution or reproduction in other forums is permitted, provided the original author(s) and the copyright owner(s) are credited and that the original publication in this journal is cited, in accordance with accepted academic practice. No use, distribution or reproduction is permitted which does not comply with these terms.





# Presence of Phylloquinone in the Intraerythrocytic Stages of *Plasmodium falciparum*

Rodrigo A. C. Sussmann<sup>1,2</sup>, Heloisa B. Gabriel<sup>1</sup>, Alejandro García Ríos<sup>3,4</sup>, Danielle S. Menchaca Vega<sup>1</sup>, Lydia F. Yamaguchi<sup>5</sup>, Antonio Doménech-Carbó<sup>6</sup>, Gerardo Cebrián-Torrejón<sup>7</sup>, Emilia A. Kimura<sup>1</sup>, Massuo J. Kato<sup>5</sup>, Ignasi Bofill Verdaguer<sup>1</sup>, Marcell Crispim<sup>1</sup> and Alejandro M. Katzin<sup>1\*</sup>

<sup>1</sup> Department of Parasitology, Institute of Biomedical Sciences, University of São Paulo, São Paulo, Brazil, <sup>2</sup> Center for Environmental Sciences, Institute of Humanities, Arts and Sciences, Federal University of Southern Bahia, Porto Seguro, Brazil, <sup>3</sup> Laboratory of Environmental Chemistry and Metalopharmaceuticals, Institute of Chemistry at the University of São Paulo, São Paulo, Brazil, <sup>4</sup> Chemistry Program, Universidad del Quindío, Quindío, Colombia, <sup>5</sup> Department of Fundamental Chemistry, Institute of Chemistry, University of São Paulo, São Paulo, Brazil, <sup>6</sup> Departament of Analytic Chemistry, Facultat de Química, Universitat de València, Valencia, Spain, <sup>7</sup> Laboratoire Connaissance et Valorisation Equipes d'Accueil (COVACHIM-M2E EA) 3592, Université des Antilles, Pointe-à-Pitre Cedex, Pointe-à-Pitre, Guadeloupe, France

## OPEN ACCESS

### Edited by:

Vipan Kumar,  
Guru Nanak Dev University, India

### Reviewed by:

Peter Doermann,  
University of Bonn, Germany  
Mithun Rudrapal,  
Rasiklal M. Dhariwal Institute of  
Pharmaceutical Education and  
Research, India

### \*Correspondence:

Alejandro M. Katzin  
amkatzin@icb.usp.br

### Specialty section:

This article was submitted to  
Clinical Microbiology,  
a section of the journal  
Frontiers in Cellular and  
Infection Microbiology

Received: 03 February 2022

Accepted: 21 March 2022

Published: 21 April 2022

### Citation:

Sussmann RAC, Gabriel HB, Ríos AG, Menchaca Vega DS, Yamaguchi LF, Doménech-Carbó A, Cebrián-Torrejón G, Kimura EA, Bofill Verdaguer I, Crispim M, Kato MJ and Katzin AM (2022) Presence of Phylloquinone in the Intraerythrocytic Stages of *Plasmodium falciparum*. *Front. Cell. Infect. Microbiol.* 12:869085. doi: 10.3389/fcimb.2022.869085

Malaria is one of the most widespread parasitic diseases, especially in Africa, Southeast Asia and South America. One of the greatest problems for control of the disease is the emergence of drug resistance, which leads to a need for the development of new antimalarial compounds. The biosynthesis of isoprenoids has been investigated as part of a strategy to identify new targets to obtain new antimalarial drugs. Several isoprenoid quinones, including menaquinone-4 (MK-4/vitamin K2),  $\alpha$ - and  $\gamma$ -tocopherol and ubiquinone (UQ) homologs UQ-8 and UQ-9, were previously detected in *in vitro* cultures of *Plasmodium falciparum* in asexual stages. Herein, we described for the first time the presence of phylloquinone (PK/vitamin K1) in *P. falciparum* and discuss the possible origins of this prenylquinone. While our results in metabolic labeling experiments suggest a biosynthesis of PK prenylation *via* phytyl pyrophosphate (phytyl-PP) with phytol being phosphorylated, on the other hand, exogenous PK attenuated atovaquone effects on parasitic growth and respiration, showing that this metabolite can be transported from extracellular environment and that the mitochondrial electron transport system (ETS) of *P. falciparum* is capable to interact with PK. Although the natural role and origin of PK remains elusive, this work highlights the PK importance in plasmodial metabolism and future studies will be important to elucidate in seeking new targets for antimalarial drugs.

**Keywords:** malaria, plasmodium, isoprenoid, phylloquinone, phytol, phytyl, naphthoquinone, atovaquone

## INTRODUCTION

Malaria is one of the most widespread parasitic diseases, with a high social and economic impact that contributes to poverty in Africa, Southeast Asia and South America (World Health Organization, 2021). In 2020, malaria affected 241 million people and resulted in 627,000 deaths, most of them in Africa, due to *Plasmodium falciparum* infections (World Health Organization,



2021). One of the greatest problems for controlling the disease is the emergence of drug-resistant strains, which demands efforts to discover new antimalarial compounds (World Health Organization, 2021).

One leading drug development strategy is to target plant-like pathways of the parasites involved in the formation of essential compounds. The presence of these pathways results from an endosymbiotic event between a red algae and the apicomplexan phagotrophic ancestor (Janouskovec et al., 2010). Due to this phenomenon, *P. falciparum* possess a non-photosynthetic plastid called apicoplast, which physically and metabolically interacts with mitochondria during the asexual life cycle (van Dooren et al., 2005; Seeber and Soldati-Favre, 2010).

The most studied plant-like biosynthesis pathways in parasites include the shikimate and methylerythritol 4-phosphate (MEP) pathways, which are responsible for chorismate and isoprenoid biosynthesis, respectively (Keeling et al., 1999; Cassera et al., 2004; Seeber and Soldati-Favre, 2010). The MEP pathway provides the basic isoprene unit of five carbons called isopentenyl pyrophosphate (IPP) and its isomer dimethylallyl pyrophosphate (DMAPP). IPP and DMAPP are the simplest isoprene units used by prenyltransferases/synthases to build up all meroterpenes, polyisoprenoids and higher terpenes (Lange et al., 2000). All living organisms produce isoprene chain-based compounds such as geranyl pyrophosphate (GPP, 10 carbons), farnesyl pyrophosphate (FPP, 15 carbons) and geranylgeranyl pyrophosphate (GGPP, 20 carbons) (Ogura et al., 1997). Moreover, compounds with C-20 partially saturated isoprene chains (also known as phytyl pyrophosphate, phytyl-PP) are found in photosynthetic prokaryotes, archaea, and plants (Ischebeck et al., 2006; Sasaki et al., 2011; Meadows et al., 2018). Partially or fully saturated 20-carbon polyisoprenoids can be formed by the hydrogenation of the geranylgeranyl chain attached to chlorophyll intermediates in photosynthetic organisms or directly from geranylgeraniol/GGPP in prokaryotes, archaea and plants (Sasaki et al., 2011; Meadows et al., 2018). This last process is catalyzed by geranylgeranyl reductases (GGRs) dependent on NADH or FADH (Sasaki et al., 2011; Meadows et al., 2018). Moreover, the ability of plants to “recycle” phytol from chlorophyll degradation through its phosphorylation has been described (Ischebeck et al., 2006). Specifically, phytol is phosphorylated to phytyl-phosphate and phytyl-pyrophosphate by the action of kinases dependent on cytidine triphosphate (CTP), guanidine triphosphate (GTP), uridine triphosphate (UTP) or adenine nucleoside triphosphate (ATP) (Ischebeck et al., 2006).

The presence of  $\alpha$ - and  $\gamma$ -tocopherol (vitamin E), phytylated isoprenoid quinones, in *P. falciparum* was previously discovered by our group (Sussmann et al., 2011), as well as the biosynthesis of other isoprenoid quinones such as UQ-8 and 9 (Ellis, 1994) and menaquinone-4 (vitamin K2, MK-4) (Tonhosolo et al., 2010). Tocopherol can be part of the parasitic antioxidant defense since its biosynthesis is stimulated under high oxygen saturation (Sussmann et al., 2017). Regarding vitamin K2, it was demonstrated that mitochondrial NADH dehydrogenase from *P. falciparum* can use MK-4/menadione to oxidize NADH (Dong et al., 2009; Tonhosolo et al., 2010), and the ubiquinone (UQ)/MK-4 pool ratio was reversed when a parasite culture was

maintained under microaerophilic conditions, suggesting that MK-4 has a role in the mitochondrial electron transport system (ETS) (Tonhosolo et al., 2010).

Since the biosynthesis of tocopherol and MK-4 has been described, it was suggested that the biosynthetic pathway for phytyl-PP and the naphthoquinone ring that composes phylloquinone (2-methyl-3-phytyl-1,4-naphthoquinone/PK/vitamin K1) could also be active (Nowicka and Kruk, 2010). Briefly, the classic route for PK biosynthesis in plants requires chorismate, which is provided by the shikimate pathway and then converted to isochorismate by the isochorismate synthase enzyme (MenF, EC number: 5.4.4.2). Isochorismate undergoes six modifications of its aromatic head group up to the first specific metabolite of PK biosynthesis: 2-carboxy-1,4-naphthoquinone, which is phytylated by the enzyme 1,4-dihydroxy-2-naphthoate polyprenyltransferase (MenA; EC number: 2.5.1.130). Finally, a S-adenosyl-L-methionine-dependent methylation is carried out by the enzyme 2-methoxy-6-polyprenyl-1,4-benzoquinol methylase (MenG; EC number: 2.1.1.329).

As part of the group of vitamin K, along with MK-4 and menadione (Nowicka and Kruk, 2010), the well-known function of PK in plants is to act as an electron carrier for oxygenic photosynthesis coupled to photosystem I (PSI) and oxidative folding of photosystem II subunits (Basset et al., 2017). However, recent findings demonstrated an alternative targeting of phylloquinone for transmembrane redox signaling associated with parasitism in nonphotosynthetic holoparasites plants (Xi et al., 2021). The presence of PK in plant membranes suggests the involvement of PK-mediated ETS acting as a redox mediator (Lochner et al., 2003; Xi et al., 2021). Herein, we described the identification of PK in the intraerythrocytic stages of *P. falciparum* and discuss about the probable functions and origins of this molecule in the parasite.

## MATERIALS AND METHODS

### Reagents

Albumax I and RPMI-1640 were purchased from Fisher Scientific® (Leicestershire, UK). All solvents used were HPLC-grade or higher quality and purchased from Sigma-Aldrich (St. Louis, Missouri USA). Radiolabeled isoprenic precursors [1-(n)-<sup>3</sup>H] geranylgeranyl pyrophosphate triammonium salt {[1-(n)-<sup>3</sup>H]-GGPP; 14 Ci/mmol}, [1-(n)-<sup>3</sup>H] phytol (20 Ci/mmol), and {[1-(n)-<sup>3</sup>H] phytyl-PP ([<sup>3</sup>H]-phytyl-PP; 20 Ci/mmol) were obtained from Amersham-Pharmacia Biotech (Buckinghamshire, UK). Adenosyl-L-methionine, S-[methyl-<sup>3</sup>H] ([<sup>3</sup>H]-SAM, 82 Ci/mmol) and [1-(n)-<sup>3</sup>H] FPP triammonium salt ([<sup>3</sup>H]-FPP 23 Ci/mmol) were purchased from Perkin Elmer® (Waltham, Massachusetts, EUA). PK,  $\alpha$ -tocopherol,  $\gamma$ -tocopherol, phytol, phytyl-PP, GGPP, UQ-8, UQ-9 and MK-4 pure standards were purchased from Sigma-Aldrich. Saponin, hypoxanthine, gentamycin sulfate, D-sorbitol, glucose, 4-(2-hydroxyethyl)-1-piperazineethanesulfonic acid (HEPES) and another reagent not cited here were also purchased from Sigma-Aldrich.

## P. falciparum In Vitro Culture

*P. falciparum* clone 3D7 was cultured *in vitro* by the classic culture methodology reported by Trager and Jensen (Trager and Jensen, 1976) employing RPMI-1640 medium completed supplemented with Albumax I (0.5%) in 75 cm<sup>3</sup> cell culture flasks (Radfar et al., 2009). The pH was adjusted to 7.4, and a gas mixture of 5% CO<sub>2</sub>, 5% O<sub>2</sub>, and 90% N<sub>2</sub> was employed. Culture synchronization at ring stages was performed with 5% (w/v) D-sorbitol solution as described by Lambros & Vanderberg (Lambros and Vanderberg, 1979). Parasite development was monitored by Giemsa-stained thin smear microscopy. Blood was leuco-depleted, and PCR (for mycoplasma) and optic microscopy were used to monitor culture contamination (Rowe et al., 1998).

## Metabolic Labeling

Synchronous cultures of *P. falciparum* were labeled at ring stages with 15 µCi/ml [<sup>3</sup>H]-GGPP, [<sup>3</sup>H]-FPP, [<sup>3</sup>H]-phytyl-PP or [<sup>3</sup>H]-phytol or 2.5 µCi/ml [<sup>3</sup>H]-SAM in complete RPMI 1640 medium for 16–18 h. After the labeling period, infected erythrocytes containing late trophozoite or schizont stages were isolated by magnetic separation (see below) or purified discontinuous Percoll® (see below). For all metabolic labeling experiments, approximately 4x10<sup>8</sup> infected erythrocytes were used.

## Isolation of Rings, Trophozoites and Schizonts From Infected Erythrocytes

Cultures at the schizont stage were purified by a magnetic column (MACS separation column, Manual Cell Separation) (Ribaut et al., 2008). Briefly, the column was equilibrated and washed at room temperature with RPMI-1640 complete medium. The culture was centrifuged, and the pellet was suspended in complete culture medium (1:10 v/v) and loaded into the column. Then, the column was washed with RPMI-1640 complete medium, and the retained parasites were collected (Ribaut et al., 2008). Infected red blood cells were centrifuged at 600 x g for 5 min, and the pellet was frozen in liquid nitrogen for further analysis.

Ring (1–20 h after reinvasion), trophozoite (20–30 h after reinvasion) and schizont (30–45 h after reinvasion) forms were purified with a 40/70/80% discontinuous Percoll® gradient (10,000 x g, 30 min, 25°C) (Braun-Breton et al., 1986). In the fraction containing the ring stage and uninfected erythrocytes (80%), parasites were isolated by treatment with 0.1% (w/v) saponin for 5 min followed by two washes with PBS, pH 7.2, at 10,000 x g for 10 min. The fractions containing trophozoite stages or schizont stages were centrifuged at 600 x g for 5 min, and the pellets were frozen in liquid nitrogen for further analysis.

## Isolation of Free Parasites

The parasitophorous vacuole/erythrocyte-free parasites for phytol phosphorylation assays were obtained by saponin lysis (Christophers and Fulton, 1939). For this purpose, erythrocytes were suspended in 30 mL of PBS (30 mM Na<sub>2</sub>HPO<sub>4</sub>, 6 mM KH<sub>2</sub>PO<sub>4</sub>, pH 7.4, 120 mM NaCl) with 2 g/L glucose and 0.2% (v/v) saponin at 4°C and centrifuged at 700 x g for 4°C. The resulting pellet was washed twice in 30 ml of complete cold RPMI-1640

medium. Finally, the pellet was frozen in liquid nitrogen for posterior analysis.

## PK Extraction

Lyophilized infected erythrocytes (1 x 10<sup>10</sup>) were suspended in 4 mL of deionized water in glass tubes. Cell lysis was carried out at 4°C by ultrasonication with 4 pulses of 5 seconds with 10% intensity and 15 second intervals between them. The proteins were precipitated by adding 800 µL of ethanol. After mixing for 1 min, extraction was performed three times with 8 mL of hexane. The sample was shaken for 1 min and centrifuged at 2700 x g for 10 min at 4°C (Ischebeck et al., 2006). The hexane extract of erythrocytes infected with *P. falciparum* was concentrated under nitrogen flow and analyzed by RP-HPLC.

## Phytyl-PP Extraction

The lysis of 1 x 10<sup>10</sup> erythrocytes infected with *P. falciparum* was achieved by sonication as described for PK and phytol extraction. The extraction of phytyl-PP was carried out three times with 6 mL of n-butyl alcohol saturated with water. The solution was centrifuged at 3000 x g for 10 min at 4°C. The n-butyl alcohol phases were combined and evaporated under nitrogen stream and analyzed by TLC.

The samples were dissolved in a small volume of n-butyl alcohol saturated with water and applied on a silica 250-PA TLC plate (Mallinckrodt Baker, Griesheim, Germany). The plate was developed with isopropyl alcohol/ammonia (32%)/H<sub>2</sub>O (6:3:1 v/v). Phytyl-PP was identified by retention factor (R<sub>f</sub>) and coelution with a commercial standard (Ischebeck et al., 2006).

## Phytol Phosphorylation Assay

The methodology for measuring phytol phosphorylation activity in parasite extracts was carried out as previously reported (Ischebeck et al., 2006). Approximately 4x10<sup>9</sup> saponin-purified free schizonts were resuspended in a solution containing 100 mM Tris-HCl buffer, pH 7.5, 1 mM dithiothreitol (DDT); 1 mM MgCl<sub>2</sub>; 1 mM isoascorbate; 1 mM KCl; 0.1% albumin serum; and a protease inhibitor cocktail purchased from Sigma. Then, parasites were successively frozen and thawed 4 times in liquid nitrogen. Subsequently, parasites were lysed three times by 10 second sonications at 30 second intervals. Then, samples were centrifuged at 100,000 x g for 30 min at 4°C (Ischebeck et al., 2006), yielding a membrane fraction (pellet) and a cytoplasmic fraction (supernatant).

Both phases were separated, and 300 µL of reaction buffer was added (50 mM MgCl<sub>2</sub>; 20 mM NaF; 50 mM Tris-HCl, pH 8; 20 mM sodium orthovanate; 1 mM DTT; 50 mM CaCl<sub>2</sub>; 100 pmol [<sup>3</sup>H]-phytol). Finally, ATP, CTP, UTP and GTP were added to a final concentration of 200 mM each. After 30 min incubation at 37°C, the reaction was stopped by adding 300 µL of saturated n-butanol (1:1 v/v). The sample was then vortexed and centrifuged at 10,000 x g for 10 min. The supernatant was collected, and the extraction procedure was repeated twice again by adding the same volume of saturated butanol (1:1 v/v). The three collected supernatants were transferred to a single glass tube and dried under a nitrogen stream. For chromatographic analysis, the

sample was suspended on the RP-HPLC initial mobile phase (system II, see below) using phytol, phytol-P and phytol-PP as internal standards (Ischebeck et al., 2006).

## RP-HPLC Analysis

The stationary phase was a Phenomenex Luna<sup>®</sup> C18 column (250 mm x 4.6 mm x 5  $\mu$ m) (Phenomenex<sup>®</sup>, CA, USA) coupled to a pre-C18 column (Phenomenex<sup>®</sup>, CA, USA). A UV-vis or a 170 diode array detector (DAD) (Gilson<sup>®</sup>, Villiers-le Bel, France) and an FC203B fraction collector were used. The software used for data processing was the Trilution<sup>™</sup> LC 3.0 System Software. Three different elution systems were used to analyze the samples.

**System I:** A linear gradient with methanol (solvent A) and acetonitrile (solvent B) was used at a flow rate of 1 mL/min. The ratio was initially 50% (B), which increased to 70% (B) in 30 min and was then maintained for 20 min. The fractions were collected once per minute. Pure standards of UQ-8, UQ-9, MK-4 and PK were co-injected. As the intraerythrocytic stages of *P. falciparum* biosynthesize UQ-8, UQ-9 and MK-4, the pure standards of these compounds were injected in this system to show that they do not co-elute with PK and tocopherol. UQs were monitored at 290 nm, MK-4 at 270 nm and PK at 245 nm.

**System II:** The system consisted of a linear gradient elution with 25 mM NaHCO<sub>3</sub> (A) and acetonitrile (B). The gradient started at 30% (B) and increased to 0% (B) in 20 min, was maintained for 19 min and returned to initial conditions in two minutes. The flow rate was set at 1 mL/min, the fractions were collected once per minute, and internal standards were monitored at 214 nm.

**System III:** An isocratic system with methanol/ethanol (1:1 v/v) was used at a flow rate of 0.5 mL/min. Samples were collected once per minute. The pure standards of UQ-8, UQ-9 and MK-4 were injected into this system to assess whether they co-eluted with PK and were monitored at the wavelengths described above.

## Gas Chromatography-Mass Spectrometry Analysis

An electron impact gas chromatography-mass spectrometer (GC-MS) with a Trace GC and Y2K ion trap PolarisQ MS System (Finnigan, ThermoQUEST Inc., San Jose, CA) with a data analysis program (Xcalibur version 1.3) was used. The device was equipped with a TR-1MS column (30 m, 0.25 mm, 0.25  $\mu$ m, Thermo Scientific, USA, CA). The injector temperature was set at 220°C, and there was a splitless liner. An oven temperature of 100°C was initially maintained for 2 min and then increased to 300°C at a rate of 25°C/min. The temperature was maintained for 10 min and then reduced to its initial value. The transfer line was maintained at 260°C, and the helium flow was 1.5 mL/min. The MS was operated in positive mode with an ion source at 200°C. The mass range monitored was  $m/z$  40 to 500 (full scan). Vitamin K1 and its derivatives were identified by the ions at  $m/z$  450 for PK (Sussmann et al., 2016),  $m/z$  452 for KH<sub>2</sub> and  $m/z$  480 for methylated hydrophylloquinone.

## LC/MS Analysis

**System I:** The analysis was performed in an LCQ Duo<sup>™</sup> MS (ThermoFinnigan, EUA) coupled with Nano RP-HPLC (LC-Packings, model Ultimate) operated with a flux of 250  $\mu$ L/min. The

solvent was 80% acetonitrile with 0.2% lithium iodide. Electrospray ionization (ESI) was used, and the MS was operated in positive mode with a potential of 4.5 kV and a capillary temperature of 180°C. The mass spectra were processed with Xcalibur<sup>®</sup> 2.0 software (Copyright<sup>©</sup> Thermo Electron Corporation, USA).

**System II:** The analysis was performed with a MicrOTOF-QII MS (Bruker<sup>®</sup>). The equipment was operated in negative mode with capillary voltage of 3500 V, N<sub>2</sub> as a mixture gas at 2 bar, N<sub>2</sub> as a drying gas at 4 L/min and a drying temperature of 180°C. Funnel 1 was an RF funnel with 400 Vpp, a quadrupole energy of 6 eV, collision energy of 12 eV and the hexapole RF was operated at 200 Vpp. In tandem MS (MS/MS), collision energies of 0 to 20 eV were used.

**System III:** The analysis was performed with a High-Resolution LC-QToF - maXis II<sup>™</sup> (Bruker<sup>®</sup>). The column was a Shimadzu XR ODSIII (150x2 mm) with flux 0.2 mL/min. The solvent was 60% acetonitrile and 40% methanol at 40°C.

The equipment was operated with atmospheric pressure chemical ionization (APCI) in positive mode with capillary voltage of 3500 V, N<sub>2</sub> as a mixture gas at 3 bar, N<sub>2</sub> as a drying gas at 4 L/min and a drying temperature of 250°C. Funnel 1 was an RF funnel with 400 Vpp, a quadrupole energy of 7 eV, collision energy of 6 eV and the hexapole RF was operated at 700 Vpp.

Each extract obtained from infected erythrocytes, uninfected erythrocytes and standard were filtered and injected into the LC-QToF equipment. Prior to the injection of the samples, system suitability tests and blanks were carried out between each of them.

## Electrochemical Study

Electrochemical measurements were performed at 298  $\pm$  1 K in a thermostatic cell with CH 660I equipment. A BAS MF2012 glassy carbon working electrode (geometrical area 0.071 cm<sup>2</sup>), a platinum wire auxiliary electrode and an Ag/AgCl (3 M NaCl) reference electrode were used in a conventional three-electrode arrangement. Cyclic and square wave voltammetry (CV and SWV, respectively) were used as detection modes. Eventually, derivative convolution of the data was performed to increase the peak resolution. Thin films of vitamin K1 and lyophilized blood samples were prepared on GCEs following a previously reported procedure (Doménech-Carbó et al., 2013b) by pipetting 10  $\mu$ L of the liquid vitamin or 20  $\mu$ L of a dispersion (1 mg/mL) of blood in ethanol and allowing the solvent to evaporate in air. As a result, a uniform, fine coating of the solid was adhered to the working electrode. Aqueous 0.10 M potassium PBS at physiological pH that had been previously degassed by bubbling argon for 10 min was used as a supporting electrolyte.

## Methylation of Hydrophylloquinone

The stabilization of hydrophylloquinone was achieved by di-O-methylation as described (Sussmann et al., 2016). Briefly, 4x10<sup>8</sup> infected erythrocytes labeled with [<sup>3</sup>H]-phytyl-PP were lysed by ultrasonication in a Branson sonicator at 4°C with three pulses of 5 second duration with 10% potency and 10 second intervals between them. Then, 50 mg of potassium hydroxide and 60  $\mu$ L of methyl iodide (CH<sub>3</sub>I) were added. The reaction was stirred overnight under a nitrogen atmosphere at room temperature in the dark. The reaction mixture was partitioned between water



(2 mL) and dichloromethane ( $3 \times 2$  mL). The organic phase was evaporated under nitrogen stream, and the residue was submitted to RP-HPLC analysis and scintillation counting.

## Atovaquone Rescue Assays

For atovaquone (ATO)  $IC_{50}$  value estimation, parasites were incubated for 48 h in the absence or presence of several concentrations of PK: (i) 0.010  $\mu$ M was used as the first concentration of ATO, which reached 0.000156  $\mu$ M by serial dilution (1:1/vol:vol), and (ii) 5.63  $\mu$ M was used as the first concentration of PK, which reached 0.09  $\mu$ M by serial dilution (1:1/vol:vol). For MK-4  $IC_{50}$  value estimation, parasites were incubated for 48 h in the absence or presence of MK-4; 16  $\mu$ M was the first of several concentrations of MK-4 used.

Assays were performed in 96-well plates starting at 2% parasitemia in the ring stage and 2% hematocrit as described (Desjardins et al., 1979). Parasite growth was monitored after 48 h by SYBR Green I<sup>®</sup> DNA staining (Smilkstein et al., 2004). For this purpose, 100  $\mu$ L of culture was incubated in darkness and at room temperature after adding 100  $\mu$ L of Syber Green I<sup>®</sup> 2/10,000 (v/v) in lysis buffer [20 mM Tris, pH 7.5; 5 mM EDTA; 0.008% saponin (w/v); 0.08% Triton X-100 (v/v)]. After 1 h, fluorescence was measured with a POLARstar Omega fluorometer<sup>®</sup> (BMG Labtech<sup>®</sup>, Ortenberg, Germany) with excitation and emission bands centered at wavelengths of 485 and 530 nm, respectively. Inhibition of parasite growth was analyzed in relation to the logarithm of the concentration using a nonlinear regression (dose-response slope/variable sigmoid equation) by using GraphPad Prism<sup>®</sup> software. Only experiments showing R-squared values ( $R^2$ )  $\geq 0.95$  were accepted. All experiments were performed at least three times with three technical triplicates for each experiment.

## Oxygen Consumption Assays

Oxygen consumption assays were performed in cultures at the trophozoite/young schizont stages (Murphy et al., 1997). Red blood cells were centrifuged at 1500  $\times g$  for 5 min at 4°C and lysed with 30 mL of 0.03% saponin in PBS at 25°C for 5 min. The obtained sample was centrifuged at 1500  $\times g$  for 5 min at 4°C and washed in respiration buffer (125 mM sucrose, 65 mM KCl, 10 mM HEPES-KOH, pH 7.2, 5 mM  $MgCl_2$ , 2 mM  $KH_2PO_4$ , 0.5 mM EGTA). Free parasites were suspended to  $1 \times 10^9$  cells/mL in respiration buffer, and the samples were utilized immediately for oxygen consumption measurements with a high-resolution oxygraph (Oxygraph-2k Oroboros Instruments, Innsbruck, Austria). ATO, PK, carbonyl cyanide-4-(trifluoromethoxy) phenylhydrazone (FCCP) or antimycin A (AntA) additions were performed during the assay as described in the results.

## RESULTS

### Detection of Phylloquinone During the Intraerythrocytic Stages of *P. falciparum*

Radioactive fractions with retention times coincident with the standards  $\alpha$ -tocopherol,  $\gamma$ -tocopherol and phylloquinone (PK) were observed in schizont stages of *P. falciparum* when [<sup>3</sup>H]-phytyl (Figure 1A), [<sup>3</sup>H]-GGPP (Figure 1B), [<sup>3</sup>H]-FPP

(Figure 1C), [<sup>3</sup>H]-SAM (Figure 1D), [<sup>3</sup>H]-phytyl-PP (Figure 4) were used as precursors and analyzed by reverse-phase high-performance liquid chromatography (RP-HPLC) using solvent system I. Using another RP-HPLC method (solvent system III) peaks with retention times coincident with the standards MK-4 and PK in the three stages of intraerythrocytic *P. falciparum* labeled with [<sup>3</sup>H]-GGPP were identified (supplemental data, Figure S1A). The greatest incorporation of the radioactive precursor was detected in the schizont stage. Similar results were found in the schizont stage when [<sup>3</sup>H]-FPP was used as a precursor and samples were analyzed by the system III RP-HPLC method (supplemental data, Figure S1B). The incorporation of [<sup>3</sup>H]-FPP and [<sup>3</sup>H]-GGPP into phytylated quinones suggests that parasites biosynthesize *de novo* phytyl-PP. Moreover, the use of [<sup>3</sup>H]-SAM shows that the probable PK and tocopherols were methylated as expected (Threlfall et al., 1968; Gaudillière et al., 1984).

### Phylloquinone Mass Spectrometry Analysis

The presence of PK in the parasite was confirmed by two methods of mass spectrometry. First, using liquid chromatographic separation and high-resolution mass spectrometry with atmospheric pressure chemical ionization LC-APCI-QToF. Chromatographic signal (Figure 2A) detected at 20.3 min in infected erythrocytes with molecular ion mass  $[M-H]^+$  of  $m/z$  451.3611 Da was only 2.2 ppm different from the signal presented by phylloquinone standard,  $m/z$  451.3601 Da (Figure 2B). Uninfected erythrocytes showed no signal (Figure 2C). Second, using the liquid chromatography/electrospray ionization mass spectrometry (LC/ESI) system I. The molecular ion peaks at  $m/z$  456 and 439 Da corresponded to  $[M + Li]$  and  $[M + Li-H_2O]$ , respectively, considering the molecular formula  $C_{31}H_{46}O_2$  (supplemental data, Figure S2). The fragmentary ions at  $m/z$  204, 221 and 245 Da were identified as the aromatic moieties of PK (supplemental data, Figure S2A). A similar profile was detected in infected erythrocytes ( $1 \times 10^{10}$  parasite extracts) (supplemental data, Figure S2B) but with 3.5-fold higher intensity than the same amounts of uninfected erythrocytes (supplemental data, Figure S2C), comparing peak area and total ion count (TIC) for each sample.

The presence of PK was not detected in 100 mL of lyophilized complete culture medium extracted as described for the parasites (Figure S2D), suggesting that this vitamin is inherent to the complex erythrocyte-parasite. Although vitamin K1 is not biosynthesized by humans, when provided in the diet, it can be transported by plasma lipoproteins and found in the bloodstream (Shearer, 1992; Shearer et al., 2012).

### Electrochemical Study

The structure of PK determined by mass spectrometry was further analyzed by electrochemical studies to confirm its presence and the oxidation state of this compound in infected erythrocytes. The proposed methodology explores the electroactive character of both vitamin K1, which is dominated by a quinone/hydroquinone redox interconversion (Munir et al., 2012; Webster, 2012), and Fe-heme, where the Fe(III)/Fe(II) redox pair has been widely studied (Lexa et al., 1988; Chen et al., 1990; Tieman et al., 1990; Jeon and Bruice, 1992; Sagara et al.,

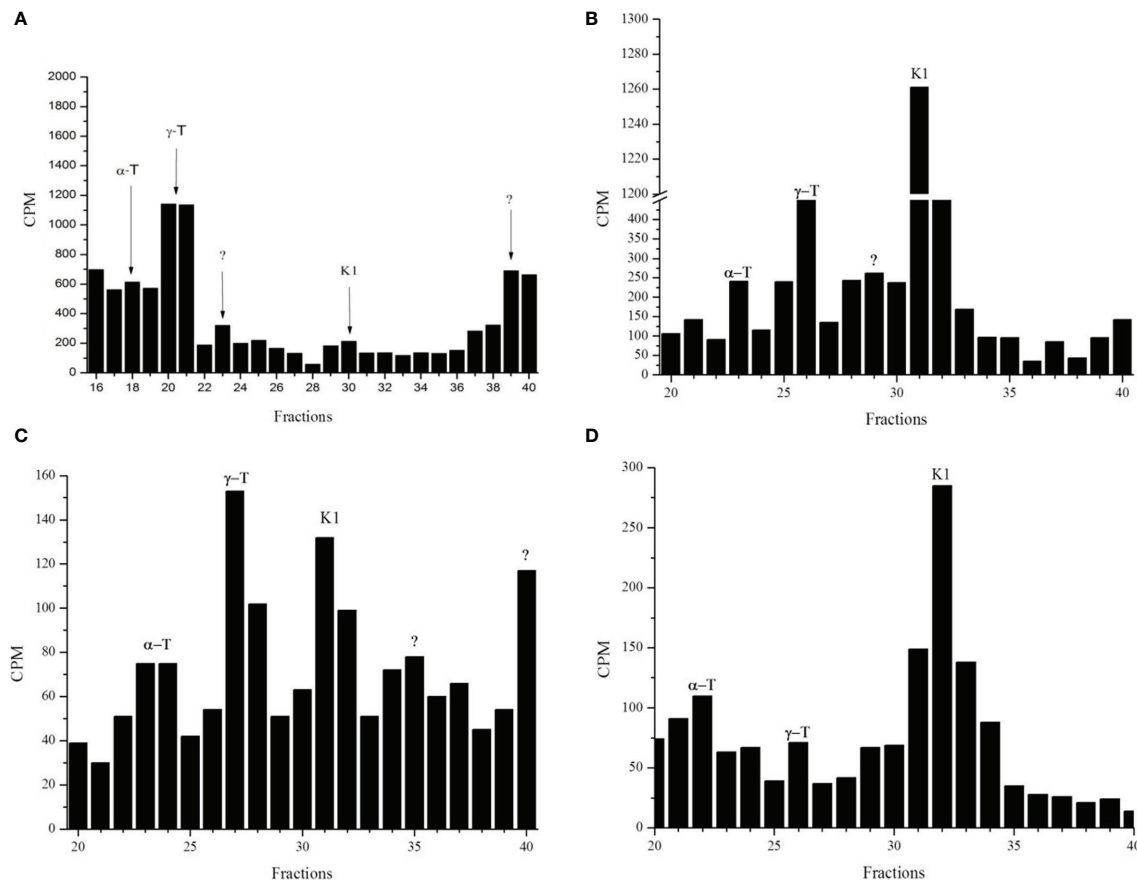


**FIGURE 1** | Radioactive incorporation profile for phyltated quinones in *P. falciparum* in schizont stage. Infected erythrocytes with schizont stages metabolically labeled with  $[^3\text{H}]$ -phytyl (A),  $[^3\text{H}]$ -GGPP (B),  $[^3\text{H}]$ -FPP (C) or  $[^3\text{H}]$ -SAM (D) were subjected to hexane extraction. These extracts were separated by RP-HPLC (System I). Radioactive fractions were coincident with the corresponding standards  $\gamma$ -T ( $\gamma$ -tocopherol),  $\alpha$ -T ( $\alpha$ -tocopherol), K1 (phylloquinone), and “?” (not identified). The experiment was performed three times by using isoprene precursors and twice by using  $[^3\text{H}]$ -SAM.

1998; de Groot et al., 2005). The electrochemistry of vitamin K3 was studied by Zhu and Li (Zhu and Li, 1999). Here, the voltammetry of microparticles (VMP), a technique that enables the determination of the voltammetric response of sparingly soluble solid materials (Doménech-Carbó et al., 2013a), was applied to vitamin K1 films deposited on glassy carbon electrodes (GCEs) and microparticulate deposits of uninfected blood and infected erythrocytes following reported procedures (Doménech-Carbó et al., 2013b).

**Figure 3** compares the square wave voltammetry of vitamin K1, uninfected blood and infected erythrocytes in contact with phosphate-buffered saline (PBS) when the potential is scanned in the negative direction. Vitamin K1 displayed a unique cathodic signal ( $C_1$ ) at  $-0.52$  V (**Figure 3A**), which can be assigned to the proton-assisted reduction of the quinone unit, whereas for uninfected blood, a reduction signal at  $-0.20$  V ( $C_2$ ) was recorded (**Figure 3B**). This signal appears as a single, undifferentiated peak, which can be attributed to the reduction of Fe (III)-heme to Fe(II)-heme. Remarkably, the voltammograms for *P. falciparum*-infected erythrocytes showed both peaks  $C_1$  and  $C_2$  (**Figure 3C**), thus denoting the presence of PK accompanying Fe-heme

to some extent forming a hemoglobin-phylloquinone complex (Zhu and Li, 1999).

When the potential is scanned in the positive direction, the vitamin K1 displays an anodic signal at  $0.0$  V ( $A_1$ ) corresponding to the anodic counterpart of the process  $C_1$ . Similarly, the uninfected erythrocytes (**Figure 3D**) yielded peak  $A_2$  at  $-0.20$  V, corresponding to the reversal of the process  $C_2$ . Remarkably, the voltammogram of the infected erythrocytes (**Figure 3E**) showed overlapping peaks at  $-0.30$  ( $A_3$ ),  $-0.20$  ( $A_2$ ),  $0.00$  ( $A_1$ ) and  $+0.10$  V ( $A_4$ ). Peak  $A_3$  can in principle be attributed to the oxidation of a Fe(II)-heme form differing from the pristine Fe (II)-heme produced in uninfected erythrocytes conceivably the farnesylated species generated by action of *P. falciparum*. However, the multiple anodic peak profile suggests that other reduced species were generated in the infected erythrocytes.

## Methylation of Hydrophylloquinone

To determine whether probable PK *P. falciparum* can be found in the reduced form, schizonts stages were metabolically labeled with  $[^3\text{H}]$ -phytyl-PP. The di-*O*-methylation of hydrophylloquinone was



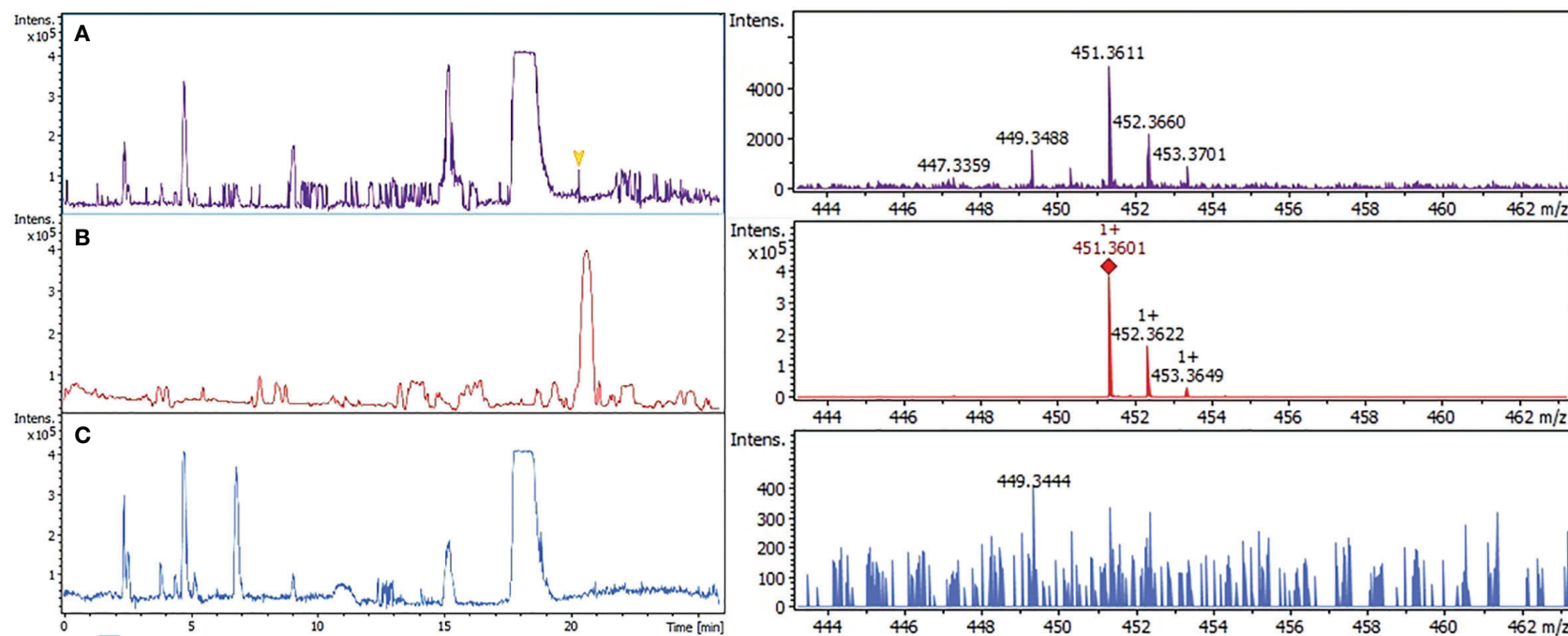


**FIGURE 2 |** Confirmation of phylloquinone by high resolution mass spectrometry (LC-QToF/system III). Three different extracts were analyzed. Infected erythrocytes (A); phylloquinone standard (B); uninfected erythrocytes (C). The signal obtained at 20.3 min of all fractions were compared with their mass spectrum.

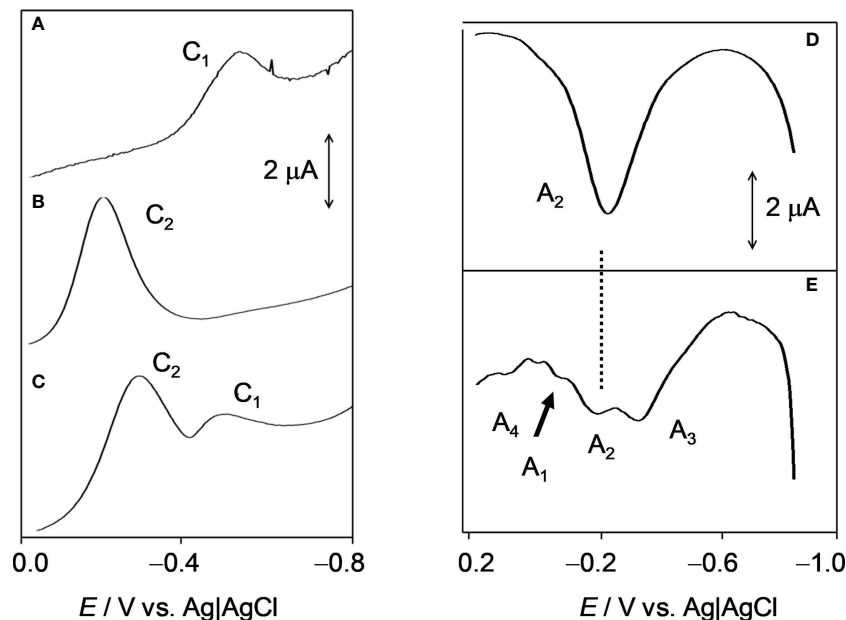


**FIGURE 3** | Square wave voltammetric curves of a vitamin K1 film on a glassy carbon electrode (**A**) and deposits of uninfected blood (**B**) and infected erythrocytes (**C**) on a glassy carbon electrode in contact with 0.10 M phosphate buffer saline at pH 7.4. Potential scan initiated at 0.0 V in the negative direction (potential step increment, 4 mV; square wave amplitude, 25 mV; frequency, 10 Hz). Square wave voltammetric curves of deposits of uninfected (**D**) and *P. falciparum*-infected erythrocytes (**E**) on glassy carbon electrode in contact with 0.10 M PBS at pH 7.4. Potential scan initiated at -0.85 V in the positive direction; potential step increment, 4 mV; square wave amplitude, 25 mV; frequency, 10 Hz. C<sub>1</sub>, C<sub>2</sub>, (A<sub>1</sub>, A<sub>2</sub>, A<sub>3</sub>, A<sub>4</sub>) denote cathodic (anodic) signals corresponding to electrochemical reduction (oxidation) processes described in detail in the text.

performed as previously described to stabilize the compound's redox state (Sussmann et al., 2016). The presence of di-*O*-methylated hydrophyllquinone was confirmed by RP-HPLC using system I. The identity of derivatized hydrophyllquinone was confirmed by gas chromatography/mass spectrometry (GC/MS) analysis as described (Sussmann et al., 2016). The radioactive fractions of the parasites coincide with the  $\alpha$ -tocopherol, methylated hydrophyllquinone and PK standards, but were not detected in uninfected blood, demonstrating that the phytylated molecule is not biosynthesized by erythrocytes (Figure 4).

### Presence of *Phytyl-PP* Intermediate

Once the metabolite, probable PK, was characterized in both redox states in the parasite *P. falciparum*, we further investigate the biosynthesis of the isoprenoid quinone side chain. For this purpose, parasites were labeled with [<sup>3</sup>H]-GGPP as described. Extracts were obtained using the phytyl-PP extraction protocol and analyzed by RP-HPLC system II. The metabolic profile obtained showed radioactive incorporation in fractions containing a phytyl-PP co-injected standard (Figure 5) indicating the formation of phytyl-PP having GGPP as a precursor.

Identification of phytyl-PP in the parasite was also performed by mass spectrometry (HRESIMS). For this purpose, 5 × 10<sup>9</sup> infected and uninfected cells and the corresponding amount (50 mL) of lyophilized complete culture medium were used. The crude extract was submitted to thin-layer chromatography (TLC) purification as described (Ischebeck et al., 2006), and

the bands corresponding to phytyl-PP were scraped, extracted with saturated butanol (1:1 v/v) and analyzed by direct injection into the LC/MS using system II (Figure 6). The phytyl-PP was detected in infected erythrocytes based on the ion at *m/z* 455.2324 Da corresponding to [M-H]<sup>-</sup> with an error of 2 ppm comparing to calculated formulae for C<sub>20</sub>H<sub>42</sub>P<sub>2</sub>O<sub>7</sub> (calc. *m/z* 455.2333 Da) and with the same isotopic profile as the standard. The sodium adduct [M+Na-2H]<sup>-</sup> was also detected.

### Phytol Phosphorylation

Another question we faced was whether parasites could also produce phytyl-PP *via* phytol phosphorylation. For this purpose, we followed the methods of Ischebeck et al. and Valentin et al. in previous studies (Ischebeck et al., 2006; Valentin et al., 2006). The plasmodial phosphorylation of phytol was detected (Figure 7) as described for *Arabidopsis* (Ischebeck et al., 2006; Valentin et al., 2006). Phytol kinase activity requires phosphate donors such as ATP, CTP, UTP, or GTP. In most organisms, various isoprenoid phosphorylation reactions are mediated by CTP (Heller et al., 1992; Inoue et al., 1994; Bentinger et al., 2007).

### Phylloquinone Attenuates Atovaquone Effects on Parasitic Growth and Respiration Rate

The antiplasmodial effect of 0.6 nM atovaquone {ATO, *trans*-2-[4-(4-chlorophenyl) cyclohexyl]-3-hydroxy-1,4-naphthalenedione} was investigated (Figure 8A). After treatment with different

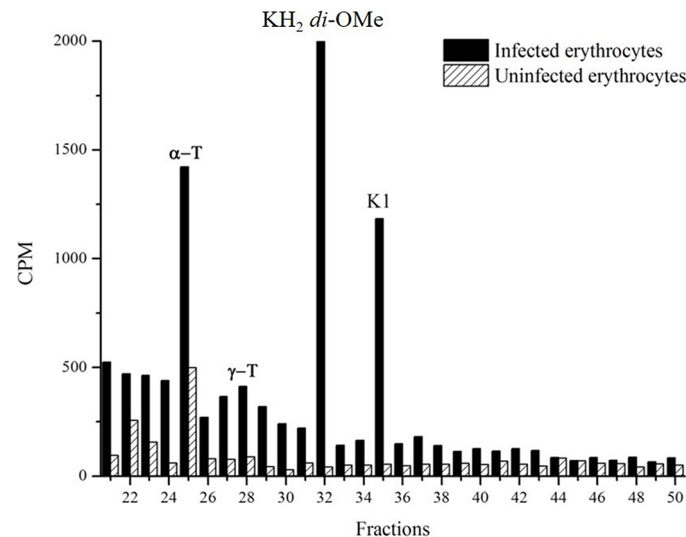


**FIGURE 4** | Detection of methylated hydrophyllquinone. The hydrophyllquinone were stabilized by adding methyl iodide in infected erythrocytes extract labeled with  $[^3\text{H}]$ -phytyl. After the extraction with dichloromethane, samples were analyzed by RP-HPLC (system I). Demonstration of the presence of radioactive fractions coincident with the standards  $\alpha$ -T ( $\alpha$ -tocopherol);  $\gamma$ -T ( $\gamma$ -tocopherol);  $\text{KH}_2$  di-O-Me (methylated hydrophyllquinone) and K1 (phyllquinone). The experiment was performed five times with similar results.

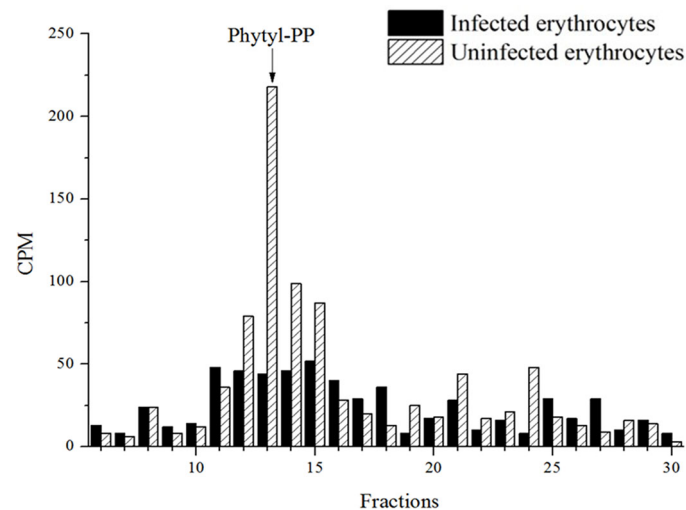


**FIGURE 5** |  $[^3\text{H}]$ -GGPP radioactive incorporation profile for *P. falciparum* and uninfected erythrocytes. Infected erythrocytes with mature forms and uninfected erythrocytes metabolically labeled with  $[^3\text{H}]$ -GGPP were subjected to extraction with n-butyl alcohol saturated with water as described for phytol-PP extraction. The extracts were purified by RP-HPLC (system II). The experiment was performed twice with similar results.

concentrations of PK, the parasite proliferation was recovered. After treatment with  $1.41 \mu\text{M}$  PK, the effect of ATO was almost nullified, with growing rates similar to the control (untreated parasites). With this result, it was decided to expand the experiment by estimating the ATO  $\text{IC}_{50}$  value at different PK concentrations. The interference of PK in the antimalarial effect of ATO was confirmed by treatment with  $2.81$  and  $5.63 \mu\text{M}$  PK, which significantly increased the ATO  $\text{IC}_{50}$  value by 2.6- and 3-fold, respectively (**Figure 8B**). It is

important to note that PK by itself and at the concentrations used in our experiments does not affect parasite proliferation or the oxygen concentrations in the oxygraph (data not shown).

Since a supposed role of MK-4 in the electron transport chain had already been indicated (Tonhosolo et al., 2010), we also tried to perform tests to recover the effect of ATO with this metabolite. However, we found that when administered exogenously, MK-4 had an antimalarial effect, with an  $\text{IC}_{50}$  of

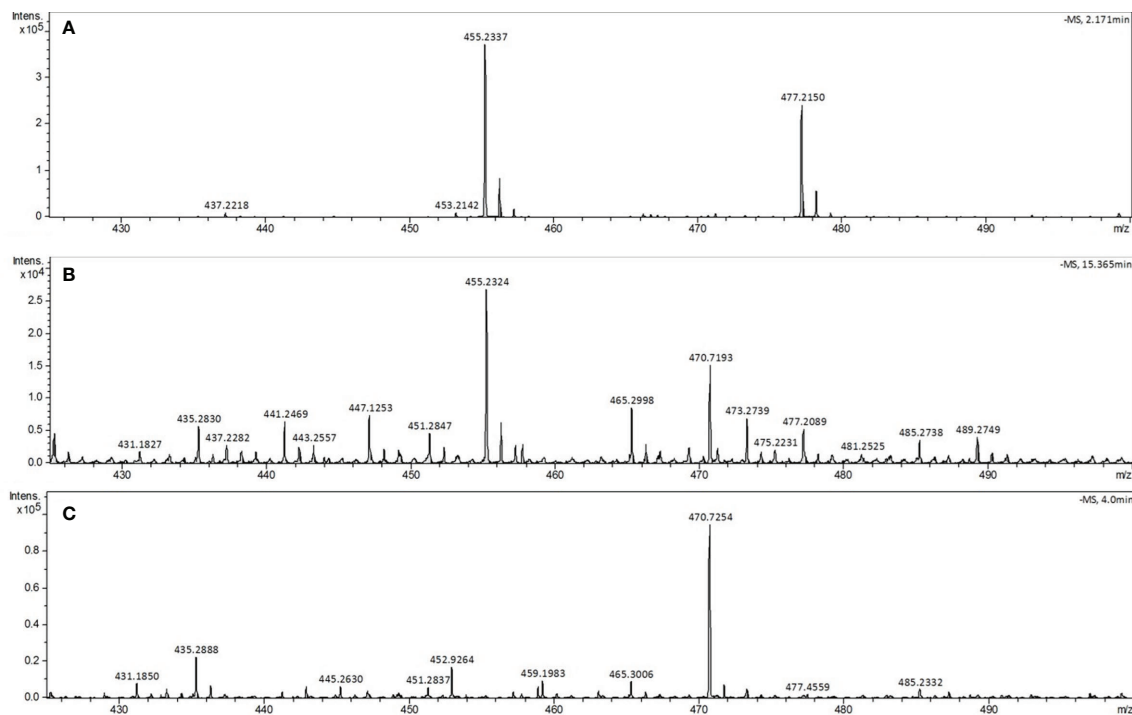


**FIGURE 6** | Analysis of phytol-PP by LC-MS system II. The phytol-PP spectra were obtained from TLC bands recovered from the samples with the same  $R_f$  as the phytol-PP standard. **(A)** Phytol-PP standard, **(B)** infected erythrocytes and **(C)** uninfected erythrocytes. Ions:  $[M] - m/z$  455.2337 and  $[M + Na] - m/z$  477.2150. The experiment was performed twice with similar results.

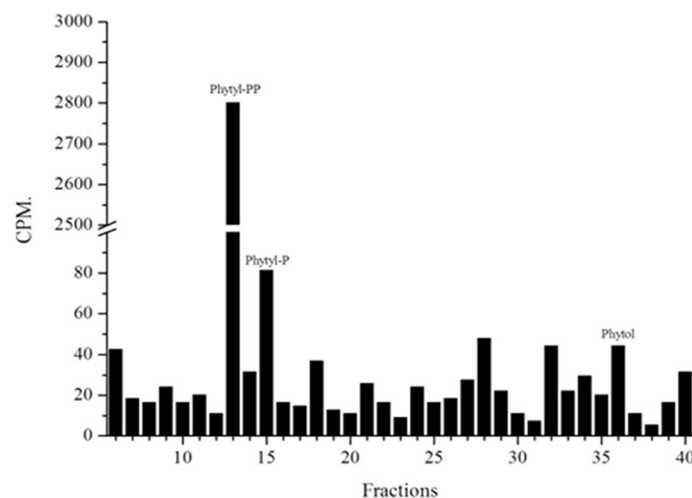
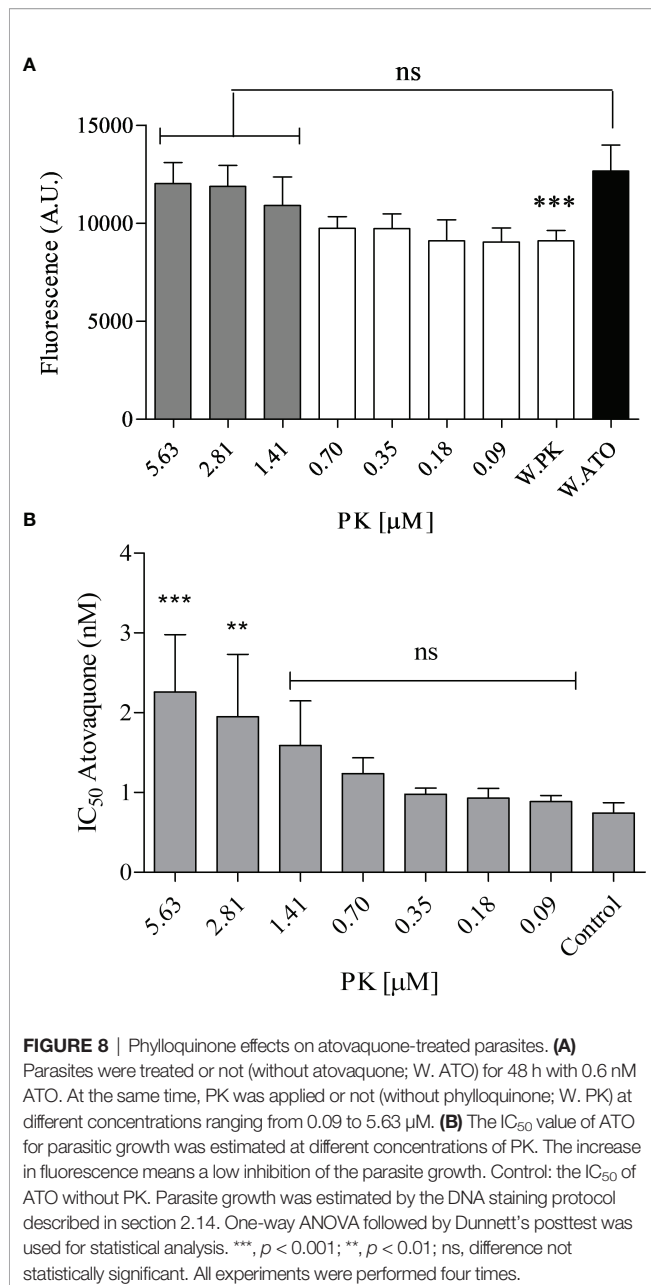


**FIGURE 7** | Phytol phosphorylation assay. Parasitic protein extracts labeled with  $[1-(n-^3H)]$ -phytol were prepared as described and studied by Ischebeck et al. (9) and Valentin et al. (35) and analyzed by RP-HPLC (system II). Extracts rich in parasitic membranes were used. Fractions containing phytol-P, phytol-PP and phytol are indicated.

$1.18 \pm 0.23 \mu\text{M}$  (**Figure S3A**). At  $0.25 \mu\text{M}$  concentration, MK-4 had an antiplasmodial effect; therefore, we used concentrations of 20 and 50 nM for recovery tests. As seen in **Figure S3B**, MK-4 does not recover the antiplasmodial effect of ATO at the

tested concentrations. Since PK attenuated ATO, oxygen consumption assays were used to investigate whether this vitamin could directly interfere with the mechanism of action of ATO *in vitro*.



The rates of  $O_2$  consumption were measured after the addition of erythrocyte-free schizonts and gave the total cellular oxygen consumption rate ( $R'$ ) (**Figure 9A**). The parasites were treated with ATO (up to a final concentration of 1 nM). ATO is an inhibitor of mitochondrial ETS complex III and therefore, as expected, reduced the oxygen consumption. Afterward, PK was titrated up to 30  $\mu$ M. Our results demonstrate that PK triggered an oxygen consumption rate similar to  $R'$  at 20  $\mu$ M and started to decrease the rate at above 30  $\mu$ M (**Figure 9B**). An additional titration with carbonyl cyanide-4-(trifluoromethoxy) phenylhydrazone (FCCP) was performed to obtain the optimum concentration of the protonophore that triggers the maximum oxygen flux/electron transfer through the ETS ( $E/E_T$  capacity). It was verified that at 30–35  $\mu$ M FCCP, the

oxygen consumption slope reached  $E$  (**Figure 9B**), ensuring mitochondrial integrity and proper functioning of all ETS components. Furthermore, after treatment with 50  $\mu$ M antimycin A (AntA), was possible to estimate that approximately 18% of  $R'$  corresponded to residual oxygen consumption (ROX).

## DISCUSSION

The first report of a prenylquinone in *Plasmodium* was made by Skelton et al. (Skelton et al., 1970), who detected UQ homologs in *Plasmodium knowlesi*, *P. cynomolgi* and *P. berghei*. However, they were not able to detect vitamin K in these parasites (Skelton et al., 1970). Only 40 years later the structure and biosynthesis of vitamin K2 (MK-4) were suggested in *P. falciparum* (Tonhosolo et al., 2010). Afterwards, the detection of tocopherol in *P. falciparum* by Sussmann et al. (Sussmann et al., 2011) indicated a source for phytol-PP to the parasite, since it is the isoprene precursor for vitamin E. Therefore, our findings indicate two hypotheses for phylloquinone fate in the parasite: (i) *P. falciparum* possess an active phylloquinone biosynthesis pathway or (ii) *P. falciparum* incorporate phylloquinone from erythrocytes and/or human plasma.

Importantly, *P. falciparum* is not the first organism that could produce different vitamin K homologs with unsaturated and saturated isoprene side chains. Full and partial reduction of the double bonds in the isoprene side chains of several menaquinones (MQs) was previously demonstrated in bacteria and archaea, including *Mycobacterium tuberculosis* (Scholes and King, 1965; Tindall, 1989; Hemmi et al., 2005; Upadhyay et al., 2015). In the parasite, radiolabeled phytol/phytyl incorporation into PK indicates phytylation, but the possibility of enzymatically reducing the MQ-4 side chain cannot be ruled out.

Metabolic labeling with [ $^3H$ ]-GGPP or [ $^3H$ ]-FPP and their incorporation into tocopherols and PK suggests that the parasite would be able to *de novo* biosynthesize the PK side chain. Moreover, incorporation with S-adenosyl-L-[methyl- $^3H$ ] methionine in peaks coinciding with those of the PK suggests the presence of SAM-mediated methylations through PK biosynthesis, which is required for most prenylquinone biosynthesis (Threlfall et al., 1968; Nowicka and Kruk, 2010; Basset et al., 2017; Verdaguer et al., 2019). In addition, when cultures of *P. falciparum* in its intraerythrocytic stages were labeled with [ $^3H$ ]-phytyl, peaks coinciding with those of the PK and tocopherol standards were detected.

The presence of PK in the parasite was confirmed by high-resolution mass spectrometry using chromatographic separation and atmospheric pressure chemical ionization LC-APCI-QToF. The chromatographic signal and the intensity of the fragments and related ions were above the detection limit, allowing unequivocal confirmation of phylloquinone in infected erythrocytes.

The PK in the parasite was also characterized by electrochemistry techniques. Electrochemistry experiments were performed on films of the vitamin K1 standard, uninfected erythrocytes and *P. falciparum*-infected erythrocytes in contact with PBS. Erythrocytes displayed well-defined signals for the Fe(III)-heme/Fe(II)-heme redox couple, whereas vitamin



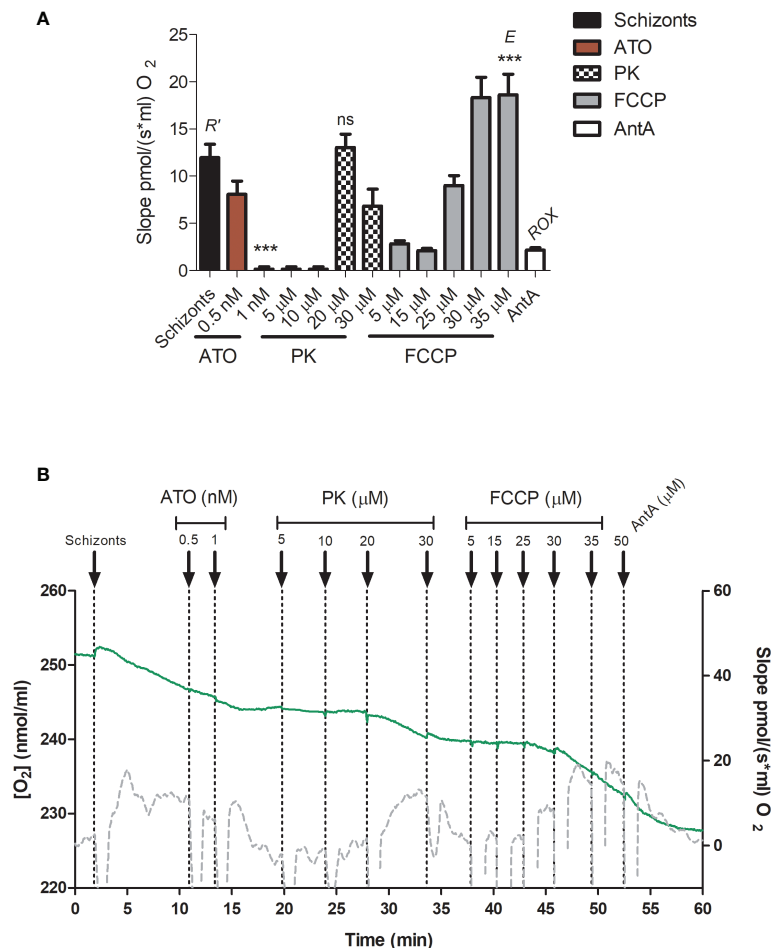


**FIGURE 9 |** Phylloquinone effect on respiration. Oxygen consumption was measured in erythrocyte-free schizonts. **(A)** The respiration slopes obtained under particular treatments are shown. *R'*, total cellular oxygen consumption. ATO, atovaquone 0.5 and 1 nM. PK: phylloquinone 5, 10, 20 and 30 μM. FCCP: carbonyl cyanide p-trifluoro-methoxyphenyl hydrazine (5, 15, 25, 30 and 35 μM. *E*, ET capacity. AntA, Antimycin A (50 μM). ROX, residual oxygen consumption, not related to *R'*. **(B)** Green lines represent the O<sub>2</sub> concentration in an oxygraph chamber as a function of time (left axis). The gray lines indicate the slope variation of oxygen concentration (right axis). As a positive control, the schizonts were maintained in respiratory buffer. One-way ANOVA followed by Dunnett's posttest was used for statistical analysis to compare the values to *R'*. \*\*\*, *p* < 0.001; ns, difference not statistically significant. All experiments were performed three times.

K1 produced signals associated with the interconversion between its oxidized and reduced forms, involving the two-proton, two-electron transfer associated with quinone/catechol motifs. Analysis of such signals confirmed the presence of vitamin K1 in the erythrocytes infected with *P. falciparum*, some of which (5–10%) was in its reduced form. The presence of reduced PK was also confirmed by stabilizing the redox state of prenylquinone through methylations and then detecting it by metabolic labeling techniques (Sussmann et al., 2016).

The most studied function of PK is related to electron transport in photosystem I, but other functions have been suggested, such as oxidative folding of photosystem II subunits (Nowicka and Kruk, 2010); however, this is not the only PK function in plants. For example, PK can also participate in protection from ROS under stress conditions and against pathogen attacks in plants (Collins et al., 1977; Soballe and Poole, 1999; Lochner et al., 2003; Nowicka

and Kruk, 2010; Sogi et al., 2016). Furthermore, some studies indicate that vitamin K, in its reduced form (hydroquinone), acts as an antioxidant in the lipid phase of cells (Fiorentini et al., 1997; Vervoort et al., 1997). Recently, it was demonstrated an alternative targeting of phylloquinone for transmembrane redox signaling associated with parasitism in nonphotosynthetic holoparasites plants (Xi et al., 2021). The presence of PK in plant membranes suggests the involvement of PK-mediated ETS in plant plasma membranes acting as a redox mediator (Lochner et al., 2003). Considering that *P. falciparum* is not a photosynthetic organism, PK should participate in other cellular redox processes.

Therefore, we investigated the effects of PK on mitochondrial ETS. We tested using PK to replace UQ in its classically described function in mitochondrial ETS. It is important to note that ATO is considered an analog of UQ, but the molecule is structurally more related to PK.

ATO is an antimalarial agent (Hudson, 1993) whose mechanism of action is believed to specifically be competing with ubiquinol (UQH<sub>2</sub>) to interact with the mitochondrial bc<sub>1</sub> complex to prevent protozoa from redox-recycling UQ, which is required for dihydroorotate dehydrogenase (DHODH) activity (Painter et al., 2007). Importantly, ATO toxicity is extremely decreased in recombinant parasites because of a DHODH enzyme is not dependent on UQ (Painter et al., 2007), which suggests that the major lethal effects of the compound are caused by the lack of UQ redox regeneration required for pyrimidine biosynthesis. Therefore, soluble UQ analogs can probably rescue the antimalarial effects on parasitic growth by replacing ATO at the mitochondrial bc<sub>1</sub> complex or directly being used by DHODH (Canfield et al., 1995). Similarly, we examined how exogenous addition of 20 μM vitamin K1 can attenuate ATO effects on parasitic growth. In contrast, vitamin K2 does not possess this capacity, at least at the nontoxic concentrations tested here on the nanomolar scale (**Figure S3**). Moreover, PK also effectively restored the parasitic oxygen uptake inhibited by ATO.

All the above-mentioned results suggest that PK can functionally act as an electron carrier for at least DHODH and mitochondrial complex III. In addition to DHODH research, further study is needed to determine whether other cellular dehydrogenases/oxidases can functionally use PK for their activity. For now, it was demonstrated only that mitochondrial NADH dehydrogenase from *P. falciparum* can bind to both MK-4 and menadione *in vitro* (Dong et al., 2009; Tonhosolo et al., 2010). It is important to note that all results presented here were obtained by the addition of exogenous PK; thus, it is unknown whether the prenylquinone involvement in the respiratory process occurs naturally and is involved in other cellular processes. Since ATO was demonstrated to be an excellent antimalarial agent, the biosynthesis of respiratory quinones may be related to its efficacy and resistance phenomena. Therefore, PK and/or UQ biosynthesis inhibitors could be effective drugs for malaria. Moreover, vitamin K1 studies could lead to the development of parasite-specific drugs since their biosynthesis and potential mitochondrial function did not occur in humans (Nowicka and Kruk, 2010; Verdaguer et al., 2019).

In addition to PK eventual involvement in mitochondrial processes, two other functions for prenylquinone in the apicomplexan parasite can be suggested. First, it has been speculated that hydrophylloquinone (**Figure 4**) can participate in the adhesion of infected erythrocytes to capillaries due to the associated coagulation mechanism (Basset et al., 2017). Therefore, the possibility of the parasite biosynthesizing vitamin K1 to promote this process cannot be ruled out. The second possibility is that vitamin K1 could be involved in plasma membrane redox systems, as was described for other similar naphthoquinones identified in *Leishmania donovani* (chlorobiumquinone) and *Entamoeba histolytica* (thermoplasmaquinone) (Fiorentini et al., 1997; Vervoort et al., 1997; Biswas et al., 2008; Nandi et al., 2011). Similar to vitamin K biosynthesis in *Plasmodium*, the formation of chlorobiumquinone and thermoplasmaquinone in protozoa has not been elucidated. In fact, bioinformatics approaches do not

reveal sequences involved in vitamin K biosynthesis in the *L. donovani* and *E. histolytica* genomes (based on information from the EuPathDB database, <https://eupathdb.org/eupathdb/>. Last access: January 2022).

Phylloquinone and tocopherols have different aromatic rings, a chromanol group for tocopherol and a 1,4-naphthoquinone in the case of PK. However, the isoprene side chain derived from phytyl-PP is the same for both prenylquinones. Metabolic techniques were used to demonstrate the incorporation of phytyl-PP, phytol and GGPP into PK. These results are indirect evidence that phytol/phytyl-PP biosynthesis and phytol phosphorylation pathways must be active in the parasite for PK biosynthesis. Therefore, we attempted to directly observe phytol phosphorylation by the parasite, as it occurs in other organisms (Ischebeck et al., 2006; Valentin et al., 2006). A chromatographic study of schizont extracts showed that phytol kinase activity was especially high in parasitic membranes.

Finally, since the parasite supposedly has no chlorophyll, phytol/phytyl-PP are probably obtained through the direct incorporation from extracellular medium or *via* hydrogenation of GGPP/geranylgeraniol, catalyzed by GGRs (Sasaki et al., 2011; Meadows et al., 2018). GGRs are NADPH- or FADH-dependent enzymes already characterized in archaea, algae, plants, cyanobacteria and bacteria (Sasaki et al., 2011; Meadows et al., 2018). Additionally, several *P. falciparum* strains possess a putative polyprenol reductase in their genomic database (PF3D7\_1455900 in *P. falciparum* 3D7; based on information from the PlasmoDB database, [https://plasmodb.org/plasmo/app/record/gene/PF3D7\\_1455900](https://plasmodb.org/plasmo/app/record/gene/PF3D7_1455900). Last access: January 2022). Further studies will be required to better understand the transport of phytol/phytyl-PP and/or the enzymatic hydrogenation of GGPP/geranylgeraniol in the parasite.

Here, we report the first proposal of PK mitochondrial function and the first evidence of PK in the malaria parasite. PK and phytol/phytyl-PP biosynthesis together with the phytol salvage pathway are typical pathways in photosynthetic organisms. Their presence in the parasite could be another consequence of *Plasmodium* evolutionary history, and their study allows us to understand parasite biology. Both pathways are absent from humans, so further confirmatory experiments involving the PK biosynthesis pathway, its biological role, and phytol-PP metabolism as potential drug targets against malaria is suggested.

## DATA AVAILABILITY STATEMENT

The original contributions presented in the study are included in the article/**Supplementary Material**. Further inquiries can be directed to the corresponding author.

## AUTHOR CONTRIBUTIONS

RS and AK designed the study. Experiments were performed by RS, HG, AR, DM, LY, AD-C, GC-T, IB, and MC. RS, HG, AR, DM, LY, AD-C, GC-T, EK, MK, and AK analyzed the data and contributed to interpretation of the data. The first draft of the

manuscript was written by RS. All authors commented and contributed to the article and approved the final version of the manuscript.

## FUNDING

This research was supported by grants from the FAPESP (project 2017/2245-1 AK and 2014/50316-7 MK), CAPES and the CNPq.

## ACKNOWLEDGMENTS

The authors would like to thank William Tadeu Lara Festuccia and Érique de Castro from the Laboratório de Fisiologia

Molecular e Metabolismo in ICB/USP, for providing the platform and helping with oximetry experiments. We also thank S. Wendel (Blood center of Sírío Libanês Hospital, São Paulo, Brazil) for the gift of erythrocytes. RS, HG, IB and MC are fellows funded by the *Fundação de Amparo à Pesquisa do Estado de São Paulo* (FAPESP).

## SUPPLEMENTARY MATERIAL

The Supplementary Material for this article can be found online at: <https://www.frontiersin.org/articles/10.3389/fcimb.2022.869085/full#supplementary-material>

## REFERENCES

- Basset, G. J., Latimer, S., Fatihi, A., Soubeyrand, E., and Block, A. (2017). Phylloquinone (Vitamin K1): Occurrence, Biosynthesis and Functions. *Mini-Rev. Med. Chem.* 17, 1028–38. doi: 10.2174/1389557516666160623082714
- Bentinger, M., Brismar, K., and Dallner, G. (2007). The Antioxidant Role of Coenzyme Q. *Mitochondrion* 7, S41–S50. doi: 10.1016/j.mito.2007.02.006
- Biswas, S., Haque, R., Bhuyan, N. R., and Bera, T. (2008). Participation of Chlorobiumquinone in the Transplasma Membrane Electron Transport System of Leishmania Donovanii Promastigote: Effect of Near-Ultraviolet Light on the Redox Reaction of Plasma Membrane. *Biochim. Biophys. Acta - Gen. Subj.* 1780, 116–127. doi: 10.1016/j.bbagen.2007.09.006
- Braun-Breton, C., Jendoubi, M., Brunet, E., Perrin, L., Scaife, J., and Da Silva, L. P. (1986). In Vivo Time Course of Synthesis and Processing of Major Schizont Membrane Polypeptides in Plasmodium Falciparum. *Mol. Biochem. Parasitol.* 20 (1), 33–43. doi: 10.1016/0166-6851(86)90140-4
- Canfield, C. J., Pudney, M., and Gutteridge, W. E. (1995). Interactions of Atovaquone With Other Antimalarial Drugs Against Plasmodium Falciparum In Vitro. *Exp. Parasitol.* 80, 373–381. doi: 10.1006/expr.1995.1049
- Cassera, M. B., Gozzo, F. C., D’Alexandri, F. L., Merino, E. F., del Portillo, H. A., Peres, V. J., et al. (2004). The Methylerythritol Phosphate Pathway is Functionally Active in All Intraerythrocytic Stages of Plasmodium Falciparum. *J. Biol. Chem.* 279, 51749–51759. doi: 10.1074/jbc.M408360200
- Chen, S.-M., Sun, P.-J., and Oliver Su, Y. (1990). Characterization of Iron Tetrakis (N-Methyl-2-Pyridyl)Porphine in Aqueous Media: Electrochemical Generation of Stable Iron(I), Iron(II), Iron(III) and Iron(IV) Porphyrins at Room Temperature. *J. Electroanal. Chem. Interfacial Electrochem.* 294, 151–164. doi: 10.1016/0022-0728(90)87142-7
- Christophers, S. R., and Fulton, J. D. (1939). Experiments With Isolated Malaria Parasites (Plasmodium Knowlesi) Free From Red Cells. *Ann. Trop. Med. Parasitol.* 33, 161–170. doi: 10.1080/00034983.1939.11685064
- Collins, M. D., Pirouz, T., Goodfellow, M., and Minnikin, D. E. (1977). Distribution of Menaquinones in Actinomycetes and Corynebacteria. *J. Gen. Microbiol.* 100, 221–230. doi: 10.1099/00221287-100-2-221
- de Groot, M. T., Merks, M., Wonders, A. H., and Koper, M. T. M. (2005). Electrochemical Reduction of NO by Hemin Adsorbed at Pyrolytic Graphite. *J. Am. Chem. Soc.* 127, 7579–7586. doi: 10.1021/ja051151a
- Desjardins, R. E., Canfield, C. J., Haynes, J. D., and Chulay, J. D. (1979). Quantitative Assessment of Antimalarial Activity In Vitro by a Semiautomated Microdilution Technique. *Antimicrob. Agents Chemother.* 16 (6), 710–8. doi: 10.1128/AAC.16.6.710
- Doménech-Carbó, A., Labuda, J., and Scholz, F. (2013a). Electroanalytical Chemistry for the Analysis of Solids: Characterization and Classification (IUPAC Technical Report). *Pure Appl. Chem.* 85, 609–631. doi: 10.1351/PAC-REP-11-11-13
- Doménech-Carbó, A., MacLuk, A., Figadère, B., Poupon, E., and Cebrián-Torrejón, G. (2013b). Solid-State Electrochemical Assay of Heme-Binding Molecules for Screening of Drugs With Antimalarial Potential. *Anal. Chem.* 85, 4014–4021. doi: 10.1021/ac303746k
- Dong, C. K. K., Patel, V., Yang, J. C. C., Dvorin, J. D. D., Duraisingh, M. T. T., Clardy, J., et al. (2009). Type II NADH Dehydrogenase of the Respiratory Chain of Plasmodium Falciparum and its Inhibitors. *Bioorg. Med. Chem. Lett.* 19, 972–975. doi: 10.1016/j.bmcl.2008.11.071
- Ellis, J. E. (1994). Coenzyme Q Homologs in Parasitic Protozoa as Targets for Chemotherapeutic Attack. *Parasitol. Today* 10, 296–301. doi: 10.1016/0169-4758(94)90079-5
- Fiorentini, D., Cipollone, M., Galli, M. C., and Landi, L. (1997). Antioxidant Activity of Reduced Menadiol in Solvent Solution and in Model Membranes. *Free Radic. Res* 26(5), 419–29. doi: 10.3109/10715769709084478
- Gaudillière, J. P., d’Harlingue, A., Camara, B., and Monéger, R. (1984). Prenylation and Methylation Reactions in Phylloquinone (Vitamin K1) Synthesis in Capsicum Annuum Plastids. *Plant Cell Rep* 6 (3), 240–2. doi: 10.1007/BF00269302
- Heller, L., Orlean, P., and Adair, W. L. (1992). Saccharomyces Cerevisiae Sec59 Cells are Deficient in Dolichol Kinase Activity (Accessed October 17, 2018).
- Hemmi, H., Takahashi, Y., Shibuya, K., Nakayama, T., and Nishino, T. (2005). Menaquinone-Specific Prenyl Reductase From the Hyperthermophilic Archaeon Archaeoglobus Fulgidus. *J. Bacteriol.* 187 (6), 1937–44. doi: 10.1128/JB.187.6.1937-1944.2005
- Hudson, A. T. (1993). Atovaquone - a Novel Broad-Spectrum Anti-Infective Drug. *Parasitol. Today* 9, 66–68. doi: 10.1016/0169-4758(93)90040-M
- Inoue, H., Korenaga, T., Sagami, H., Koyama, T., and Ogura, K. (1994). Phosphorylation of Farnesol by a Cell-Free System From Botryococcus Braunii. *Biochem. Biophys. Res. Commun.* 200, 1036–1041. doi: 10.1006/bbrc.1994.1554
- Ischebeck, T., Zbierzak, A. M., Kanwischer, M., and Dörmann, P. (2006). A Salvage Pathway for Phytol Metabolism in Arabidopsis. *J. Biol. Chem.* 281, 2470–2477. doi: 10.1074/jbc.M509222200
- Janouskovec, J., Horak, A., Obornik, M., Lukes, J., and Keeling, P. J. (2010). A Common Red Algal Origin of the Apicomplexan, Dinoflagellate, and Heterokont Plastids. *Proc. Natl. Acad. Sci.* 107, 10949–10954. doi: 10.1073/pnas.1003335107
- Jeon, S., and Bruce, T. C. (1992). Redox Chemistry of Water-Soluble Iron, Manganese, and Chromium Metalloporphyrins and Acid-Base Behavior of Their Lyate Axial Ligands in Aqueous Solution: Influence of Electronic Effects. *Inorg. Chem.* 31, 4843–4848. doi: 10.1021/ic00049a023
- Keeling, P. J., Palmer, J. D., Donald, R. G. K. K., Roos, D. S., Waller, R. F., and McFadden, G. I. (1999). Shikimate Pathway in Apicomplexan Parasites. *Nature* 397, 219–220. doi: 10.1038/16618
- Lambros, C., and Vanderberg, J. P. (1979). Synchronization of Plasmodium Falciparum Erythrocytic Stages in Culture. *J. Parasitol.* 65(3), 418–20. doi: 10.2307/3280287
- Lange, B. M., Rujan, T., Martin, W., and Croteau, R. (2000). Isoprenoid Biosynthesis: The Evolution of Two Ancient and Distinct Pathways Across Genomes. *Proc. Natl. Acad. Sci. U. S. A.* 97, 13172–13177. doi: 10.1073/pnas.240454797
- Lexa, D., Saveant, J. M., Binh, S. K., and Wang, D. L. (1988). Single Electron Transfer and Nucleophilic Substitution. Reaction of Alkyl Bromides With

- Aromatic Anion Radicals and Low Oxidation State Iron Porphyrins. *J. Am. Chem. Soc.* 110, 7617–7625. doi: 10.1021/ja00231a006
- Lochner, K., Döring, O., and Böttger, M. (2003). Phylloquinone, What can We Learn From Plants? *BioFactors* 18 (1–4), 73–78. doi: 10.1002/biof.5520180209
- Meadows, C. W., Mingardon, F., Garabedian, B. M., Baidoo, E. E. K., Benites, V. T., Rodrigues, A. V., et al (2018) Discovery of Novel Geranylgeranyl Reductases and Characterization of Their Substrate Promiscuity. *Biotechnol. Biofuels*. 11, 1–17. doi: 10.1186/s13068-018-1342-2
- Munir, S., Shah, A., Zafar, F., Badshah, A., Wang, X., Rehman, Z. U., et al. (2012). Redox Behavior of a Derivative of Vitamin K at a Glassy Carbon Electrode. *J. Electrochem. Soc.* 159, G112–G116. doi: 10.1149/2.032210jes
- Murphy, A. D., Doeller, J. E., Hearn, B., and Lang-Unnasch, N. (1997). Plasmodium Falciparum: Cyanide-Resistant Oxygen Consumption. *Exp. Parasitol* 87, 112–120. doi: 10.1006/expr.1997.4194
- Nandi, N., Bera, T., Kumar, S., Purkait, B., Kumar, A., and Das, P. (2011). Involvement of Thermoplasmaquinone-7 in Transplasma Membrane Electron Transport of Entamoeba Histolytica Trophozoites: A Key Molecule for Future Rational Chemotherapeutic Drug Designing. *J. Bioenerg. Biomembr.* 43, 203–215. doi: 10.1007/s10863-011-9347-6
- Nowicka, B., and Kruk, J. (2010). Occurrence, Biosynthesis and Function of Isoprenoid Quinones. *Biochim. Biophys. Acta - Bioenerg.* 1797, 1587–1605. doi: 10.1016/j.bbabi.2010.06.007
- Ogura, K., Koyama, T., and Sagami, H. (1997). Polyprenyl Diphosphate Synthases. *Subcell. Biochem.* 28, 57–87. doi: 10.1007/978-1-4615-5901-6\_3
- Painter, H. J., Morrissey, J. M., Mather, M. W., and Vaidya, A. B. (2007). Specific Role of Mitochondrial Electron Transport in Blood-Stage Plasmodium Falciparum. *Nature* 446, 88–91. doi: 10.1038/nature05572
- Radfar, A., Méndez, D., Moneriz, C., Linares, M., Marín-García, P., Puyet, A., et al. (2009). Synchronous Culture of Plasmodium Falciparum at High Parasitemia Levels. *Nat. Protoc* 4, 1899–915. doi: 10.1038/nprot.2009.198
- Ribaut, C., Berry, A., Chevalley, S., Reybier, K., Morlais, L., Parzy, D., et al. (2008). Concentration and Purification by Magnetic Separation of the Erythrocytic Stages of All Human Plasmodium Species. *Malar. J.* 7, 1–5. doi: 10.1186/1475-2875-7-45
- Rowe, J. A., Scragg, I. G., Kwiatkowski, D., Ferguson, D. J. P., Carucci, D. J., and Newbold, C. I. (1998). Implications of Mycoplasma Contamination in Plasmodium Falciparum Cultures and Methods for its Detection and Eradication. *Mol. Biochem. Parasitol* 92 (1), 177–80. doi: 10.1016/S0166-6851(97)00237-5
- Sagara, T., Fukuda, M., and Nakashima, N. (1998). Electoreflectance Study of Hemin Adsorbed on a HOPG Electrode: Estimation of Molecular Orientation and Analysis of Nonfaradaic Electoreflectance Signal Due to the Stark Effect. *J. Phys. Chem. B* 102 (15), 2835. doi: 10.1021/jp981160o
- Sasaki, D., Fujihashi, M., Iwata, Y., Murakami, M., Yoshimura, T., Hemmi, H., et al. (2011). Structure and Mutation Analysis of Archaeal Geranylgeranyl Reductase. *J. Mol. Biol.* 409 (4), 543–57. doi: 10.1016/j.jmb.2011.04.002
- Scholes, P. B., and King, H. K. (1965). Isolation of a Naphthaquinone With Partly Hydrogenated Side Chain From Corynebacterium Diphtheriae. *Biochem. J* 97 (3), 766–8. doi: 10.1042/bj0970766
- Seeber, F., and Soldati-Favre, D. (2010). Metabolic Pathways in the Apicoplast of Apicomplexa. *Int. Rev. Cell Mol. Biol* 281, 161–228. doi: 10.1016/S1937-6448(10)81005-6
- Shearer, M. J. (1992). Vitamin K Metabolism and Nutriture. *Blood Rev.* 6, 92–104. doi: 10.1016/0268-960X(92)90011-E
- Shearer, M. J., Fu, X., and Booth, S. L. (2012). Vitamin K Nutrition, Metabolism, and Requirements: Current Concepts and Future Research. *Adv. Nutr.* 3, 182–195. doi: 10.3945/an.111.001800
- Skelton, F. S., Rietz, P. J., and Folkers, K. (1970). Coenzyme Q. CXXII. Identification of Ubiquinone-8 Biosynthesized by Plasmodium Knowlesi, P. Cynomolgi, and P. Berghei. *J. Med. Chem.* 13, 602–606. doi: 10.1021/jm00298a004
- Smilkstein, M., Sriwilaijaroen, N., Kelly, J. X., Wilairat, P., and Riscoe, M. (2004). Simple and Inexpensive Fluorescence-Based Technique for High-Throughput Antimalarial Drug Screening. *Antimicrob. Agents Chemother.* 48, 1803–1806. doi: 10.1128/AAC.48.5.1803-1806.2004
- Soballe, B., and Poole, R. K. (1999). Microbial Ubiquinones: Multiple Roles in Respiration, Gene Regulation and Oxidative Stress Management. *Microbiology* 145, 1817–1830. doi: 10.1099/13500872-145-8-1817
- Sogi, K. M., Holsclaw, C. M., Fragiadakis, G. K., Nomura, D. K., Leary, J. A., and Bertozzi, C. R. (2016). Biosynthesis and Regulation of Sulfomenaquinone, a Metabolite Associated With Virulence in Mycobacterium Tuberculosis. *ACS Infect. Dis.* 2, 800–806. doi: 10.1021/acsinfecdis.6b00106
- Sussmann, R. A. C. C., Angeli, C. B., Peres, V. J., Kimura, E. A., and Katzin, A. M. (2011). Intraerythrocytic Stages of Plasmodium Falciparum Biosynthesize Vitamin E. *FEBS Lett.* 585, 3985–3991. doi: 10.1016/j.febslet.2011.11.005
- Sussmann, R. A. C., de Moraes, M. M., Cebrían-Torrejón, G., Porta, E. O., Doménech-Carbó, A., Yamaguchi, L. F., et al. (2016). Stabilization and Detection of Hydrophyllquinone as Di- O -Methyl Derivative. *J. Chromatogr. B* 1033–1034, 368–371. doi: 10.1016/j.jchromb.2016.09.011
- Sussmann, R. A. C. C., Fotoran, W. L., Kimura, E. A., and Katzin, A. M. (2017). Plasmodium Falciparum Uses Vitamin E to Avoid Oxidative Stress. *Parasites Vectors* 10, 461. doi: 10.1186/s13071-017-2402-3
- Threlfall, D. R., Whistance, G. R., and Goodwin, T. W. (1968). Biosynthesis of Phytoquinones. Incorporation of L-[Me-<sup>14</sup>C,<sup>3</sup>H]Methionine Into Terpenoid Quinones and Chromanols in Maize Shoots. *Biochem. J.* 106, 107–112. doi: 10.1042/bj1060107
- Tieman, R. S., Coury, L. A., Kirchhoff, J. R., and Heineman, W. R. (1990). The Electrochemistry of Hemin in Dimethylsulfoxide. *J. Electroanal. Chem.* 281, 133–145. doi: 10.1016/0022-0728(90)87035-I
- Tindall, B. (1989). Fully Saturated Menaquinones in the Archaeobacterium Pyrobaculum Islandicum. *FEMS Microbiol. Lett* 60, 251–254. doi: 10.1016/0378-1097(89)90405-9
- Tonhosolo, R., Gabriel, H. B., Matsumura, M. Y., Cabral, F. J., Yamamoto, M. M., D’Alexandri, F. L., et al. (2010). Intraerythrocytic Stages of Plasmodium Falciparum Biosynthesize Menaquinone. *FEBS Lett.* 584, 4761–4768. doi: 10.1016/j.febslet.2010.10.055
- Trager, W., and Jensen, J. B. (1976). Human Malaria Parasites in Continuous Culture. *Science* 193, 673–675. doi: 10.1126/science.781840
- Upadhyay, A., Fontes, F. L., Gonzalez-Juarrero, M., McNeil, M. R., Crans, D. C., Jackson, M., et al. (2015). Partial Saturation of Menaquinone in Mycobacterium Tuberculosis: Function and Essentiality of a Novel Reductase, MenJ. *ACS Cent. Sci* 1(6), 292–302. doi: 10.1021/acscentsci.5b00212
- Valentin, H. E., Lincoln, K., Moshiri, F., Jensen, P. K., Qi, Q., Venkatesh, T. V., et al. (2006). The Arabidopsis Vitamin E Pathway Gene5-1 Mutant Reveals a Critical Role for Phytol Kinase in Seed Tocopherol Biosynthesis. *Plant Cell Online* 18, 212–224. doi: 10.1105/tpc.105.037077
- van Dooren, G. G., Marti, M., Tonkin, C. J., Stimmler, L. M., Cowman, A. F., and McFadden, G. I. (2005). Development of the Endoplasmic Reticulum, Mitochondrion and Apicoplast During the Asexual Life Cycle of Plasmodium Falciparum. *Mol. Microbiol.* 57, 405–419. doi: 10.1111/j.1365-2958.2005.04699.x
- Verdaguer, I. B., Zafra, C. A., Crispim, M., Sussmann, R. A. C., Kimura, E. A., and Katzin, A. M. (2019). Prenylquinones in Human Parasitic Protozoa: Biosynthesis, Physiological Functions, and Potential as Chemotherapeutic Targets. *Molecules* 24 (20), 3721. doi: 10.3390/molecules24203721
- Vervoort, L. M. T., Ronden, J. E., and Thijssen, H. H. W. (1997). The Potent Antioxidant Activity of the Vitamin K Cycle in Microsomal Lipid Peroxidation. *Biochem. Pharmacol* 54(8), 871–6. doi: 10.1016/S0006-2952(97)00254-2
- Webster, R. D. (2012). Voltammetry of the Liposoluble Vitamins (A, D, E and K) in Organic Solvents. *Chem. Rec.* 12, 188–200. doi: 10.1002/tcr.201100005
- World Health Organization (2021). *WHO | the World Malaria Report 2021*. Geneva: WHO.
- Xi, G., Ing-Gin, C., Harding, S. A., Nyamdari, B., Ortega, M. A., Clermont, K., et al. (2021). Plasma Membrane Phylloquinone Biosynthesis in Nonphotosynthetic Parasitic Plants. *Plant Physiol.* 185, 1443–1456. doi: 10.1093/plphys/kiab031
- Zhu, Z., and Li, N.-Q. (1999). Electrochemical Studies of Vitamin K3 Interacting With Hemoglobin and Determination of Hemoglobin. *Electroanalysis* 11, 1145–1148. doi: 10.1002/(sici)1521-4109(199911)11:15<1145:aid-elan1145>3.3.co;2-#

**Conflict of Interest:** The authors declare that the research was conducted in the absence of any commercial or financial relationships that could be construed as a potential conflict of interest.

**Publisher’s Note:** All claims expressed in this article are solely those of the authors and do not necessarily represent those of their affiliated organizations, or those of

the publisher, the editors and the reviewers. Any product that may be evaluated in this article, or claim that may be made by its manufacturer, is not guaranteed or endorsed by the publisher.

Copyright © 2022 Sussmann, Gabriel, Ríos, Menchaca Vega, Yamaguchi, Doménech-Carbó, Cebrián-Torrejón, Kimura, Kato, Bofill Verdaguer, Crispim and Katzin. This

*is an open-access article distributed under the terms of the Creative Commons Attribution License (CC BY). The use, distribution or reproduction in other forums is permitted, provided the original author(s) and the copyright owner(s) are credited and that the original publication in this journal is cited, in accordance with accepted academic practice. No use, distribution or reproduction is permitted which does not comply with these terms.*





# An Overview of Mucosa-Associated Protozoa: Challenges in Chemotherapy and Future Perspectives

Helena Lucia Carneiro Santos\* and Karina M. Rebello

Laboratório de Estudos Integrados em Protozoologia, Instituto Oswaldo Cruz, Fundação Oswaldo Cruz (FIOCRUZ), Rio de Janeiro, Brazil

## OPEN ACCESS

### Edited by:

Vipan Kumar,  
Guru Nanak Dev University, India

### Reviewed by:

Shannon Moonah,  
University of Virginia, United States  
M. Guadalupe Ortega-Pierres,  
Instituto Politécnico Nacional de  
México (CINVESTAV),  
Mexico

### \*Correspondence:

Helena Lucia Carneiro Santos  
helenalucias@ioc.fiocruz.br;  
helenalucias@gmail.com

### Specialty section:

This article was submitted to  
Clinical Microbiology,  
a section of the journal  
Frontiers in Cellular and  
Infection Microbiology

**Received:** 22 January 2022

**Accepted:** 29 March 2022

**Published:** 25 April 2022

### Citation:

Santos HLC and Rebello KM  
(2022) An Overview of Mucosa-Associated Protozoa: Challenges in Chemotherapy and Future Perspectives.  
Front. Cell. Infect. Microbiol. 12:860442.  
doi: 10.3389/fcimb.2022.860442

Parasitic infections caused by protozoans that infect the mucosal surfaces are widely neglected worldwide. Collectively, *Entamoeba histolytica*, *Giardia lamblia*, *Cryptosporidium* spp. and *Trichomonas vaginalis* infect more than a billion people in the world, being a public health problem mainly in developing countries. However, the exact incidence and prevalence data depend on the population examined. These parasites ultimately cause pathologies that culminate in liver abscesses, malabsorption syndrome, vaginitis, and urethritis, respectively. Despite this, the antimicrobial agents currently used to treat these diseases are limited and often associated with adverse side effects and refractory cases due to the development of resistant parasites. The paucity of drug treatments, absence of vaccines and increasing problems of drug resistance are major concerns for their control and eradication. Herein, potential candidates are reviewed with the overall aim of determining the knowledge gaps and suggest future perspectives for research. This review focuses on this public health problem and focuses on the progress of drug repositioning as a potential strategy for the treatment of mucosal parasites.

**Keywords:** *Entamoeba histolytica*, *Giardia lamblia*, *Cryptosporidium* spp., *Trichomonas vaginalis*, reinfection, treatment-refractory, repurposed drug

## 1 INTRODUCTION

Pathogenic protozoa associated with mucosal surfaces represent a significant threat to global health and development. Their control and elimination rely on prevention, diagnosis, and effective treatment. Altogether, *Entamoeba histolytica*, *Cryptosporidium* spp., *Giardia intestinalis* (syn. *Giardia lamblia*, *Giardia duodenalis*) contribute significantly to the global burden of gastroenteritis and fit well into the One Health concept (Collaborators, 2017; Shrivastav et al., 2020; Li et al., 2021). In turn, *Trichomonas vaginalis* accounts for one of the most prevalent non-viral sexually transmitted infections (STIs) (Vivancos et al., 2018). However, to a lesser extent, sexual activity that promotes faecal-oral contact can also lead to the transmission of *E. histolytica*, *Cryptosporidium* spp., and *G. intestinalis*. These intestinal infections of interest within the STI scope

pose an important public health challenge and seem to be significantly underestimated (Hung et al., 2012; Escobedo et al., 2014; Billet et al., 2019).

Globally, these mucosa-associated protozoa are one of the leading causes of morbidity and mortality, mainly in areas of intense poverty, in marginal communities of urban centres and rural areas in developing countries (Iyer et al., 2017). The clinical spectrum of diseases produced by these protozoa ranges from asymptomatic (up to 50%) to severe disease, which includes liver abscesses, malabsorption syndrome, vaginitis, and urethritis (Collaborators, 2017; Leung et al., 2019; Li et al., 2021). Moreover, despite a low frequency, trichomoniasis has been implicated in leading to serious adverse effects, such as infertility and cervical cancer (Yang et al., 2018). In pregnancy, *T. vaginalis* is frequently linked with complications, such as premature birth and low birth weight babies (Silver et al., 2014; Leitsch, 2016). While in men, symptomatic infections are rarer (urethritis and prostatitis), but in the long term, trichomoniasis may lead to impaired sperm quality (Mielczarek and Blaszkowska, 2016) and an increased risk of acquisition and transmission of human immunodeficiency virus (HIV) and other STIs (Kissinger and Adamski, 2013; Lazenby et al., 2019) in both sexes.

Remarkably, despite the good and high coverage of sanitary quality, these parasites are still a matter of concern to developed countries (e.g., in European countries and the North American states) (Nisha et al., 2013; Gharpure et al., 2019). The outbreaks seem to be concentrated in the USA, Canada, Australia and the UK (Karanis et al., 2007; Painter et al., 2016). Large outbreaks are associated with treated (disinfected) recreational water venues in the USA. In the last decade, *Cryptosporidium* has emerged as one of the major causes of outbreaks associated with treated aquatic venues. Each year, in the USA, 748,000 cases of cryptosporidiosis (Scallan et al., 2011) and more than 1.2 million cases of *G. intestinalis* are diagnosed (Collier et al., 2021). These parasites are zoonotic agents that are often identified during outbreaks caused by contaminated public water supplies (Nisha et al., 2013; Painter et al., 2015). It is noteworthy that outbreaks of cryptosporidiosis have been related to public drinking water (failures at water treatment facilities), as in the massive Milwaukee cryptosporidiosis outbreak that affected nearly 400,000 people (Mac Kenzie et al., 1994; Efstratiou et al., 2017). However, in some outbreaks, recreational, drinking and fountain waters have been identified as important sources of community infections worldwide (Karanis et al., 2007). As a result, children are more at risk for infection, and cryptosporidiosis is more prevalent in children and immunosuppressed patients. Similarly, children are more likely to have giardiasis and amebiasis than adults (Iyer et al., 2017).

In regard to *T. vaginalis*, in the USA it is one of the most common causes of protozoal infections (Satterwhite et al., 2013; Secor et al., 2014). There were an estimated 2.6 million infections in 2018, and it is also a common cause of symptomatic vaginitis in women (Newman et al., 2015; Hlavsa et al., 2017; Connors et al., 2021). Globally, trichomoniasis mostly affects women between 35 and 40 years of age (Hung et al., 2012; Escobedo et al., 2014).

## 2 TREATMENT AND SIDE EFFECTS

For many years, some pathogenic protozoa parasites associated with mucosal surfaces were considered “neglected infections of poverty”, had low visibility and their studies were unable to attract funding, leading to insufficient development of their diagnosis and treatment options. Currently, they are underdiagnosed, and due to the lack of an effective vaccine, chemotherapy is the only option against these infections.

There are only a small number of drugs available that are effective against these microorganisms. Noteworthy, with different availability across countries, basically two classes of drugs are used in treatment—the nitroimidazole derivatives (MTZ, tinidazole, secnidazole and ornidazole) and benzimidazole derivatives (albendazole and mebendazole), Nitazoxanide, furazolidone, quinacrine, chloroquine and paromomycin. Consequently, rational use of available antiparasitic agents is essential to maintain their usefulness. Although, the cure rate is great, treatment failure can be owing to several factors including noncompliance, resistance and reinfection.

A non-exhaustive list of treatments selected from the literature is depicted in **Table 1**.

Some of the current pharmacological treatments of amebiasis, giardiasis, cryptosporidiosis, and trichomoniasis are discussed in more detail. The most effective and widely used compound is MTZ (a nitroimidazole derivative) that has been the mainstay of protozoan parasite treatment for decades (Leitsch, 2019).

This compound has the ability to reduce and produce nitro radicals in anaerobic microorganisms that inhibit pathogen DNA synthesis (Leitsch, 2019). Events associated with MTZ therapy, such as drug adverse effects or the need for continued dosing past the resolution of disease symptoms, are common (Hernandez Ceruelos et al., 2019). In addition, there is emerging evidence for an increased frequency of therapeutic failure (Leitsch, 2015). In spite of this, the most used medication against these protozoa, except for *Cryptosporidium* spp., is still MTZ. Although its mechanism of action is not fully elucidated, MTZ is activated by thioredoxin reductase and possibly by ferredoxin to generate a nitro-radical anion and a nitroimidazole compound on subsequent reduction. These metabolites compete with the energy metabolism pathway of anaerobic microorganisms, causing toxic effects on trophozoites by inhibiting nucleic acid synthesis, thereby inhibiting protein synthesis and parasite growth (Shrivastav et al., 2020; Weir and Le, 2021). MTZ has been prescribed for over 60 years for luminal and tissue action on *G. intestinalis* and *T. vaginalis*, respectively. Moreover, this drug is currently the standard therapy for treating adults and children with invasive amebiasis. However, treatment for amebiasis is reliant on a single class of agents, the nitroimidazole compounds (Haque et al., 2003). Advantages of MTZ are that it is effective at killing trophozoites, cheap, and can be orally dosed. However, it is unable to kill the infective cyst stage of *E. histolytica* from the colonic lumen, necessitating a multi-drug treatment regimen. Consequently, around 40% of patients treated with MTZ will continue to have parasites in the

**TABLE 1 |** Current treatment options for amoebiasis, giardiasis, cryptosporidiosis and trichomoniasis.

Diseases	Parasite	Drug	References
Amoebiasis	<i>E. histolytica</i>	Nitroimidazoles (Metronidazole, tinidazole, ornidazole, secnidazole), Emetine, Paromomycin Nitazoxanide	(Shirley et al., 2018; Gonzales et al., 2019; Sharma and Ahuja, 2021)
Giardiasis	<i>G. intestinalis</i>	Nitroimidazoles (Mebendazole and Tinidazole) Benzimidazole (Albendazole and Mebendazole) Furazolidone, Paromomycin nitazoxanide	(Morgan et al., 1993; Rossignol, 2010; Kappagoda et al., 2011; Vivancos et al., 2018)
Trichomoniasis	<i>T. vaginalis</i>	Nitroimidazoles (Metronidazole and Tinidazole)	(Gulmezoglu and Garner, 1998; Meites et al., 2015; Sherrard et al., 2018; Workowski et al., 2021)
Cryptosporidiosis	<i>Cryptosporidium</i> spp.	Nitazoxanide	(Rossignol, 2010; Innes et al., 2020)

colonic lumen (Haque et al., 2003) and a second agent (paromomycin or iodoquinol) should be administered to completely clear the remaining trophozoites and cysts from the colonic lumen. Other unwanted side effects include alcohol intolerance and problems with use during pregnancy and lactation (Roe, 1977).

Unfortunately, resistance to MTZ and tinidazole have been reported in *G. intestinalis* and *T. vaginalis* for several decades (Schwebke and Barrientes, 2006; Kirkcaldy et al., 2012; Paulish-Miller et al., 2014; Leitsch, 2015). Several investigations have identified MTZ-resistant *T. vaginalis* strains associated with treatment-refractory vaginal trichomoniasis (Coelho, 1997; Meri et al., 2000; Schmid et al., 2001; Lin et al., 2020). However, nitroimidazole resistance is relative not absolute, ranging from slight to strong. Similar findings were reported for refractory giardiasis due to MTZ resistance in the parasite in both healthy and immunocompromised individuals (Morch et al., 2008; Nabarro et al., 2015; Carter et al., 2018; Lalle and Hanevik, 2018). So far, there is slight evidence for MTZ resistance in *E. histolytica* (Victoria-Hernandez et al., 2020), but a decrease in 5-nitroimidazole susceptibility can be induced experimentally (Wassmann et al., 1999; Iyer et al., 2017). Notoriously, increased drug resistance leads to higher doses used in the treatment and, therefore, more severe side effects (Hernandez Ceruelos (Hernandez Ceruelos et al., 2019). MTZ is generally well tolerated, but unpleasant side effects are often reported. The most common adverse effects are dose dependent, mild and reversible. Among them, common secondary effects of the nitroimidazoles are gastrointestinal tract symptoms, such as nausea, anorexia, vomiting and metallic or bitter taste, dizziness, ataxia and headache (Hernandez Ceruelos et al., 2019; Diptyanusa and Sari, 2021).

It is also important to note that the risk of treatment failure is linked to reinfection, suboptimal drug dose and drug resistance. In particular, *G. intestinalis* could be sequestered in the gallbladder or the pancreatic duct, which promotes treatment failure (Escobedo et al., 2016; Lalle and Hanevik, 2018). In turn, except for *T. vaginalis*, it is hard to make this distinction in an endemic area, because reinfection is frequent related to high environmental contamination by infective cysts/oocysts, in association with precarious sanitation conditions. However, treatment failure must be excluded in the case of a recurrence of symptoms after appropriate therapy.

Nitazoxanide (NTZ) is a nitrothiazole pro-drug that also needs to be reduced at its nitro group to be active. NTZ has

been shown to be a non-competitive inhibitor of the pyruvate: ferredoxin/flavodoxin oxidoreductases (PFORs) of *T. vaginalis*, *E. histolytica* and *G. intestinalis* (Adagu et al., 2002). Protein disulphide isomerases (PDI) have also been identified as potential targets of NTZ activity. In *G. intestinalis*, which expresses PDI variants, PDI2 and PDI4 expression was shown to be significantly downregulated during *in vitro* treatment with NTZ, indicating that the drug is targeting this enzyme (Muller et al., 2007).

In general, the effects of NTZ on the trophozoite ultrastructure of *T. vaginalis*, *E. histolytica* and *G. intestinalis* include cell swelling and distorted cell shape, a redistribution of vacuoles, plasma membrane damage and the formation of extensive empty areas in the cytoplasm of the protozoa (Cedillo-Rivera et al., 2002). Conversely, NTZ is currently the single approved medicine for the treatment of cryptosporidiosis in individuals who have healthy immune systems. It exhibits moderate clinical efficacy in children and immunocompromised individuals, although the treatment of immunosuppressed patients is remarkably difficult, even with higher doses (Abubakar et al., 2007; Amadi et al., 2009). Common side effects may include: nausea, diarrhoea, dry mouth, skin rash, stomach pain, fatigue, headache, and scleral and urine discoloration (Andersson, 1981; Diptyanusa and Sari, 2021).

### 3 PROSPECTS ABOUT OF MUCOSA-ASSOCIATED PROTOZOA INFECTIONS PERSISTENCE: A CHALLENGE AHEAD

Mucosa-associated protozoa infections have distinct characteristics that, when considered together, set them apart from other diseases. Of note, the persistence of infection is linked to several causes, including suboptimal drug concentrations, incomplete treatment regimens, reinfection, an immunocompromised state and drug resistance. Understanding of these factors is, thus, relevant and has been demonstrated. With mass drug administration (MDA), continued campaigns have substantially reduced soil-transmitted helminth (STH) infections in many countries. Albendazole is frequently used in MDA campaigns as a principal control tool for intestinal helminth infections. The collateral benefits of preventive chemotherapy might also affect conditions beyond its originally intended targets, such as enteric protozoa like *G. lamblia*, *E. histolytica*

and *Cryptosporidium* spp. However, the therapeutic regimen of treatment with albendazole is suboptimal for these protozoa and may lead to drug resistance (Quihui-Cota and Morales-Figueroa, 2012; Oliveira et al., 2020), although no surveillance system exists to detect resistance. In Pemba Island, Tanzania, persistent parasitic infection was reported following single-dose albendazole, NTZ and albendazole-nitazoxanide (Speich et al., 2013). Conversely, the rates of *Giardia*, *Cryptosporidium* and *E. histolytica* are high in communities where basic sanitary conditions are unsatisfactory or non-existent; consequently, the frequent episodes of reinfection and protozoan persistence are remarkable in these communities, even after treatment (Fantinatti et al., 2020). In turn, cases of recurrent trichomoniasis are likely to occur due to a lack of adherence to the medication or reinfection from an untreated sexual partner (Sena et al., 2014). However, decreased sensitivity to nitroimidazoles has been identified in 2% to 10% of vaginal trichomoniasis cases (Perez et al., 2001; Schwebke and Barrientes, 2006; Kirkcaldy et al., 2012).

Notably, there are important challenges in the context of these infections. The first challenge is the lack of reliable epidemiological data, which precludes one from estimating the actual burden of pathogenic protozoa associated with mucosal surfaces. However, the heart of this challenge is mainly associated with two (some) factors: a high percentage of asymptomatic individuals and limited tests for diagnosis, which are biased and likely contribute to the epidemiological data underestimating the actual global burden of these diseases (Soares et al., 2020).

The second challenge are factors intrinsic to the host and/or parasite. The complex parasite-host relationship involves multiple mechanisms that have been characterized as one of the most important challenges of these times. Despite being complex and poorly investigated, the existence of one organism within another is not uncommon between protists and bacteria and/or viruses. There is an increasing recognition that endosymbionts in protozoa could influence the outcome of a disease as an eco-evolutionary process, such as drug resistance (Barrow et al., 2020). Parasites infected by viruses modify this relationship, adding more complexity to the system that now becomes tripartite. However, these issues remain largely unknown and evidence is conflicting.

Globally, some strains of *T. vaginalis*, *G. intestinalis*, *E. histolytica*, and *Cryptosporidium* spp. carry endosymbiotic double-stranded RNA (dsRNA) viruses (Banik et al., 2014; Jenkins et al., 2015), which share common characteristics, with uncharted implications to both the human host and protozoa (Fichorova et al., 2012). However, increasing evidence is accumulating that these protozoa harbour different classes of viruses that are absent from humans, but their role in pathogenicity is still poorly understood. Indeed, much of our understanding of viral endosymbionts of mucosa-associated protozoa is based on the *Trichomonasvirus* (TVV), which has been relatively more studied in some details than other protozoa. The TVV is a dsRNA virus that belongs to the Totiviridae family, which was described and characterized in the 1980s and has at least two core proteins, a capsid protein (CP) and an

RNA-dependent RNA polymerase (RdRp). Currently, the TVV has been divided into four distinct viral strains (TVV1, TVV2, TVV3, and TVV4), ranging in size from 4.5 to 5 kbp, based on phylogenetic analyses and comparisons of genomic sequences (Su and Tai, 1996; Liu et al., 1998). The viral genome is never found free in the protozoan cell, and the positive strand viral transcripts synthesized within the viral particle by the CP/RdRp are translocated to the cell cytoplasm to be translated (Barrow et al., 2020). Despite their non-lytic life mode, dsRNA viruses may induce various phenotypic changes that may interfere with the virulence of *T. vaginalis* (Provenzano et al., 1997; Fraga et al., 2012). In the last few years, some studies have reported experimental findings that point toward a positive association between infection and the exacerbation of trichomoniasis symptoms (El-Gayar et al., 2016) while other authors have shown the absence of any correlation (El-Gayar et al., 2016; Graves et al., 2019). Of note, more than one TVV species can coexist in the same *T. vaginalis* cell (Benchimol et al., 2002), and a high percentage of *Trichomonasvirus* in different protozoan isolates have been reported worldwide, ranging from 30% to 100% (Fichorova et al., 2017), which may lead to the discrepancy of the findings. The implications of these co-infections so far are unclear, but evidence has shown that the TVV released from infected *T. vaginalis* cells induced inflammation upon treatment with metronidazole (MTZ) and may suppress host immune activation (Fichorova et al., 2012; Govender et al., 2020). Each viral strain affects different aspects of the parasite. TVV2 and TVV3 infections are strongly enfolded in the upregulation of the protozoan cysteine proteases (Provenzano et al., 1997), which are involved in modulating *T. vaginalis* cytoadherence to human host cells and in the degradation of the basement membrane, human cellular molecules, and secretory IgAs. While, TVV1 and TVV2 are related to the severity of clinical symptoms of trichomoniasis in humans (Fraga et al., 2012). Conversely, one study reported increased MTZ susceptibility in TVV-infected *T. vaginalis* (Malla et al., 2011), while another report observed drug resistance (Snipes et al., 2000). However, additional research is needed to clarify the effect of TVV infection on 5-nitroimidazole resistance in *T. vaginalis*.

Similar to TVV, *Giardiavirus* was first isolated from assemblage A of *G. intestinalis* (Wang and Wang, 1986) as a dsRNA virus and is a member of the family Totiviridae, which specifically infects trophozoites of the parasite *G. intestinalis*. The virus makes capsids that are released from the host to infect other cells, and when a high viral titre is observed, the growth of the parasite is suspended (Marucci et al., 2021). However, unlike *Leishmanivirus* and *Trichomonasvirus*, the *Giardiavirus* does not seem to be linked with the virulence of the parasite (Gomez-Arreaza et al., 2017). Another *Giardiavirus* of the family Totiviridae is *G. canis* virus (GCV) (Cao et al., 2009), which was isolated from the *G. canis* strain. However, it is important to note that knowledge on *Giardiavirus* has unfortunately made little progress in recent years. Similarly, there are few reports on *Cryptosporidium* and *E. histolytica* virus. *Cryspovirus* is a new genus of protozoan viruses in the family Partitiviridae, which infect different species of *Cryptosporidium* oocysts (Nibert et al., 2009).



Although viruses can have complex effects on *Cryptosporidium*, there is so far no well-established information on whether the pathogenicity of parasites is either positively or negatively modulated by *Cryspovirus* infection (Banik et al., 2014; Sharma et al., 2016). Likewise, the presence of virus-like particles in an *E. histolytica* trophozoite has been reported. This virus was described in the 1960s based on electron microscopy studies, which revealed characteristics closely related to Rhabdoviridae (a family of negative-strand RNA viruses) (Ludvik and Shipstone, 1970). Despite being discovered a number of years ago, little was investigated about the viruses involved and their impact on amoebiasis, and no investigation based on clinical perspective has been done (Bird et al., 1974; Banik et al., 2014).

## 4 PARASITE DRUG-RESISTANCE MECHANISMS

The nitroimidazole metronidazole is clearly one of the best-studied drugs affecting intermediary metabolism in *Entamoeba histolytica*, *G. lamblia* and *Trichomonas vaginalis* (Lofmark et al., 2010), but resistance mechanisms against NTZ and albendazole were also investigated. Notoriously, Metronidazole's mechanism of action describes that of the other nitroimidazoles. However, not all mechanisms that reduce susceptibility to the nitroimidazoles have been described. Resistance to metronidazole is complex but appears to be owing to activation of the prodrug to the active nitroso free radical. Laboratory-induced resistant isolates (Upcroft and Upcroft, 1993) is associated with an downregulation of pyruvate:flavodoxin/ferredoxin oxidoreductase (PFOR) activity, a protein absenting in higher eukaryotic cells (Horner et al., 1999). Metronidazole is a prodrug that present an ability to intracellularly reduce to intermediates nitro radical (Sisson et al., 2000) by electrons coming from PFOR (Upcroft and Upcroft, 2001). This radical causes irreversible damage on intracellular structures of parasites. Some enzymatic pathways of *G. lamblia* and *Trichomonas vaginalis*, were identified that are probable to play a function in 5-nitroimidazole reduction, inclusive of the central metabolic enzyme pyruvate:ferredoxin oxidoreductase (PFOR) together with ferredoxin (Townson et al., 1996; Rasoloson et al., 2002; Leitsch et al., 2011) and thioredoxin reductase (TrxR).

In *Giardia*, pyruvate:ferredoxin oxidoreductases (PFORs), *Giardia lamblia* nitroreductase 1 (GLNR1), and thioredoxin reductase (TrxR) are capable to induce the partial reduction reaction that to convert MTZ into toxic metabolites (Nillius et al., 2011; Lalle and Hanevik, 2018).

It is worth to mention that large predictor studies for therapeutic failure are unavailable so far. The resistance slowly induced in laboratory lines could be of a different nature than the rapidly increasing clinical resistance occurred the past decades. Laboratory-induced resistance were obtained from patients several decades ago, most of them belong to the zoonotic assemblage AI, and may not currently represent the main circulating strains (Lalle and Hanevik, 2018). The results

reported from laboratory-induced resistant lines showed a variation in the infectivity and molecular phenotypes, suggesting that multiple molecular resistance phenotypes are possible. However, stability of laboratory-induced resistance is generally lost or reduced after removing the drug. MTZ resistances in clinical isolates from patients were demonstrated in a study reported that some isolates were also less MTZ susceptible when tested in a neonatal mouse model (Lemee et al., 2000). Studies with metronidazole-resistant strains have reported, however, that resistance is not always correlated with reduced POR activity (Leitsch, 2015). A study on resistance of clinical isolates of *T. vaginalis* reported that flavin reductase activity was downregulated (Leitsch et al., 2012), or even absent, in metronidazole-resistant strains. It is important to considerate that flavin reductase can reduce oxygen to hydrogen peroxide (Leitsch et al., 2014), so its downregulation might impair oxygen scavenging, and with activation of nitroimidazoles by either inhibiting drug-activating pathways or by reoxidizing a critical, toxic, nitroradical anion intermediate, consequently reduce metronidazole uptake. Likewise, resistance to metronidazole in *E. histolytica* has been associated with oxidative stress mechanisms, including superoxide dismutase and peroxiredoxin, without a significant decrease of the PFOR activity (Wassmann et al., 1999).

NTZ resistance is thought to be due to altered expression of stress response proteins. An expression study on the NTZ laboratory-induced resistance showed several protein chaperones (Hsp70, Hsp90, and Cpn60), (Leitsch, 2015) and surface antigens to be upregulated in expression (Muller et al., 2008). Levels of PFOR were practically unaltered in nitazoxanide-resistant cell lines (Muller et al., 2007), whereas nitroreductase 1 was found downregulated (Nillius et al., 2011). It is important to point out that resistance to NTZ has been reported not only on experimentally induced resistant strains, but also in clinical isolates (Lemee et al., 2000; Reyes-Vivas et al., 2014).

Benzimidazole affect the microtubules assembly, and induction of oxidative stress may also play a role in the antiparasitic mechanism. Albendazole resistance in *Giardia* is correlated with cytoskeletal changes (Upcroft et al., 1996), in the particular emphasis on the median body. Moreover, resistance has been attributable mutation in the beta-giardin gene, leading in amino acid changes have also been associated with reduced susceptibility to albendazole (Jimenez-Cardoso et al., 2009). However, treatment failure has also been reported for ABZ either administered alone or in combination with MTZ. The higher levels of efficacy with albendazole require multiple doses.

In fact, given their significant impact on human health and infections of mucosa-associated protozoa being difficult to eradicate, it is necessary to focus on finding preventive and curative therapeutics to control their spread. Thereby, there is an urgent need to develop new therapeutic options that will help fight resistance and increase effectiveness. However, a great barrier is the high costs associated with developing a new drug and low economic returns (Dimasi et al., 2003). In recent years, one alternative approach for lowering the costs of drug discovery



and development for these diseases is to repurpose drugs developed for other indications (Ashburn and Thor, 2004; Jourdan et al., 2020). It is an alternative viable to the identification of a new indication for a known drug or compound with previously established preclinical studies or clinical data can significantly decrease the overall cost and reduce the time required to bring a drug to market (Muller and Hemphill, 2013).

Recent strategies for the development of drugs in the context of these mucosa-associated parasitic protozoa will be discussed in the next section.

## 5 RECENT APPROACHES TO DRUG DEVELOPMENT

Over the past six decades, the lack of financial incentives has strongly reduced efforts to develop effective treatments. Because of this, new drugs are urgently required for parasitic protozoan infections, and repurposing drugs is a promising approach for the drug development process, a rapid mode and reduces cost. The discovery of new uses for approved drugs has the potential to identify and reveal new targets that aim to maximize the pre-existing preclinical and clinical knowledge accumulated on registered drugs for a new indication outside the scope of its original indication. Thus, it opens a promising avenue for identifying targets for treatment.

Nevertheless, the treatment of parasitic diseases is often complex, owing to the multiple life stages of parasites with differing sensitivities to chemical agents. High-throughput screens of repurposed drug libraries have been used to the screening of drugs for *E. histolytica*, *G. intestinalis*, *Cryptosporidium* spp. and *T. vaginalis*, and some of these compounds are shown below. However, one of the available practical approaches to find novel potential candidates with antiprotozoal activity are FDA-approved drugs, which is an attractive way to identify new drugs.

### 5.1 Advances in Research for Novel Anti-*Giardia* Activity Agents and FDA-Approved Drugs

#### 5.1.1 Fumagilin

This is an antibiotic compound isolated from *Aspergillus fumigatus*, and its efficacy has been demonstrated in the treatment of diarrheal disease caused by *Microsporidia* spp. (Goodgame, 2003; Agholi et al., 2013). Similarly, fumagillin also showed activity against *Giardia* assemblages A and B at submicromolar concentrations in the mouse giardiasis model. The anti-giardiasis properties of fumagilin have exhibited effectiveness, even against *in vitro* MTZ resistance, and the *in vivo* animal model was superior to MTZ, being a promising drug candidate for the treatment of giardiasis (Kulakova et al., 2014).

#### 5.1.2 Proton Pump Inhibitors

PPIs are a class of medications widely used for the treatment of gastroesophageal reflux disease and other acid-related disorders. Repurposing of PPIs, such as omeprazole, is effective *in vitro* against

*G. lamblia*, and the toxic activity is associated with the inhibition of triosephosphate isomerase (*GLTIM*), which is a key enzyme in glucose and glycogen metabolism of the parasite (Reyes-Vivas et al., 2014; Lopez-Velazquez et al., 2019). Hernández-Ochoa and colleagues (2017) described two novel PPI derivatives, named BHO2 and BHO3, that showed better anti-giardiasis activity than omeprazole in micromolar concentrations, without a cytotoxic effect on mammal cell cultures (Hernandez-Ochoa et al., 2017; Hernandez-Ochoa et al., 2020).

#### 5.1.3 Tetrahydrolipstatin (orlistat)

This is a specific lipase inhibitor derived from lipstatin, which is a lipid produced by *Streptomyces toxytricini* used in the treatment of obesity. Hahn and colleagues (2013) showed experimentally that orlistat inhibited *in vitro* growth of *G. duodenalis* at low micromolar concentrations compared to that of the standard drug MTZ (Hahn et al., 2013).

#### 5.1.4 Spiro Compounds of Isatin

Spiro compounds represent an important class of a small and versatile organic molecule that are known to exhibit versatile biological properties. *In vitro* test of 1*H*-1,2,3-triazole and  $\beta$ -amino-alcohol tethered isatin- $\beta$ -lactam conjugates displayed anti-*T. vaginalis* activity (Nisha et al., 2013). Also, 1*H*-1,2,3-triazole-tethered isatin-MTZ conjugates also exhibited activity *in vitro* against *T. vaginalis*, *E. histolytica*, and *G. lamblia* in submicromolar concentrations (Kumar et al., 2018).

#### 5.1.5 Auranofin

The gold(I) complex auranofin was approved by the FDA in 1985 as an oral anti-arthritis agent (used in the treatment of rheumatoid arthritis) was shown to be effective against MTZ-resistant *Giardia*, and auranofin has now progressed into clinical trials (Capparelli et al., 2017).

#### 5.1.6 Disulfiram

This drug blocks an enzyme that is involved in metabolizing alcohol. It is an inhibitor of acetaldehyde dehydrogenase, which is used to support the treatment of alcohol use disorder. It also acts as a cysteine modifying agent. The anti-giardiasis activity of disulfiram has shown to be effective against *G. lamblia* trophozoites *in vitro* and in a murine model of giardiasis. Interestingly, the drug has been demonstrated to be more than 2–4 times active against MTZ-resistant than MTZ-sensitive (WB and GS/B) parasites (Kulakova et al., 2014). This drug may act as a novel inactivator of *G. lamblia* triosephosphate isomerase (the endogenous activity and carbamate kinase *in vitro*), which demonstrates that its giardicidal effect may involve the inactivation of more than a single enzyme, increasing its potential as an anti-giardial drug (Castillo-Villanueva et al., 2017).

### 5.2 Advances in Research for Novel Anti-*Entamoeba histolytica* Activity Agents and FDA-Approved Drugs

#### 5.2.1 Antineoplastic Kinase Inhibitors

Recently, antineoplastic kinase inhibitors have emerged as potent amebicidal drugs for amebiasis. The drugs tested

were able to kill *E. histolytica* trophozoites as quickly as MTZ. Moreover, one of these drugs (ibrutinib) also exhibited both amebicidal and cysticidal properties, in contrast to all the drugs currently used in the therapeutic strategy (Sauvey et al., 2021).

### 5.2.2 Rabeprazole

The thioredoxin system catalyses several redox reactions essential in maintaining a variety of important biological functions in the *Entamoeba*. It is considered a fundamental enzyme system (reducing the redox system and detoxifying the intracellular oxygen) for *E. histolytica* survival under both aerobic *in vitro* and *in vivo* conditions. Consequently, the TrxR/Trx system is an excellent target for antiamebic drug. Rabeprazole (RB), a drug widely used to treat heartburn, is able to inhibit the EhTrxR recombinant enzyme, amebic proliferation and several functions required for parasite virulence, such as cytotoxicity, oxygen reduction to hydrogen peroxide, erythrophagocytosis, proteolysis, and oxygen and complement resistances (Martinez-Perez et al., 2020).

### 5.2.3 Pencolide

It is a fungal secondary metabolite that shows cysteine deprivation-dependent antiamebic activity. This compound targets cysteine synthase, which is essential for the proliferation and antioxidative defence of *E. histolytica* trophozoites, and is implicated in various important biological processes, including attachment, motility, proliferation, and antioxidative defence (Mori et al., 2018).

### 5.2.4 Anisomycin and Prodigiosin

Anisomycin, an antibiotic isolated from *Streptomyces*, and prodigiosin, a natural red water-insoluble pigment isolated from *Serratia marcescens*, have already shown therapeutic effects over 50 years ago to treat amebiasis in small cohorts (Gonzalez Constandse, 1956; Ehrenkaufer et al., 2018). Ehrenkaufer and coworkers recently performed a screen of repurposed compounds against *E. histolytica*, anisomycin and prodigiosin were both able to kill MTZ-resistant parasites, while prodigiosin was active against mature cysts (Ehrenkaufer et al., 2018). This is the first compound showing efficacy against the dormant cyst form, which is highly resistant to environmental stresses and to the major drug used to treat amebiasis (MTZ).

Importantly, obatoclax an analogue of prodigiosin, which has been used in human clinical trials, had significant activity against both trophozoites and cysts. Development of this molecule as a therapeutic may be possible, given the established safety record in patients (Ehrenkaufer et al., 2020).

### 5.2.5 Auranofin

It is a gold-containing compound originally developed to treat rheumatoid arthritis that showed antiparasitic activity against *E. histolytica* (Debnath et al., 2013; Andrade and Reed, 2015). This compound targets the thioredoxin reductase in *E. histolytica*, thereby making the parasite sensitive to oxidative stress (Debnath et al., 2012). It also showed 10-fold better activity against *E. histolytica* than the standard drug MTZ.

Unsurprisingly, auranofin was equally active against *G. lamblia*, both in *in vitro* and *in vivo* studies (Debnath et al., 2013; Tejman-Yarden et al., 2013), indicating the possibility of its use for a more general treatment of protozoan parasites. However, it presented side effects, such as abdominal pain, nausea, anaemia, and elevated liver enzymes, and its use is prohibited during pregnancy.

### 5.2.6 Disulfiram

This drug is an inexpensive orally administered drug used in the treatment of chronic alcoholism. It is rapidly metabolized to diethyldithiocarbamate (ditiocarb, DTC), which in the presence of zinc forms zinc diethyldithiocarbamate (ZnDTC). Gosh and colleagues demonstrated that the ZnDTC complex has a high *in vivo* activity against *E. histolytica* parasites (Ghosh et al., 2020). This metabolite of disulfiram showed the ability to inhibit COP9 signalosome, a critical upstream regulator of parasite protein degradation (Ghosh et al., 2020; Shirley et al., 2021).

## 5.3 Advances in Research for Novel Anti-*T. vaginalis* Activity Agents and FDA-Approved Drugs

### 5.3.1 Ixazomib and Carmaphycin-17

The proteasome is a multicatalytic proteinase complex, and proteasome inhibitors have also been shown to be toxic for other pathogens and useful in parasitic treatment (Khare et al., 2016). O'Donoghue and colleagues (2019) validated the proteasome as a drug target for the development of a novel class of trichomonacidal agents (O'Donoghue et al., 2019). They showed experimentally that two clinically approved anticancer drugs, ixazomib and carmaphycin-17 (CP-17), were active against vaginal trichomonad infections. In addition, CP-17 was able to overcome MTZ resistance in *T. vaginalis* and had significant *in vitro* and *in vivo* efficacy against trichomonads (O'Donoghue et al., 2019).

### 5.3.2 Benznidazole

In silico analyses classified 20 compounds as potentially active against *T. vaginalis*. From these, ipronidazole, dimetridazole and NTZ showed the highest cytotoxic activity superior to MTZ and secnidazole, respectively. Besides, the *in vivo* assay revealed similar activity for benznidazole and MTZ, suggesting the former as a novel alternative in antitrichomonal therapy (Meneses-Marcel et al., 2018).

### 5.3.3 Disulfiram

The antiprotozoal activities of disulfiram have been studied over the past decade. Disulfiram, when complexed to divalent metal ions (such as zinc) has been demonstrated as an anti-parasitic agent against protozoan parasites *Trypanosoma*, *Leishmania*, *Giardia* and *E. histolytica*. It also appears to be similarly effective against *T. vaginalis*.

This drug has shown antitrichomonal activity, and its metabolite, ditiocarb, has been shown to be more effective than MTZ against both sensitive and resistant trichomonads (Bouma et al., 1998).

## 5.4 Advances in Research for Novel Anti-*Cryptosporidium* Activity Agents and FDA-Approved Drugs

### 5.4.1 FDA-Approved Drugs Phenotypic Screen

Even though promising targets and lead compounds have been identified, robust therapies to eliminate parasites are still lacking. Some of them (paromomycin, clarithromycin, azithromycin, rifaximin, rifabutin, and roxithromycin) (Shrivastava et al., 2017) have demonstrated limited potential when used in animal models, and all were ineffective in controlled trials in AIDS patients. Also, preclinical activity with miltefosine (originally developed as an anticancer drug) and clofazimine (leprosy drug) has been demonstrated, which had no efficacy in phase II studies in AIDS patients (Gavrilov, 1989; Croft et al., 2003; Sinkala et al., 2011; Huston, 2021).

Indeed, activity against an organism found by *in vitro* screening does not necessarily correlate to *in vivo* activity. Moreover, several aspects might explain unsuccessful drug discovery. One of the major bottlenecks to the development of specific anticryptosporidial drugs is the unavailability of a reproducible axenic *in vitro* culture system for *Cryptosporidium* spp., as well as being unable to genetically manipulate the organism.

The genomes of parasites have shown a limited biosynthetic capability that may be targets to identify promising new chemical entities. For example, there are approaches based on data mining of genome data to provide new insights into aspects of *Cryptosporidium* biology focused on novel targets. Recently, the identification of some ligands/inhibitors and parasite-specific molecules, such as parasite kinases; nucleic acid synthesis and processing; proteases; and lipid metabolism have paved the way for new therapies against *Cryptosporidium*, which is considered an attractive strategy. However, alternative salvage pathways could reduce the efficacy of many of these targets as one remarkable case demonstrated with the thymidylate synthase-dihydrofolate reductase target (Pawlowicz et al., 2019).

### 5.4.2 Bumped Kinase Inhibitors

Protein kinases play essential roles in the biology of *Cryptosporidium* and can identify essential pathways to potential new targets. Bumped kinase inhibitors (BKIs) targeting calcium-dependent protein kinase 1 (CDPK1) have shown effect against *Cryptosporidium* *in vitro* and in mice. Pyrazolopyrimidine analogues inhibit *C. parvum* CDPK1 and block *C. parvum* growth in tissue culture *in vitro*. However, the effect on parasite growth was variable and did not correlate well with enzyme inhibition (Kuhlenschmidt et al., 2016), conversely as demonstrated by *Toxoplasma gondii*. It also has shown issue challenges related to cardiovascular toxicity, teratogenicity, and varying efficacy (Choi et al., 2020; Love and Choy, 2021). Another series of BKI compounds have been developed which inhibit CDPK. However, this class of drugs has presented significant adverse reactions because of inhibited binding to mammalian protein kinases (Wang et al., 2020).

Another, kinase target is phosphatidylinositol-4-OH kinase, which phosphorylates lipid molecules to participate in intracellular signalling and trafficking, and is a target for

pyrazolopyridines. Screening a library of compounds with antiparasitic activity found pyrazolopyridine KDU731 as a promising anticryptosporidial drug candidate [(*Cryptosporidium* lipid kinase PI(4)K (phosphatidylinositol-4-OH kinase)] that is active against both *C. parvum* and *C. hominis* (Manjunatha et al., 2017; Funkhouser-Jones et al., 2020). However, safety and pharmacological preclinical evaluations are necessary in order to support the initiation of human clinical trials.

### 5.4.3 Inhibitors of Inosine Monophosphate Dehydrogenase

Another essential pathway in *Cryptosporidium* spp. is purine synthesis. Oxidoreductase inosine 5'-monophosphate dehydrogenase (IMPDH) is required for the conversion of adenosine into guanine nucleotides. IMPDH is a target for immunosuppressive, antiviral, and anticancer drugs. However, inhibitors of IMPDH have shown *in vitro* efficacy against *Cryptosporidium* spp (Jefferies et al., 2015).

### 5.4.4 tRNA Synthetase

tRNA synthetases comprise a family of enzymes that couple specific amino acid residues to selected tRNA for protein peptide synthesis. *Cryptosporidium* spp. are inhibited by a benzoxaborole (a 3-aminomethyl benzoxaborole, AN6426) targeting leucyl-tRNA synthetase. Despite the fact that homologous proteins exist in humans, this molecule has the potential for antimicrobial drug design, since structural and sequence divergences can be modified to enhance specificity and avoid toxicity (Palencia et al., 2016). Besides this one, quinazoline-based derivative shows potent activity against *Cryptosporidium* prolyl-tRNA synthetase (Jain et al., 2017); imidazopyridine derivatives are also potent inhibitors of *Cryptosporidium* methionyl-tRNA synthetase (Buckner et al., 2019). Similar results have been observed with cladospirin derivatives, also exhibiting potent activity against *Cryptosporidium* lysyl-tRNA synthetases (KRSs) (Baragana et al., 2019).

### 5.4.5 Cysteine Protease (Cryptopains)

Five genes coding cathepsin L-like proteases (cryptopains), a representative of clan CA, were identified in the *C. parvum* genome that are expressed during the sporozoite stage and are important for cell invasion and survival. The discovery that a cysteine protease inhibitor provides potent anticryptosporidial activity in an animal model of infection encourages the investigation and development of this class as a new (and urgently needed) therapy for cryptosporidiosis (Ndao et al., 2013).

## 6 ALTERNATIVE CHEMOTHERAPEUTIC AGENTS AGAINST PROTOZOAN PARASITES

### 6.1 Natural Compounds

Natural products remain an important source of biologically active substances and are an alternative source for parasitic



control. In this context, several research groups are focused on the isolation and identification of novel compounds with antimicrobial activity from plant and fungal extracts, aiming to use them in the discovery of new antiprotozoal drugs. A list of natural compounds with antiprotozoal activity is described in **Supplementary Table 1**.

## 6.2 Hybrid Compounds

Studies have shown that hybrid molecules display high protozoal activity, making them potentially promising agents for antiprotozoal therapy. Evaluation of nitazoxanide-N-methylbenzimidazole hybrid compounds showed strong activity *in vitro* against *G. intestinalis*, *E. histolytica* and *T. vaginalis*, especially with *E. histolytica*, where the IC<sub>50</sub> values ranged between 3 and 69 nM (Soria-Arteche et al., 2013).

Other compounds with antiprotozoal properties are 1H-1,2,3-triazole-tethered metronidazole-isatin conjugates, which presented inhibitory activity against *T. vaginalis*, *Trichomonas foetus*, *G. lamblia* and *E. histolytica* *in vitro*. Curiously, compounds with thiosemicarbazone moieties showed better results against *G. lamblia* and *E. histolytica* and were similar to MTZ against trichomonads (Kumar et al., 2018). Matadamas-Martínez and colleagues (2016) showed that a nitazoxanide-N-methyl-1H-benzimidazole hybrid molecule exhibited giardicidal activity at nanomolar concentrations and was more active *in vitro* than both MTZ and albendazole, and equipotent to NTZ. This compound induced ultrastructural changes and alterations in cytoskeleton proteins and in proteins that play an important role in the encystment process (Matadamas-Martínez et al., 2016). Further *in vitro* and *in vivo* studies revealed that the hybrid compound also exhibited broad activity against susceptible and resistant strains to albendazole and NTZ (Matadamas-Martínez et al., 2020).

MTZ-chalcone conjugates exhibited activity against MTZ-susceptible and resistant strains of *T. vaginalis* (Anthwal et al., 2014). 3-(3,5-Difluoro-phenyl)-1-{4-[2-(2-methyl-5-nitroimidazol-1-yl)-ethoxy]-phenyl}-propenone and 3-(3-chloro-phenyl)-1-{4-[2-(2-methyl-5-nitroimidazol-1-yl)-ethoxy]-phenyl}-propenone compounds were four times more potent than MTZ and safe against HeLa *in vitro*, being a candidate drug capable of overcoming the MTZ resistance of *T. vaginalis* (Anthwal et al., 2014).

## 6.3 Synthetic Compounds

The *in vitro* antiprotozoal activities of 2H-indazole derivatives have been reported for *E. histolytica*, *G. lamblia* and *T. vaginalis* at lower concentrations and are usually more potent compared to MTZ, appearing to be a good alternative (Perez-Villanueva et al., 2017; Rodríguez-Villar et al., 2021). In turn, 2'-hydroxychalcone showed trichomonocidal *in vitro* analysis: at 12.5 µM associated with MTZ (40 µM), a reduction of 95.31% in the trophozoite's viability was displayed after 24 hours of incubation (Das Neves et al., 2020). Furanyl N-acylhydrazones also presented activity against *T. vaginalis*, with IC<sub>50</sub> values ranging from 1.69 µM to 1.98 µM (Alves et al., 2020).

MTZ thiosemicarbazones and ethyl- and methyl-quinoxaline-7-carboxylate 1,4-di-N-oxide derivatives showed a significant antiamebic activity *in vitro*, with an IC<sub>50</sub> of 0.56 µM and IC<sub>50</sub> values ranging from 1.41 µM to 1.47 µM, respectively (Abid et al., 2008; Duque-Montano et al., 2013).

Muller and colleagues (2006) showed experimentally that NTZ-related thiazolide/thiadiazolide derivatives exhibited inhibitory activity *in vitro* against a *G. duodenalis* axenic culture and coculture with Caco2 cells (Muller et al., 2006). Another study revealed that 2-ethenyl- and 2-ethanyl-5-NI derivatives exhibited anti-giardial activity without toxicity and were more potent than MTZ *in vitro*. Furthermore, they were more effective than MTZ in a murine giardiasis model (Valdez et al., 2009).

NTZ-related thiazolide/thiadiazolide compounds also exhibited *in vitro* inhibitory activity against *C. parvum*. Modifications of the NTZ chemical structure showed that anticryptosporidial activity is thought to be independent of the presence of a nitro group on the thiazole moiety, with IC<sub>50</sub> lower than NTZ (Gargala et al., 2010).

Recently, *in vitro* and *in vivo* studies revealed that L-tert-leucyl thiazolide (aminoxadine), a soluble drug of tizoxanide (TIZ), possesses potency of cryptosporidiosis. *In vitro*, this compound dose-dependently inhibited *C. parvum* growth, and no toxicity was observed, since the IC<sub>50</sub> for *C. parvum* (1.55 ± 0.21 µM) was at least 20-fold lower than the CC<sub>50</sub> for HCT-8 cells. Surprisingly, in gerbils, a 5-day course of daily intramuscular aminoxanide treatment (100 mg/kg) resulted in a 72.5% oocyst excretion inhibition, statistically equivalent to 75.5% in rodents treated with a 4-fold lower oral dose of NTZ (Diawara et al., 2021). Until now, the only two injected drugs to inhibit *C. parvum* infection are aminoxanide and MMV665917, a new drug based on piperazine (Jumani et al., 2018).

## 6.4 Nanotechnology Against Protozoan Parasites

Nanotechnology-based drug delivery has emerged as a promising approach for several illnesses, including parasitic diseases, improving the ability to specifically target pathogens, penetrate barriers within the host to allow a drug to access areas of pathogen residence, reduce toxicity by lowering dose amount and frequency of administration, and increase the uptake of poorly soluble drugs (Sun et al., 2019). A summary of the types of nanoparticles susceptible to parasites is shown in **Table 2**.

## 7 CONCLUSION

Parasitic mucosa-associated protozoa cause severe health, social, and economic impacts, mainly in low-income settings that are resource constrained. Considering the scarcity of drugs available to treat these diseases and the threat of resistant cases, the search for new therapeutics is urgently needed.



**TABLE 2** | List of the types of nanoparticles susceptibility to protozoa parasites.

Type of nanoparticle	Drug	Parasite	Effect	Reference
<b>Polymeric nanoparticles</b>	Chitosan	<i>C. parvum</i>	Reduced the number of Cryptosporidium oocysts	(Ahmed et al., 2019)
<b>Polymeric nanoparticles</b>	Clofazimine	<i>C. parvum</i>	Increased solubility by 90 times	(Zhang et al., 2017; Feng et al., 2018)
<b>Nano-suspension</b>	Bupravaquone	<i>C. parvum</i>	Enhanced mucosal adsorption and targeting	(Lemke et al., 2010)
<b>Polymeric nanoparticles</b>	Nano-Nitazoxanide (NTZ)	<i>C. parvum</i>	decreased the number of parasites, been more effective at day 6 of treatment	(Sedighi et al., 2016)
<b>Polymeric nanoparticles</b>	antibody-engineered with Indinavir	<i>C. parvum</i>	were able to target <i>C. parvum</i> in infected cells	(Bondioli et al., 2011)
<b>Polymeric nanoparticles</b>	Silver	<i>C. parvum</i>	high concentrations are able to fully break the oocyst wall	(Cameron et al., 2016)
<b>Polymeric nanoparticles</b>	Cooper oxide and silver	<i>E. histolytica</i> ; <i>C. parvum</i>	significant reduction for cysts viability	(Saad et al., 2015)
<b>Polymeric nanoparticles</b>	Silver, chitosan, and curcumin	<i>G. lamblia</i>	Highest effect was combining the three nanoform drugs. Parasite was eliminated from feces and intestine.	(Said et al., 2012)
<b>Polymeric nanoparticles</b>	Gold	<i>G. lamblia</i>	concentration of 0.3 mg/ml was effective to eliminated cysts	(Bavand et al., 2014)
<b>Polymeric nanoparticles</b>	Metronidazole	<i>G. lamblia</i>	completely eliminated cyst shedding and trophozoite count compared with Giardia-infected mice	(Madbouly et al., 2020)
<b>Nano-emulsion</b>	Micana cordifolia	<i>T. vaginalis</i>	anti- <i>T. vaginalis</i> activity was observed to be 100% at 1000 ppm	(Vazini, 2017)
<b>Polymeric nanoparticles</b>	Chitosan	<i>T. vaginalis</i>	showed a strong at 100 µg/mL	(Pradines et al., 2015)

However, despite considerable effort, no new novel drugs have been approved as a novel option for treatment. Also, there are no new compounds currently in clinical trials. Most of the targets and compounds were able to show some efficacy *in vitro*, *in vivo*, or both. Also, they have already proven effective in large animal models, although the compounds so far have not reached clinical application. Ahead, the huge challenge is to get the best candidates for clinical studies.

## AUTHOR CONTRIBUTIONS

KMR and HLCS contributed equally to this work and approved the submitted version.

## REFERENCES

- Abid, M., Agarwal, S. M., and Azam, A. (2008). Synthesis and Antiamoebic Activity of Metronidazole Thiosemicarbazone Analogues. *Eur. J. Med. Chem.* 43, 2035–2039. doi: 10.1016/j.ejmech.2007.12.007
- Abubakar, I., Aliyu, S. H., Arumugam, C., Hunter, P. R., and Usman, N. K. (2007). Prevention and Treatment of Cryptosporidiosis in Immunocompromised Patients. *Cochrane Database Syst. Rev.* 24 (1), CD004932. doi: 10.1002/14651858.CD004932.pub2
- Adagu, I. S., Nolder, D., Warhurst, D. C., and Rossignol, J. F. (2002). *In Vitro* Activity of Nitazoxanide and Related Compounds Against Isolates of Giardia Intestinalis, Entamoeba Histolytica and Trichomonas Vaginalis. *J. Antimicrob. Chemother.* 49, 103–111. doi: 10.1093/jac/49.1.103
- Agholi, M., Hatam, G. R., and Motazedian, M. H. (2013). Microsporidia and Coccidia as Causes of Persistence Diarrhea Among Liver Transplant Children: Incidence Rate and Species/Genotypes. *Pediatr. Infect. Dis. J.* 32 (2) 185–187. doi: 10.1097/INF.0b013e318273d95f

## FUNDING

This work was supported by the Fundação de Amparo à Pesquisa do Estado do Rio de Janeiro, Conselho Nacional de Desenvolvimento Científico e Tecnológico, Coordenação de Aperfeiçoamento de Pessoal de Nível Superior and Fundação Oswaldo Cruz.

## SUPPLEMENTARY MATERIAL

The Supplementary Material for this article can be found online at: <https://www.frontiersin.org/articles/10.3389/fcimb.2022.860442/full#supplementary-material>

**Supplementary Table 1** | List of natural compounds with antiprotozoa activity.

- Ahmed, S. A., El-Mahallawy, H. S., and Karanis, P. (2019). Inhibitory Activity of Chitosan Nanoparticles Against Cryptosporidium Parvum Oocysts. *Parasitol. Res.* 118, 2053–2063. doi: 10.1007/s00436-019-06364-0
- Alves, M. S. D., Das Neves, R. N., Sena-Lopes, A., Domingues, M., Casaril, A. M., Segatto, N. V., et al. (2020). Antiparasitic Activity of Furanyl N-Acylhydrazones Derivatives Against Trichomonas Vaginalis: *In Vitro* and *In Silico* Analyses. *Parasitol. Vectors* 13, 59. doi: 10.1186/s13071-020-3923-8
- Amadi, B., Mwiya, M., Sianongo, S., Payne, L., Watuka, A., Katubulushi, M., et al. (2009). High Dose Prolonged Treatment With Nitazoxanide is Not Effective for Cryptosporidiosis in HIV Positive Zambian Children: A Randomised Controlled Trial. *BMC Infect. Dis.* 9, 195. doi: 10.1186/1471-2334-9-195
- Andersson, K. E. (1981). Pharmacokinetics of Nitroimidazoles. Spectrum of Adverse Reactions. *Scand. J. Infect. Dis. Suppl.* 26, 60–67.
- Andrade, R. M., and Reed, S. L. (2015). New Drug Target in Protozoan Parasites: The Role of Thioredoxin Reductase. *Front. Microbiol.* 6, 975. doi: 10.3389/fmicb.2015.00975

- Anthwal, A., Rajesh, U. C., Rawat, M. S., Kushwaha, B., Maikhuri, J. P., Sharma, V. L., et al. (2014). Novel Metronidazole-Chalcone Conjugates With Potential to Counter Drug Resistance in Trichomonas Vaginalis. *Eur. J. Med. Chem.* 79, 89–94. doi: 10.1016/j.ejmech.2014.03.076
- Ashburn, T. T., and Thor, K. B. (2004). Drug Repositioning: Identifying and Developing New Uses for Existing Drugs. *Nat. Rev. Drug Discovery* 3, 673–683. doi: 10.1038/nrd1468
- Banik, G. R., Stark, D., Rashid, H., and Ellis, J. T. (2014). Recent Advances in Molecular Biology of Parasitic Viruses. *Infect. Disord. Drug Targets* 14, 155–167. doi: 10.2174/1871526514666140713160905
- Baragana, B., Forte, B., Choi, R., Nakazawa Hewitt, S., Bueren-Calabuig, J. A., Pisco, J. P., et al. (2019). Lysyl-tRNA Synthetase as a Drug Target in Malaria and Cryptosporidiosis. *Proc. Natl. Acad. Sci. U.S.A.* 116, 7015–7020. doi: 10.1073/pnas.1814685116
- Barrow, P., Dujardin, J. C., Fasel, N., Greenwood, A. D., Osterrieder, K., Lomonosoff, G., et al. (2020). Viruses of Protozoan Parasites and Viral Therapy: Is the Time Now Right? *Virol. J.* 17, 142. doi: 10.1186/s12985-020-01410-1
- Bavand, Z., Gholami, S., Honari, S., Rahimi Esboei, B., Torabi, N., and Borabadi, H. (2014). Effect of Gold Nanoparticles on Giardia Lambliacyst stage in *In Vitro*? *Arak. Med. Univ. J.* 16, 27–37.
- Benchimol, M., Chang, T. H., and Alderete, J. F. (2002). Trichomonas Vaginalis: Observation of Coexistence of Multiple Viruses in the Same Isolate. *FEMS Microbiol. Lett.* 215, 197–201. doi: 10.1111/j.1574-6968.2002.tb11391.x
- Billet, A. C., Salmon Rousseau, A., Piroth, L., and Martins, C. (2019). An Underestimated Sexually Transmitted Infection: Amoebiasis. *BMJ Case Rep.* 12 (5), e228942. doi: 10.1136/bcr-2018-228942
- Bird, R. G., Mccaul, T. F., and Knight, R. (1974). Proceedings: Rhabdo-Virus Like Particles of Entamoeba Histolytica. *Trans. R. Soc. Trop. Med. Hyg.* 68, 2. doi: 10.1016/0035-9203(74)90214-4
- Bondioli, L., Ludovisi, A., Tosi, G., Ruozzi, B., Forni, F., Pozio, E., et al. (2011). The Loading of Labelled Antibody-Engineered Nanoparticles With Indinavir Increases its *In Vitro* Efficacy Against Cryptosporidium Parvum. *Parasitology* 138, 1384–1391. doi: 10.1017/S0031182011001119
- Bouma, M. J., Snowdon, D., Fairlamb, A. H., and Ackers, J. P. (1998). Activity of Disulfiram (Bis(Diethylthiocarbamoyl)Disulphide) and Ditiocarb (Diethylthiocarbamate) Against Metronidazole-Sensitive and -Resistant Trichomonas Vaginalis and Trichomonas Foetus. *J. Antimicrob. Chemother.* 42, 817–820. doi: 10.1093/jac/42.6.817
- Buckner, F. S., Ranade, R. M., Gillespie, J. R., Shibata, S., Hulverson, M. A., Zhang, Z., et al. (2019). Optimization of Methionyl tRNA-Synthetase Inhibitors for Treatment of Cryptosporidium Infection. *Antimicrob. Agents Chemother.* 63 (4), e02061-18. doi: 10.1128/AAC.02061-18
- Cameron, P., Gaiser, B. K., Bhandari, B., Bartley, P. M., Katzer, F., and Bridle, H. (2016). Silver Nanoparticles Decrease the Viability of Cryptosporidium Parvum Oocysts. *Appl. Environ. Microbiol.* 82, 431–437. doi: 10.1128/AEM.02806-15
- Cao, L., Gong, P., Li, J., Zhang, X., Zou, X., Tuo, W., et al. (2009). Giardia Canis: Ultrastructural Analysis of G. Canis Trophozoites Transfected With Full Length G. Canis Virus cDNA Transcripts. *Exp. Parasitol.* 123, 212–217. doi: 10.1016/j.exppara.2009.07.001
- Capparelli, E. V., Bricker-Ford, R., Rogers, M. J., Mckerrow, J. H., and Reed, S. L. (2017). Phase I Clinical Trial Results of Auranofin, a Novel Antiparasitic Agent. *Antimicrob. Agents Chemother.* 61 (1), e01947-16. doi: 10.1128/AAC.01947-16
- Carter, E. R., Nabarro, L. E., Hedley, L., and Chiodini, P. L. (2018). Nitroimidazole-Refractory Giardiasis: A Growing Problem Requiring Rational Solutions. *Clin. Microbiol. Infect.* 24, 37–42. doi: 10.1016/j.cmi.2017.05.028
- Castillo-Villanueva, A., Rufino-Gonzalez, Y., Mendez, S. T., Torres-Arroyo, A., Ponce-Macotela, M., Martinez-Gordillo, M. N., et al. (2017). Disulfiram as a Novel Inactivator of Giardia Lambli Triosephosphate Isomerase With Antigiardial Potential. *Int. J. Parasitol. Drugs Drug Resist.* 7, 425–432. doi: 10.1016/j.ijppdr.2017.11.003
- Cedillo-Rivera, R., Chavez, B., Gonzalez-Robles, A., Tapia, A., and Yopez-Mulia, L. (2002). *In Vitro* Effect of Nitazoxanide Against Entamoeba Histolytica, Giardia Intestinalis and Trichomonas Vaginalis Trophozoites. *J. Eukaryot. Microbiol.* 49, 201–208. doi: 10.1111/j.1550-7408.2002.tb00523.x
- Choi, R., Hulverson, M. A., Huang, W., Vidadala, R. S. R., Whitman, G. R., Barrett, L. K., et al. (2020). Bumped Kinase Inhibitors as Therapy for Apicomplexan Parasitic Diseases: Lessons Learned. *Int. J. Parasitol.* 50, 413–422. doi: 10.1016/j.ijpara.2020.01.006
- Coelho, D. D. (1997). Metronidazole Resistant Trichomoniasis Successfully Treated With Paromomycin. *Genitourin. Med.* 73, 397–398. doi: 10.1136/sti.73.5.397
- Collaborators, G. B. D. D. (2017). Estimates of Global, Regional, and National Morbidity, Mortality, and Aetiologies of Diarrhoeal Diseases: A Systematic Analysis for the Global Burden of Disease Study 2015. *Lancet Infect. Dis.* 17, 909–948. doi: 10.1016/S1473-3099(17)30276-1
- Collier, S. A., Deng, L., Adam, E. A., Benedict, K. M., Beshearse, E. M., Blackstock, A. J., et al. (2021). Estimate of Burden and Direct Healthcare Cost of Infectious Waterborne Disease in the United States. *Emerg. Infect. Dis.* 27, 140–149. doi: 10.3201/eid2701.190676
- Connors, E. E., Miller, A. D., Balachandran, N., Robinson, B. M., and Benedict, K. M. (2021). Giardiasis Outbreaks - United States-2017. *MMWR Morb. Mortal Wkly Rep.* 70, 304–307. doi: 10.15585/mmwr.mm7009a2
- Croft, S. L., Seifert, K., and Duchene, M. (2003). Antiprotozoal Activities of Phospholipid Analogues. *Mol. Biochem. Parasitol.* 126, 165–172. doi: 10.1016/S0166-6851(02)00283-9
- Das Neves, R. N., Sena-Lopes, A., Alves, M. S. D., Da Rocha Fonseca, B., Da Silva, C. C., Casaril, A. M., et al. (2020). 2'-Hydroxychalcones as an Alternative Treatment for Trichomoniasis in Association With Metronidazole. *Parasitol. Res.* 119, 725–736. doi: 10.1007/s00436-019-06568-4
- Debnath, A., Ndao, M., and Reed, S. L. (2013). Reprofiled Drug Targets Ancient Protozoans: Drug Discovery for Parasitic Diarrheal Diseases. *Gut. Microbes* 4, 66–71. doi: 10.4161/gmic.22596
- Debnath, A., Parsonage, D., Andrade, R. M., He, C., Cobo, E. R., Hirata, K., et al. (2012). A High-Throughput Drug Screen for Entamoeba Histolytica Identifies a New Lead and Target. *Nat. Med.* 18, 956–960. doi: 10.1038/nm.2758
- Diawara, E. H., Francois, A., Stachulski, A. V., Razakandrainibe, R., Costa, D., Favennec, L., et al. (2021). Systemic Efficacy on Cryptosporidium Parvum Infection of Aminoxanide (RM-5061), a New Amino-Acid Ester Thiazolidine Prodrug of Tizoxanide. *Parasitology* 148, 975–984. doi: 10.1017/S0031182021000524
- Dimasi, J. A., Hansen, R. W., and Grabowski, H. G. (2003). The Price of Innovation: New Estimates of Drug Development Costs. *J. Health Econ.* 22, 151–185. doi: 10.1016/S0167-6296(02)00126-1
- Diptyanusa, A., and Sari, I. P. (2021). Treatment of Human Intestinal Cryptosporidiosis: A Review of Published Clinical Trials. *Int. J. Parasitol. Drugs Drug Resist.* 17, 128–138. doi: 10.1016/j.ijppdr.2021.09.001
- Duque-Montano, B. E., Gomez-Caro, L. C., Sanchez-Sanchez, M., Monge, A., Hernandez-Baltazar, E., Rivera, G., et al. (2013). Synthesis and *In Vitro* Evaluation of New Ethyl and Methyl Quinoxaline-7-Carboxylate 1,4-Di-N-Oxide Against Entamoeba Histolytica. *Bioorg. Med. Chem.* 21, 4550–4558. doi: 10.1016/j.bmc.2013.05.036
- Efstratiou, A., Ongerth, J. E., and Karanis, P. (2017). Waterborne Transmission of Protozoan Parasites: Review of Worldwide Outbreaks - An Update 2011-2016. *Water Res.* 114, 14–22. doi: 10.1016/j.watres.2017.01.036
- Ehrenkauf, G., Li, P., Stebbins, E. E., Kangussu-Marcolino, M. M., Debnath, A., White, C. V., et al. (2020). Identification of Anisomycin, Prodigiosin and Obatoxas as Compounds With Broad-Spectrum Anti-Parasitic Activity. *PloS Negl. Trop. Dis.* 14, e0008150. doi: 10.1371/journal.pntd.0008150
- Ehrenkauf, G. M., Suresh, S., Solow-Cordero, D., and Singh, U. (2018). High-Throughput Screening of Entamoeba Identifies Compounds Which Target Both Life Cycle Stages and Which Are Effective Against Metronidazole Resistant Parasites. *Front. Cell Infect. Microbiol.* 8, 276. doi: 10.3389/fcimb.2018.00276
- El-Gayar, E. K., Mokhtar, A. B., and Hassan, W. A. (2016). Molecular Characterization of Double-Stranded RNA Virus in Trichomonas Vaginalis Egyptian Isolates and its Association With Pathogenicity. *Parasitol. Res.* 115, 4027–4036. doi: 10.1007/s00436-016-5174-3
- Escobedo, A. A., Almirall, P., Alfonso, M., Cimerman, S., and Chacin-Bonilla, L. (2014). Sexual Transmission of Giardiasis: A Neglected Route of Spread? *Acta Trop.* 132, 106–111. doi: 10.1016/j.actatropica.2013.12.025
- Escobedo, A. A., Lalle, M., Hrastnik, N. I., Rodriguez-Morales, A. J., Castro-Sanchez, E., Cimerman, S., et al. (2016). Combination Therapy in the Management of Giardiasis: What Laboratory and Clinical Studies Tell Us, So Far. *Acta Trop.* 162, 196–205. doi: 10.1016/j.actatropica.2016.06.026
- Fantinati, M., Lopes-Oliveira, L. A. P., Cascais-Figueroa, T., Austriaco-Teixeira, P., Verissimo, E., Bello, A. R., et al. (2020). Recirculation of Giardia Lambli

- Assemblage A After Metronidazole Treatment in an Area With Assemblages A, B, and E Sympatric Circulation. *Front. Microbiol.* 11, 571104. doi: 10.3389/fmicb.2020.571104
- Feng, J., Zhang, Y., Mcmanus, S. A., Ristroph, K. D., Lu, H. D., Gong, K., et al. (2018). Rapid Recovery of Clofazimine-Loaded Nanoparticles With Long-Term Storage Stability as Anti-Cryptosporidium Therapy. *ACS Appl. Nano Mater.* 1, 2184–2194. doi: 10.1021/acsanm.8b00234
- Fichorova, R., Fraga, J., Rappelli, P., and Fiori, P. L. (2017). Trichomonas Vaginalis Infection in Symbiosis With Trichomonasvirus and Mycoplasma. *Res. Microbiol.* 168, 882–891. doi: 10.1016/j.resmic.2017.03.005
- Fichorova, R. N., Lee, Y., Yamamoto, H. S., Takagi, Y., Hayes, G. R., Goodman, R. P., et al. (2012). Endobiont Viruses Sensed by the Human Host - Beyond Conventional Antiparasitic Therapy. *PLoS One* 7, e48418. doi: 10.1371/journal.pone.0048418
- Fraga, J., Rojas, L., Sario, I., Fernandez-Calienes, A., and Nunez, F. A. (2012). Species Typing of Cuban Trichomonas Vaginalis Virus by RT-PCR, and Association of TVV-2 With High Parasite Adhesion Levels and High Pathogenicity in Patients. *Arch. Virol.* 157, 1789–1795. doi: 10.1007/s00705-012-1353-4
- Funkhouser-Jones, L. J., Ravindran, S., and Sibley, L. D. (2020). Defining Stage-Specific Activity of Potent New Inhibitors of Cryptosporidium Parvum Growth *In Vitro*. *mBio* 11 (2), e00052-20. doi: 10.1128/mBio.00052-20
- Gargala, G., Le Goff, L., Ballet, J. J., Favennec, L., Stachulski, A. V., and Rossignol, J. F. (2010). Evaluation of New Thiazolidine/Thiadiazolidine Derivatives Reveals Nitro Group-Independent Efficacy Against *In Vitro* Development of Cryptosporidium Parvum. *Antimicrob. Agents Chemother.* 54, 1315–1318. doi: 10.1128/AAC.00614-09
- Gavrilov, O. K. (1989). Gravitational Surgical Correction of the Aggregative Status of the Blood in Ischemic Heart Disease. *Klin. Med. (Mosk)* 67, 8–12.
- Gharpure, R., Perez, A., Miller, A. D., Wikswo, M. E., Silver, R., and Hlavsa, M. C. (2019). Cryptosporidiosis Outbreaks - United States 2009–2017. *MMWR Morb. Mortal Wkly Rep.* 68, 568–572. doi: 10.15585/mmwr.mm6825a3
- Ghosh, S., Farr, L., Singh, A., Leaton, L. A., Padalia, J., Shirley, D. A., et al. (2020). COP9 Signalingosome is an Essential and Druggable Parasite Target That Regulates Protein Degradation. *PLoS Pathog.* 16, e1008952. doi: 10.1371/journal.ppat.1008952
- Gomez-Arreaza, A., Haenni, A. L., Dunia, I., and Avilan, L. (2017). Viruses of Parasites as Actors in the Parasite-Host Relationship: A "Menage a Trois". *Acta Trop.* 166, 126–132. doi: 10.1016/j.actatropica.2016.11.028
- Gonzales, M. L. M., Dans, L. F., and Sio-Agular, J. (2019). Antiamoebic Drugs for Treating Amoebic Colitis. *Cochrane Database Syst. Rev.* 1, CD006085. doi: 10.1002/14651858.CD006085.pub3
- Gonzalez Constandse, R. (1956). Anisomycin in Intestinal Amebiasis; Study of 30 Clinical Cases. *Prensa Med. Mex* 21, 114–115.
- Goodgame, R. (2003). Emerging Causes of Traveler's Diarrhea: Cryptosporidium, Cyclospora, Isospora, and Microsporidia. *Curr. Infect. Dis. Rep.* 5, 66–73. doi: 10.1007/s11908-003-0067-x
- Govender, Y., Chan, T., Yamamoto, H. S., Budnik, B., and Fichorova, R. N. (2020). The Role of Small Extracellular Vesicles in Viral-Protozoan Symbiosis: Lessons From Trichomonasvirus in an Isogenic Host Parasite Model. *Front. Cell Infect. Microbiol.* 10, 591172. doi: 10.3389/fcimb.2020.591172
- Graves, K. J., Ghosh, A. P., Schmidt, N., Augustini, P., Secor, W. E., Schwebke, J. R., et al. (2019). Trichomonas Vaginalis Virus Among Women With Trichomoniasis and Associations With Demographics, Clinical Outcomes, and Metronidazole Resistance. *Clin. Infect. Dis.* 69, 2170–2176. doi: 10.1093/cid/ciz146
- Gulmezoglu, A. M., and Garner, P. (1998). Trichomoniasis Treatment in Women: A Systematic Review. *Trop. Med. Int. Health* 3, 553–558. doi: 10.1046/j.1365-3156.1998.00273.x
- Hahn, J., Seeber, F., Kolodziej, H., Ignatius, R., Laue, M., Aebischer, T., et al. (2013). High Sensitivity of Giardia Duodenalis to Tetrahydropyridazinol (Orlistat) *In Vitro*. *PLoS One* 8, e71597. doi: 10.1371/journal.pone.0071597
- Haque, R., Huston, C. D., Hughes, M., Houpt, E., and Petri, W. A. Jr. (2003). Amebiasis. *N. Engl. J. Med.* 348, 1565–1573. doi: 10.1056/NEJMra022710
- Hernandez Ceruelos, A., Romero-Quezada, L. C., Ruvalcaba Ledezma, J. C., and Lopez Contreras, L. (2019). Therapeutic Uses of Metronidazole and its Side Effects: An Update. *Eur. Rev. Med. Pharmacol. Sci.* 23, 397–401. doi: 10.26355/eurrev\_201901\_16788
- Hernandez-Ochoa, B., Gomez-Manzo, S., Sanchez-Carrillo, A., Marcial-Quino, J., Rocha-Ramirez, L. M., Santos-Segura, A., et al. (2020). Enhanced Anti-giardial Effect of Omeprazole Analog Benzimidazole Compounds. *Molecules* 25 (17), 3979. doi: 10.3390/molecules25173979
- Hernandez-Ochoa, B., Navarrete-Vazquez, G., Nava-Zuazo, C., Castillo-Villanueva, A., Mendez, S. T., Torres-Arroyo, A., et al. (2017). Novel Giardicidal Compounds Bearing Proton Pump Inhibitor Scaffold Proceeding Through Triosephosphate Isomerase Inactivation. *Sci. Rep.* 7, 7810. doi: 10.1038/s41598-017-07612-y
- Hlavsa, M. C., Roellig, D. M., Seabolt, M. H., Kahler, A. M., Murphy, J. L., Mckitt, T. K., et al. (2017). Using Molecular Characterization to Support Investigations of Aquatic Facility-Associated Outbreaks of Cryptosporidiosis - Alabama, Arizona, and Ohio. *MMWR Morb. Mortal Wkly Rep.* 66, 493–497. doi: 10.15585/mmwr.mm6619a2
- Horner, D. S., Hirt, R. P., and Embley, T. M. (1999). A Single Eubacterial Origin of Eukaryotic Pyruvate: Ferredoxin Oxidoreductase Genes: Implications for the Evolution of Anaerobic Eukaryotes. *Mol. Biol. Evol.* 16, 1280–1291. doi: 10.1093/oxfordjournals.molbev.a026218
- Hung, C. C., Chang, S. Y., and Ji, D. D. (2012). Entamoeba Histolytica Infection in Men Who Have Sex With Men. *Lancet Infect. Dis.* 12, 729–736. doi: 10.1016/S1473-3099(12)70147-0
- Huston, C. D. (2021). The Clofazimine for Treatment of Cryptosporidiosis in HIV-Infected Adults (CRYPTOFAZ) and Lessons Learned for Anticryptosporidial Drug Development. *Clin. Infect. Dis.* 73, 192–194. doi: 10.1093/cid/ciaa425
- Innes, E. A., Chalmers, R. M., Wells, B., and Pawlowic, M. C. (2020). A One Health Approach to Tackle Cryptosporidiosis. *Trends Parasitol.* 36, 290–303. doi: 10.1016/j.pt.2019.12.016
- Iyer, L. R., Banyal, N., Naik, S., and J., P. (2017). Antioxidant Enzyme Profile of Two Clinical Isolates of Entamoeba Histolytica Varying in Sensitivity to Antiamoebic Drugs. *World J. Clin. Infect. Dis.* 7, 6. doi: 10.5495/wjcid.v7.i2.21
- Jain, V., Yogavel, M., Kikuchi, H., Oshima, Y., Hariguchi, N., Matsumoto, M., et al. (2017). Targeting Prolyl-tRNA Synthetase to Accelerate Drug Discovery Against Malaria, Leishmaniasis, Toxoplasmosis, Cryptosporidiosis, and Coccidiosis. *Structure* 25, 1495–1505 e6. doi: 10.1016/j.str.2017.07.015
- Jefferies, R., Yang, R., Woh, C. K., Weldt, T., Milech, N., Estcourt, A., et al. (2015). Target Validation of the Inosine Monophosphate Dehydrogenase (IMPDH) Gene in Cryptosporidium Using Phylomer(R) Peptides. *Exp. Parasitol.* 148, 40–48. doi: 10.1016/j.exppara.2014.11.003
- Jenkins, M. C., O'Brien, C. N., Santin, M., and Fayer, R. (2015). Changes in the Levels of Cryptosporidium During *In Vitro* Development of Cryptosporidium Parvum. *Parasitol. Res.* 114, 2063–2068. doi: 10.1007/s00436-015-4390-6
- Jimenez-Cardoso, E., Eligio-Garcia, L., Cortes-Campos, A., Flores-Luna, A., Valencia-Mayoral, P., and Lozada-Chavez, I. (2009). Changes in Beta-Giardin Sequence of Giardia Intestinalis Sensitive and Resistant to Albendazole Strains. *Parasitol. Res.* 105, 25–33. doi: 10.1007/s00436-009-1363-7
- Jourdan, J. P., Bureau, R., Rochais, C., and Dallemagne, P. (2020). Drug Repositioning: A Brief Overview. *J. Pharm. Pharmacol.* 72, 1145–1151. doi: 10.1111/jphp.13273
- Jumani, R. S., Bessoff, K., Love, M. S., Miller, P., Stebbins, E. E., Teixeira, J. E., et al. (2018). A Novel Piperazine-Based Drug Lead for Cryptosporidiosis From the Medicines for Malaria Venture Open-Access Malaria Box. *Antimicrob. Agents Chemother.* 62 (4), e01505-17. doi: 10.1128/AAC.01505-17
- Kappagoda, S., Singh, U., and Blackburn, B. G. (2011). Antiparasitic Therapy. *Mayo Clin. Proc.* 86, 561–583. doi: 10.4065/mcp.2011.0203
- Karanis, P., Kourenti, C., and Smith, H. (2007). Waterborne Transmission of Protozoan Parasites: A Worldwide Review of Outbreaks and Lessons Learnt. *J. Water Health* 5, 1–38. doi: 10.2166/wh.2006.002
- Khare, S., Nagle, A. S., Biggart, A., Lai, Y. H., Liang, F., Davis, L. C., et al. (2016). Proteasome Inhibition for Treatment of Leishmaniasis, Chagas Disease and Sleeping Sickness. *Nature* 537, 229–233. doi: 10.1038/nature19339
- Kirkcaldy, R. D., Augustini, P., Asbel, L. E., Bernstein, K. T., Kerani, R. P., Mettenbrink, C. J., et al. (2012). Trichomonas Vaginalis Antimicrobial Drug Resistance in 6 US Cities, STD Surveillance Network 2009–2010. *Emerg. Infect. Dis.* 18, 939–943. doi: 10.3201/eid1806.111590
- Kissinger, P., and Adamski, A. (2013). Trichomoniasis and HIV Interactions: A Review. *Sex Transm. Infect.* 89, 426–433. doi: 10.1136/sextrans-2012-051005



- Kuhlenschmidt, T. B., Rutaganira, F. U., Long, S., Tang, K., Shokat, K. M., Kuhlenschmidt, M. S., et al. (2016). Inhibition of Calcium-Dependent Protein Kinase 1 (CDPK1) *In Vitro* by Pyrazolopyrimidine Derivatives Does Not Correlate With Sensitivity of *Cryptosporidium Parvum* Growth in Cell Culture. *Antimicrob. Agents Chemother.* 60, 570–579. doi: 10.1128/AAC.01915-15
- Kulakova, L., Galkin, A., Chen, C. Z., Southall, N., Marugan, J. J., Zheng, W., et al. (2014). Discovery of Novel Anti-giardiasis Drug Candidates. *Antimicrob. Agents Chemother.* 58, 7303–7311. doi: 10.1128/AAC.03834-14
- Kumar, S., Bains, T., Won Kim, A. S., Tam, C., Kim, J., Cheng, L. W., et al. (2018). Highly Potent 1h-1,2,3-Triazole-Tethered Isatin-Metronidazole Conjugates Against Anaerobic Foodborne, Waterborne, and Sexually-Transmitted Protozoal Parasites. *Front. Cell Infect. Microbiol.* 8, 380. doi: 10.3389/fcimb.2018.00380
- Lalle, M., and Hanevik, K. (2018). Treatment-Refractory Giardiasis: Challenges and Solutions. *Infect. Drug Resist.* 11, 1921–1933. doi: 10.2147/IDR.S141468
- Lazenby, G. B., Thompson, L., Powell, A. M., and Soper, D. E. (2019). Unexpected High Rates of Persistent *Trichomonas Vaginalis* Infection in a Retrospective Cohort of Treated Pregnant Women. *Sex Transm. Dis.* 46, 2–8. doi: 10.1097/OLQ.0000000000000902
- Leitsch, D. (2015). Drug Resistance in the Microaerophilic Parasite *Giardia Lamblia*. *Curr. Trop. Med. Rep.* 2, 128–135. doi: 10.1007/s40475-015-0051-1
- Leitsch, D. (2016). Recent Advances in the *Trichomonas Vaginalis* Field. *F1000Res* 5 (F1000 Faculty Rev), 162. doi: 10.12688/f1000research.7594.1
- Leitsch, D. (2019). A Review on Metronidazole: An Old Warhorse in Antimicrobial Chemotherapy. *Parasitology* 146, 1167–1178. doi: 10.1017/S003182017002025
- Leitsch, D., Burgess, A. G., Dunn, L. A., Krauer, K. G., Tan, K., Duchene, M., et al. (2011). Pyruvate:ferredoxin Oxidoreductase and Thioredoxin Reductase are Involved in 5-Nitroimidazole Activation While Flavin Metabolism is Linked to 5-Nitroimidazole Resistance in *Giardia Lamblia*. *J. Antimicrob. Chemother.* 66, 1756–1765. doi: 10.1093/jac/ckr192
- Leitsch, D., Drinic, M., Kolarich, D., and Duchene, M. (2012). Down-Regulation of Flavin Reductase and Alcohol Dehydrogenase-1 (ADH1) in Metronidazole-Resistant Isolates of *Trichomonas Vaginalis*. *Mol. Biochem. Parasitol.* 183, 177–183. doi: 10.1016/j.molbiopara.2012.03.003
- Leitsch, D., Janssen, B. D., Kolarich, D., Johnson, P. J., and Duchene, M. (2014). *Trichomonas Vaginalis* Flavin Reductase 1 and its Role in Metronidazole Resistance. *Mol. Microbiol.* 91, 198–208. doi: 10.1111/mmi.12455
- Lemee, V., Zaharia, I., Nevez, G., Rabodonirina, M., Brasseur, P., Ballet, J. J., et al. (2000). Metronidazole and Albendazole Susceptibility of 11 Clinical Isolates of *Giardia Duodenalis* From France. *J. Antimicrob. Chemother.* 46, 819–821. doi: 10.1093/jac/46.5.819
- Lemke, A., Kiderlen, A. F., Petri, B., and Kayser, O. (2010). Delivery of Amphotericin B Nanosuspensions to the Brain and Determination of Activity Against *Balamuthia Mandrillaris* Amebas. *Nanomedicine* 6, 597–603. doi: 10.1016/j.nano.2009.12.004
- Leung, A. K. C., Leung, A. A. M., Wong, A. H. C., Sergi, C. M., and Kam, J. K. M. (2019). Giardiasis: An Overview. *Recent Pat. Inflammation Allergy Drug Discovery* 13, 134–143. doi: 10.2174/1872213X13666190618124901
- Li, J., Cui, Z., Li, X., and Zhang, L. (2021). Review of Zoonotic Amebiasis: Epidemiology, Clinical Signs, Diagnosis, Treatment, Prevention and Control. *Res. Vet. Sci.* 136, 174–181. doi: 10.1016/j.rvsc.2021.02.021
- Lin, H. C., Chu, L. J., Huang, P. J., Cheng, W. H., Zheng, Y. H., Huang, C. Y., et al. (2020). Proteomic Signatures of Metronidazole-Resistant *Trichomonas Vaginalis* Reveal Novel Proteins Associated With Drug Resistance. *Parasitol. Vectors* 13, 274. doi: 10.1186/s13071-020-04148-5
- Liu, H. W., Chu, Y. D., and Tai, J. H. (1998). Characterization of *Trichomonas Vaginalis* Virus Proteins in the Pathogenic Protozoan *T. Vaginalis*. *Arch. Virol.* 143, 963–970. doi: 10.1007/s007050050345
- Liu, J., Kanetake, S., Wu, Y. H., Tam, C., Cheng, L. W., Land, K. M., et al. (2016). Antiprotozoal Effects of the Tomato Tetrasaccharide Glycoalkaloid Tomatine and the Aglycone Tomatidine on Mucosal Trichomonads. *J. Agric. Food Chem.* 64, 8806–8810. doi: 10.1021/acs.jafc.6b04030
- Lofmark, S., Edlund, C., and Nord, C. E. (2010). Metronidazole is Still the Drug of Choice for Treatment of Anaerobic Infections. *Clin. Infect. Dis.* 50 Suppl 1, S16–S23. doi: 10.1086/647939
- Lopez-Velazquez, G., Fernandez-Lainez, C., de la Mora-De La Mora, J. I., Caudillo de la Portilla, D., Reynoso-Robles, R., Gonzalez-Macié, A., et al. (2019). On the Molecular and Cellular Effects of Omeprazole to Further Support its Effectiveness as an Anti-giardial Drug. *Sci. Rep.* 9, 8922. doi: 10.1038/s41598-019-45529-w
- Love, M. S., and Choy, R. K. M. (2021). Emerging Treatment Options for Cryptosporidiosis. *Curr. Opin. Infect. Dis.* 34, 455–462. doi: 10.1097/QCO.0000000000000761
- Ludvik, J., and Shipstone, A. C. (1970). The Ultrastructure of *Entamoeba Histolytica*. *Bull. World Health Organ* 43, 301–308.
- Mac Kenzie, W. R., Hoxie, N. J., Proctor, M. E., Gradus, M. S., Blair, K. A., Peterson, D. E., et al. (1994). A Massive Outbreak in Milwaukee of *Cryptosporidium* Infection Transmitted Through the Public Water Supply. *N. Engl. J. Med.* 331, 161–167. doi: 10.1056/NEJM199407213310304
- Madbouly, N. A., Nashee, H., Elgendy, A. A., Rabee, I., and El Amir, A. (2020). Encapsulation of Low Metronidazole Dose in Poly (D,L-Lactide-Co-Glycolide) (PLGA) Nanoparticles Improves *Giardia Intestinalis* Treatment. *Infect. Chemother.* 52, 550–561. doi: 10.3947/ic.2020.52.4.550
- Malla, N., Kaul, P., Sehgal, R., and Gupta, I. (2011). The Presence of dsRNA Virus in *Trichomonas Vaginalis* Isolates From Symptomatic and Asymptomatic Indian Women and its Correlation With *In Vitro* Metronidazole Sensitivity. *Indian J. Med. Microbiol.* 29, 152–157. doi: 10.4103/0255-0857.81801
- Manjunatha, U. H., Vinayak, S., Zambriski, J. A., Chao, A. T., Sy, T., Noble, C. G., et al. (2017). A *Cryptosporidium* Pi(4)K Inhibitor is a Drug Candidate for Cryptosporidiosis. *Nature* 546, 376–380. doi: 10.1038/nature22337
- Martinez-Perez, Y., Nequiz-Avendano, M., Garcia-Torres, I., Gudino-Zayas, M. E., Lopez-Velazquez, G., Enriquez-Flores, S., et al. (2020). Rabepazole Inhibits Several Functions of *Entamoeba Histolytica* Related With its Virulence. *Parasitol. Res.* 119, 3491–3502. doi: 10.1007/s00436-020-06868-0
- Marucci, G., Zullino, I., Bertuccini, L., Camerini, S., Cecchetti, S., Pietrantonio, A., et al. (2021). Re-Discovery of *Giardiavirus*: Genomic and Functional Analysis of Viruses From *Giardia Duodenalis* Isolates. *Biomedicine* 9 (6), 654. doi: 10.3390/biomedicine9060654
- Matadamas-Martinez, F., Castillo, R., Hernandez-Campos, A., Mendez-Cuesta, C., De Souza, W., Gadelha, A. P., et al. (2016). Proteomic and Ultrastructural Analysis of the Effect of a New Nitazoxanide-N-Methyl-1H-Benzimidazole Hybrid Against *Giardia Intestinalis*. *Res. Vet. Sci.* 105, 171–179. doi: 10.1016/j.rvsc.2016.02.006
- Meites, E., Gaydos, C. A., Hobbs, M. M., Kissinger, P., Nyirjesy, P., Schwebke, J. R., et al. (2015). A Review of Evidence-Based Care of Symptomatic Trichomoniasis and Asymptomatic *Trichomonas Vaginalis* Infections. *Clin. Infect. Dis.* 61 (Suppl 8), S837–S848. doi: 10.1093/cid/civ738
- Meneses-Marcel, A., Marrero-Ponce, Y., Ibanez-Escribano, A., Gomez-Barrio, A., Escario, J. A., Barigye, S. J., et al. (2018). Drug Repositioning for Novel Antitrichomonas From Known Antiprotozoan Drugs Using Hierarchical Screening. *Future Med. Chem.* 10, 863–878. doi: 10.4155/fmc-2016-0211
- Meri, T., Jokiranta, T. S., Suhonen, L., and Meri, S. (2000). Resistance of *Trichomonas Vaginalis* to Metronidazole: Report of the First Three Cases From Finland and Optimization of *In Vitro* Susceptibility Testing Under Various Oxygen Concentrations. *J. Clin. Microbiol.* 38, 763–767. doi: 10.1128/JCM.38.2.763-767.2000
- Mielczarek, E., and Blaszkowska, J. (2016). *Trichomonas Vaginalis*: Pathogenicity and Potential Role in Human Reproductive Failure. *Infection* 44, 447–458. doi: 10.1007/s15010-015-0860-0
- Morch, K., Hanevik, K., Robertson, L. J., Strand, E. A., and Langeland, N. (2008). Treatment-Ladder and Genetic Characterisation of Parasites in Refractory Giardiasis After an Outbreak in Norway. *J. Infect.* 56, 268–273. doi: 10.1016/j.jinf.2008.01.013
- Morgan, U. M., Reynoldson, J. A., and Thompson, R. C. (1993). Activities of Several Benzimidazoles and Tubulin Inhibitors Against *Giardia* Spp. *In Vitro. Antimicrob. Agents Chemother.* 37, 328–331. doi: 10.1128/AAC.37.2.328
- Mori, M., Tsuge, S., Fukasawa, W., Jeelani, G., Nakada-Tsukui, K., Nonaka, K., et al. (2018). Discovery of Antiamebic Compounds That Inhibit Cysteine Synthase From the Enteric Parasitic Protist *Entamoeba Histolytica* by Screening of Microbial Secondary Metabolites. *Front. Cell Infect. Microbiol.* 8, 409. doi: 10.3389/fcimb.2018.00409
- Muller, J., and Hemphill, A. (2013). New Approaches for the Identification of Drug Targets in Protozoan Parasites. *Int. Rev. Cell Mol. Biol.* 301, 359–401. doi: 10.1016/B978-0-12-407704-1.00007-5
- Muller, J., Ley, S., Felger, I., Hemphill, A., and Muller, N. (2008). Identification of Differentially Expressed Genes in a *Giardia Lamblia* WB C6 Clone Resistant to

- Nitazoxanide and Metronidazole. *J. Antimicrob. Chemother.* 62, 72–82. doi: 10.1093/jac/dkn142
- Muller, J., Ruhle, G., Muller, N., Rossignol, J. F., and Hemphill, A. (2006). *In Vitro* Effects of Thiazolidines on Giardia Lamblia WB Clone C6 Cultured Asexually and in Coculture With Caco2 Cells. *Antimicrob. Agents Chemother.* 50, 162–170. doi: 10.1128/AAC.50.1.162-170.2006
- Muller, J., Wastling, J., Sanderson, S., Muller, N., and Hemphill, A. (2007). A Novel Giardia Lamblia Nitroreductase, GINR1, Interacts With Nitazoxanide and Other Thiazolidines. *Antimicrob. Agents Chemother.* 51, 1979–1986. doi: 10.1128/AAC.01548-06
- Nabarro, L. E., Lever, R. A., Armstrong, M., and Chiodini, P. L. (2015). Increased Incidence of Nitroimidazole-Refractory Giardiasis at the Hospital for Tropical Diseases, London: 2008–2013. *Clin. Microbiol. Infect.* 21, 791–796. doi: 10.1016/j.cmi.2015.04.019
- Ndao, M., Nath-Chowdhury, M., Sajid, M., Marcus, V., Mashiyama, S. T., Sakanari, J., et al. (2013). A Cysteine Protease Inhibitor Rescues Mice From a Lethal Cryptosporidium Parvum Infection. *Antimicrob. Agents Chemother.* 57, 6063–6073. doi: 10.1128/AAC.00734-13
- Newman, L., Rowley, J., Vander Hoorn, S., Wijesooriya, N. S., Unemo, M., Low, N., et al. (2015). Global Estimates of the Prevalence and Incidence of Four Curable Sexually Transmitted Infections in 2012 Based on Systematic Review and Global Reporting. *PloS One* 10, e0143304. doi: 10.1371/journal.pone.0143304
- Nibbel, M. L., Woods, K. M., Upton, S. J., and Ghabrial, S. A. (2009). Crystovirus: A New Genus of Protozoan Viruses in the Family Partitiviridae. *Arch. Virol.* 154, 1959–1965. doi: 10.1007/s00705-009-0513-7
- Nillius, D., Muller, J., and Muller, N. (2011). Nitroreductase (GINR1) Increases Susceptibility of Giardia Lamblia and Escherichia Coli to Nitro Drugs. *J. Antimicrob. Chemother.* 66, 1029–1035. doi: 10.1093/jac/dkr029
- Nisha, G., Mehra, V., Hopper, M., Patel, N., Hall, D., Wrischnik, L. A., et al. (2013). Design and Synthesis of B-Amino Alcohol Based B-Lactam-Isatin Chimeras and Preliminary Analysis of *In Vitro* Activity Against the Protozoal Pathogen Trichomonas Vaginalis. *Med. Chem. Commun.* 4, 1018–1024. doi: 10.1039/c3md00057e
- O'donoghue, A. J., Bibo-Verdugo, B., Miyamoto, Y., Wang, S. C., Yang, J. Z., Zuill, D. E., et al. (2019). 20s Proteasome as a Drug Target in Trichomonas Vaginalis. *Antimicrob. Agents Chemother.* 63 (11), e00448-19. doi: 10.1128/AAC.00448-19
- Oliveira, Y., Oliveira, L. M., Oliveira, Y. L. M., Nascimento, A. M. D., La Corte, R., Geraldi, R. M., et al. (2020). Changes in the Epidemiological Profile of Intestinal Parasites After a School-Based Large-Scale Treatment for Soil-Transmitted Helminths in a Community in Northeastern Brazil: Epidemiological Profile After Large-Scale School-Based Treatment for STH. *Acta Trop.* 202, 105279. doi: 10.1016/j.actatropica.2019.105279
- Painter, J. E., Gargano, J. W., Yoder, J. S., Collier, S. A., and Hlavsa, M. C. (2016). Evolving Epidemiology of Reported Cryptosporidiosis Cases in the United States-2012. *Epidemiol. Infect.* 144, 1792–1802. doi: 10.1017/S0950268815003131
- Painter, J. E., Hlavsa, M. C., Collier, S. A., Xiao, L., Yoder, J. S. Centers For Disease, C. & Prevention (2015). Cryptosporidiosis Surveillance – United States 2011–2012. *MMWR Suppl.* 64, 1–14.
- Palencia, A., Liu, R. J., Lukarska, M., Gut, J., Bougdour, A., Touquet, B., et al. (2016). Cryptosporidium and Toxoplasma Parasites Are Inhibited by a Benzoxaborole Targeting Leucyl-tRNA Synthetase. *Antimicrob. Agents Chemother.* 60, 5817–5827. doi: 10.1128/AAC.00873-16
- Paulish-Miller, T. E., Augustini, P., Schuyler, J. A., Smith, W. L., Mordechai, E., Adelson, M. E., et al. (2014). Trichomonas Vaginalis Metronidazole Resistance is Associated With Single Nucleotide Polymorphisms in the Nitroreductase Genes Ntr4tv and Ntr6tv. *Antimicrob. Agents Chemother.* 58, 2938–2943. doi: 10.1128/AAC.02370-13
- Pawlowic, M. C., Somepalli, M., Sateriale, A., Herbert, G. T., Gibson, A. R., Cuny, G. D., et al. (2019). Genetic Ablation of Purine Salvage in Cryptosporidium Parvum Reveals Nucleotide Uptake From the Host Cell. *Proc. Natl. Acad. Sci. U.S.A.* 116, 21160–21165. doi: 10.1073/pnas.1908239116
- Perez, S., Fernandez-Verdugo, A., Perez, F., and Vazquez, F. (2001). Prevalence of 5-Nitroimidazole-Resistant Trichomonas Vaginalis in Oviedo, Spain. *Sex Transm. Dis.* 28, 115–116. doi: 10.1097/00007435-200102000-00010
- Perez-Villanueva, J., Yopez-Mulia, L., Gonzalez-Sanchez, I., Palacios-Espinosa, J. F., Soria-Arteche, O., Sainz-Espunes, T. D. R., et al. (2017). Synthesis and Biological Evaluation of 2H-Indazole Derivatives: Towards Antimicrobial and Anti-Inflammatory Dual Agents. *Molecules* 22 (11), 1864. doi: 10.3390/molecules22111864
- Pradines, B., Bories, C., Vauthier, C., Ponchel, G., Loiseau, P. M., and Bouchemal, K. (2015). Drug-Free Chitosan Coated Poly(Isobutylcyanoacrylate) Nanoparticles are Active Against Trichomonas Vaginalis and non-Toxic Towards Pig Vaginal Mucosa. *Pharm. Res.* 32, 1229–1236. doi: 10.1007/s11095-014-1528-7
- Provenzano, D., Khoshnan, A., and Alderete, J. F. (1997). Involvement of dsRNA Virus in the Protein Composition and Growth Kinetics of Host Trichomonas Vaginalis. *Arch. Virol.* 142, 939–952. doi: 10.1007/s007050050130
- Quihui-Cota, L., and Morales-Figueroa, G. G. (2012). Persistence of Intestinal Parasitic Infections During the National De-Worming Campaign in Schoolchildren of Northwestern Mexico: A Cross-Sectional Study. *Ann. Gastroenterol.* 25, 57–60.
- Rasoloson, D., Vanacova, S., Tomkova, E., Razga, J., Hrdy, I., Tachezy, J., et al. (2002). Mechanisms of *In Vitro* Development of Resistance to Metronidazole in Trichomonas Vaginalis. *Microbiol. (Reading)* 148, 2467–2477. doi: 10.1099/00221287-148-8-2467
- Reyes-Vivas, H., de la Mora-De La Mora, I., Castillo-Villanueva, A., Yopez-Mulia, L., Hernandez-Alcantara, G., Figueroa-Salazar, R., et al. (2014). Giardial Triosephosphate Isomerase as Possible Target of the Cytotoxic Effect of Omeprazole in Giardia Lamblia. *Antimicrob. Agents Chemother.* 58, 7072–7082. doi: 10.1128/AAC.02900-14
- Rodriguez-Villar, K., Yopez-Mulia, L., Cortes-Gines, M., Aguilera-Perdomo, J. D., Quintana-Salazar, E. A., Olascoaga Del Angel, K. S., et al. (2021). Synthesis, Antiprotozoal Activity, and Cheminformatic Analysis of 2-Phenyl-2h-Indazole Derivatives. *Molecules* 26 (8), 2145. doi: 10.3390/molecules26082145
- Roe, F. J. (1977). Metronidazole: Review of Uses and Toxicity. *J. Antimicrob. Chemother.* 3, 205–212. doi: 10.1093/jac/3.3.205
- Rossignol, J. F. (2010). Cryptosporidium and Giardia: Treatment Options and Prospects for New Drugs. *Exp. Parasitol.* 124, 45–53. doi: 10.1016/j.exppara.2009.07.005
- Saad, H. A., Soliman, M. I., Azzam, A. M., and Mostafa, B. (2015). Antiparasitic Activity of Silver and Copper Oxide Nanoparticles Against Entamoeba Histolytica and Cryptosporidium Parvum Cysts. *J. Egypt Soc. Parasitol.* 45, 593–602. doi: 10.12816/0017920
- Said, D. E., Elsamad, L. M., and Gohar, Y. M. (2012). Validity of Silver, Chitosan, and Curcumin Nanoparticles as Anti-Giardia Agents. *Parasitol. Res.* 111, 545–554. doi: 10.1007/s00436-012-2866-1
- Satterwhite, C. L., Torrone, E., Meites, E., Dunne, E. F., Mahajan, R., Ocfemia, M. C., et al. (2013). Sexually Transmitted Infections Among US Women and Men: Prevalence and Incidence Estimates 2008. *Sex Transm. Dis.* 40, 187–193. doi: 10.1097/OLQ.0b013e318286bb53
- Sauvey, C., Ehrenkauf, G., Shi, D., Debnath, A., and Abagyan, R. (2021). Antineoplastic Kinase Inhibitors: A New Class of Potent Anti-Amoebic Compounds. *PloS Negl. Trop. Dis.* 15, e0008425. doi: 10.1371/journal.pntd.0008425
- Scallan, E., Hoekstra, R. M., Angulo, F. J., Tauxe, R. V., Widdowson, M. A., Roy, S. L., et al. (2011). Foodborne Illness Acquired in the United States—major Pathogens. *Emerg. Infect. Dis.* 17, 7–15. doi: 10.3201/eid1701.P11101
- Schmid, G., Narcisi, E., Mosure, D., Secor, W. E., Higgins, J., and Moreno, H. (2001). Prevalence of Metronidazole-Resistant Trichomonas Vaginalis in a Gynecology Clinic. *J. Reprod. Med.* 46, 545–549. doi: 10.1097/00006254-200111000-00015
- Schwabe, J. R., and Barrientes, F. J. (2006). Prevalence of Trichomonas Vaginalis Isolates With Resistance to Metronidazole and Tinidazole. *Antimicrob. Agents Chemother.* 50, 4209–4210. doi: 10.1128/AAC.00814-06
- Secor, W. E., Meites, E., Starr, M. C., and Workowski, K. A. (2014). Neglected Parasitic Infections in the United States: Trichomoniasis. *Am. J. Trop. Med. Hyg.* 90, 800–804. doi: 10.4269/ajtmh.13-0723
- Sedighi, F., Abbasali, P. R., Maghsood, A., and Fallah, M. (2016). Comparison of Therapeutic Effect of Anti-Cryptosporidium Nano-Nitazoxanide (ntz) with Free Form of This Drug in Neonatal Rat. *Scientific J. Hamadan Univ. Med. Sci.* 23, 134–140.
- Sena, A. C., Bachmann, L. H., and Hobbs, M. M. (2014). Persistent and Recurrent Trichomonas Vaginalis Infections: Epidemiology, Treatment and Management Considerations. *Expert Rev. Anti Infect. Ther.* 12, 673–685. doi: 10.1586/14787210.2014.887440
- Sharma, S., and Ahuja, V. (2021). Liver Abscess: Complications and Treatment. *Clin. Liver Dis. (Hoboken)* 18, 122–126. doi: 10.1002/cld.1128



- Sharma, P., Khurana, S., Sharma, A., Sehgal, R., and Malla, N. (2016). Presence of Intracellular Viruses in Human Cryptosporidium Isolates. *Ann. Parasitol.* 62, 139–147. doi: 10.17420/ap6202.46
- Sherrard, J., Wilson, J., Donders, G., Mendling, W., and Jensen, J. S. (2018). 2018 European (IUSTI/WHO) International Union Against Sexually Transmitted Infections (IUSTI) World Health Organisation (WHO) Guideline on the Management of Vaginal Discharge. *Int. J. STD AIDS* 29, 1258–1272. doi: 10.1177/0956462418785451
- Shirley, D. T., Farr, L., Watanabe, K., and Moonah, S. (2018). A Review of the Global Burden, New Diagnostics, and Current Therapeutics for Amebiasis. *Open Forum Infect. Dis.* 5, ofy161. doi: 10.1093/ofid/ofy161
- Shirley, D. A., Sharma, I., Warren, C. A., and Moonah, S. (2021). Drug Repurposing of the Alcohol Abuse Medication Disulfiram as an Anti-Parasitic Agent. *Front. Cell Infect. Microbiol.* 11, 633194. doi: 10.3389/fcimb.2021.633194
- Shrivastava, A. K., Kumar, S., Smith, W. A., and Sahu, P. S. (2017). Revisiting the Global Problem of Cryptosporidiosis and Recommendations. *Trop. Parasitol.* 7, 8–17. doi: 10.4103/2229-5070.202290
- Shrivastav, M. T., Malik, Z., and Somlata, (2020). Revisiting Drug Development Against the Neglected Tropical Disease, Amebiasis. *Front. Cell Infect. Microbiol.* 10, 628257. doi: 10.3389/fcimb.2020.628257
- Silver, B. J., Guy, R. J., Kaldor, J. M., Jamil, M. S., and Rumbold, A. R. (2014). Trichomonas Vaginalis as a Cause of Perinatal Morbidity: A Systematic Review and Meta-Analysis. *Sex Transm. Dis.* 41, 369–376. doi: 10.1097/OLQ.0000000000000134
- Sinkala, E., Katubulushi, M., Sianongo, S., Obwaller, A., and Kelly, P. (2011). In a Trial of the Use of Miltefosine to Treat HIV-Related Cryptosporidiosis in Zambian Adults, Extreme Metabolic Disturbances Contribute to High Mortality. *Ann. Trop. Med. Parasitol.* 105, 129–134. doi: 10.1179/136485911X12899838683160
- Sisson, G., Jeong, J. Y., Goodwin, A., Bryden, L., Rossler, N., Lim-Morrison, S., et al. (2000). Metronidazole Activation is Mutagenic and Causes DNA Fragmentation in Helicobacter Pylori and in Escherichia Coli Containing a Cloned H. Pylori RdxA(+) (Nitroreductase) Gene. *J. Bacteriol.* 182, 5091–5096. doi: 10.1128/JB.182.18.5091-5096.2000
- Snipes, L. J., Gamard, P. M., Narcisi, E. M., Beard, C. B., Lehmann, T., and Secor, W. E. (2000). Molecular Epidemiology of Metronidazole Resistance in a Population of Trichomonas Vaginalis Clinical Isolates. *J. Clin. Microbiol.* 38, 3004–3009. doi: 10.1128/JCM.38.3.3004-3009.2000
- Soares, F. A., Benitez, A. D. N., Santos, B. M. D., Loiola, S. H. N., Rosa, S. L., Nagata, W. B., et al. (2020). A Historical Review of the Techniques of Recovery of Parasites for Their Detection in Human Stools. *Rev. Soc. Bras. Med. Trop.* 53, e20190535. doi: 10.1590/0037-8682-0535-2019
- Soria-Arteche, O., Hernandez-Campos, A., Yopez-Mulia, L., Trejo-Soto, P. J., Hernandez-Luis, F., Gres-Molina, J., et al. (2013). Synthesis and Antiprotozoal Activity of Nitazoxanide-N-Methylbenzimidazole Hybrids. *Bioorg. Med. Chem. Lett.* 23, 6838–6841. doi: 10.1016/j.bmcl.2013.10.011
- Speich, B., Marti, H., Ame, S. M., Ali, S. M., Bogoch, I. I., Utzinger, J., et al. (2013). Prevalence of Intestinal Protozoa Infection Among School-Aged Children on Pemba Island, Tanzania, and Effect of Single-Dose Albendazole, Nitazoxanide and Albendazole-Nitazoxanide. *Parasitol. Vectors* 6, 3. doi: 10.1186/1756-3305-6-3
- Sun, Y., Chen, D., Pan, Y., Qu, W., Hao, H., Wang, X., et al. (2019). Nanoparticles for Antiparasitic Drug Delivery. *Drug Delivery* 26, 1206–1221. doi: 10.1080/10717544.2019.1692968
- Su, H. M., and Tai, J. H. (1996). Genomic Organization and Sequence Conservation in Type I Trichomonas Vaginalis Viruses. *Virology* 222, 470–473. doi: 10.1006/viro.1996.0446
- Tejman-Yarden, N., Miyamoto, Y., Leitsch, D., Santini, J., Debnath, A., Gut, J., et al. (2013). A Repurposed Drug, Auranofin, is Effective Against Metronidazole-Resistant Giardia Lamblia. *Antimicrob. Agents Chemother.* 57, 2029–2035. doi: 10.1128/AAC.01675-12
- Townson, S. M., Upcroft, J. A., and Upcroft, P. (1996). Characterisation and Purification of Pyruvate:Ferredoxin Oxidoreductase From Giardia Duodenalis. *Mol. Biochem. Parasitol.* 79, 183–193. doi: 10.1016/0166-6851(96)02661-8
- Upcroft, J., Mitchell, R., Chen, N., and Upcroft, P. (1996). Albendazole Resistance in Giardia is Correlated With Cytoskeletal Changes But Not With a Mutation at Amino Acid 200 in Beta-Tubulin. *Microb. Drug Resist.* 2, 303–308. doi: 10.1089/mdr.1996.2.303
- Upcroft, J. A., and Upcroft, P. (1993). Drug Resistance and Giardia. *Parasitol. Today* 9, 187–190. doi: 10.1016/0169-4758(93)90144-5
- Upcroft, P., and Upcroft, J. A. (2001). Drug Targets and Mechanisms of Resistance in the Anaerobic Protozoa. *Clin. Microbiol. Rev.* 14, 150–164. doi: 10.1128/CMR.14.1.150-164.2001
- Valdez, C. A., Tripp, J. C., Miyamoto, Y., Kalisiak, J., Hruz, P., Andersen, Y. S., et al. (2009). Synthesis and Electrochemistry of 2-Ethenyl and 2-Ethanyl Derivatives of 5-Nitroimidazole and Antimicrobial Activity Against Giardia Lamblia. *J. Med. Chem.* 52, 4038–4053. doi: 10.1021/jm900356n
- Vazini, H. (2017). Anti-Trichomonas Vaginalis Activity of Nano Micana Cordifolia and Metronidazole: An In Vitro Study. *J. Parasitol. Dis.* 41, 1034–1039. doi: 10.1007/s12639-017-0930-6
- Victoria-Hernandez, J. A., Ventura-Saucedo, A., Lopez-Morones, A., Martinez-Hernandez, S. L., Medina-Rosales, M. N., Munoz-Ortega, M., et al. (2020). Case Report: Multiple and Atypical Amoebic Cerebral Abscesses Resistant to Treatment. *BMC Infect. Dis.* 20, 669. doi: 10.1186/s12879-020-05391-y
- Vivancos, V., Gonzalez-Alvarez, I., Bermejo, M., and Gonzalez-Alvarez, M. (2018). Giardiasis: Characteristics, Pathogenesis and New Insights About Treatment. *Curr. Top. Med. Chem.* 18, 1287–1303. doi: 10.2174/1568026618666181002095314
- Wang, B., Castellanos-Gonzalez, A., and White, A. C.Jr. (2020). Novel Drug Targets for Treatment of Cryptosporidiosis. *Expert Opin. Ther. Targets* 24, 915–922. doi: 10.1080/14728222.2020.1785432
- Wang, A. L., and Wang, C. C. (1986). Discovery of a Specific Double-Stranded RNA Virus in Giardia Lamblia. *Mol. Biochem. Parasitol.* 21, 269–276. doi: 10.1016/0166-6851(86)90132-5
- Wassmann, C., Hellberg, A., Tannich, E., and Bruchhaus, I. (1999). Metronidazole Resistance in the Protozoan Parasite Entamoeba Histolytica is Associated With Increased Expression of Iron-Containing Superoxide Dismutase and Peroxiredoxin and Decreased Expression of Ferredoxin 1 and Flavin Reductase. *J. Biol. Chem.* 274, 26051–26056. doi: 10.1074/jbc.274.37.26051
- Weir, C. B., and Le, J. K. (2021). “Metronidazole,” in *StatPearls* (Treasure Island (FL): StatPearlsPublishing). Available at: <http://www.ncbi.nlm.nih.gov/books/NB>.
- Workowski, K. A., Bachmann, L. H., Chan, P. A., Johnston, C. M., Muzny, C. A., Park, I., et al. (2021). Sexually Transmitted Infections Treatment Guideline. *MMWR Recomm. Rep.* 70, 1–187. doi: 10.15585/mmwr.rr7004a1
- Yang, S., Zhao, W., Wang, H., Wang, Y., Li, J., and Wu, X. (2018). Trichomonas Vaginalis Infection-Associated Risk of Cervical Cancer: A Meta-Analysis. *Eur. J. Obstet. Gynecol. Reprod. Biol.* 228, 166–173. doi: 10.1016/j.ejogrb.2018.06.031
- Zhang, Y., Feng, J., Mcmanus, S. A., Lu, H. D., Ristroph, K. D., Cho, E. J., et al. (2017). Design and Solidification of Fast-Releasing Clofazimine Nanoparticles for Treatment of Cryptosporidiosis. *Mol. Pharm.* 14, 3480–3488. doi: 10.1021/acs.molpharmaceut.7b00521

**Conflict of Interest:** The authors declare that the research was conducted in the absence of any commercial or financial relationships that could be construed as a potential conflict of interest.

**Publisher's Note:** All claims expressed in this article are solely those of the authors and do not necessarily represent those of their affiliated organizations, or those of the publisher, the editors and the reviewers. Any product that may be evaluated in this article, or claim that may be made by its manufacturer, is not guaranteed or endorsed by the publisher.

Copyright © 2022 Santos and Rebello. This is an open-access article distributed under the terms of the Creative Commons Attribution License (CC BY). The use, distribution or reproduction in other forums is permitted, provided the original author(s) and the copyright owner(s) are credited and that the original publication in this journal is cited, in accordance with accepted academic practice. No use, distribution or reproduction is permitted which does not comply with these terms.



# Targeting the *Plasmodium falciparum*'s Thymidylate Monophosphate Kinase for the Identification of Novel Antimalarial Natural Compounds

Kweku S. Enninful<sup>1</sup>, Samuel K. Kwofie<sup>2,3</sup>, Mark Tetteh-Tsifoanya<sup>1</sup>, Amanda N. L. Lamptey<sup>1</sup>, Georgina Djameh<sup>1</sup>, Samuel Nyarko<sup>1</sup>, Anita Ghansah<sup>1</sup> and Michael D. Wilson<sup>1,4\*</sup>

<sup>1</sup> Department of Parasitology, Noguchi Memorial Institute for Medical Research, University of Ghana, Accra, Ghana,

<sup>2</sup> Department of Biomedical Engineering, School of Engineering Sciences, University of Ghana, Accra, Ghana, <sup>3</sup> West African Centre for Cell Biology of Infectious Pathogens, College of Basic and Applied Sciences, University of Ghana, Accra, Ghana,

<sup>4</sup> Stritch School of Medicine, Loyola University of Chicago, Maywood, IL, United States

## OPEN ACCESS

### Edited by:

Vipin Kumar,  
Guru Nanak Dev University, India

### Reviewed by:

Conrad Simoben Veranso,  
University of Buea, Cameroon  
Tingxiang Yan,  
Shanghai Jiao Tong University, China

### \*Correspondence:

Michael D. Wilson  
mwilson@noguchi.ug.edu.gh

### Specialty section:

This article was submitted to  
Clinical Microbiology,  
a section of the journal  
Frontiers in Cellular and  
Infection Microbiology

**Received:** 02 February 2022

**Accepted:** 25 April 2022

**Published:** 25 May 2022

### Citation:

Enninful KS, Kwofie SK,  
Tetteh-Tsifoanya M, Lamptey  
ANL, Djameh G, Nyarko S,  
Ghansah A and Wilson MD (2022)  
Targeting the *Plasmodium*  
*falciparum*'s Thymidylate  
Monophosphate Kinase for the  
Identification of Novel Antimalarial  
Natural Compounds.  
Front. Cell. Infect. Microbiol. 12:868529.  
doi: 10.3389/fcimb.2022.868529

Recent reports of resistance to artemisinin-based combination drugs necessitate the need to discover novel antimalarial compounds. The present study was aimed at identifying novel antimalarial compounds from natural product libraries using computational methods. *Plasmodium falciparum* is highly dependent on the pyrimidine biosynthetic pathway, a *de novo* pathway responsible for the production of pyrimidines, and the parasite lacks the pyrimidine salvage enzymes. The *P. falciparum* thymidylate monophosphate kinase (*PfTMPK*) is an important protein necessary for rapid DNA replication; however, due to its broad substrate specificity, the protein is distinguished from its homologs, making it a suitable drug target. Compounds from AfroDB, a database of natural products originating from Africa, were screened virtually against *PfTMPK* after filtering the compounds for absorption, distribution, metabolism, excretion, and toxicity (ADMET)-acceptable compounds with FAF-Drugs4. Thirteen hits with lower binding energies than thymidine monophosphate were selected after docking. Among the thirteen compounds, ZINC13374323 and ZINC13365918 with binding energies of  $-9.4$  and  $-8.9$  kcal/mol, respectively, were selected as plausible lead compounds because they exhibited structural properties that ensure proper binding at the active site and inhibitory effect against *PfTMPK*. ZINC13374323 (also called aurantiamide acetate) is known to exhibit anti-inflammatory and antiviral activities, and ZINC13365918 exhibits antileishmanial activity. Furthermore, aurantiamide acetate, which is commercially available, is a constituent of *Artemisia annua*, the herb from which artemisinin was derived. The compound also shares interactions with several residues with a potent thymidine analog inhibitor of *PfTMPK*. The anti-plasmodial activity of aurantiamide acetate was evaluated *in vitro*, and the mean half-maximal inhibitory concentration ( $IC_{50}$ ) was  $69.33 \mu M$  when synchronized *P. falciparum* 3D7 culture was used as

compared to  $IC_{50} > 100 \mu M$  with asynchronized culture. The significance of our findings within the context of malaria treatment strategies and challenges is discussed.

**Keywords:** *Plasmodium falciparum*, aurantiamide acetate, *PfTMPK*, *Artemisia annua*, natural compounds

## INTRODUCTION

*Plasmodium falciparum* is among the five *Plasmodium* parasites that cause human malaria and is also responsible for the most severe form of the disease (Tuteja, 2007; Ludin et al., 2012; Spitzmüller and Mestres, 2013; Bhatt et al., 2015). Recent studies have reported *P. falciparum* to be developing resistance to current major antimalarial drugs (Egwu et al., 2022), which warrants the identification and development of new antimalarials as a necessity. Throughout the history of malaria chemotherapy, the most successful antimalarials have been natural products. Antimalarials such as chloroquine were developed from quinine, which was extracted from the bark of the *Cinchona* tree from South America. Artemisinin was also obtained from *Artemisia annua* originating from China (Tajuddeen and Van Heerden, 2019). Medicinal herbs have generally proven to be very effective drugs against parasitic diseases (Siddiqui et al., 2014). Even though both chloroquine and artemisinin have been plagued with resistance to the parasite, research into natural product antimalarials remains a priority. Out of about 1,524 compounds with anti-plasmodial activity reported between 2010 and 2017, 39% were natural products, with 29% of the compounds having half-maximal inhibitory concentration ( $IC_{50}$ )  $\leq 3.0 \mu M$  against at least one *Plasmodium* strain (Tajuddeen and Van Heerden, 2019). This reinforces the urgent need to exploit natural products to unravel future potent biotherapeutic molecules.

Research efforts at developing new antimalarials have uncovered diverse pathways and protein targets of which some are novel (Belete, 2020; Agamah et al., 2021). It is worthwhile to mention that new antimalarials, currently in the clinical trial phase, have been identified against critical pathways and targets (Kumar et al., 2018; Belete, 2020). However, a good number remain unexploited, while others have not yielded any potent drugs. Identification of new antimalarial targets from novel pathways not associated with resistance must be explored by screening diverse compound libraries (Ludin et al., 2012; Spitzmüller and Mestres, 2013).

Thymidylate monophosphate kinase catalyzes the reversible phosphorylation of dTMP to deoxythymidine diphosphate (dTDP), which is an important step for cellular DNA synthesis (Cassera et al., 2011; Krungkrai and Krungkrai, 2016; Vanoevelen et al., 2022). It has a broad substrate specificity, which distinguishes it from other homologs, making it a suitable target (Reyes et al., 1982; Cassera et al., 2011; Krungkrai and Krungkrai, 2016). *P. falciparum* thymidylate monophosphate kinase (*PfTMPK*) is involved in the pyrimidine biosynthetic pathway, a *de novo* pathway responsible for the production of pyrimidines, which are necessary for rapid DNA replication (Reyes et al., 1982; Cassera et al., 2011; Krungkrai and Krungkrai, 2016). The pathway

is preferred because the parasite is highly dependent on it since it lacks pyrimidine salvage enzymes (Cassera et al., 2011; Krungkrai and Krungkrai, 2016).

So far, thiourea has been shown to exhibit inhibitory activity against *PfTMPK*, the compound that was first discovered to inhibit the TMPK of *Mycobacterium tuberculosis* (*MtTMPK*) (Cui et al., 2012; Patrick and Turner, 2020). The inhibitory effect of thiourea on *PfTMPK* is however weaker than that of *MtTMPK*. Several analogs containing thiourea or urea have since been tested for antimalarial activity through the inhibition of *PfTMPK* (Cui et al., 2012). However, the analogs have mostly exhibited weak inhibition against *PfTMPK*. The most active analog, phenylurea, exhibited an  $EC_{50}$  of 28 nM but was reported to be a weak inhibitor of *PfTMPK* with a binding affinity of 200  $\mu M$  (Cui et al., 2012; Chen et al., 2018). It was also observed that ureas showed more antimalarial activities than thioureas (Cui et al., 2012; Patrick and Turner, 2020).

In this study, new antimalarials are predicted for *P. falciparum* by virtually screening an African natural product library against *PfTMPK*. Recently, the development of quantitative structure–activity relationship (QSAR) models has contributed significantly to antimalarial discovery (Neves et al., 2020). As such, this study explores the structural insights for *PfTMPK* inhibition using QSAR modeling, pharmacophore mapping, and docking studies (Ojha and Roy, 2013) to select the most plausible antimalarial lead compounds with good pharmacological profiles from compounds in the AfroDB database. Molecular dynamic simulations were also undertaken to provide insights into the binding mechanisms of *PfTMPK*.

## METHODOLOGY

### *In-Silico* Absorption, Distribution, Metabolism, Excretion, and Toxicity Filtering of the Natural Product Database

A total of 885 African natural products were retrieved from AfroDB (Ntie-Kang et al., 2013) in “.sdf” format for absorption, distribution, metabolism, excretion, and toxicity (ADMET) analysis. The compounds were screened via FAF-Drugs4 (Lagorce et al., 2017) to elucidate their pharmacokinetic, structural, and physicochemical properties. The physicochemical filter used for the compounds was “Drug likeness”. The compounds were categorized as “rejected”, “intermediate”, or “accepted” by FAF-Drugs4. “Accepted” compounds were then chosen for molecular docking.

### Virtual Screening

The “accepted” compounds from the FAF-Drugs4 ADMETox prediction were docked against *PfTMPK*, using AutoDock Vina

(Trott and Olson, 2010) integrated with PyRx (Dallakyan and Olson, 2015). The substrate of *Pf*TMPPK (TMP) was also extracted from the complex (Protein Data Bank (PDB) ID: 2wwf) and added to the library of “accepted” compounds for docking. Before the docking, the compounds were energy minimized with OpenBabel using the universal force field (uff) before converting to “.pdbqt” formats (Kwofie et al., 2021). A grid box size of 17.3, 9.7, and 11.2 Å and center dimensions of 42.5, 46.7, and 47.6 Å all in the x, y, and z coordinate axes were used, respectively.

## Docking Method Validation

For validation of the performance of the docking technique, the SMILES of five potent inhibitors (compounds 28, 30, 53, 54, and 55) against *Pf*TMPPK (Cui et al., 2012) were used to generate their decoys via Rapid DEcoy Retriever (RADER) (Wang et al., 2017). A total of 243 decoys were obtained and screened together with the five inhibitors against *Pf*TMPPK using AutoDock Vina. The docking results were used to generate a receiver operating characteristic (ROC) curve, and the area under the curve (AUC) was computed using easy ROC Ver. 1.3 (Goksuluk et al., 2016). Parameters used for the ROC generation and calculation of AUC were a non-parametric method for curve fitting (DeLong et al., 1988) for SE estimation and CI as well as a Type I error of 0.05.

The co-crystallized ligands of *Pf*TMPPK were removed from their binding site and re-docked against *Pf*TMPPK. The best-predicted docking pose of each ligand was superimposed with its respective experimental co-crystallized ligand pose, and their root mean square deviation (RMSD) was calculated using LigAlign (Heifets and Lilien, 2010).

## Molecular Dynamic Simulations of Complexes

Molecular dynamics simulations were performed using the *Pf*TMPPK in complex with TMP and the respective chosen potential lead compounds. GROningen MACHine for Chemical Simulation (GROMACS) version 5.1.4 (Van Der Spoel et al., 2005) was used to perform the molecular dynamics simulations using the GROMOS96 43A1 force field. The topology of the compounds was generated using PRODRG (Schüttelkopf and Van Aalten, 2004). As part of the preparation before the simulation, the complexes were first solvated in a 1-nm dodecahedron water box and neutralized by adding one positive ion. The complexes were relaxed through energy minimization to remove any steric clashes or bad geometry and equilibrated to the required temperature (300K) and density (1,020 kg/m<sup>3</sup>). After the respective systems were equilibrated and set in the desired temperature and density, a 100-ns production run was performed, and the results of the simulations were analyzed using Xmgrace version 5.1.25 (Vaught, 1996).

## In-Vitro Parasite Growth Inhibition Assay

One of the potential lead compounds, aurantiamide acetate, was tested for anti-plasmodial activity using the SYBR Green I fluorescence assay as described previously (Smilkstein et al., 2004). Stock concentrations of 100 mM [100% dimethyl

sulfoxide (DMSO)] of compounds were diluted with culture media to a working concentration of 100 µM (0.1% DMSO). A serial dilution of 1:2 concentrations of the compound (10 to 0.781 µM) was prepared for the assay. Artesunate was the reference drug diluted from 100 to 3.125 nM. Test wells were initially seeded with 90 µl of ring-stage (synchronized) parasitized red blood cells (pRBCs), culture media, and pRBCs at 2% hematocrit and 1% parasitemia. An aliquot of 10 µl of each concentration was dispensed into each well in triplicates. The wells containing RBCs (2% hematocrit), pRBCs, and cultured protoplast washing (CPW) media served as negative and blank controls and were then incubated for 48 h. An aliquot of 100 µl of 4× buffered SYBR Green I (0.20 µl of 10,000× SYBR Green I/ml of 1× phosphate-buffered saline) was then added for a further 30 min at 37°C. The presence and amount of pRBCs were detected by fluorescence using the Guava EasyCyte HT FACS machine (Millipore, Billerica, MA, USA), and parasitemia was recorded in percentages. The IC<sub>50</sub> was extrapolated from non-linear regression curves of percentage inhibition versus log-concentration curves from GraphPad Prism (Graph Pad Software, San Diego, CA, USA) using algorithms obtained from flow cytometry (fluorescence-activated cell sorting (FACS)) data. The experiment was repeated using an asynchronized parasite culture using the same protocol.

## RESULTS AND DISCUSSION

### Target Structure

The three-dimensional structure of *Pf*TMPPK retrieved from the PDB (PDB ID: 2wwf) was solved using X-ray crystallography at a resolution of 1.89 Å (Whittingham et al., 2010). The 2wwf is a homo-oligomer (homodimer) consisting of three chains of *Pf*TMPPK in complex adenosine diphosphate (ADP) and thymidine monophosphate (TMP), which is a natural substrate. Other ligands like sodium-ion and glycerol are also present. **Figure 1** shows chain A of 2wwf with the active site, and TMP is highlighted. The protein has a sequence length of 212 and is significantly different from the human TMPPK with a sequence identity of 36.9%.

### Absorption, Distribution, Metabolism, Excretion, and Toxicity-Acceptable Compounds

ADMET tests are performed to eliminate compounds that may be weak drug candidates so that potential drug-like compounds are prioritized (Sliwoski et al., 2013). FAF drug server uses quantitative QSAR models to predict specific properties or toxicological endpoints of compounds (Lagorce et al., 2017). The predicted properties were compared with the standard range of accepted values concerning the chosen physicochemical filter, which was “drug-likeness”. The filtered compounds were categorized as “rejected”, “intermediate”, or “accepted”. The “accepted” compounds are those with no structural alerts and satisfy the physicochemical filter. Intermediate and rejected compounds show some structural alerts and do not satisfy



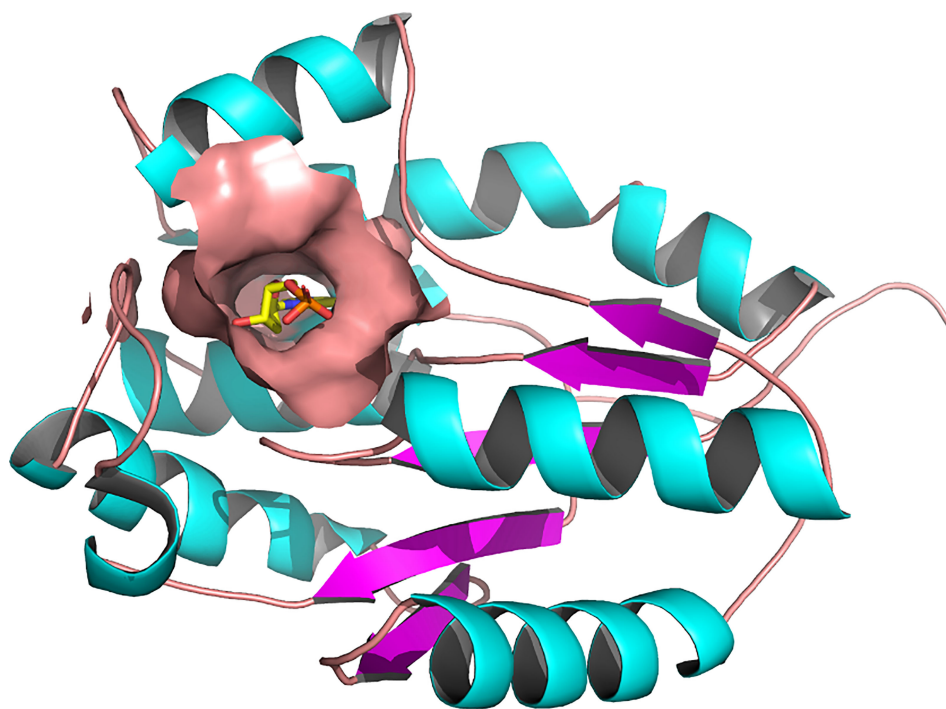


**FIGURE 1** | Three-dimensional structure of *Plasmodium falciparum* thymidylate monophosphate kinase (PDB ID: 2WWF) and its active site (Whittingham et al., 2010). A cartoon representation of the 3D structure of *PfTMPK*. The surface representation shows the active site of *PfTMPK* and binding in its natural substrate, thymidine monophosphate (TMP), represented by yellow sticks. Active site residues include Asp17, Lys21, Leu59, Phe44, Arg47, Pro45, Phe74, Arg78, Arg99, Tyr100, Ser103, Gly104, Tyr107, and Tyr153 (Kandeel et al., 2009). The protein structure was retrieved from the Protein Data Bank, and image was generated with PyMOL.

completely the physicochemical filter. Structural alerts are substructures that are related to mutagenic and carcinogenic properties, which are undesirable for drug-likeness (Benigni and Bossa, 2006). After the compounds were screened using the FAF drug, 91 compounds categorized as “accepted” were used for docking against *PfTMPK*.

### Docking Protocol Validation

To validate AutoDock Vina’s ability to distinguish between active and inactive compounds concerning *PfTMPK*, a ROC curve (**Figure 2**) was generated after virtually screening five potent inhibitors of *PfTMPK* (Cui et al., 2012) (**Table 1**) and their decoys against the receptor. The AUC value was calculated to assess the docking performance. AUC value less than 0.5 is considered a poor discrimination ability, from 0.5 to 0.7 is considered moderate, and greater than 0.7 is acceptable (Mandrekar, 2010). AUC value very close to 1 indicates an excellent discriminatory ability of the docking model for the receptor (Mandrekar, 2010). The AUC obtained was 0.95 with a p-value of  $9.776159 \times 10^{-78}$ , indicating an excellent discriminatory ability of AutoDock Vina to distinguish between active compounds and decoys of *PfTMPK*.

To validate further the docking approach used, four co-crystallized *PfTMPK* ligands (three of which are complexed with inhibitors and a substrate) were retrieved from their PDB crystal structures and re-docked against the *PfTMPK* protein

structures. The co-crystallized binding poses of the ligands were superimposed to their respective predicted docking poses, and RMSDs less than 2 Å were obtained for all of them. This suggests that AutoDock Vina reasonably distinguished between active and inactive compounds for *PfTMPK* and accurately predicted binding poses.

### Virtual Screening Analysis and Lead Identification

Ninety-one pre-filtered drug-like compounds were screened against *PfTMPK* together with its natural substrate and known potent inhibitors. After docking, thirteen of the drug-like compounds had binding affinities greater than the protein’s substrate and were selected as hits (**Table 2**). The binding energies of three potent inhibitors were −8.9, −9.3, and −9.7 kcal/mol for compounds 28, 53, and 55, respectively, which fell within the same range as the hits. The lowest energies among them were −10.5 and −10.2 kcal/mol for compounds 54 and 30, respectively, which were not far from the lowest among the hits (−9.9 kcal/mol). This is a good indication of the potential antimalarial activity of the hits. Lead compounds were then selected among the hits. Four structural properties of a molecule that ensure proper binding at the active site and inhibitory effect against *PfTMPK*, developed using QSAR analysis, pharmacophore modeling, and docking studies with a set of thymidine analogs that have well-defined *PfTMPK* inhibitory



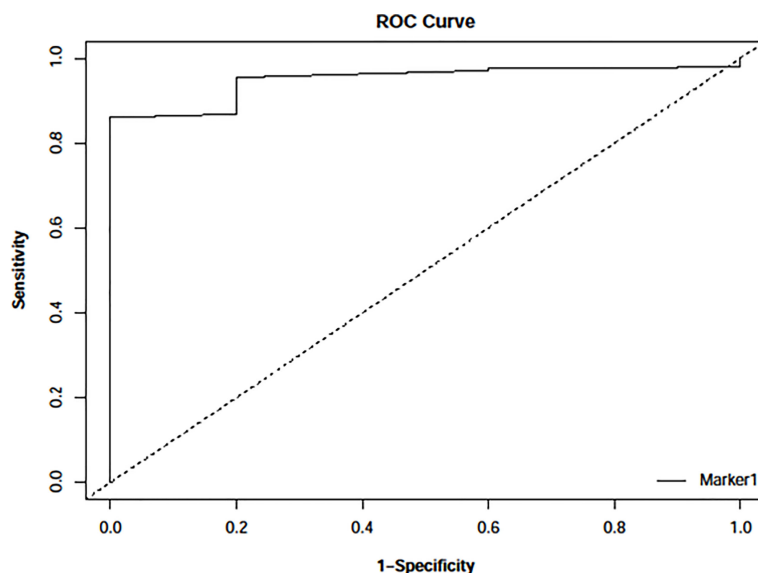


**FIGURE 2** | Receiver operating characteristic (ROC) curve generated with easyROC (Goksuluk et al., 2016) after docking 243 decoys and 5 potent inhibitors against *Pf*TMPK using AutoDock Vina via PyRx version 0.8. The area under the curve (AUC) obtained was 0.94897 with a p-value of  $9.776159 \times 10^{-78}$ .

activity, were considered in selecting possible lead compounds (Ojha and Roy, 2013). These properties are the presence of –NH fragment, –OH group, urea moiety, and a considerable amount of oxygen atoms (Ojha and Roy, 2013).

The molecular structures of the hit compounds were analyzed to identify any of the aforementioned structural properties. ZINC13374323 possesses –NH group, urea moiety, and a considerable amount of oxygen atoms, while ZINC13365918 also has all the properties but lacks oxygen atoms. ZINC14644461, ZINC95486293, ZINC95486295, and ZINC87493012 all have –OH groups and considerable amounts of oxygen atoms, while ZINC13282986 possesses none of the structural properties. The rest of the six compounds only possess oxygen atoms among the aforementioned structural properties. Most of the compounds seem to possess considerable amounts of O-atoms, which is an essential requirement for high binding affinity toward *Pf*TMPK. The most distinctive structural properties were the presence of NH fragment and urea moiety, which were exhibited only by

ZINC13374323 and ZINC13365918. Although all four properties are essential for good inhibitory activity against *Pf*TMPK (Ojha and Roy, 2013), a ligand with at least three of the properties, placing priority on the distinctive properties (presence of –NH fragment and urea moiety), may exhibit a good inhibitory effect against the compound with no or little modifications. As such, ZINC13374323 and ZINC13365918 were considered the potential lead compounds among the 13 hits.

## Protein–Ligand Interactions

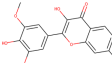
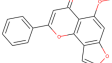
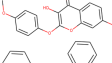
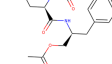
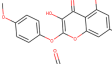
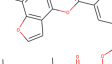
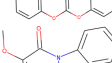
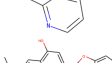
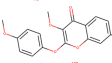
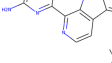
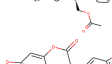
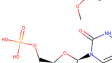
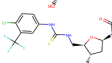
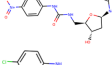
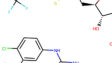
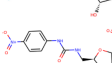
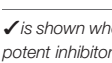
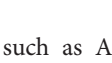
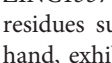
Protein–ligand molecular interactions of ZINC13374323 and ZINC13365918 were further studied and compared to the protein–ligand molecular interaction of compound 25, a *Pf*TMPK inhibitor thymidine analog, which has been shown to exhibit very high activity against the protein (Ojha and Roy, 2013). Compound 25 has been reported to share molecular interactions with protein residues Arg78, Arg99, Arg47, Asp17, Ser22, Phe74, and Tyr43 (Ojha and Roy, 2013). In **Figure 3A**, we show the substrate to share interactions with similar residues

**TABLE 1** | List of potent inhibitors and co-crystallized ligands showing the  $K_i$  values (Cui et al., 2012), the respective PDB IDs, and RMSD values of the aligned co-crystallized and re-docked ligands.

Compound	Type	$K_i$ ( $\mu$ M)	Ligand	PDB ID	RMSD ( $\text{\AA}$ )
Thymidine monophosphate	Substrate	( $K_m = 11 \mu\text{M}$ )	TMP	2wwf	0.376
Compound 28	Inhibitor	31	74W	2yof (chain C)	1.768
Compound 30	Inhibitor	11	74X	2yog	1.741
Compound 53	Inhibitor	25	WMJ	2yoh	1.073
Compound 54	Inhibitor	27	–	–	–
Compound 55	Inhibitor	11	–	–	–

PDB, Protein Data Bank; RMSD, root mean square deviation.

**TABLE 2 |** List of hits showing their structures, binding energies, and structural properties.

Compound	Binding energy (kcal/mol)	Structural properties			
		NH fragment	OH group	More O-atoms	Urea moiety
 ZINC14644461	−9.9	✗	✓	✓	✗
 ZINC14677166	−9.7	✗	✗	✓	✗
 ZINC95486297	−9.6	✗	✗	✓	✗
 ZINC13374323	−9.4	✓	✗	✓	✓
 ZINC95486293	−9.4	✗	✓	✓	✗
 ZINC14504006	−9.3	✗	✗	✓	✗
 ZINC95486295	−9.2	✗	✓	✓	✗
 ZINC13282986	−9	✗	✗	✗	✗
 ZINC87493012	−9	✗	✓	✓	✗
 ZINC95486296	−9	✗	✓	✗	✗
 ZINC13365918	−8.9	✓	✗	✓	✓
 ZINC95486004	−8.9	✗	✗	✓	✗
 ZINC05357841	−8.8	✗	✗	✓	✗
 TMP	−8.7	. —	. —	. —	. —
 Compound 28	−9.3	. —	. —	. —	. —
 Compound 30	−10.2	. —	. —	. —	. —
 Compound 53	−8.9	. —	. —	. —	. —
 Compound 54	−10.5	. —	. —	. —	. —
 Compound 55	−9.7	. —	. —	. —	. —

✓ is shown when the structural property applies to the compound, while ✗ is shown when the property does not apply. Structures and binding energies of the substrate (TMP) and the five potent inhibitors are included.

such as Arg78, Arg99, Arg47, and Phe74. From **Figure 3C**, ZINC13374323 is also shown to have interactions with common residues such as compound 25. ZINC13365918, on the other hand, exhibited interactions with Asp17 and Phe74 among the listed residues (**Figure 3B**). This warranted the experimental

characterization of ZINC13374323 to corroborate potential inhibitory activity against *Pf*TMPK. H-bond interactions with Asp17 and Pi-Pi stacked interactions with Tyr107 and Phe74 are common among both ligands. This may indicate the importance of the residues for effective binding. One can suggest that the lack

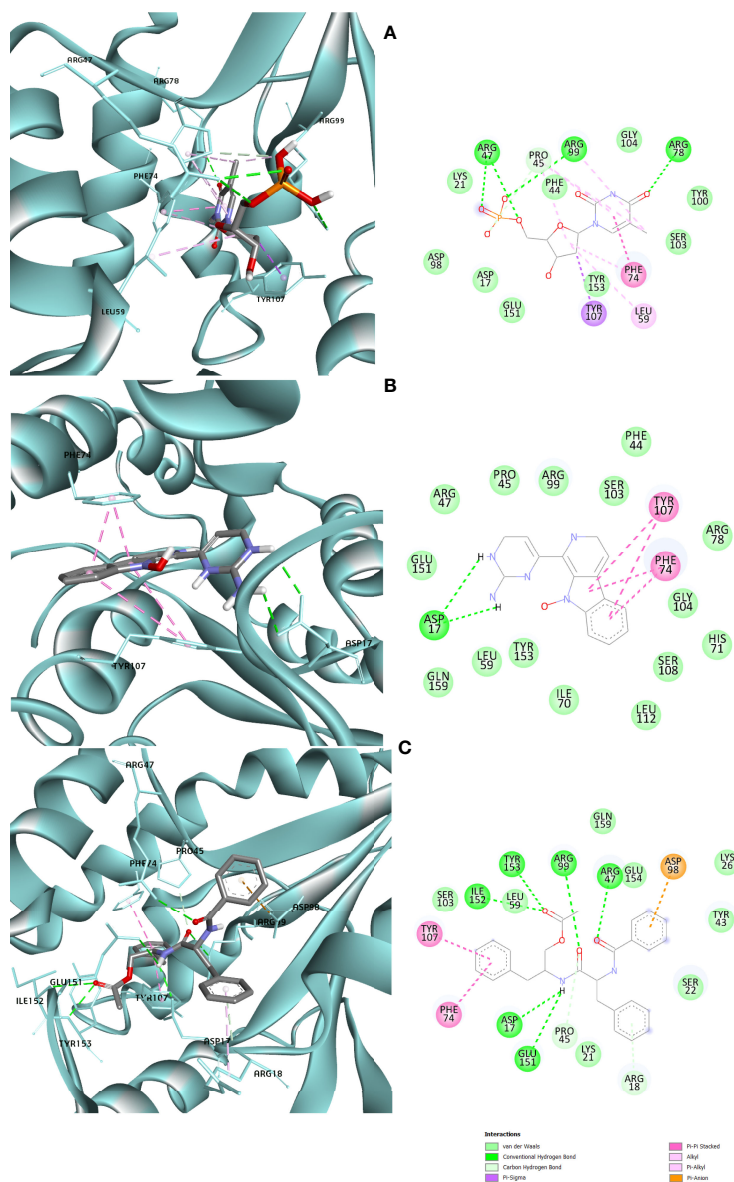


**FIGURE 3** | 3D and 2D images of the protein–ligand interactions between *Pf*TMPK and (A) TMP, (B) ZINC13365918, and (C) ZINC13374323. TMP forms H-bonds with Arg47, Arg99, and Arg78; ZINC13374323 is shown to have H-bond interactions with Arg99, Arg47, Asp17, Glu151, Ile152, and Tyr153; ZINC13365918 forms H-bonds with only Asp17.

of more O-atoms in ZINC13365918 significantly affects its ability to form H-bonds with important residues such as Arg47 and Arg99. TMP and ZINC13374323 were able to form H-bonds with both Arg47 and Arg99 using their O-atoms. However, a lack of an OH-group did not seem to affect the ligands' interactions, since none of them formed any bonds with it.

## Molecular Dynamics Simulations

### Stability of Protein–Ligand Complexes

Molecular dynamics simulations were performed to compare the stability of the distinctive protein–ligand complexes of *Pf*TMPK

with TMP, ZINC13374323, and ZINC13365918. To accomplish that, the RMSDs of the complexes were generated after the simulation (**Figure 4**). The results showed that *Pf*TMPK–ZINC13374323 behaved very similarly to *Pf*TMPK–TMP in terms of stability. Complex *Pf*TMPK–ZINC13365918 shows a higher RMSD but has much fewer fluctuations than *Pf*TMPK–TMP and *Pf*TMPK–ZINC13374323, maintaining an RMSD of 0.34 nm from 15- to 90-ns simulation time. Complexes *Pf*TMPK–TMP and *Pf*TMPK–ZINC13374323 exhibited RMSD from 0.25 nm at the first 20 ns of the simulation to 0.26 nm between 20 ns and 60 ns and 0.27 nm in the final 10 ns of the simulation.

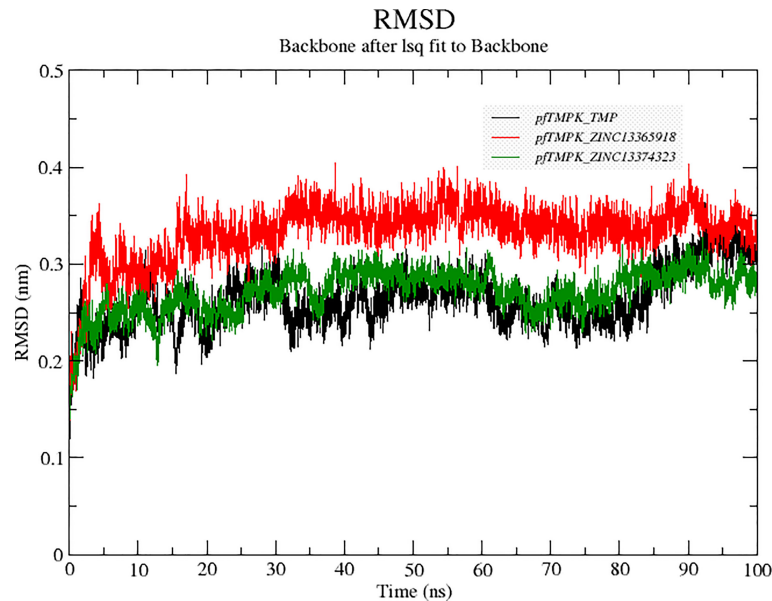


**FIGURE 4** | Root mean square deviation (RMSD) graphs comparing the RMSDs of *PfTMPK* in complex with its natural substrate (TMP) and the respective lead compounds. The RMSD graph for *PfTMPK*–TMP is colored black, for *PfTMPK*–ZINC13365918 red, and for *PfTMPK*–ZINC13374323 green.

### Influence of Ligand Binding on the Flexibility of *PfTMPK*

A comparison of the behavior of the protein residues in each complex was also done using the root mean square fluctuations (RMSFs) (**Figure 5**). It can be observed from the graph that the

protein residues experienced higher fluctuations in *PfTMPK*–ZINC13365918 than in the other complexes and the unbounded *PfTMPK*. The fluctuations of *PfTMPK*–ZINC13374323 and *PfTMPK*–TMP seem to be very close, indicating a similar margin of flexibility within the protein when complexed with

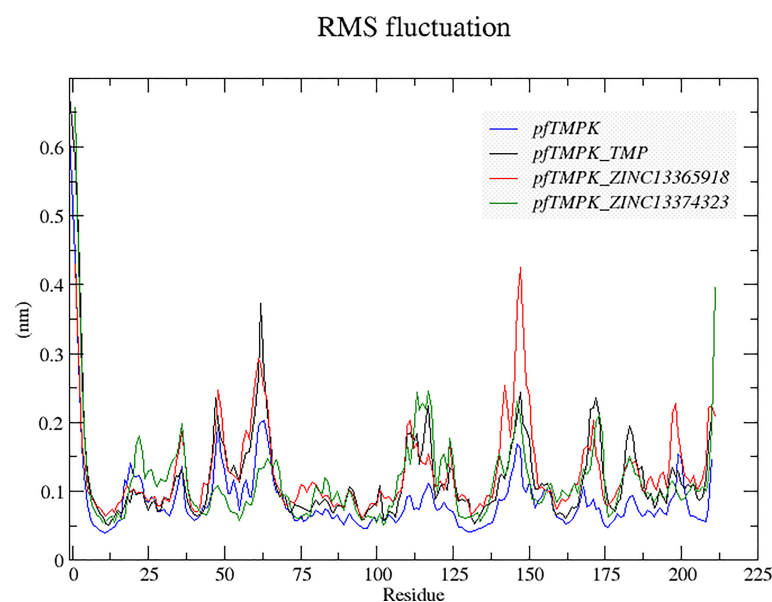


**FIGURE 5** | Root mean square fluctuation (RMSF) graphs comparing the behaviors of the residues of *PfTMPK* in complex with its natural substrate (TMP) and the respective compounds with those of the unbound protein. The RMSF graph for the unbound *PfTMPK* is shown in blue, for *PfTMPK*–TMP black, for *PfTMPK*–ZINC13365918 red, and green for *PfTMPK*–ZINC13374323.



either ZINC13374323 or TMP. A similar observation was made with their RMSDs. However, all the complexes generally experienced more fluctuations than the unbound protein throughout the simulation. The fluctuations were most probably induced by the effect of the binding of the ligands.

### Binding Interactions During Molecular Dynamics Simulations

To determine if ZINC13374323 and ZINC13365918 can maintain strong interactions with *Pf*TMPK, the numbers of hydrogen bonds formed between the respective compounds and *Pf*TMPK throughout the simulation were analyzed. This suggests a continuous bind of the ligand in the binding site under harsh dynamic conditions. The average number of hydrogen bonds (**Figure 6**) shared between *Pf*TMPK–ZINC13365918 and *Pf*TMPK–ZINC13374323 complexes during the entire simulation decreased to between 1 and 2. Complex *Pf*TMPK–ZINC13374323 formed 3 and 4 hydrogen bonds more frequently during the simulation as compared to *Pf*TMPK–ZINC13365918. Complex *Pf*TMPK–ZINC13365918 reached as high as 5 and 6 hydrogen bonds, but this happened very few times in the simulation. The average hydrogen bonds shown were consistent with the H-bond interactions obtained after molecular docking (**Figures 3B, C**).

### Exploring Biological Activities of Potential Lead Compounds

The common name of ZINC13374323 is aurantiamide acetate, which has been shown to exhibit anti-inflammatory and antiviral activities in influenza-infected cells (Zhou et al., 2017). The compound is a constituent of herbs such as the bark of *Albizia adianthifolia* and *Brillantaisia lamium*, where it has been shown to exhibit antimicrobial activity (Tamokou et al., 2011; Tamokou et al., 2012). Interestingly, aurantiamide acetate is also an ingredient of *A. annua*, the Chinese herb from which artemisinin was discovered (Milne et al., 2018). ZINC13365918 is a pyrimidine analog with the name *N*-hydroxyannomontine. *N*-Hydroxyannomontine has been shown to exhibit antileishmanial activity against *Leishmania braziliensis* and *Leishmania guyanensis* (Costa et al., 2006). The toxicity profiles of both compounds as shown in **Table 3** indicate the compounds to be generally safe, with aurantiamide acetate tending to cause some irritation. The toxicity profile was generated with OSIRIS DataWarrior version 5.5.0 (Sander et al., 2015).

We explored the anti-plasmodial activity of aurantiamide acetate further since it is commercially available. *N*-Hydroxyannomontine is currently not commercially available; as such, *in vitro* experimentation for this analog was not

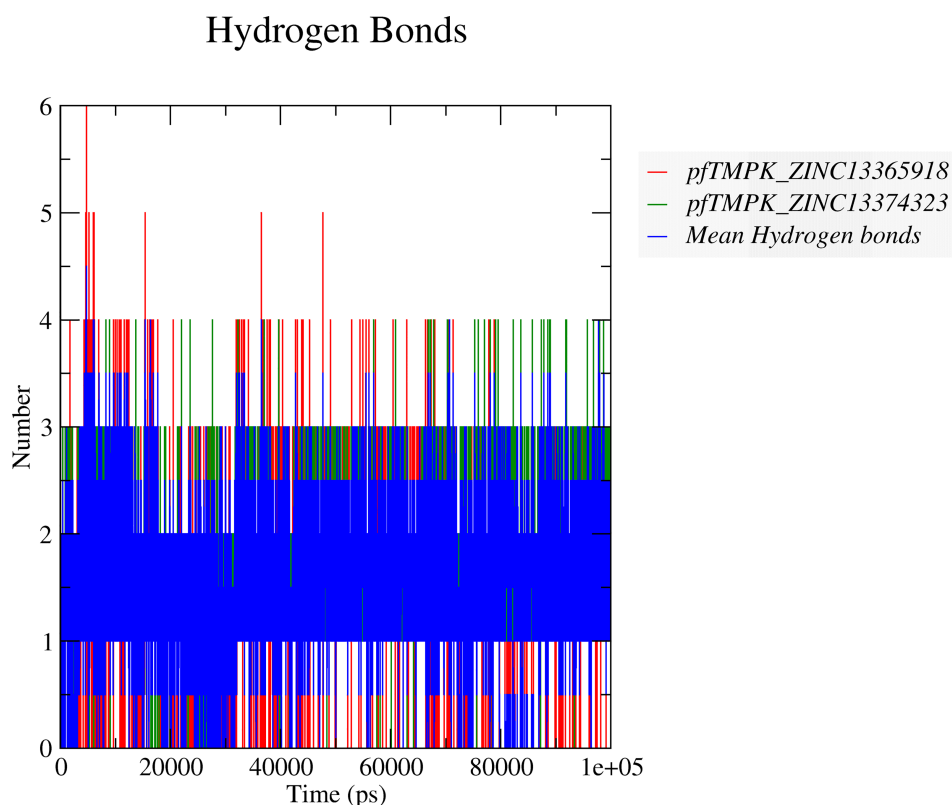


**FIGURE 6** | Hydrogen bond predictions between the complexes of *Pf*TMPK and the respective potential lead compounds. The hydrogen bonds formed between *Pf*TMPK and ZINC13365918 are shown as red lines, while those of the protein and ZINC13374323 are shown as green lines. The mean hydrogen bonds formed throughout the simulation in both complexes are highlighted in blue.

**TABLE 3 |** Toxicity profile of potential lead compounds.

	Mutagenicity	Tumorigenic	Reproductive effectiveness	Irritant
<b>ZINC13374323</b> (aurantiamide acetate)	None	None	None	High
<b>ZINC13365918</b> ( <i>N</i> -hydroxyannomontine)	None	None	None	None

carried out. An *in vitro* parasite growth inhibition assay was prepared for the *P. falciparum* 3D7 strain using the SYBR Green I fluorescence assay (Smilkstein et al., 2004). Artesunate was used as the positive control. The compounds were added to synchronized cultures of the ring stages, and inhibition of the parasite's growth was determined through IC<sub>50</sub>, with the experiment conducted in triplicates. The IC<sub>50</sub> values obtained for artesunate were comparable to those reported previously with the average being 23.22 nM (Touré et al., 2008; Quashie et al., 2013). The average IC<sub>50</sub> value obtained for aurantiamide acetate was 69.33 μM (Table 4). The inhibition curves of both compounds are shown in Figure 7. A single screen of aurantiamide acetate was also performed on asynchronized cultures of *P. falciparum* 3D7 strain. The IC<sub>50</sub> value achieved for the asynchronized culture was >100 μM (Supplementary Figure 1), which indicates an increase in the potency of the compound when screened against the ring stages of the parasite. This could imply a clue into the target specificity of the compound but requires further investigation; therefore, a stage-of-action study to assess the potency of the compound against different asexual stages is recommended. The activity of aurantiamide acetate, despite being appreciable for a natural compound, must be further improved through optimization to cater to its lack of O-atoms, which is necessary for PfTMPK inhibition.

## SIGNIFICANCE OF THE STUDY

In recent years, a minimal number of natural products have made it to antimalarial lead optimization projects (Guantai and Chibale, 2011). Natural products have proven to be a rich source of antimalarials throughout the history of malaria drug discovery, with breakthroughs like quinine and artemisinin being prime examples (Saxena et al., 2003; Itokawa et al., 2008). Most other drugs like clindamycin and

azithromycin have also had their foundation in natural products (Guantai and Chibale, 2011). This shows that developing new drug candidates from natural product sources remains a favorable line of research for antimalarial drug development. It is evident, however, that most compounds developed from natural products show moderate inhibition activity (Saxena et al., 2003; Guantai and Chibale, 2011). As such, through the incorporation of *in silico* techniques, we can focus on compounds with desirable properties with the potential to become lead compounds and later become drug candidates through further optimization. The thirteen hits obtained after molecular docking represent compounds that can compete with the natural substrate of PfTMPK based on their binding affinity. By screening those compounds against important structural properties obtained through extensive *in silico* work (Ojha and Roy, 2013), we have been able to highlight two natural products, namely, aurantiamide acetate and *N*-hydroxyannomontine, as potential lead compounds. The binding affinities of the compounds as compared to known active inhibitors of PfTMPK corroborate this claim. Also, further experimental *in vitro* studies of the biological activity of aurantiamide acetate against the *P. falciparum* 3D7 strain show the compound to express appreciable antimalarial activity (IC<sub>50</sub> of 69.33). *In vitro* experimentation could not be done for *N*-hydroxyannomontine because it is not commercially available. It will be necessary to synthesize and test the compound in future studies and also develop cytotoxicity assays for both compounds. To develop these compounds into lead compounds, it is crucial to optimize them, taking into account the structural properties needed for effective binding as earlier described (Ojha and Roy, 2013).

Resistance to chloroquine, a cheap and efficacious antimalarial drug, has led to the change to artemisinin-based combination therapy (ACT) as the recommended first-line treatment option. Chloroquine resistance was first observed in Southeast Asia (in Thailand in 1957), which spread globally (Packard, 2014) and rendered chloroquine useless. However, resistance to ACT has been detected again in Southeast Asia with hints of delayed parasite clearance in Africa (Global Malaria Program, 2015). Delayed parasite clearance, however, may not necessarily lead to treatment failure, but in the Greater Mekong Subregion, treatment failures following treatment with an ACT have only been observed where there is resistance to the partner drug (World Health Organization, 2018). The drugs used in the ACT are few, necessitating the need to have additional compounds, thus the significance of our finding of aurantiamide acetate as a potential antimalarial compound. Moreover, it is known to possess anti-inflammatory properties (Zhou et al., 2017), which is good. Although its anti-plasmodial activity *in vitro* is not comparable

**TABLE 4 |** IC<sub>50</sub> values of artesunate and aurantiamide acetate for the synchronized culture of *Plasmodium falciparum* 3D7 ring stages.

	Artesunate (nM)	Aurantiamide acetate (μM)
IC <sub>50</sub> —Experiment 1	2.76	73.48
IC <sub>50</sub> —Experiment 2	15.88	76.32
IC <sub>50</sub> —Experiment 3	51.02	58.19
Mean IC <sub>50</sub>	23.22	69.33
SD	24.95	9.751
SEM	14.41	5.630

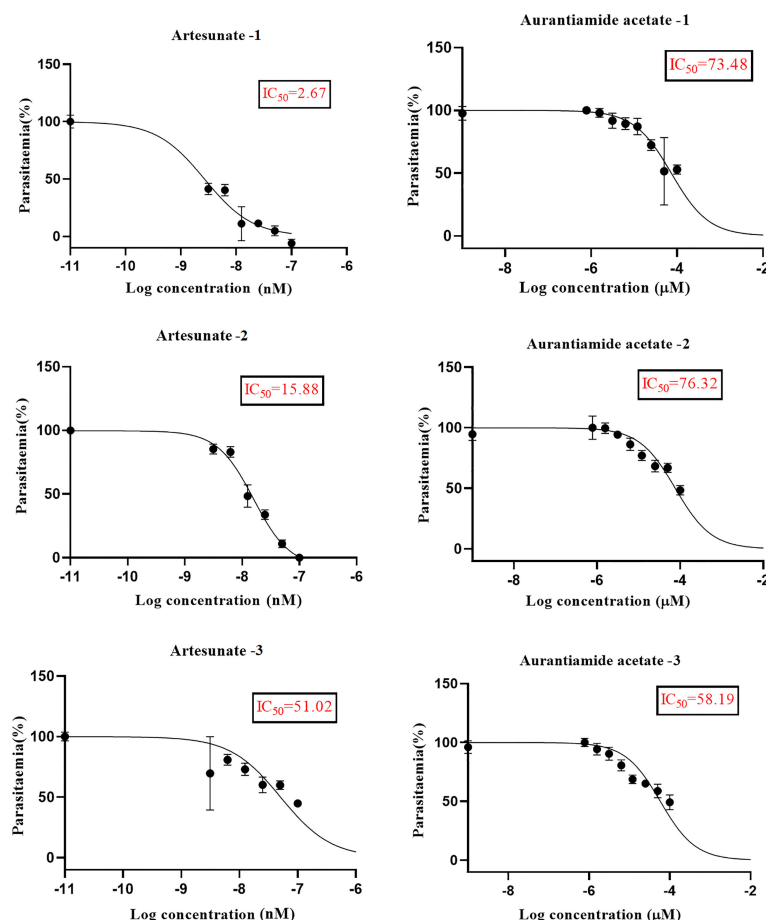


**FIGURE 7** | The inhibition curves of artesunate and aurantiamide acetate for the synchronized culture of *Plasmodium falciparum* 3D7 ring stages.

to that of artesunate, we believe that the addition of oxygen atoms to the molecule will significantly increase its performance. Studies have reported that dried leaves of *A. annua* used as a tea infusion in treating malaria have a higher potency than pure artemisinin (Weathers, 2014). Using the dried-leaf treatment has also been shown to overcome resistance to artemisinin. These effects may be due to the other chemical components of *A. annua*, which enhance the bioavailability and efficacy of artemisinin even though they have significantly less potent anti-plasmodial activity than artemisinin (Weathers, 2014). Since aurantiamide acetate is a constituent of *A. annua*, we recommend further studies to determine its ability to reduce resistance to artemisinin and/or enhance anti-plasmodial activity when used as a partner drug in ACT.

## CONCLUSION

A total of 885 compounds retrieved from AfroDB were screened in FAF-Drugs4 server, which produced 91 ADMET-acceptable compounds. Thirteen compounds out of the 91, which scored

higher binding energy than the substrate of *Pf*TMPPK, were selected as hits. Four structural properties of a molecule that ensures proper binding at the active site and inhibitory effect against *Pf*TMPPK were considered in selecting lead compounds. ZINC13374323 and ZINC13365918 were selected as plausible lead compounds since they exhibited three of the structural properties. ZINC13374323 shares interactions with many similar residues as a *Pf*TMPPK inhibitor thymidine analog, which has been shown to exhibit high activity against the protein. ZINC13374323, also known as aurantiamide acetate, is an ingredient of *A. annua* and exhibits anti-inflammatory, antiviral, and antimicrobial activities. ZINC13365918, on the other hand, is a pyrimidine analog that has been shown to exhibit antileishmanial activity. Analysis of the molecular dynamics simulations of the lead compounds complexed with the protein showed the complex of *Pf*TMPPK and ZINC13374323 to have similar RMSD and RMSF as that of the protein in complex with its natural substrate, TMP. *In vitro* testing of aurantiamide acetate for anti-plasmodial activity resulted in an IC<sub>50</sub> of 69.33 μM. The compounds could be used as scaffolds for lead optimization.

## DATA AVAILABILITY STATEMENT

The original contributions presented in the study are included in the article/**Supplementary Material**. Further inquiries can be directed to the corresponding author.

## AUTHOR CONTRIBUTIONS

AG, MW, and SK developed the concept and designed the study. KE conducted the computational aspects of the study and drafted the manuscript. MT-T, AL, SN, and GD performed the *in vitro* experiments of the study. AG, MW, and SK edited and proofread the manuscript. All authors contributed to the manuscript.

## REFERENCES

- Agamah, F. E., Damena, D., Skelton, M., Ghansah, A., Mazandu, G. K., and Chimusa, E. R. (2021). Network-Driven Analysis of Human-*Plasmodium falciparum* Interactome: Processes for Malaria Drug Discovery and Extracting *In Silico* Targets. *Malar. J.* 20, 421. doi: 10.1186/s12936-021-03955-0
- Belete, T. M. (2020). Recent Progress in the Development of New Antimalarial Drugs With Novel Targets. *Drug Des. Devel. Ther.* 14, 3875–3889. doi: 10.2147/DDDT.S265602
- Benigni, R., and Bossa, C. (2006). Structural Alerts of Mutagens and Carcinogens. *Curr. Comput. Aided-Drug Des.* 2, 169–176. doi: 10.2174/157340906777441663
- Bhatt, S., Weiss, D. J., Cameron, E., Bisanzio, D., Mappin, B., Dalrymple, U., et al. (2015). The Effect of Malaria Control on *Plasmodium falciparum* in Africa Between 2000 and 2015. *Nature* 526, 207–211. doi: 10.1038/nature15535
- Cassera, M. B., Zhang, Y., Hazleton, K. Z., and Schramm, V. L. (2011). Purine and Pyrimidine Pathways as Targets in *Plasmodium falciparum*. *Curr. Top. Med. Chem.* 11, 2103–2115. doi: 10.2174/156802611796575948
- Chen, M.D., Sinha, K., Rule, G. S., and Ly, D. H. (2018). Interaction of  $\alpha$ -Thymidine Inhibitors With Thymidylate Kinase From *Plasmodium falciparum*. *Biochemistry* 57, 2868–2875. doi: 10.1021/acs.biochem.8b00162
- Costa, E. V., Pinheiro, M. L. B., Xavier, C. M., Silva, J. R. A., Amaral, A. C. F., Souza, A. D. L., et al. (2006). A Pyrimidine- $\beta$ -Carboline and Other Alkaloids From *Annona F. Oetida* With Antileishmanial Activity. *J. Nat. Prod.* 69, 292–294. doi: 10.1021/np050422s
- Cui, H., Carrero-Lérida, J., Silva, A. P. G., Whittingham, J. L., Brannigan, J. A., Ruiz-Pérez, L. M., et al. (2012). Synthesis and Evaluation of  $\alpha$ -Thymidine Analogues as Novel Antimalarials. *J. Med. Chem.* 55, 10948–10957. doi: 10.1021/jm301328h
- Dallakyan, S., and Olson, A. J. (2015). Small-Molecule Library Screening by Docking With Pyrx. *Methods Mol. Biol.* 1263, 243–250. doi: 10.1007/978-1-4939-2269-7\_19
- DeLong, E. R., DeLong, D. M., and Clarke-Pearson, D. L. (1988). Comparing the Areas Under Two or More Correlated Receiver Operating Characteristic Curves: A Nonparametric Approach. *Biometrics* 44, 837. doi: 10.2307/2531595
- Egwu, C. O., Pério, P., Augereau, J.-M., Tsamesidis, I., Benoit-Vical, F., and Reybier, K. (2022). Resistance to Artemisinin in *Falciparum* Malaria Parasites: A Redox-Mediated Phenomenon. *Free Radic. Biol. Med.* 179, 317–327. doi: 10.1016/j.freeradbiomed.2021.08.016
- Global Malaria Program. (2015). *Status Report on Artemisinin and ACT Resistance*. Available at: <https://www.who.int/malaria/publications/atoz/status-rep-artemisinin-act-resistance-sept2015.pdf?ua=1> (Accessed February 2, 2022).
- Goksuluk, D., Korkmaz, S., Zararsiz, G., and Karaagaoglu, A. E. (2016). Easyroc: An Interactive Web-Tool for Roc Curve Analysis Using R Language Environment. *R J.* 8, 213–230. doi: 10.32614/RJ-2016-042
- Guantai, E., and Chibale, K. (2011). How can Natural Products Serve as a Viable Source of Lead Compounds for the Development of New/Novel Anti-Malarials? *Malar. J.* 10, S2. doi: 10.1186/1475-2875-10-S1-S2
- Heifets, A., and Lilien, R. H. (2010). Lalign: Flexible Ligand-Based Active Site Alignment and Analysis. *J. Mol. Graph. Model.* 29, 93–101. doi: 10.1016/j.jmgm.2010.05.005

## ACKNOWLEDGMENTS

We are grateful to Dr. Rita Afriyie Boateng for her support in the molecular dynamics simulations and the director of Noguchi Memorial Institute for Medical Research for allowing us to publish this paper.

## SUPPLEMENTARY MATERIAL

The Supplementary Material for this article can be found online at: <https://www.frontiersin.org/articles/10.3389/fcimb.2022.868529/full#supplementary-material>.

- Itokawa, H., Morris-Natschke, S. L., Akiyama, T., and Lee, K. H. (2008). Plant-Derived Natural Product Research Aimed at New Drug Discovery. *J. Nat. Med.* 62, 263–280. doi: 10.1007/s11418-008-0246-z
- Kandeel, M., Ando, T., Kitamura, Y., Abdel-Aziz, M., and Kitade, Y. (2009). Mutational, Inhibitory and Microcalorimetric Analyses of *Plasmodium falciparum* TMP Kinase. Implications for Drug Discovery. *Parasitology* 136, 11. doi: 10.1017/S0031182008005301
- Krungkrai, S. R., and Krungkrai, J. (2016). Insights Into the Pyrimidine Biosynthetic Pathway of Human Malaria Parasite *Plasmodium falciparum* as Chemotherapeutic Target. *Asian Pac. J. Trop. Med.* 9, 525–534. doi: 10.1016/j.apjtm.2016.04.012
- Kumar, S., Bhardwaj, T. R., Prasad, D. N., and Singh, R. K. (2018). Drug Targets for Resistant Malaria: Historic to Future Perspectives. *Biomed. Pharmacother.* 104, 8–27. doi: 10.1016/j.biopha.2018.05.009
- Kwofie, S. K., Broni, E., Asiedu, S. O., Kwarko, G. B., Dankwa, B., Enninful, K. S., et al. (2021). Cheminformatics-Based Identification of Potential Novel Anti-SARS-CoV-2 Natural Compounds of African Origin. *Molecules* 26, 406. doi: 10.3390/molecules26020406
- Lagorce, D., Bouslama, L., Becot, J., Miteva, M. A., and Villoutreix, B. O. (2017). Faf-Drugs4: Free ADME-Tox Filtering Computations for Chemical Biology and Early Stages Drug Discovery. *Bioinformatics* 33, 3658–3660. doi: 10.1093/bioinformatics/btx491
- Ludin, P., Woodcroft, B., Ralph, S. A., and Mäser, P. (2012). *In Silico* Prediction of Antimalarial Drug Target Candidates. *Int. J. Parasitol. Drugs Drug Resist.* 2, 191–199. doi: 10.1016/j.ijpddr.2012.07.002
- Mandrekar, J. N. (2010). Receiver Operating Characteristic Curve in Diagnostic Test Assessment. *J. Thorac. Oncol.* 5, 1315–1316. doi: 10.1097/JTO.0b013e3181ec173d
- Milne, G. W. A., Zhou, J., Xie, G., and Yan, X. (2018). *Traditional Chinese Medicines: Molecular Structures, Natural Sources and Applications*. Eds. X. Yan, G. Xie, J. Zhou and G. W. A. Milne Routledge. (London: Routledge). doi: 10.4324/9781315193441
- Neves, B. J., Braga, R. C., Alves, V. M., Lima, M. N. N., Cassiano, G. C., Muratov, E. N., et al. (2020). Deep Learning-driven Research for Drug Discovery: Tackling Malaria. *PLoS Comput. Biol.* 16, e1007025. doi: 10.1371/journal.pcbi.1007025
- Ntie-Kang, F., Zofou, D., Babiaka, S. B., Meudom, R., Scharfe, M., Lifongo, L. L., et al. (2013). AfrodB: A Select Highly Potent and Diverse Natural Product Library From African Medicinal Plants. *PLoS One* 8, e78085. doi: 10.1371/journal.pone.0078085
- Ojha, P. K., and Roy, K. (2013). First Report on Exploring Structural Requirements of Alpha and Beta Thymidine Analogs for PFTMPK Inhibitory Activity Using *In Silico* Studies. *BioSystems* 113, 177–195. doi: 10.1016/j.biosystems.2013.07.005
- Packard, R. M. (2014). The Origins of Antimalarial-Drug Resistance. *N. Engl. J. Med.* 371, 397–399. doi: 10.1056/NEJMp1403340
- Patrick, G. L., and Turner, H. (2020). “Kinases and Kinase Inhibitors,” in *Antimalarial Agents* (Amsterdam: Elsevier). doi: 10.1016/B978-0-08-101210-9.00013-5
- Quashie, N. B., Duah, N. O., Abuaku, B., Quaye, L., Ayanful-Torgby, R., Akwoviah, G. A., et al. (2013). A SYBR Green 1-Based *In Vitro* Test of



- Susceptibility of Ghanaian *Plasmodium falciparum* Clinical Isolates to a Panel of Anti-Malarial Drugs. *Malar. J.* 12, 450. doi: 10.1186/1475-2875-12-450
- Reyes, P., Rathod, P. K., Sanchez, D. J., Mrema, J. E., Rieckmann, K. H., and Heidrich, H. G. (1982). Enzymes of Purine and Pyrimidine Metabolism From the Human Malaria Parasite, *Plasmodium falciparum*. *Mol. Biochem. Parasitol.* 5, 275–290. doi: 10.1016/0166-6851(82)90035-4
- Sander, T., Freyss, J., von Korff, M., and Rufener, C. (2015). Datawarrior: An Open-Source Program for Chemistry Aware Data Visualization And Analysis. *J. Chem. Inf. Model.* 55, 460–473. doi: 10.1021/ci500588j
- Saxena, S., Pant, N., Jain, D. C., and Bhakuni, R. S. (2003). Antimalarial Agents From Plant Sources. *Curr. Sci.* 85, 1314–1329.
- Schüttelkopf, A. W., and Van Aalten, D. M. F. (2004). Prodrgr: A Tool for High-Throughput Crystallography of Protein-Ligand Complexes. *Acta Crystallogr. Sect. D Biol. Crystallogr.* 60, 1355–1363. doi: 10.1107/S0907444904011679
- Siddiqui, A. A., Iram, F., Siddiqui, S., and Sahu, K. (2014). Role of Natural Products in Drug Discovery Process. *Int. J. Drug Dev. Res.* 6, 172–204.
- Sliwoski, G., Kothiwale, S., Meiler, J., and Lowe, E. W. (2013). Computational Methods in Drug Discovery. *Pharmacol. Rev.* 66, 334–395. doi: 10.1124/pr.112.007336
- Smilkstein, M., Sriwilajaroen, N., Kelly, J. X., Wilairat, P., and Riscoe, M. (2004). Simple and Inexpensive Fluorescence-Based Technique for High-Throughput Antimalarial Drug Screening. *Antimicrob. Agents Chemother.* 48, 1803–1806. doi: 10.1128/AAC.48.5.1803-1806.2004
- Spitzmüller, A., and Mestres, J. (2013). Prediction of the *P. falciparum* Target Space Relevant to Malaria Drug Discovery. *PLoS Comput. Biol.* 9, e1003257. doi: 10.1371/journal.pcbi.1003257
- Tajudeen, N., and Van Heerden, F. R. (2019). Antiplasmodial Natural Products: An Update. *Malar. J.* 18, 404. doi: 10.1186/s12936-019-3026-1
- Tamokou, J., de, D., Kuiaite, J. R., Tene, M., Kenla Nwemeguela, T. J., and Tane, P. (2011). The Antimicrobial Activities of Extract and Compounds Isolated From *Brilliantaisia Lamium*. *Iran. J. Med. Sci.* 36, 24–31.
- Tamokou, J., de, D., Simo Mpetga, D. J., Keilah Lunga, P., Tene, M., Tane, P., et al. (2012). Antioxidant and Antimicrobial Activities of Ethyl Acetate Extract, Fractions and Compounds From Stem Bark of *Albizia Adianthifolia* (Mimosoideae). *BMC Complement. Altern. Med.* 12, 1074. doi: 10.1186/1472-6882-12-99
- Touré, A. O., Koné, L. P., Jambou, R., Konan, T. D., Demba, S., Beugre, G. E., et al. (2008). Sensibilité *In Vitro* De *P. falciparum* À La Quinine, L'artésunate Et La Chloroquine À Abidjan (Côte d'Ivoire). *Cah. Santé* 18, 043–047. doi: 10.1684/san.2008.0103
- Trott, O., and Olson, A. J. (2010). Software News and Update AutoDock Vina: Improving the Speed and Accuracy of Docking With a New Scoring Function, Efficient Optimization, and Multithreading. *J. Comput. Chem.* 31, 455–461. doi: 10.1002/jcc.21334
- Tuteja, R. (2007). Helicases - Feasible Antimalarial Drug Target for *Plasmodium falciparum*. *FEBS J.* 274, 4699–4704. doi: 10.1111/j.1742-4658.2007.06000.x
- Van Der Spoel, D., Lindahl, E., Hess, B., Groenhof, G., Mark, A. E., and Berendsen, H. J. C. (2005). Gromacs: Fast, Flexible, and Free. *J. Comput. Chem.* 26, 1701–1718. doi: 10.1002/jcc.20291
- Vanoevelen, J. M., Bierau, J., Grashorn, J. C., Lambrichs, E., Kamsteeg, E.-J., Bok, L. A., et al. (2022). DTYMK is Essential for Genome Integrity and Neuronal Survival. *Acta Neuropathol.* 143, 245–262. doi: 10.1007/s00401-021-02394-0
- Vaught, A. (1996). Graphing With Gnuplot and Xmgr: Two Graphing Packages Available Under Linux. *Linux J.* 1996, 7.
- Wang, L., Pang, X., Li, Y., Zhang, Z., and Tan, W. (2017). Rader: A Rapid DEcoy Retriever to Facilitate Decoy Based Assessment of Virtual Screening. *Bioinformatics* 33, 1235–1237. doi: 10.1093/bioinformatics/btw783
- Weathers, P. J. (2014). Dried-Leaf *Artemisia Annua*: A Practical Malaria Therapeutic for Developing Countries? *World J. Pharmacol.* 3, 39. doi: 10.5497/wjp.v3.i4.39
- Whittingham, J. L., Carrero-Lerida, J., Brannigan, J. A., Ruiz-Perez, L. M., Silva, A. P. G., Fogg, M. J., et al. (2010). Structural Basis for the Efficient Phosphorylation of AZT-MP (3'-azido-3'-deoxythymidine Monophosphate) and dGMP by *Plasmodium falciparum* Type I Thymidylate Kinase. *Biochem. J.* 428, 499–509. doi: 10.1042/BJ20091880
- World Health Organization (2018) *Status Report on Artemisinin Resistance and ACT Efficacy (August 2018)* (World Heal. Organ). Available at: <https://www.who.int/publications/i/item/WHO-CDS-GMP-2019.17> (Accessed February 2, 2022).
- Zhou, B., Yang, Z., Feng, Q., Liang, X., Li, J., Zanin, M., et al. (2017). Aurantiamide Acetate From *Baphicacanthus cusia* Root Exhibits Anti-Inflammatory and Anti-Viral Effects via Inhibition of the NF-κB Signaling Pathway in Influenza A virus-Infected Cells. *J. Ethnopharmacol.* 199, 60–67. doi: 10.1016/j.jep.2017.01.038

**Conflict of Interest:** The authors declare that the research was conducted in the absence of any commercial or financial relationships that could be construed as a potential conflict of interest.

**Publisher's Note:** All claims expressed in this article are solely those of the authors and do not necessarily represent those of their affiliated organizations, or those of the publisher, the editors and the reviewers. Any product that may be evaluated in this article, or claim that may be made by its manufacturer, is not guaranteed or endorsed by the publisher.

Copyright © 2022 Enninful, Kwofie, Tetteh-Tsifoanya, Lamptey, Djameh, Nyarko, Ghansah and Wilson. This is an open-access article distributed under the terms of the Creative Commons Attribution License (CC BY). The use, distribution or reproduction in other forums is permitted, provided the original author(s) and the copyright owner(s) are credited and that the original publication in this journal is cited, in accordance with accepted academic practice. No use, distribution or reproduction is permitted which does not comply with these terms.



# Homology Modeling, *de Novo* Design of Ligands, and Molecular Docking Identify Potential Inhibitors of *Leishmania donovani* 24-Sterol Methyltransferase

Patrick O. Sakyi<sup>1,2</sup>, Emmanuel Broni<sup>3,4</sup>, Richard K. Amewu<sup>1</sup>, Whelton A. Miller III<sup>5,6,7</sup>, Michael D. Wilson<sup>4,5</sup> and Samuel Kojo Kwofie<sup>3,8\*</sup>

<sup>1</sup> Department of Chemistry, School of Physical and Mathematical Sciences, College of Basic and Applied Sciences, University of Ghana, Accra, Ghana, <sup>2</sup> Department of Chemical Sciences, School of Sciences, University of Energy and Natural Resources, Sunyani, Ghana, <sup>3</sup> Department of Biomedical Engineering, School of Engineering Sciences, College of Basic & Applied Sciences, University of Ghana, Accra, Ghana, <sup>4</sup> Department of Parasitology, Noguchi Memorial Institute for Medical Research (NMIMR), College of Health Sciences (CHS), University of Ghana, Accra, Ghana, <sup>5</sup> Department of Medicine, Loyola University Medical Center, Maywood, IL, United States, <sup>6</sup> Department of Molecular Pharmacology and Neuroscience, Loyola University Medical Center, Maywood, IL, United States, <sup>7</sup> Department of Chemical and Biomolecular Engineering, School of Engineering and Applied Science, University of Pennsylvania, Philadelphia, PA, United States, <sup>8</sup> Department of Biochemistry, Cell and Molecular Biology, West African Centre for Cell Biology of Infectious Pathogens, College of Basic and Applied Sciences, University of Ghana, Accra, Ghana

## OPEN ACCESS

### Edited by:

Vipan Kumar,  
Guru Nanak Dev University, India

### Reviewed by:

Marcus Scotti,  
Federal University of Paraíba, Brazil  
Wanderley De Souza,  
Federal University of Rio de Janeiro,  
Brazil

### \*Correspondence:

Samuel Kojo Kwofie  
skkwofie@ug.edu.gh

### Specialty section:

This article was submitted to  
Clinical Microbiology,  
a section of the journal  
Frontiers in Cellular and  
Infection Microbiology

**Received:** 22 January 2022

**Accepted:** 28 April 2022

**Published:** 02 June 2022

### Citation:

Sakyi PO, Broni E, Amewu RK,  
Miller WA III, Wilson MD and Kwofie SK  
(2022) Homology Modeling, *de Novo*  
Design of Ligands, and Molecular  
Docking Identify Potential  
Inhibitors of *Leishmania donovani*  
24-Sterol Methyltransferase.  
Front. Cell. Infect. Microbiol. 12:859981.  
doi: 10.3389/fcimb.2022.859981

The therapeutic challenges pertaining to leishmaniasis due to reported chemoresistance and toxicity necessitate the need to explore novel pathways to identify plausible inhibitory molecules. *Leishmania donovani* 24-sterol methyltransferase (*LdSMT*) is vital for the synthesis of ergosterols, the main constituents of *Leishmania* cellular membranes. So far, mammals have not been shown to possess SMT or ergosterols, making the pathway a prime candidate for drug discovery. The structural model of *LdSMT* was elucidated using homology modeling to identify potential novel 24-SMT inhibitors *via* virtual screening, scaffold hopping, and *de-novo* fragment-based design. Altogether, six potential novel inhibitors were identified with binding energies ranging from  $-7.0$  to  $-8.4$  kcal/mol with e-LEA3D using 22,26-azasterol and **S1–S4** obtained from scaffold hopping *via* the ChEMBL, DrugBank, PubChem, ChemSpider, and ZINC15 databases. These ligands showed comparable binding energy to 22,26-azasterol ( $-7.6$  kcal/mol), the main inhibitor of *LdSMT*. Moreover, all the compounds had plausible ligand efficiency-dependent lipophilicity (LELP) scores above 3. The binding mechanism identified Tyr92 to be critical for binding, and this was corroborated *via* molecular dynamics simulations and molecular mechanics Poisson–Boltzmann surface area (MM-PBSA) calculations. The ligand **A1** was predicted to possess antileishmanial properties with a probability of activity (Pa) of 0.362 and a probability of inactivity (Pi) of 0.066, while **A5** and **A6** possessed dermatological properties with Pa values of 0.205 and 0.249 and Pi values of 0.162 and 0.120, respectively. Structural similarity search *via* DrugBank identified vabicaserin, daledalin, zanapezil, imipramine, and cefradine with antileishmanial properties

suggesting that the *de-novo* compounds could be explored as potential antileishmanial agents.

**Keywords:** leishmaniasis, 24-sterol methyltransferase, *Leishmania donovani*, *de-novo* drug design, molecular docking, molecular dynamics simulation

## 1 INTRODUCTION

Visceral leishmaniasis, the most debilitating form of leishmaniasis, is caused by *Leishmania donovani* and *Leishmania infantum* (Ikeogu et al., 2020). It is one of the oldest neglected tropical diseases that remain a major challenge to the global community. It is estimated to affect over 10 million people and cause up to 30,000 deaths annually (Hernández-Bojorge et al., 2020). The present chemotherapeutic options comprising pentavalent antimony, pentamidine (PTM), amphotericin B (Amp B), miltefosine (Milt), paromomycin, and liposomal Amp B suffer from numerous inefficiencies such as long treatment durations, cytotoxicity, resistance, and high cost, necessitating the urgent need for alternative therapeutic agents (Ghorbani and Farhodi, 2018; Sakyi et al., 2021a).

Target identification and validation are pivotal for rational drug designs (Lionta et al., 2014). Contemporary strategies comprising experimental (metabolomic and transcriptomic approaches) and computational (structure- and ligand-based) approaches have led to the identification of numerous biological targets necessary for the survival of *Leishmania* parasites (Mandal et al., 2009; Mavromoustakos et al., 2011; Rinschen et al., 2019; Kwofie et al., 2020). However, the incomplete knowledge on *Leishmania* biology and the limited studies on the exact functions of sterols in intracellular organelles have hampered the exploitation of effective sterol inhibitors against leishmaniasis. While cholesterol is biosynthesized in humans, *Leishmania* and other protozoa synthesize ergosterol. Due to this difference, a number of drugs including bisphosphonates, statins, azoles, and quinuclidine have been used for leishmaniasis treatment *via* the inhibition of the ergosterol biosynthetic pathway (Sakyi et al., 2021b). Sterol methyltransferase (SMT) is an enzyme involved in ergosterol biosynthesis which is understudied partly due to the paucity of structural genomics data. This notwithstanding, investigations are ongoing to explore SMT in designing drugs against leishmaniasis due to its absence in the human host coupled with the fact that it is highly conserved among all *Leishmania* parasites (Magaraci et al., 2003; Kidane et al., 2017).

SMT belongs to the family of transferases and functions by catalyzing methyl transfer from S-adenosyl methionine onto the C24 position of the lanosterol or the cycloartenol side chain during ergosterol biosynthesis. For example, genetic ablation studies of 24-SMT orthologs involved in the sterol biosynthetic pathway have demonstrated that ergosterol, one of the widely recognized classes of lipids in the cellular membrane of protozoans, plays a significant role in plasma membrane stabilization and mitochondrion function (Mukherjee et al., 2019). Studies have demonstrated the crucial functions of SMT to *Leishmania* survival, and hence, it is considered as a plausible target for drug design (Urbina et al., 1995; Mukherjee

et al., 2019; Sakyi et al., 2021a). For instance, vaccine evaluation studies against *Leishmania* 24-SMT identified 24-SMT as an essential drug target (Goto et al., 2009). *Leishmania* 24-SMT dysfunction results in the increased generation of reactive oxygen species and vesicular trafficking (Mukherjee et al., 2019). In addition, 24-alkyl sterols have been shown to be essential growth factors of *Trypanosoma cruzi* to the extent that its perturbation during ergosterol biosynthesis leads to cell cycle defects and DNA fragmentation (Urbina et al., 1995; Pérez-Moreno et al., 2012). Furthermore, RNA-seq analysis has revealed genomic instability at the locus of SMT, resulting in the promotion of amphotericin B resistance in *Leishmania* parasites (Pountain et al., 2019). Similarly, gigantol and imipramine suppressed the growth and proliferation of promastigotes and amastigotes *via* inhibition of SMT (Andrade-Neto et al., 2016; Rahman et al., 2021). Similarly, the antiproliferative effects of sterol biosynthesis inhibition on *Pneumocystis carinii* have hinted sterol methyltransferase suppressors as potential chemotherapeutic options for the treatment of *P. carinii* infections (Urbina et al., 1997). However, the recent resistance associated with 22,26-azasterol targeting SMT warrants the identification of novel inhibitors.

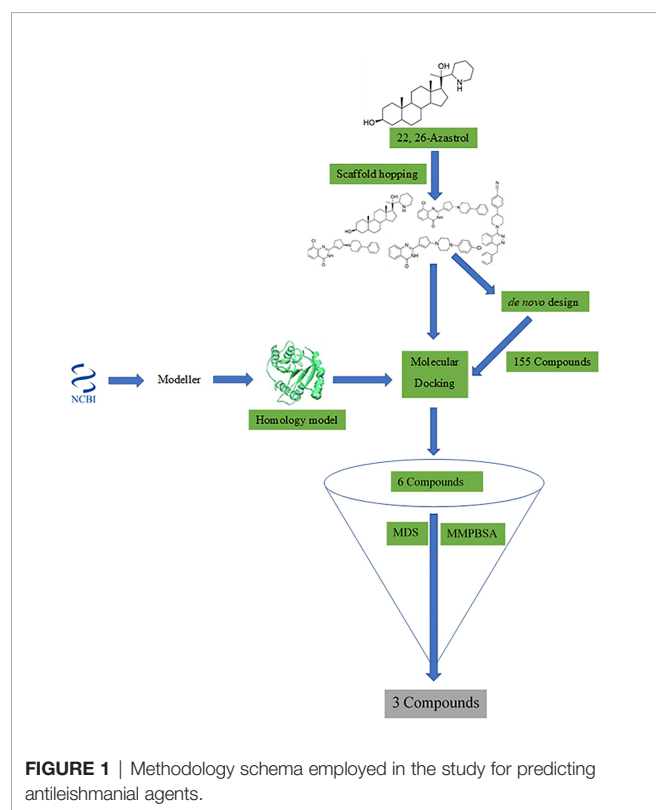
*In-silico* techniques in drug design are advantageous due to the reduced cost, time, and energy compared with traditional high-throughput screening (HTS) (Mak and Pichika, 2019). One of the strategies employed in the identification of lead compounds with improved efficacy in rational drug design includes scaffold hopping (Hu et al., 2017). It starts with a known active compound and ends up with new chemotypes with different core structures but with equal or improved efficacy (Hu et al., 2017). A typical example is the discovery of cyproheptadine from pheniramine, an antihistamine used to treat allergic conditions, such as hay fever or urticaria (Sun et al., 2012). Pheniramine has two aromatic rings joined to one carbon or nitrogen atom and a positive charge center. Cyproheptadine, an analog of pheniramine, has significantly improved binding affinity against the H1 receptor. This rigidified molecule with better absorption was achieved by locking both aromatic rings of pheniramine to the active conformation through ring closure and by introducing the piperidine ring to further reduce the flexibility of the molecule (Sun et al., 2012). In addition, these structural changes gave other medical benefits including cyproheptadine as a prophylaxis for migraine, pizotifen for the treatment of migraine, and azatadine as a typical potent sedating antihistamine (Sun et al., 2012). Tramadol was obtained through scaffold hopping of morphine (Sun et al., 2012). The recent interest in *de-novo* drug design compared with repurposing presents a new paradigm shift, not only in terms of time and cost but also innovation (Talevi and Bellera, 2019). The identification of leads from hits and then

optimization to druggable candidates in the drug design pipeline result not only in an increase in potency and selectivity but also improved drug-like properties (Gil and Martinez, 2021). In addition, *de-novo* drug design has increased the areas explored in the chemical space of molecules leading to improvements in chemotherapeutic efficacy (Lin et al., 2020). This strategy has also been used in the design of drugs including vemurafenib, venetoclax, and dihydroorotate dehydrogenase inhibitors against malaria and aryl sulfonamide, a new aurora A kinase inhibitor (Jacquemard and Kellenberger, 2019). Despite the success achieved using the *de-novo* design, its use in the search for potential hits against *L. donovani* 24-sterol methyltransferase (LdSMT) is limited.

The study sought to utilize *in-silico* approaches to predict putative inhibitors targeting LdSMT. To accomplish this, the three-dimensional (3D) structure of LdSMT was first elucidated *via* modeling followed by subjection of 22,26-azasterol to *de-novo* drug design. Next, molecular docking and molecular dynamics simulation studies of the complexes were undertaken to identify potential novel LdSMT inhibitors. Furthermore, the biological activity and pharmacological profiles of the compounds were predicted to reinforce their lead-likeness.

## 2 METHODS

A workflow schema detailing the stepwise techniques employed in this study is shown in **Figure 1**. The compound 22,26-azasterol was submitted to balanced rapid and unrestricted server for



extensive ligand-aimed screening (BRUSELAS) (Banegas-Luna et al., 2019) to generate non-steroidal inhibitors. Meanwhile, a reasonably good structure of LdSMT was modeled and validated. The non-steroidal inhibitors were virtually screened against the LdSMT to identify compounds with high binding affinity to the receptor. The complexes of these compounds then served as input to the e-LEA3D (Douguet, 2010) for the generation of the novel compounds. Molecular dynamics (MD) simulation and molecular mechanics Poisson–Boltzmann surface area (MM-PBSA) were computed on the LdSMT–ligand complexes to determine the molecular interactions as well as the stability during the simulation. Absorption, distribution, metabolism, excretion, and toxicity (ADMET) predictions were performed to evaluate the pharmacological profiles of the selected compounds. The inhibitory constant, ligand efficiency, ligand efficiency scale, fit quality, binding efficiency index, surface efficiency index, and ligand efficiency-dependent lipophilicity were also calculated to assess the quality parameters of the ligands in binding to the target protein. In addition, the biological activity of the selected hits was predicted using the open Bayesian machine learning technique (Lagunin et al., 2000).

### 2.1 Sequence Retrieval

The protein sequence of LdSMT (SCMT1/GenBank ID: AAR92099.1) was retrieved from the National Center for Biotechnology Information (NCBI) database (Boratyn et al., 2013). To identify similar proteins as templates for building the 3D structure of LdSMT, the fast-all (FASTA) format of the sequence was aligned with the homologous sequences of crystal protein structures in the Protein Data Bank (PDB) (Berman et al., 2000) using the Basic Local Alignment and Sequencing Tool (BLAST) (Burley et al., 2017).

### 2.2 LdSMT Model Generation

Due to the unavailability of an experimentally elucidated 3D structure for LdSMT, molecular modeling techniques were used to predict a reasonably accurate protein structure (Crentsil et al., 2020). Modeller version 10.2 (Eswar et al., 2008) was employed in building the 3D structure using three different templates: i) the 3BUS template was used to generate five models of the LdSMT (Eswar et al., 2008), ii) the protein structure with PDB ID 4PNE was also used to model five different structures of the LdSMT (Eswar et al., 2008), and iii) multitemplate homology modeling was employed to generate five structures of the LdSMT (Eswar et al., 2008). A total of three templates comprising 4PNE, 3BUS, and 6UAK were used in the multitemplate homology modeling approach. Modeller 10.2 was employed in generating all the potential structures of the LdSMT (Fiser and Šali, 2003; Eswar et al., 2008). The reasonably best model in each approach was selected based on the discrete optimized protein energy (DOPE) scores (Eswar et al., 2008).

### 2.3 Structural Validation

The structural quality and accuracy of the best models from each approach were assessed using PROCHECK (Laskowski et al., 2012) with results reported as Ramachandran plots (Anderson et al., 2005). Further validation with VERIFY 3D



(Sasin and Bujnicki, 2004), ERRAT (Colovos and Yeates, 1993; Messaoudi et al., 2013), and PROVE (Sasin and Bujnicki, 2004) was also performed. The reasonably best model was selected based on all the quality assessments for the molecular docking studies. Protein Structure Analysis (ProSA) (Wiederstein and Sippl, 2007) was then used to investigate the problematic regions of the selected model.

## 2.4 Determining Binding Sites

The plausible binding sites of the selected protein were determined using the Computed Atlas of Surface Topology of proteins (CASTp) (Dundas et al., 2006; Tian et al., 2018). The predicted sites were visualized using PyMOL (PyMOL Molecular Graphics System, Version 1.5.0.4, Schrödinger, LLC, New York, USA) (Lighthall et al., 2010) and Chimera 1.16 (Pettersen et al., 2004). The predicted binding sites with relatively small areas and volumes, where no ligand could fit, were ignored (Agyapong et al., 2021).

## 2.5 Scaffold Hopping

Shape similarity searching and pharmacophore screening were undertaken using the spatial data file (sdf) format of 22,26-azasterol via BRUSELAS (Banegas-Luna et al., 2019). A total of 100 ligands were generated with varying degrees of similarities to the input ligand, 22,26-azasterol. All ligands devoid of the steroidal core with varying degrees of similarities were selected for binding affinity prediction using AutoDock Vina v1.2.0 (Trott and Olson, 2010).

## 2.6 Molecular Docking Studies

AutoDock Vina (Trott and Olson, 2010) was used for molecular docking. The molecular docking process was performed in two different stages. The first docking stage involved ligands obtained from the scaffold hopping process (Pathania et al., 2021), while the second involved compounds obtained from the *de-novo* design studies (Agyapong et al., 2021). Altogether, 1,448 ligands were used for the docking studies.

For the first stage, the ligands were obtained from the scaffold hopping and their structural derivatives fetched from the DrugBank (Wishart et al., 2018), PubChem (Kim et al., 2021), ZINC15 (Sterling and Irwin, 2015), and ChemSpider databases (Pence and Williams, 2010). Compounds labeled X1, X2, X3, X4, X5, X6, and X7 which showed good half-maximum inhibitory concentration (IC<sub>50</sub>) values against *Leishmania* parasite's sterol methyltransferase together with amphotericin B, miltefosine, paromomycin, and 22,26-azasterol were also used.

The ligands generated from the *de-novo* design were virtually screened against the LdSMT in the second stage. For both stages, the ligands and the protein were prepared using the AutoDock Tools (Morris et al., 2009) and saved in the input format of AutoDock Vina (Trott and Olson, 2010). The charge, hydrogen bond network, and histidine protonation state of the protein were assigned after pdbqt conversion. Grid box size was set to (91.445 × 73.502 × 78.352) Å<sup>3</sup> with the center at (72.200, 58.009, 13.302) Å. Ligands were then screened against the LdSMT protein with exhaustiveness set to default 8.

## 2.7 De-Novo Drug Design

The potential protein–ligand complex from the scaffold hopping was submitted to e-LEA3D (Douguet, 2010) for further *de-novo* design. The binding site radius was set to 15 Å and the final score set to 1 with the same active site coordinates as used in the molecular docking study. Conformational search was set to 10, number of generations to 30, and population size to 30 with the rest of the options left as default.

## 2.8 Characterization of the Mechanism of Binding

The atomistic details of binding between the LdSMT and small molecules upon ligand binding were determined using the BIOVIA discovery studio visualizer v19.1.0.18287 (BIOVIA, San Diego, CA, USA) (Šudomová et al., 2019).

## 2.9 Quality Evaluation of Shortlisted Molecules

The inhibitory constant ( $K_i$ ) of the ligands was calculated from the binding energies of the selected compounds and the LdSMT protein (Islam and Pillay, 2020). In addition, ligand efficiency (LE) metrics including ligand efficiency scale (LE\_Scale), fit quality (FQ), ligand efficiency-dependent lipophilicity (LELP), and surface binding efficiency were also determined (Hopkins et al., 2014).

## 2.10 ADMET Properties and Drug-Likeness Assessment

The ADMET properties were determined using SwissADME (Daina et al., 2017) and the OSIRIS Property Explorer in Data Warrior (Sander et al., 2015). Pan-assay interference compounds (PAINS) (Daina et al., 2017) and synthetic accessibility (Daina et al., 2017) search using SwissADME (Daina et al., 2017) were performed to eliminate false positive compounds that possess good physiochemical properties as well as those with complex structures.

## 2.11 Prediction of Biological Activity of Selected Compounds

The biological activity of the selected compounds was predicted using prediction of activity spectra for substance (PASS) (Lagunin et al., 2000) with the simplified molecular input line entry system (SMILES) as inputs.

## 2.12 Molecular Dynamics Simulation

A 100-ns MD simulation was performed for the unbound LdSMT and the protein–hit complexes using GROMACS 2018 (Van Der Spoel et al., 2005; Abraham et al., 2015). QtGrace (Dahiya et al., 2019) was used to plot the graphs generated from the MD simulation. The binding free energies of the complexes were calculated using MM-PBSA (Kumari et al., 2014). The energy contribution of each residue was also determined using g\_MMPBSA. The graphs from the MM-PBSA computations were generated using the R programming language (Tippmann, 2014; Alkarkhi and Alqaraghuli, 2020).

## 2.13 Antileishmanial Exploration of Potential Leads

Structural similarity search of all the hits was done *via* DrugBank (Wishart et al., 2018) to identify drugs with potential antileishmanial activity and possible mechanisms of action from similar compounds.

## 3 RESULTS AND DISCUSSION

### 3.1 Template Search

The 3D structure of LdSMT is yet to be experimentally elucidated; therefore, the structure was modeled. A BLAST (Boratyn et al., 2013) search of the protein sequence of LdSMT (SCMT1/GenBank ID: AAR92099.1) was performed *via* NCBI BLAST (Boratyn et al., 2013) to identify suitable identical templates to the LdSMT. The search revealed 12 experimentally determined protein structures that are identical to the LdSMT (**Supplementary Table 1**). The most widely used criteria in selecting a template is to choose the template with the highest sequence identity to the query sequence (Broni et al., 2021) and that was used for the modeling. However, the resolution at which the template protein structure was experimentally determined must also be taken into consideration. Also, the coverage of the template sequence to the query is another important factor. Herein, the *E*-value, sequence identity, query coverage, and the resolution of the 3D structures were used to select the most suitable templates as previously done (Meier and Söding, 2015; Haddad et al., 2020; Kwofie et al., 2021).

All the 12 identical protein structures had sequence identity less than 30% to the LdSMT, and 5WP4 demonstrated the highest with an identity of 29.01% (**Supplementary Table 1**); however, 5WP4 had a relatively low coverage of 45% to the LdSMT (**Supplementary Table 1**) and an *E*-value of  $1 \times 10^{-11}$ . The 3BUS template had the least *E*-value of  $6 \times 10^{-20}$  and identity of 24.12%. The 3BUS protein has previously been used in modeling the SMT of *L. infantum* (Azam et al., 2014). Although 3BUS had a low resolution (2.65 Å), it was selected as one of the structures for modeling. 3BUS is the crystal structure of the rebeccamycin 4'-O-methyltransferase (RebM) in complex with S-adenosyl-L-homocysteine (Singh et al., 2008). On the other hand, the 4PNE template was also shortlisted as a suitable template due to its high coverage to the LdSMT (61%), high resolution (1.50 Å), and sequence identity similar to that of 3BUS (24.15%). 4PNE is the SpnF enzyme in *Saccharopolyspora spinosa* involved in the biosynthesis of the insecticide spinosyn A (Fage et al., 2015; Jeon et al., 2017). SpnF has been reported to be structurally similar to S-adenosyl-L-methionine (SAM)-dependent methyltransferases (Fage et al., 2015).

Furthermore, a BLAST search *via* the SWISS-MODEL (Waterhouse et al., 2018) revealed that 4PNE covered residues 43 to 258 while 3BUS spanned from residues 47 to 276 of the LdSMT. From residues 258 to 353 of the LdSMT sequence, both templates do not share similarities with the LdSMT. Thus, the protein structure with PDB ID 6UAK was selected in addition to 3BUS and 4PNE for the multitemplate homology modeling.

The 6UAK shared similarity with the LdSMT mostly from residues 100 to 345. 6UAK is a SAM-dependent methyltransferase (LahS<sub>B</sub>) from the *Lachnospiraceae* bacterium C6A11 (Huo et al., 2020). Both 3BUS and 6UAK templates, like the LdSMT, are methyltransferases, while the 4PNE is a methyltransferase-like protein.

### 3.2 Structure Prediction of LdSMT

An earlier study identified Modeller (Eswar et al., 2008) to predict the most accurate model of *L. infantum* sterol methyltransferase (Azam et al., 2014). Although the two organisms (*L. infantum* and *L. donovani*) belong to the same genus and SMT is highly conserved among *Leishmania* species (Goto et al., 2007), there was a need to model the structure of LdSMT to ascertain its accuracy. Therefore, Modeller 10.2 (Eswar et al., 2008) was employed for modeling the structure of the LdSMT.

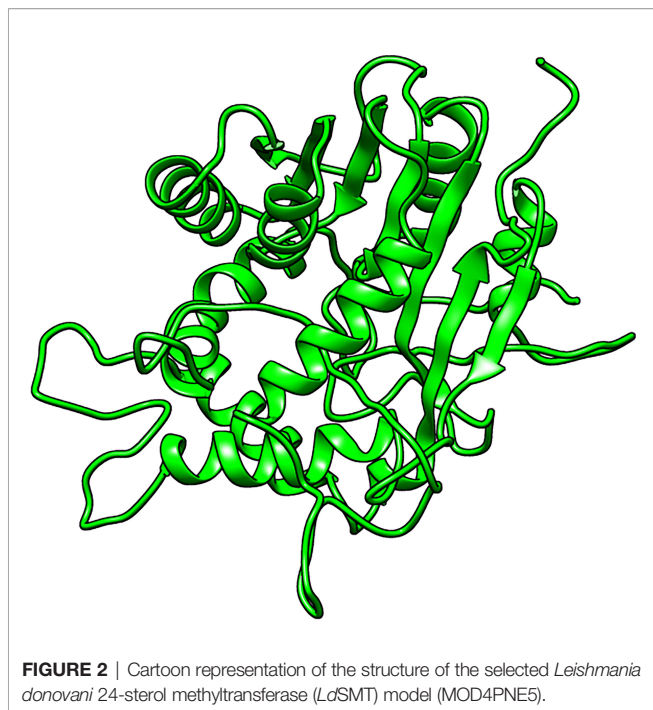
Three modeling approaches were employed to predict the most reasonably accurate LdSMT model. First, 3BUS was used as template to model five structures of the LdSMT. Secondly, 4PNE was also used to model five different structures of the LdSMT. Lastly, a multitemplate homology modeling approach was employed by using three templates comprising 3BUS, 4PNE, and 6UAK protein structures. For each approach, the best model was selected based on the DOPE score, which is an atomic distance-dependent statistical potential calculated from a sample of native protein structures (Shen and Sali, 2006). The DOPE scores were used to distinguish “good” models from “bad” ones with lower DOPE scores signifying a better model (Shen and Sali, 2006; Eswar et al., 2008).

#### 3.2.1 Structure Prediction Using 3BUS as Template

The 3BUS template with a sequence identity of 24.12% and coverage of 63% to the LdSMT was used to generate five potential models of the LdSMT (**Supplementary Table 1**). The five generated models (referred to as MOD3BUS1, MOD3BUS2, MOD3BUS3, MOD3BUS4, and MOD3BUS5) had genetic algorithm 341 (GA341) scores ranging from 0.87 to 0.99 (**Supplementary Table 2**). The GA341 score assesses the reliability of a model and has a determined threshold of 0.7. A model is said to be reliable when the GA341 score is higher than the cutoff (0.7) (Broni et al., 2021). For all the 3BUS-based models, the GA341 scores were greater than the cutoff signifying their reliability. Model MOD3BUS2 had the least DOPE score of -30,234.79297 and was selected as the most reasonable structure among the three models (**Supplementary Table 2** and **Supplementary Figure 2A**).

#### 3.2.2 Structure Prediction Using 4PNE as Template

A total of five structures were predicted using 4PNE as template. 4PNE had a sequence identity of 24.15% and a coverage of 61% to the LdSMT (**Supplementary Table 1**). For the 4PNE-based models, the GA341 scores ranged between 0.73 and 0.98, signifying their high level of reliability (**Supplementary Table 2** and **Figure 2**). Model MOD4PNE5 had the least DOPE score of -31,608.05664 and was thus selected as the most reasonably accurate model for the 4PNE-based structures (**Supplementary Table 2** and **Figure 2**).



### 3.2.3 Structure Prediction Using 3BUS, 4PNE, and 6UAK as Templates

For the third set of models, three templates comprising 3BUS, 4PNE, and 6UAK were used for the modeling because it has been reported that the use of multiple templates can help increase the accuracy of a model (Larsson et al., 2008). Model MOD3TEMP2 had a GA341 score of 0.64307, lower than the 0.7 cutoff. However, the other four models had good GA341 scores ranging from 0.7 to 0.94 (Supplementary Table 2). Among the multiple template-generated models, MOD3TEMP3 had the least DOPE score and was thus selected as the most accurate (Supplementary Table 2 and Supplementary Figure 2B).

### 3.3 Validation of the Predicted Models

Next, validation and quality assessment of the predicted 3D structures were undertaken to obtain reasonable structures of the proteins. The best models from each of the three different

approaches MOD3BUS2, MOD4PNE5, and MOD3TEMP3 were evaluated to select the most reasonably valid structure of the LdSMT.

The percentage of residues in the most favored, additionally allowed, generously allowed, and disallowed regions in a Ramachandran plot determines the quality of protein structures. From the Ramachandran plots generated from PROCHECK, model MOD3BUS2 had 270 (86.8%), 32 (10.3%), 6 (1.9%), and 3 (1.0%) residues in the most favored, additionally allowed, generously allowed, and disallowed regions, respectively (Table 1 and Supplementary Figure 3A). Model MOD3TEMP3 had 266 (85.5%), 31 (10.0%), 8 (2.6%), and 6 (1.9%) residues in the most favored, additionally allowed, generously allowed, and disallowed regions, respectively (Table 1 and Supplementary Figure 3B). For the MOD4PNE5 model, 264 (84.9%) residues were in the most favored region, 32 (10.3%) in the additionally favored region, 11 (3.5%) in the generously allowed region, and 4 (1.3%) in the disallowed region (Table 1 and Figure 3). The Ramachandran plot statistics of all three structures were comparatively close (Table 1) and are consistent with those of a previously modeled LdSMT structure using Modeller (Azam et al., 2014).

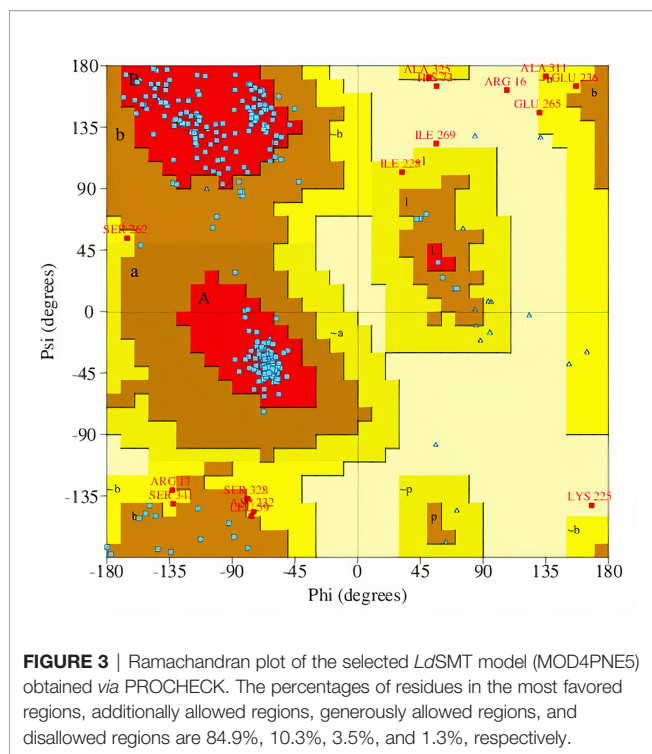
The qualities of the three structures were further assessed via SAVES v6.0 (Behera et al., 2021). The protein structure MOD3BUS2 had a VERIFY score of 62.61%, ERRAT quality factor of 41.5663, PROVE score of 11%, and four PROCHECK errors, one warning and three passes (Supplementary Table 3). For the MOD3TEMP3 model, ERRAT predicted an overall score of 45.858, VERIFY a score of 53.82%, PROVE a score of 9.6%, and five PROCHECK errors, one warning and two passes (Supplementary Table 3). Model MOD4PNE5 was predicted to have ERRAT, VERIFY, and PROVE scores of 46.9565, 62.04%, and 7.1%, respectively. MOD4PNE5 was also predicted to have four PROCHECK errors, two warnings and two passes (Supplementary Table 3). For a model to be considered high quality, 80% of its amino acids must have a score of 0.2 in the 3D-1D profile (VERIFY score). Although all the top 3 structures did not have a VERIFY score above 80%, MOD3BUS2 (VERIFY score of 62.61) and MOD4PNE5 (VERIFY score of 62.04) could be considered since a previous study has shown that a crystallized structure also performed poorly based on the

**TABLE 1** | Ramachandran plot statistics for the best models from the three modeling approaches.

Model	MOD3BUS2		MOD4PNE5		Refined MOD4PNE5		MOD3TEMP3	
	No. of residues	Percentage (%)	No. of residues	Percentage (%)	No. of residues	Percentage (%)	No. of residues	Percentage (%)
Most favored regions [A, B, L]	270	86.8	264	84.9	268	86.2	266	85.5
Additionally allowed regions [a, b, l, p]	32	10.3	32	10.3	34	10.9	31	10.0
Generously allowed regions [~a, ~b, ~l, ~p]	6	1.9	11	3.5	7	2.3	8	2.6
Disallowed regions	3	1.0	4	1.3	2	0.6	6	1.9
Non-glycine and non-proline residues	311	100.0	311	100.0	311	100.0	311	100.0

For all three models, the number of end residues (excluding Gly and Pro) = 2, glycine residues = 27, proline residues = 13, and the total number of residues = 353.





VERIFY 3D quality indicator (Mora Lagares et al., 2020). For the ERRAT predictions, MOD4PNE5 had the best score and was also predicted using PROVE to be less erroneous (Supplementary Table 3). Generally, model MOD3TEMP3 exhibited the lowest quality scores from SAVES v6.0.

Based on the quality assessments, the protein structure MOD4PNE5 was selected as the most reasonable structure of the *LdSMT* protein. Aligning the selected *LdSMT* structure and the chain A of the 4PNE structure revealed a close similarity with a root mean square deviation (RMSD) of 0.356 Å (Supplementary Figure 2C). The quality of the selected model (MOD4PNE5) was further assessed via ProSA-web (Sippl, 1993; Wiederstein and Sippl, 2007). With a Z-score (Zhang and Skolnick, 1998) of -3.97, the *LdSMT* structure was predicted to be of X-ray quality (Supplementary Figure 4A). The Z-score was used to indicate the overall protein quality (Zhang and Skolnick, 1998; Benkert et al., 2011). ProSA (Sippl, 1993; Wiederstein and Sippl, 2007) was used to plot the energies as a function of the amino acid sequence position for the *LdSMT* protein (Supplementary Figure 4B). Positive energy values signify problematic or erroneous regions of the protein structure. The residues of the protein demonstrated relatively low energies until residue 230, where positive energy values were observed until the end of the sequence.

The selected *LdSMT* structure was then refined using ModRefiner (Xu and Zhang, 2011). The refined structure of the selected *LdSMT* model showed improved Ramachandran plot statistics with 268 (86.2%), 34 (10.9%), 7 (2.3%), and 2 (0.6%) residues in the most favored, additionally allowed, generously allowed, and disallowed regions, respectively (Table 1).

### 3.4 Active Site Prediction

CASTp was used to predict the plausible binding sites within the refined *LdSMT* structure. CASTp predicted 65 potential binding sites of the *LdSMT* protein. Ligand binding sites tend to involve the largest pockets or cavities on the protein (Laskowski et al., 1996; Liang et al., 1998); thus, pockets with relatively low areas and volumes, such that no ligand could fit, were not considered (Broni et al., 2021; Kwofie et al., 2021). A total of seven binding sites were shortlisted (Supplementary Table 4), which were visualized using PyMOL (PyMOL Molecular Graphics System, Version 1.5.0.4, Schrödinger, LLC) (Lighthall et al., 2010) and Chimera 1.16 (Pettersen et al., 2004). However, superimposing the *LdSMT* on the 4PNE template revealed that pocket 1 was similar to the S-adenosyl-L-homocysteine (SAH) ligand's binding site in the 4PNE protein (Fage et al., 2015). Surprisingly, pocket 1 for *LdSMT* was predicted to have no opening in Chimera 1.16 (Pettersen et al., 2004), leaving pockets 2 to 7 as the most plausible binding cavities of the *LdSMT* (Supplementary Table 4). Pockets 5 and 7 also overlapped and occupied the same region (Supplementary Table 4).

### 3.5 Scaffold Hopping via BRUSELAS and Molecular Docking

Following the protocols of BRUSELAS, 100 ligands were generated using the ChEMBL database (Davies et al., 2015) with varying degrees of similarities to 22,26-azasterol. Out of the 100 ligands, 17 were identified to possess unique scaffolds devoid of the steroidal nucleus present in the 22,26-azasterol. The total score (comprising a combination of WEGA, LiSiCA, Screen3D, and OptiPharm) ranged from 0.38458 to 0.65814. Ten of the molecules with different scaffolds and varying scores are presented (Supplementary Table 5).

A search via the PubChem (Kim et al., 2021), ZINC15 (Sterling and Irwin, 2015), DrugBank (Wishart et al., 2018), and ChemSpider databases (Pence and Williams, 2010) generated 1,342 derivatives of all 17 scaffolds. The 1,370 compounds consisting of 17 scaffolds, 1,342 derivatives, 22,26-azasterol, 7 other known inhibitors (labeled X1–X7), and 3 already known drugs (amphotericin B, miltefosine, and paromomycin) were screened against an energy minimized *LdSMT* using a grid box of  $(91.445 \times 73.502 \times 78.352) \text{ Å}^3$  with the center at  $(72.200, 58.009, 13.302) \text{ Å}$  to cover the protein. Screening 1,370 compounds against the active site of the protein identified 25 hits which were selected based on the binding affinities and orientation within the binding site of the protein.

Among the three drugs used in leishmaniasis treatment, amphotericin B had the least binding energy of -5.3 kcal/mol followed by paromomycin (-5.0 kcal/mol) and miltefosine (-4.0 kcal/mol). Interestingly, all the known inhibitors had binding energies lower than the three drugs signifying a higher binding affinity to *LdSMT*. The binding energies of -5.9, -6.2, and -6.5 kcal/mol were obtained for X6, X3, and X4, respectively. The least binding energy of -7.7 kcal/mol was observed for X5 comparable to 22,26-azasterol (-7.6 kcal/mol). *In-vitro* studies reported that 22,26-azasterol inhibited *L. donovani* intracellular amastigotes and *Trypanosoma brucei* subsp. *brucei* with  $IC_{50}$



values of 8.9 and 1.76  $\mu\text{M}$ , respectively (Magaraci et al., 2003; Gros et al., 2006), supporting the results reported herewith. Compounds X1, X7, and X2 had binding energies of  $-7.3$ ,  $-7.2$ , and  $-7.0$  kcal/mol, respectively (**Supplementary Table 6**). Similarly, *in-vitro* studies revealed that X1, X2, X3, X4, X5, X6, and X7 inhibited the growth of *Leishmania* parasites with  $\text{IC}_{50}$  less than 10  $\mu\text{M}$ , except for X6 and X7 which were found to suppress growth with  $\text{IC}_{50}$  values of 28.6 and 30  $\mu\text{M}$ , respectively (Magaraci et al., 2003; Lorente et al., 2004; Andrade-Neto et al., 2016; Torres-Santos et al., 2016).

The 12 best hits out of the 25 selected from the scaffold hopping had lower binding energies compared with the three drugs (**Supplementary Table 6**). In addition, the binding energies of these ligands were also found to be comparable to the known inhibitors with S1 showing the least binding energy of  $-9.0$  kcal/mol. The closest to this ligand were S2, S3, and S4 with binding energies of  $-8.9$ ,  $-8.8$ , and  $-8.7$  kcal/mol, respectively (**Supplementary Table 6**). Compounds S12, S11, and S10 had the highest binding energies among the 12 best compounds with binding energies of  $-7.0$ ,  $-7.0$ , and  $-7.2$  kcal/mol, respectively. In addition, the binding energies of compounds S9 ( $-7.3$  kcal/mol), S8 ( $-7.4$  kcal/mol), and S7 ( $-7.4$  kcal/mol) were also obtained. Comparable binding energies to the two lowest binding energies of the known inhibitors were obtained for S5 ( $-7.7$  kcal/mol) and S6 ( $-7.6$  kcal/mol).

### 3.6 De-Novo Design via e-LEA3D and Molecular Docking

The *de-novo* drug design is the generation of novel chemical entities that fit a set of constraints using computational algorithms (Schneider and Schneider, 2016). Despite the challenges of synthetic accessibility associated with this method, the application of *de-novo* drug design leads to the development of drug candidates in a cost- and time-efficient manner (Mouchlis et al., 2021). In addition, the *de-novo* design generates novel compounds with improved biological activity (Mouchlis et al., 2021). A number of studies have been undertaken for the *de-novo* design of inhibitors against plausible targets (Kranthi et al., 2018; Islam and Pillay, 2020; Pathania et al., 2021). A previous study selected a lead molecule based on the least binding energy as well the accurate pose of the ligand within the protein binding pocket for the *de-novo* design of inhibitors (Pathania et al., 2021). A similar approach was used in the identification of promising anti-DNA gyrase antibacterial compounds (Islam and Pillay, 2020). Ligands with very low binding energies and accurate pose have the potential to inhibit the receptor.

Among the compounds obtained from scaffold hopping, the well-known heterocyclic quinolinone and the phenylpiperazine/phenylpiperidine moieties found in several bioactive compounds were present. These compounds with diverse pharmacological potencies have been explored for various ailments including leishmaniasis (Kshirsagar, 2015; Chanquia et al., 2019; Mishra et al., 2021). One of such derivatives is 2-(4-(4,6-di(piperidin-1-yl)-1,3,5-triazin-2-ylamino)phenyl)-2-methyl-2,3-dihydroquinazolin-4(1H)-one which had an  $\text{IC}_{50}$  value of 0.65

$\mu\text{M}$  against intracellular amastigotes when compared with miltefosine ( $\text{IC}_{50}$  of 8.4  $\mu\text{M}$ ) (Sharma et al., 2013), corroborating the fact that *de-novo* drug design could result in novel scaffolds as potential antileishmanial agents.

The e-LEA3D was used to generate 155 potential novel compounds against LdSMT after using protein-S1, S2, S3, S4, and 22,26-azasterol complexes. They were filtered based on Lipinski's rule of five (Benet et al., 2016) and redundancy to generate 78 ligands that were subjected to molecular docking studies. The six best hits (**A1**, **A2**, **A3**, **A4**, **A5**, and **A6**) (**Figure 4**) were selected for downstream analysis. The search *via* public databases including PubChem (Kim et al., 2021) and ChemSpider (Pence and Williams, 2010) showed that the six ligands do not have duplicates.

The docking analysis of the six compounds revealed the binding energies of **A1** ( $-8.4$  kcal/mol), **A2** ( $-7.5$  kcal/mol), and **A3** ( $-7.2$  kcal/mol), while **A4**, **A5**, and **A6** had  $-7.0$  kcal/mol. Though **A1**, **A2**, **A3**, and **A6** have similar core structures, they had different binding energies (**Table 2**). Interestingly, using AutoDock Vina, compounds that had shown binding energies  $\leq -7.0$  kcal/mol have been found to demonstrate significant inhibitory activities against the parasite of consideration (Chang et al., 2007; Wyllie et al., 2018; Tabrez et al., 2021). In lieu of this, the predicted compounds may have the potential of suppressing LdSMT since the binding energies were lower than  $-7.0$  kcal/mol. Altogether, compounds **A1**, **A2**, **A3**, **A4**, **A5**, and **A6** showed binding energies lower than amphotericin B, miltefosine, and paromomycin. Similarly, all the compounds had binding energies comparable to the known inhibitors and, therefore, have the potential of attenuating LdSMT.

### 3.7 Characterization of Binding Interactions

Compounds with similar activity against a receptor may possess identical chemical features in sterically consistent locations within the pocket of a macromolecule (Held et al., 2011; Du et al., 2016). Most of the compounds including 22,26-azasterol and its derivatives were observed to interact with residues Asp58, Ala88, Arg89, Tyr92, Glu85, Phe93, Phe100, Glu102, Lys198, Pro199, and Gly200, which lined binding pockets 5 and 7 (**Supplementary Tables 4 and 6**). A similar study involving *L. infantum* SMT, however, showed the ligands to interact with residues Tyr1, Gly4, Gln5, Gly45, Gly47, Asn67, Asn68, Gln72, and Ile112 within the binding pocket of the receptor (Azam et al., 2014). The nature of interactions included *pi*-anion, *pi*-*pi* stacking, *pi*-alkyl, *pi*-sigma, carbon-hydrogen, and hydrogen bonds similar to the other study (Azam et al., 2014). Among all the ligands, only amphotericin B had five hydrogen bonds, with residues Asp31, Phe307, Val308, Arg309, and Leu310 found to line pocket 2. Compounds X1 and X5 formed two hydrogen bonds each with LdSMT. Compound X1 interacted with pockets 5 and 7 and residues Asp172 and Gly200, while X5 interacted with pocket 4 and residues Asn12 and Thr319 *via* hydrogen bonds (**Supplementary Table 6**).

In addition, compounds X2, X6, X7, S1, S5, S9, S10, and S12 docked into the binding pocket of the receptor but showed no

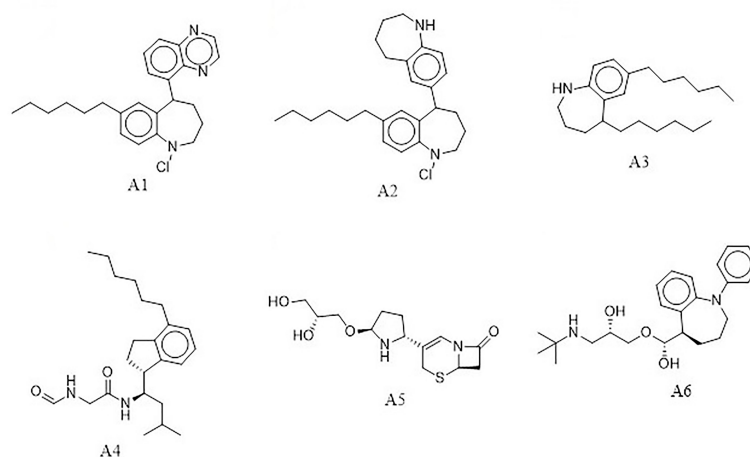


**FIGURE 4** | Top hits from *de-novo* drug design using the e-LEA3D.

hydrogen bond interactions with any of the residues. The compound 22,26-azasterol formed two hydrogen bonds with Glu102 and Gly200 as well as hydrophobic interactions with Phe100, Lys198, and Pro199. Moreover, while paromomycin, S2, S3, S4, S5, and S11 formed a hydrogen bond with Arg89, that of S6 and S7 showed a similar interaction with Asp58. Apart from paromomycin, all the other ligands which interacted with Arg89 had low binding energies, implying that it might be critical for binding. The known drugs and inhibitors formed hydrophobic interactions with one or more of the residues Phe100, Met101, Asp104, Asp172, Pro199, Gly200, Thr201, Tyr343, and Ile344, while the selected S-class compounds showed hydrophobic interactions with one or more of the residues Asp58, Ala88, Arg89, Tyr92, Phe93, and Phe264 (Supplementary Table 6).

For the e-LEA3D-generated hits, apart from A2 and A3 which were predicted not to form hydrogen bond interactions with any amino acid residues, the remaining four exhibited hydrogen bonding with at least one of the amino acid residues of LdSMT (Table 2). This notwithstanding, all six formed hydrophobic interactions with the LdSMT protein. The hydrophobic interactions for A1 were with residues Arg89, Tyr92, Ala95, Ala96, and Leu123 (Figure 5 and Table 2), and those for A2 were with Phe84, Glu85, Ala88, Arg89, and Tyr92

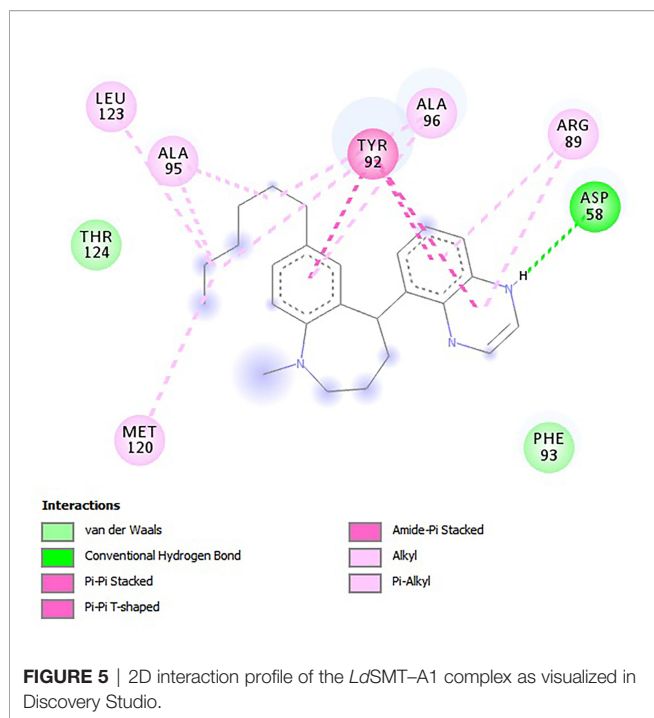
(Table 2 and Supplementary Figure 5A). The ligand A3, on the other hand, formed hydrophobic interactions with Ala88, Arg89, Tyr92, Phe93, Ala96, and Phe264 (Table 2 and Supplementary Figure 5B). Furthermore, both A4 (Supplementary Figure 5C) and A6 (Supplementary Figure 5E) formed hydrogen bonding with Cys202 and Asp58, respectively, while A5 (Supplementary Figure 5D) formed two hydrogen bonding interactions with Arg222 and Lys317.

### 3.8 Physicochemical, Pharmacological, and Toxicity Profiling

A druggable candidate must be able to reach the site of action in the body at optimized concentrations (Hughes et al., 2011). Predictions of pharmacological and physicochemical parameters are essential because they offer clues as to whether the molecule could reach the active site in the desired concentration and remain there to elicit the required biological response. The physicochemical and pharmacokinetic parameters of the six compounds were assessed using SwissADME (Hughes et al., 2011). Physicochemical profiling assessed both Lipinski's rule of five (RO5) and Veber's rule to determine if the chemical compounds with certain pharmacological or biological activity have chemical and physical properties to make them orally active

**TABLE 2** | Binding energies and predicted interacting residues in the LdSMT-hit complexes.

Compounds	Binding energies (kcal/mol)	Interacting residues	
		Hydrogen bonds	Hydrophobic bonds
22,26-Azasterol	-7.6	Glu102, Gly200	Phe100, Lys198, Pro199
A1	-8.4	Asp58	Arg89, Tyr92, Ala95, Ala96, Leu123
A2	-7.5	-	Phe84, Glu85, Ala88, Arg89, Tyr92
A3	-7.2	-	Ala88, Arg89, Tyr92, Phe93, Ala96, Phe264
A4	-7.0	Cys202	Gly98, Phe100, Asp104, Tyr343, Ile344
A5	-7.0	Arg222, Lys317	Val26, Ala30, Phe33, Phe37, Met52, Ile224
A6	-7.0	Asp58	Phe33, Ile258, Phe264



(Lipinski et al., 2001; Veber et al., 2002). **A5** and **A6** were found to obey both Lipinski's and Veber's rules, and **A1**, **A2**, **A3**, and **A4** violated one of the two rules (**Supplementary Table 7**).

Solubility, an important physicochemical property, was predicted to assess the bioavailability and bioactivity of the hit compounds (van den Anker et al., 2018). Many lead compounds have failed to reach clinical trials despite being potent because of low bioactivity attributed to insufficient solubility, making solubility predictions critical in the early stages of drug design (Das et al., 2022). Compounds **A4**, **A5**, and **A6** were, however, predicted to be soluble compared with **A1**, **A2**, and **A3** whose solubility can be improved upon by structural modification (Das et al., 2022).

Next, molar refractivity (MR) was assessed to give valuable information on the pharmacokinetics and pharmacodynamics of the compounds. This is governed by different interactions in solution such as drug-solvent, drug-drug, and drug-co-solute interactions (Sawale et al., 2016). The compounds passed for molar refractivity as the predicted values for MR (**Supplementary Table 7**) were all within the acceptable range of 40 to 130. Since compounds with topological polar surface area (tPSA) not more than 140 Å<sup>2</sup> are considered to have good oral bioavailability, all compounds are predicted to be orally active and have good bioavailability.

Furthermore, synthetic accessibility was explored to evaluate the synthetic feasibility of the *de-novo* hits and has gained importance in the prioritization of compounds in drug design (Ertl and Schuffenhauer, 2009). Many druggable candidates especially *de-novo* constructed chemical entities are unable to reach clinical trials due to their molecular complexity coupled

with difficulty in synthesis (Huang et al., 2010; de Souza Neto et al., 2020). SwissADME (Daina et al., 2017) predicted all the six compounds to possess synthetic accessibility less than 6 implying easy synthesis.

The PAINS of the chemical compounds was investigated to establish whether they will react non-specifically with numerous biological targets (Baell, 2016). A number of PAINS compounds include toxoflavin, isothiazolones, hydroxyphenyl hydrazones, curcumin, phenol-sulfonamides, rhodanines, enones, quinones, and catechols (Baell and Walters, 2014). It is reported that about 5% of US FDA-approved drugs obtained from natural and synthetic drugs still contain PAINS-recognized substructures (Baell and Nissink, 2017). All the compounds were predicted not to contain PAINS substructures.

Pharmacokinetics studies were used to evaluate the time course of absorption, distribution, metabolism, and excretion of the selected hits (Luer and Penzak, 2016). The parameters measured were blood-brain barrier (BBB), gastrointestinal absorption (GI), and permeability glycoprotein (P-gp). Compounds predicted to permeate the BBB have the potential to bind to relevant receptors of the brain to activate signal pathways (Banks, 2009). Four of the compounds (**A1**, **A2**, **A3**, and **A5**) were predicted not to cross the blood-brain barrier, while **A4** and **A6** were predicted to cross the BBB to attach to the receptors in the brain to elicit a biological response. GI absorption was probed to investigate whether the hit compounds will be absorbed into the bloodstream after metabolism when orally administered (Löbenberg et al., 2013). All ligands were predicted to have a high GI absorption score except **A2** and **A3** (**Supplementary Table 7**). Another pharmacokinetic parameter considered for this study was to explore whether the hits generated were P-gp substrates as compounds predicted to inhibit P-gp result in their increased bioavailability (Lin and Yamazaki, 2003; Prachayasittikul and Prachayasittikul, 2016). The six compounds were screened for their P-glycoprotein binding affinity and they were all predicted to be substrates except **A4**.

The toxicity profiles of all six compounds were predicted using OSIRIS Property Explorer in Data Warrior (Sander et al., 2015). Toxicity prediction has become very critical in the development of drugs as over 45% of drug candidates fail due to toxicity deficiencies (Van Norman, 2019). Moreover, between 1953 and 2013, as many as 462 medicinal products were withdrawn from the market due to adverse drug reactions (Onakpoya et al., 2016). Toxicity profiling considered for this study was mutagenicity, carcinogenicity, irritancy, and reproductive effects. Of the six compounds, only **A1** was predicted to be tumorigenic. The rest neither were mutagenic nor possessed any irritant or reproductive effects (**Supplementary Table 8**). Among all the compounds under consideration, only **X6** was predicted to possess reproductive effects. Overall, the predictions indicate that all molecules may have safe pharmacokinetic and pharmacodynamic profiles except for **A1**, which would require structural modification to improve its pharmacological properties. For instance, the prediction showed that replacement of the

chlorine substituent with a hydrogen atom could render the **A1** analog non-tumorigenic.

### 3.9 Bioactivity Prediction

The open Bayesian machine learning technique, PASS, was used to predict the biological activity of the ligands based on the structure-activity relationship between the selected hits and the training set of compounds of known biological activity (Lagunin et al., 2000; Parasuraman, 2011). A ligand is said to be biologically active and requires experimental validation if the probability of activity (Pa) is greater than the probability of inactivity (Pi) (Basanagouda et al., 2011). Among the six compounds, **A3** was predicted to possess antileishmanial properties with a Pa of 0.362 and a Pi of 0.066 and also dermatological properties with a Pa of 0.32 and a Pi of 0.091. Compounds **A5** and **A6** were also predicted as dermatologic, with Pa values of 0.205 and 0.249 and Pi values of 0.162 and 0.120, respectively. The results may suggest that **A3**, **A5**, and **A6** might be beneficial in treating post-kala-azar leishmaniasis (Momeni et al., 2003; Ali et al., 2012).

Compounds **A1** (Pa of 0.571 and Pi of 0.111), **A3** (Pa of 0.774 and Pi of 0.026), and **A6** (Pa of 0.615 and Pi of 0.079) were also predicted as mucomembrane protectors. A recent *in-vitro* study revealed that butein acting as a mucomembrane protector on human cells increased immunity against pathogenic infections (Satari et al., 2021). This may suggest that the compounds have the potential of boosting the immune system to prevent disease exacerbation. Compound **A1** was predicted as an indolepyruvate C-methyltransferase inhibitor with a Pa of 0.226 and a Pi of 0.074. Compound **A3** was also predicted to be phenol O-methyltransferase, histamine N-methyltransferase, and acetylserotonin O-methyltransferase inhibitors with Pa values greater than Pi.

### 3.10 Quality Assessment

The inhibitory constant ( $K_i$ ) and other parameters such as LE, LE\_Scale, FQ, binding efficiency index (BEI), surface efficiency index (SEI), and LELP were calculated (**Supplementary Table 9**).

$K_i$  is the concentration required to produce half-maximum inhibition and, hence, an indicator of the potency of a ligand (Fisar et al., 2010). Computation of  $K_i$  for the protein-ligand complexes was obtained using Equation (1), where  $R$  is the molar gas constant ( $1.987 \times 10^{-3}$  kcal/K mol<sup>-1</sup>) and  $T$  (298.15 K) is the absolute temperature (Du et al., 2016).

$$K_i = e^{\frac{-\Delta G}{RT}} \quad (1)$$

The  $K_i$  predicted for the ligands was low (**Supplementary Table 9**), hence has the capacity to be lead-like with possible high potency (Reynolds and Reynolds, 2017).

LE is a value that expresses the binding energy of a compound normalized by the compound's size and expressed by the number of heavy (non-hydrogen) atoms (Hopkins et al., 2004). This property is important to consider in screening for hits as larger compounds tend to show greater binding energy due to a large number of interactions but may not necessarily be the most efficient binder (Hevener et al., 2018). The LE was computed using Equation (2), where BE is the binding energy and NHA is the number of heavy atoms (Abad-Zapatero et al., 2010).

$$LE = \frac{-BE}{NHA} \quad (2)$$

Interestingly, all the ligands except **A1**, **A3**, and **A5** were within the optimal range ( $LE < 0.3$  kcal/mol/HA) (Schultes et al., 2010) for the ligand efficiency of lead-like molecules.

Results from the computation of LE being size-dependent may not be a true reflection of the binding energy of the compound, and therefore, ligand efficiency scaling (LE\_Scale), a size-independent parameter that compares ligands with the help of an exponential function to the maximal LE values, is required (Reynolds et al., 2007). LE\_Scaling was computed using Equation (3), where NHA is the number of heavy atoms (Reynolds et al., 2007).

$$LE\_Scaling = 0.873e^{-0.026 \times NHA} - 0.064 \quad (3)$$

Potential lead-like molecules are suggested to have an LE\_Scale lower than 0.3 (Islam and Pillay, 2020). The LE\_Scale values of all six molecules were, however, predicted to be in the range of 0.3 to 0.5 with **A5** having the highest LE\_Scale of 0.455.

FQ is another size-independent parameter that determines the optimal ligand binding within the receptor active site (Schultes et al., 2010), and is computed using Equation (4) (Schultes et al., 2010).

$$FQ = \frac{LE}{LE\_Scale} \quad (4)$$

FQ scores range from 0 to 1 with values close to 1 signifying an optimal ligand binding (Schultes et al., 2010). All the compounds were predicted to have an FQ score above 0.7 except **A6** (0.695), implying a stronger ligand binding. With the predicted FQ being close to 1, it suggests an optimal ligand binding.

The LELP, on the other hand, assesses the binding energy of a compound in relation to the compound's lipophilicity (Hevener et al., 2018). LELP is a parameter used in drug design and development to evaluate the quality of compounds by linking potency and lipophilicity in an attempt to estimate drug-likeness (Edwards and Price, 2010). Equation (5), where  $\log P$  is the lipophilicity, was used in calculating the LELP of the compounds (Schultes et al., 2010).

$$LELP = \frac{\log P}{LE} \quad (5)$$

The recommended range for promising molecules for LELP was  $>3$  (Schultes et al., 2010). All the analogs had LELP above 4 (**Supplementary Table 9**) suggesting an optimized affinity with respect to lipophilicity.

BEI and SEI are two alternative metrics that are also used to compare the activity of molecules according to size and area (Schultes et al., 2010). Binding efficiency index is defined by  $BEI = p(IC_{50})/MW$ , where MW is the molecular weight (Schultes et al., 2010). The relation in Equation (6) was used in computing the BEI of the ligands (Abad-Zapatero et al., 2010).

$$BEI = \frac{-\log K_i}{MW(kDa)} \quad (6)$$



SEI, on the other hand, is defined by  $SEI = p(IC_{50})/PSA$ , where PSA is the polar surface area of the ligand (Abad-Zapatero et al., 2010). Calculation of SEI was done using Equation (7) (Abad-Zapatero et al., 2010).

$$SEI = \frac{-\log K_i}{(PSA/100)} \quad (7)$$

By rule of thumb, potential inhibitors must approximately have the same BEI and SEI values (Abad-Zapatero, 2007). Compounds **A1**, **A4**, and **A6** were predicted to have BEI equal to SEI. Altogether, the parameters predicted for all the compounds were mostly within the acceptable range prompting the need for experimental analysis.

### 3.11 Molecular Dynamics Analysis

MD simulation is a computer simulation method for analyzing the physical movements of atoms and molecules (Hollingsworth and Dror, 2018). Of great concern for the MD simulation is how a biomolecular system responds to some perturbation within a short period of time (Karplus and Kuriyan, 2005; Hollingsworth and Dror, 2018). Due to its usefulness, a number of drug design studies have explored molecular dynamics simulation to analyze and validate the binding poses, stability of the complexes, and binding affinity of selected hits within the binding pocket of the receptor (Agyapong et al., 2021; Gupta et al., 2021; Pathania et al., 2021). To check the relative stability of each complex using a 100-ns time span MD simulation, parameters such as RMSD, root mean square fluctuation (RMSF), and radius of gyration (Rg) were computed.

#### 3.11.1 The Root Mean Square Deviation of the Unbound LdSMT and the Complexes

The RMSD trajectory was used to evaluate the stability of the protein–ligand complexes, and the plot shows the system was

equilibrated in the range of 0 to 0.7 nm. Averagely, the unbound LdSMT was observed to rise steadily from 0.28 nm until about 0.42 nm for 20 ns before stabilizing thereafter (**Figure 6**). Comparatively, there is no significant fluctuation observed in any of the protein–ligand complexes except for the LdSMT–**A3** complex, which rose from 0.28 to 0.62 nm during 10 ns and then stabilized for the next 10 ns and dropped to about 0.5 nm. It then rose slightly to 0.56 nm and then stabilized after 40 ns. Across the board, the LdSMT–**A2** complex had high rigidity and the frames of each complex depict a tight structural packing across the whole protein influencing the low RMSD values of LdSMT.

#### 3.11.2 Radius of Gyration of the LdSMT and the Complexes

The radius of the gyration plot, a graph of Rg against simulation time, is used to analyze the compactness and folding of the unbound protein and complexes during the molecular dynamics simulations. The Rg graph obtained showed that all the complexes had low Rg values implying that the ligands formed a stable and compact complex (Liao et al., 2014; Pandey et al., 2020; Sinha and Wang, 2020). All the complexes except for **A3** had a steady decline in Rg to about 40 ns before stabilizing afterward. Rg values for both unbound protein and the complexes were between 1.925 and 2.75 nm (**Supplementary Figure 6A**). The Rg trajectory of each complex demonstrated that each ligand forms a stable bond with the LdSMT.

#### 3.11.3 The Root Mean Square Fluctuation of the LdSMT and the Complexes

The RMSF was explored to investigate which amino acids within the binding site of the receptor interacted with the ligand resulting in the stability of the protein–ligand complex (Farmer et al., 2017). The RMSF plots showed that all the hit compounds caused fluctuations in similar positions of the protein target. The

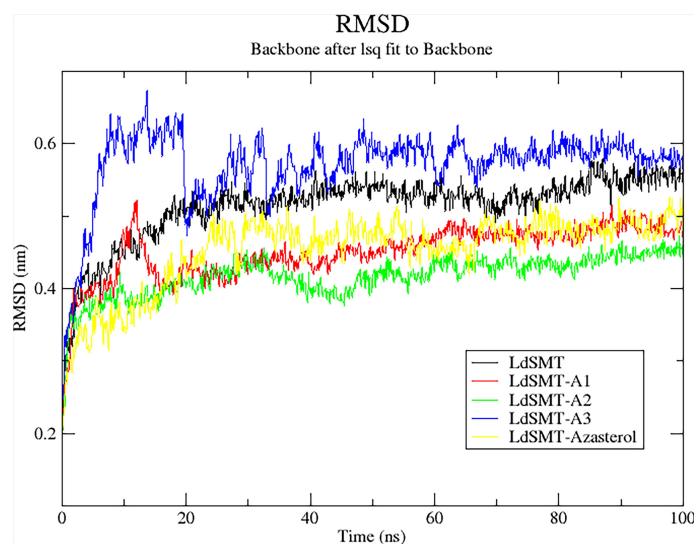


**FIGURE 6** | Root mean square deviation (RMSD) plot of 100 ns molecular dynamics (MD) simulations of the LdSMT–ligand complexes using GROMACS.

plots revealed that the amino acid residues between 15 and 100, 200 and 250, and 280 and 320 (**Supplementary Figure 6B**) fluctuated for all complexes and are predicted to be involved in the stability of the complexes (Dong et al., 2018). However, the highest fluctuation was observed around regions 200–280 for **A2** and **A3** implying it could be involved in ligand binding.

### 3.12 MM-PBSA Free Energy Computations

#### 3.12.1 Binding Energy Assessment Scores

The free energy of binding of all the protein–ligand complexes was calculated using the MM-PBSA continuum solvation method (Kumari et al., 2014). The MM-PBSA was employed to find the free energies of the bound complexes. Ligand **A1**, which was predicted to have the least binding energy from AutoDock Vina, was shown to have the lowest free binding energy of  $-282.550$  kJ/mol (**Table 3**) to the LdSMT. Among the three top compounds, only **A3** exhibited free binding energy greater than that of the reference candidate, 22,26-azasterol (**Table 3**). The dominating interaction per contribution to the free energy was electrostatic forces of attraction ranging from  $-333$  to  $-11$  kJ/mol followed by the van der Waals interactions.

#### 3.12.2 Per-Residue Energy Decomposition

Calculation of the energy contribution of each amino acid residue *via* per-residue energy analysis was performed using MM-PBSA (Congreve and Marshall, 2010; Grinter and Zou,

2014). It has previously been suggested that for a residue to contribute to the binding, the threshold must be  $>5$  or  $<5$  kJ/mol (Kwofie et al., 2019). Based on that, a detailed analysis of each complex was done (**Figure 7** and **Supplementary Figures 6A–C**), and for all the complexes, several binding site residues contributed favorable energies for ligand binding. The Tyr92 and Ala96 contributed to strong binding *via*  $\pi$ – $\pi$  stacked,  $\pi$ – $\pi$  T-shaped,  $\pi$ –alkyl, and van der Waals interactions, while Asp58 through its hydrogen bonding strengthened the affinity for ligands bound in pocket 5.

### 3.13 Exploring the Antileishmanial Potential of the Predicted Compounds

Four (**A1**, **A2**, **A3**, and **A6**) out of the six compounds possessed benzo[*b*]azepine moiety as a replacement for the steroidal core in the 22,26-azasterol. This same moiety is present in paullone and its derivatives as well as BNZ-1 (**Figure 8**), which are known to suppress growth in *Leishmania* parasites with  $IC_{50}$  values of 47 nM and 100  $\mu$ M, respectively (Clark et al., 2007; Dao Duong Thi et al., 2009), implying the possible antileishmanial potentials of the proposed hits. Moreover, the chemical structural similarity search of compounds **A1**, **A2**, **A3**, and **A6** *via* DrugBank (Wishart et al., 2018) revealed a variable similarity to antipsychotic and antidepressant drugs (Kaur, 2013; Mendonca Junior et al., 2015). For instance, compounds **A1**, **A2**, **A3**, and **A6** showed similarity scores above 0.50 to vabicaserin, sertraline,

**TABLE 3** | MM-PBSA energy assessment of the *de-novo* hits and 22,26-azasterol.

Complex	$\Delta G_{vdw}$ (kJ/mol)	$\Delta G_{ele}$ (kJ/mol)	$\Delta G_{ele, sol}$ (kJ/mol)	$\Delta G_{SASA}$ (kJ/mol)	$\Delta G_{bind}$ (kJ/mol)
<b>A1</b>	$-254 \pm 20.790$	$-276.921 \pm 49.836$	$268.533 \pm 68.275$	$-19.358 \pm 1.489$	$-282.550 \pm 35.346$
<b>A2</b>	$-165 \pm 44.344$	$-333.723 \pm 82.848$	$371.954 \pm 91.519$	$-14.820 \pm 3.992$	$-142.568 \pm 47.076$
<b>A3</b>	$-49.793 \pm 41.867$	$-11.805 \pm 11.107$	$25.031 \pm 43.156$	$-4.827 \pm 4.582$	$-41.394 \pm 44.095$
22,26-Azasterol	$-0.047 \pm 0.042$	$-56.829 \pm 37.192$	$-15.475 \pm 37.519$	$0.045 \pm 2.716$	$-72.305 \pm 59.057$

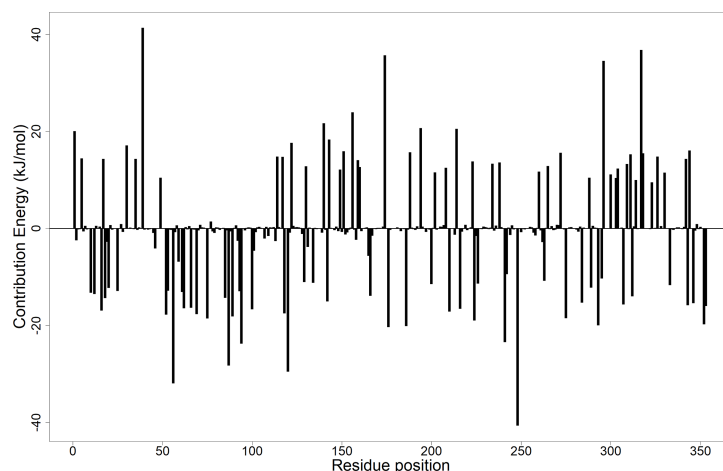


**FIGURE 7** | Molecular mechanics Poisson–Boltzmann surface area (MM-PBSA) plot showing the binding free energy contribution per residue of the LdSMT–A1 complex.

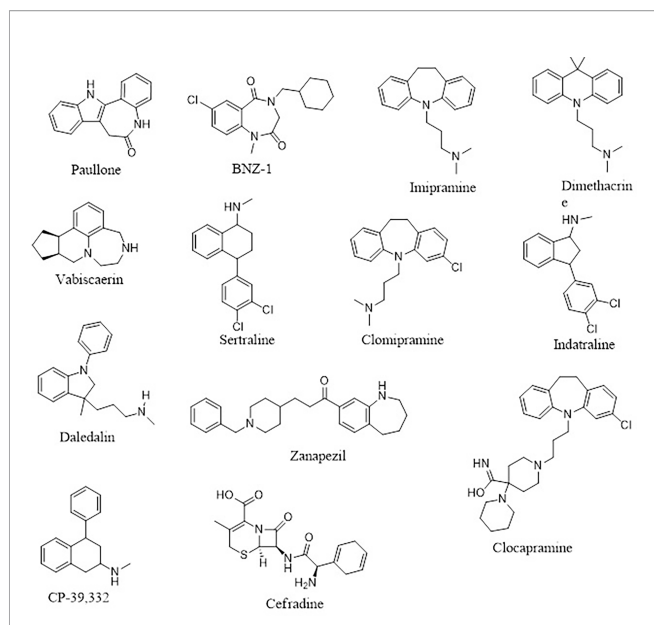


**FIGURE 8** | The 2D representations of the compounds cited from DrugBank.

and indatraline (Richardson et al., 2009; Wishart et al., 2018; Lima et al., 2018). In addition, the four compounds showed similarity scores of around 0.55, which are close to those of daledalin, zanzepzil, clocapramine, imipramine, and dimethacrine (**Figure 8**) (Mukherjee et al., 2012; da Silva Rodrigues et al., 2019). Interestingly, these drugs have been explored for their antileishmanial potentials causing *Leishmania* parasites to undergo mitochondrion depolarization in addition to inhibiting trypanothione reductase, thereby inducing strong oxidative stress in the parasite (Kaur, 2013; Andrade-Neto et al., 2016; da Silva Rodrigues et al., 2019). The similarity scores and the antileishmanial properties of these antidepressant and antipsychotic drugs warrant the testing of the compounds to assess their antileishmanial propensity.

Furthermore, compound **A4** devoid of the benzo[H]azepine also showed a chemical structural similarity score of 0.564 to CP-39,332, a serotonin–norepinephrine reuptake inhibitor. The successes emanating from other serotonin inhibitors for leishmaniasis treatment suggest **A4** as a potential antileishmanial compound. In addition, **A5** showed a similarity score of 0.538 to cefradine, a broad-spectrum antibiotic for the treatment of skin, chest, throat, and ear infections (Wishart et al., 2018). A recent study has revealed that patients exposed to antibiotics had a greater healing rate (Barakat et al., 2017), suggesting **A5** to be explored as an antileishmanial agent. In lieu of the aforementioned, the potential leads **A1**, **A2**, **A3**, **A4**, **A5**, and **A6** with diverse structural similarities with the antipsychotic and antibiotic agents are also proposed as potential antileishmanial agents *via* inhibition of sterol methyltransferase and are worthy of further experimental evaluation to assess their biological efficacy.

## 4 POTENTIAL IMPLICATIONS OF THE STUDY ON *LEISHMANIA DONOVANI* STEROL METHYLTRANSFERASE AND FUTURE PERSPECTIVE

The study modeled a reasonable structure of LdSMT with good quality parameters, which has been made available to augment the structure-based drug design. In addition, small non-steroidal molecules with negligible toxicity with the potential to suppress LdSMT were identified and could be harmonized into non-commercial databases for the design of new biotherapeutic compounds. Furthermore, the *de-novo* design was employed in making available chemical structures of compounds which can be synthesized to ascertain their antileishmanial potency.

The renewed interest in polypharmacology drugs with the added advantage of overcoming drug resistance necessitates the investigation of these compounds against plausible targets involved in the ergosterol biosynthetic pathway of *Leishmania* parasites. Furthermore, coordinating these ligands to transition metals to find multimodality metallodrugs with the potential of inhibiting two or more enzymes in the ergosterol pathway may present a possible biotherapeutic route for leishmaniasis.

## 5 CONCLUSION

*In-silico* approaches were used to predict putative inhibitors targeting LdSMT by elucidating the 3D structure of LdSMT *via* Modeller followed by subsection of 22,26-azasterol to scaffold hopping and *de-novo* drug design. In all, six potential inhibitors labeled **A1**, **A2**, **A3**, **A4**, **A5**, and **A6** were generated *via de-novo* design with binding affinities of  $-8.4$ ,  $-7.5$ ,  $-7.2$ ,  $-7.0$ ,  $-7.0$ , and  $-7.0$  kcal/mol, respectively. The compounds **A1** and **A2** demonstrated comparable binding affinity to that of 22,26-azasterol ( $-7.6$  kcal/mol), the main inhibitor of LdSMT. The study identified Tyr92 to be essential for ligand binding in the receptor binding pocket, and this was corroborated by MD simulation and MM-PBSA calculations. The physicochemical and pharmacological profiling showed that the compounds are drug-like and predicted as non-toxic. The predicted ligand quality metrics including  $K_i$ , LE, LE\_Scale, FQ, LELP, BEI, and SEI were all within the acceptable range. These findings suggest that the compounds possess antileishmanial potential and warrant experimental corroboration.

## DATA AVAILABILITY STATEMENT

The original contributions presented in the study are included in the article/**Supplementary Material**. Further inquiries can be directed to the corresponding author.

## AUTHOR CONTRIBUTIONS

POS, SKK, and RA conceptualized the project. PS designed the project and predominantly undertook the computational

analysis with inputs from SKK, RA, EB, WAM, and MDW. POS wrote the first draft of the manuscript. All the authors read, edited, and approved the manuscript before submission.

## ACKNOWLEDGMENTS

The authors are grateful to the West African Centre for Cell Biology of Infectious Pathogens (WACCBIP), University of Ghana for the use of Zuputo, a DELL high-performance

computing system, for this study. POS is grateful to the Ghana National Petroleum Corporation (GNPC) for supporting the postgraduate studies.

## SUPPLEMENTARY MATERIAL

The Supplementary Material for this article can be found online at: <https://www.frontiersin.org/articles/10.3389/fcimb.2022.859981/full#supplementary-material>

## REFERENCES

- Abad-Zapatero, C. (2007). Ligand Efficiency Indices for Effective Drug Discovery. *Expert Opin. Drug Discov.* 2, 469–488. doi: 10.1517/17460441.2.4.469
- Abad-Zapatero, C., Perišić, O., Wass, J., Bento, A. P., Overington, J., Al-Lazikani, B., et al. (2010). Ligand Efficiency Indices for an Effective Mapping of Chemico-Biological Space: The Concept of an Atlas-Like Representation. *Drug Discov. Today* 15, 804–811. doi: 10.1016/j.drudis.2010.08.004
- Abraham, M. J., Murtola, T., Schulz, R., Páll, S., Smith, J. C., Hess, B., et al. (2015). Gromacs: High Performance Molecular Simulations Through Multi-Level Parallelism From Laptops to Supercomputers. *SoftwareX* 1, 19–25. doi: 10.1016/j.softx.2015.06.001
- Agyapong, O., Asiedu, S. O., Kwofie, S. K., Miller, W. A., Parry, C. S., Sowah, R. A., et al. (2021). Molecular Modelling and De Novo Fragment-Based Design of Potential Inhibitors of Beta-Tubulin Gene of *Necator americanus* From Natural Products. *Inf. Med. Unlock.* 26, 100734/1–100734/20. doi: 10.1016/j.imu.2021.100734
- Ali, N., Ali, N. M., Fariba, J., and Elaheh, H. (2012). The Efficacy of 5% Trichloroacetic Acid Cream in the Treatment of Cutaneous Leishmaniasis Lesions. *J. Dermatolog. Treat.* 23, 136–139. doi: 10.3109/09546634.2010.500322
- Alkarkhi, A. F. M., and Alqaraghuli, W. A. A. (2020). R Statistical Software. *Appl. Stat. Environ. Sci. R.* 1, 1–17. doi: 10.1016/b978-0-12-818622-0.00002-2
- Anderson, R. J., Weng, Z., Campbell, R. K., and Jiang, X. (2005). Main-Chain Conformational Tendencies of Amino Acids. *Proteins Struct. Funct. Genet.* 60, 679–689. doi: 10.1002/PROT.20530
- Andrade-Neto, V. V., Pereira, T. M., Canto-Cavaleiro, M., and Torres-Santos, E. C. (2016). Imipramine Alters the Sterol Profile in *Leishmania Amazonensis* and Increases Its Sensitivity to Miconazole. *Parasitol. Vectors* 9, 1–8. doi: 10.1186/s13071-016-1467-8
- Azam, S. S., Abro, A., Raza, S., and Saroosh, A. (2014). Structure and Dynamics Studies of Sterol 24-C-Methyltransferase With Mechanism Based Inactivators for the Disruption of Ergosterol Biosynthesis. *Mol. Biol. Rep.* 41, 4279–4293. doi: 10.1007/s11033-014-3299-y
- Baell, J. B. (2016). Feeling Nature's PAINS: Natural Products, Natural Product Drugs, and Pan Assay Interference Compounds (PAINS). *J. Nat. Prod.* 79, 616–628. doi: 10.1021/acs.jnatprod.5b00947
- Baell, J. B., and Nissink, J. W. M. (2017). Seven Year Itch: Pan-Assay Interference Compounds (PAINS) in 2017—Utility and Limitations. *ACS Chem. Biol.* 13, 36–44. doi: 10.1021/ACSCHEMBIO.7B00903
- Baell, J., and Walters, M. A. (2014). Chemistry: Chemical Con Artists Foil Drug Discovery. *Nature* 513, 481–483. doi: 10.1038/513481a
- Banegas-Luna, A. J., Cerón-Carrasco, J. P., Puertas-Martin, S., and Pérez-Sánchez, H. (2019). BRUSELAS: HPC Generic and Customizable Software Architecture for 3D Ligand-Based Virtual Screening of Large Molecular Databases. *J. Chem. Inf. Model.* 59, 2805–2817. doi: 10.1021/ACS.JCIM.9B00279
- Banks, W. A. (2009). Characteristics of Compounds That Cross the Blood-Brain Barrier. *BMC Neurol.* 9, S3/1–S3/1. doi: 10.1186/1471-2377-9-S1-S3
- Barakat, R., Aronson, N., and Olsen, C. (2017). Microbiome Manipulation: Antibiotic Effects on Cutaneous Leishmaniasis Presentation and Healing. *Open Forum Infect. Dis.* 4, S122/1–S122/2. doi: 10.1093/OFID/OFX163.157
- Basanagouda, M., Jadhav, V. B., Kulkarni, M. V., and Nagendra Rao, R. (2011). Computer Aided Prediction of Biological Activity Spectra: Study of Correlation Between Predicted and Observed Activities for Coumarin-4-Acetic Acids. *Indian J. Pharm. Sci.* 73, 88–92. doi: 10.4103/0250-474X.89764
- Behera, S. K., Sabarinath, T., Mishra, P. K. K., Deneke, Y., Kumar, A., Chandrasekar, S., et al. (2021). Immunoinformatic Study of Recombinant Liga/Bcon1-5 Antigen and Evaluation of Its Diagnostic Potential in Primary and Secondary Binding Tests for Serodiagnosis of Porcine Leptospirosis. *Pathogens* 10, 1–20. doi: 10.3390/pathogens10091082
- Benet, L. Z., Hosey, C. M., Ursu, O., and Oprea, T. I. (2016). BDDCS, the Rule of 5 and Drugability. *Adv. Drug Deliv. Rev.* 101, 89–98. doi: 10.1016/j.addr.2016.05.007
- Benkert, P., Biasini, M., and Schwede, T. (2011). Toward the Estimation of the Absolute Quality of Individual Protein Structure Models. *Bioinformatics* 27, 343–350. doi: 10.1093/BIOINFORMATICS/BTQ662
- Berman, H. M., Westbrook, J., Feng, Z., Gilliland, G., Bhat, T. N., Weissig, H., et al. (2000). The Protein Data Bank. *Nucleic Acids Res.* 28, 235–242. doi: 10.1093/NAR/28.1.235
- Boratyn, G. M., Camacho, C., Cooper, P. S., Coulouris, G., Fong, A., Ma, N., et al. (2013). BLAST: A More Efficient Report With Usability Improvements. *Nucleic Acids Res.* 41, 29–33. doi: 10.1093/NAR/GKT282
- Broni, E., Kwofie, S. K., Asiedu, S. O., Miller, W. A., and Wilson, M. D. (2021). A Molecular Modeling Approach to Identify Potential Antileishmanial Compounds Against the Cell Division Cycle (Cdc)-2-Related Kinase 12 (CRK12) Receptor of *Leishmania Donovanii*. *Biomolecules* 11, 458/1–458/32. doi: 10.3390/biom11030458
- Burley, S. K., Berman, H. M., Kleywegt, G. J., Markley, J. L., Nakamura, H., and Velankar, S. (2017). Protein Data Bank (PDB): The Single Global Macromolecular Structure Archive. *Methods Mol. Biol.* 1607, 627–641. doi: 10.1007/978-1-4939-7000-1\_26
- Chang, M. W., Lindstrom, W., Olson, A. J., and Belew, R. K. (2007). Analysis of HIV Wild-Type and Mutant Structures via in Silico Docking Against Diverse Ligand Libraries. *J. Chem. Inf. Model.* 47, 1258–1262. doi: 10.1021/CI700044S
- Chanquia, S. N., Larregui, F., Puente, V., Labriola, C., Lombardo, E., and García Liñares, G. (2019). Synthesis and Biological Evaluation of New Quinoline Derivatives as Antileishmanial and Antitrypanosomal Agents. *Bioorg. Chem.* 83, 526–534. doi: 10.1016/j.bioorg.2018.10.053
- Clark, R. L., Carter, K. C., Mullen, A. B., Coxon, G. D., Owusu-Dapaah, G., McFarlane, E., et al. (2007). Identification of the Benzodiazepines as a New Class of Antileishmanial Agent. *Bioorg. Med. Chem. Lett.* 17, 624–627. doi: 10.1016/j.bmcl.2006.11.004
- Colovos, C., and Yeates, T. O. (1993). Verification of Protein Structures: Patterns of Nonbonded Atomic Interactions. *Protein Sci.* 2, 1511–1519. doi: 10.1002/pro.5560020916
- Congreve, M., and Marshall, F. (2010). The Impact of GPCR Structures on Pharmacology and Structure-Based Drug Design. *Br. J. Pharmacol.* 159, 986–996. doi: 10.1111/j.1476-5381.2009.00476.x
- Crentsil, J. A., Yamthe, L. R. T., Anibea, B. Z., Broni, E., Kwofie, S. K., Tetteh, J. K. A., et al. (2020). Leishmanicidal Potential of Hardwickiic Acid Isolated From *Croton Sylvaticus*. *Front. Pharmacol.* 11, 753. doi: 10.3389/fphar.2020.00753
- Dahiya, R., Mohammad, T., Gupta, P., Haque, A., Alajmi, M. F., Hussain, A., et al. (2019). Molecular Interaction Studies on Ellagic Acid for Its Anticancer Potential Targeting Pyruvate Dehydrogenase Kinase 3. *RSC Adv.* 9, 23302–23315. doi: 10.1039/C9RA02864A
- Daina, A., Michielin, O., and Zoete, V. (2017). SwissADME: A Free Web Tool to Evaluate Pharmacokinetics, Drug-Likeness and Medicinal Chemistry Friendliness of Small Molecules. *Sci. Rep.* 7, 42717/1–42717/13. doi: 10.1038/SREP42717



- Dao Duong Thi, M., Helen Grant, M., Mullen, A. B., Tettey, J. N. A., MacKay, S. P., and Clark, R. L. (2009). Metabolism of Two New Benzodiazepine-Type Anti-Leishmanial Agents in Rat Hepatocytes and Hepatic Microsomes and Their Interaction With Glutathione in Macrophages. *J. Pharm. Pharmacol.* 61, 399–406. doi: 10.1211/JPP/61.03.0017
- da Silva Rodrigues, J. H., Miranda, N., Volpato, H., Ueda-Nakamura, T., and Nakamura, C. V. (2019). The Antidepressant Clomipramine Induces Programmed Cell Death in *Leishmania Amazonensis* Through a Mitochondrial Pathway. *Parasitol. Res.* 118, 977–989. doi: 10.1007/s00436-018-06200-x
- Das, B., TK Baidya, A., Mathew, A. T., Kumar Yadav, A., and Kumar, R. (2022). Structural Modification Aimed for Improving Solubility of Lead Compounds in Early Phase Drug Discovery. *Bioorg. Med. Chem.* 56, 116614/1–116614/83. doi: 10.1016/j.bmc.2022.116614
- Davies, M., Nowotka, M., Papadatos, G., Dedman, N., Gaulton, A., Atkinson, F., et al. (2015). ChEMBL Web Services: Streamlining Access to Drug Discovery Data and Utilities. *Nucleic Acids Res.* 43, 612–620. doi: 10.1093/NAR/GKV352
- de Souza Neto, L. R., Moreira-Filho, J. T., Neves, B. J., Maidana, R. L. B. R., Guimarães, A. C. R., Furnham, N., et al. (2020). In Silico Strategies to Support Fragment-To-Lead Optimization in Drug Discovery. *Front. Chem.* 8, 93. doi: 10.3389/FCHEM.2020.00093
- Dong, Y. W., Liao, M. L., Meng, X. L., and Somero, G. N. (2018). Structural Flexibility and Protein Adaptation to Temperature: Molecular Dynamics Analysis of Malate Dehydrogenases of Marine Molluscs. *Proc. Natl. Acad. Sci. U. S. A.* 115, 1274–1279. doi: 10.1073/PNAS.1718910115
- Douguet, D. (2010). E-LEA3D: A Computational-Aided Drug Design Web Server. *Nucleic Acids Res.* 38, 615–621. doi: 10.1093/NAR/GKQ322
- Du, X., Li, Y., Xia, Y. L., Ai, S. M., Liang, J., Sang, P., et al. (2016). Insights Into Protein–Ligand Interactions: Mechanisms, Models, and Methods. *Int. J. Mol. Sci.* 17, 144/1–144/34. doi: 10.3390/IJMS17020144
- Dundas, J., Ouyang, Z., Tseng, J., Binkowski, A., Turpaz, Y., and Liang, J. (2006). CASTp: Computed Atlas of Surface Topography of Proteins With Structural and Topographical Mapping of Functionally Annotated Residues. *Nucleic Acids Res.* 34, 116–118. doi: 10.1093/nar/gkl282
- Edwards, M. P., and Price, D. A. (2010). Role of Physicochemical Properties and Ligand Lipophilicity Efficiency in Addressing Drug Safety Risks. *Annu. Rep. Med. Chem.* 45, 380–391. doi: 10.1016/S0065-7743(10)45023-X
- Ertl, P., and Schuffenhauer, A. (2009). Estimation of Synthetic Accessibility Score of Drug-Like Molecules Based on Molecular Complexity and Fragment Contributions. *J. Cheminform.* 1, 1–11. doi: 10.1186/1758-2946-1-8/TABLES/1
- Eswar, N., Eramian, D., Webb, B., Shen, M. Y., and Sali, A. (2008). Protein Structure Modeling With MODELLER. *Methods Mol. Biol.* 426, 145–159. doi: 10.1007/978-1-60327-058-8\_8
- Fage, C. D., Isiorho, E. A., Liu, Y., Wagner, D. T., Liu, H., and Keatinge-Clay, A. T. (2015). The Structure of SpnF, a Standalone Enzyme That Catalyzes [4 + 2] Cycloaddition. *Nat. Chem. Biol.* 11, 256–258. doi: 10.1038/nchembio.1768
- Farmer, J., Kanwal, F., Nikulsin, N., Tsilimigras, M. C. B., and Jacobs, D. J. (2017). Statistical Measures to Quantify Similarity Between Molecular Dynamics Simulation Trajectories. *Entropy* 19, 646/1–646/17. doi: 10.3390/E19120646
- Fisar, Z., Hroudová, J., and Raboch, J. (2010). Inhibition of Monoamine Oxidase Activity by Antidepressants and Mood Stabilizers Alzheimer's Alzheimer's Disease View Project Mitochondrial Dysfunctions in Bipolar Affective Disorder View Project. *Neuroendocrinol. Lett.* 31, 645–656.
- Fiser, A., and Šali, A. (2003). Modeller: Generation and Refinement of Homology-Based Protein Structure Models. *Methods Enzymol.* 374, 461–491. doi: 10.1016/S0076-6879(03)74020-8
- Ghorbani, M., and Farhoudi, R. (2018). Leishmaniasis in Humans: Drug or Vaccine Therapy? *Drug Des. Devel. Ther.* 12, 25–40. doi: 10.2147/DDDT.S146521
- Gil, C., and Martinez, A. (2021). Is Drug Repurposing Really the Future of Drug Discovery or Is New Innovation Truly the Way Forward? *Taylor. Fr.* 16, 829–831. doi: 10.1080/17460441.2021.1912733
- Goto, Y., Bhatia, A., Raman, V. S., Vidal, S. E. Z., Bertholet, S., Coler, R. N., et al. (2009). Leishmania Infantum Sterol 24-C-Methyltransferase Formulated With MPL-SE Induces Cross-Protection Against L. Major Infection. *Vaccine* 27, 2884–2890. doi: 10.1016/J.VACCINE.2009.02.079
- Goto, Y., Bogatzki, L. Y., Bertholet, S., Coler, R. N., and Reed, S. G. (2007). Protective Immunization Against Visceral Leishmaniasis Using *Leishmania* Sterol 24-C-Methyltransferase Formulated in Adjuvant. *Vaccine* 25, 7450–7458. doi: 10.1016/j.vaccine.2007.08.001
- Grinter, S. Z., and Zou, X. (2014). Challenges, Applications, and Recent Advances of Protein-Ligand Docking in Structure-Based Drug Design. *Molecules* 19, 10150–10176. doi: 10.3390/MOLECULES190710150
- Gros, L., Castillo-Acosta, V. M., Jiménez, C. J., Sealey-Cardona, M., Vargas, S., Estévez, A. M., et al. (2006). New Azasterols Against *Trypanosoma Brucei*: Role of 24-Sterol Methyltransferase in Inhibitor Action. *Antimicrob. Agents Chemother.* 50, 2595–2601. doi: 10.1128/AAC.01508-05
- Gupta, Y., Maciorowski, D., Zak, S. E., Jones, K. A., Kathayat, R. S., Azizi, S. A., et al. (2021). Bisindolylmaleimide IX: A Novel Anti-SARS-CoV2 Agent Targeting Viral Main Protease 3cldpro Demonstrated by Virtual Screening Pipeline and *in-Vitro* Validation Assays. *Methods* 195, 57–71. doi: 10.1016/j.ymeth.2021.01.003
- Haddad, Y., Adam, V., and Heger, Z. (2020). Ten Quick Tips for Homology Modeling of High-Resolution Protein 3D Structures. *PLoS Comput. Biol.* 16, e1007449/1–e1007449/19. doi: 10.1371/journal.pcbi.1007449
- Held, M., Metzner, P., Prinz, J. H., and Noé, F. (2011). Mechanisms of Protein-Ligand Association and Its Modulation by Protein Mutations. *Biophys. J.* 100, 701–710. doi: 10.1016/J.BPJ.2010.12.3699
- Hernández-Bojorge, S. E., Blass-Alfaro, G. G., Rickloff, M. A., Gómez-Guerrero, M. J., and Izurieta, R. (2020). Epidemiology of Cutaneous and Mucocutaneous Leishmaniasis in Nicaragua. *Parasite. Epidemiol. Contr.* 11, e00192/1–e00192/11. doi: 10.1016/j.parepi.2020.e00192
- Hevener, K. E., Pesavento, R., Ren, J., Lee, H., Ratia, K., and Johnson, M. E. (2018). Hit-To-Lead: Hit Validation and Assessment. *Methods Enzymol.* 610, 265–309. doi: 10.1016/bs.mie.2018.09.022
- Hollingsworth, S. A., and Dror, R. O. (2018). Molecular Dynamics Simulation for All. *Neuron* 99, 1129–1143. doi: 10.1016/J.NEURON.2018.08.011
- Hopkins, A. L., Groom, C. R., and Alex, A. (2004). Ligand Efficiency: A Useful Metric for Lead Selection. *Drug Discov. Today* 9, 430–431. doi: 10.1016/S1359-6446(04)03069-7
- Hopkins, A. L., Keserü, G. M., Leeson, P. D., Rees, D. C., and Reynolds, C. H. (2014). The Role of Ligand Efficiency Metrics in Drug Discovery. *Nat. Rev. Drug Discov.* 13, 105–121. doi: 10.1038/NRD4163
- Huang, Q., Li, L. L., and Yang, S. Y. (2010). PhDD: A New Pharmacophore-Based De Novo Design Method of Drug-Like Molecules Combined With Assessment of Synthetic Accessibility. *J. Mol. Graph. Model.* 28, 775–787. doi: 10.1016/J.JMGM.2010.02.002
- Hughes, J. P., Rees, S. S., Kalindjian, S. B., and Philpott, K. L. (2011). Principles of Early Drug Discovery. *Br. J. Pharmacol.* 162, 1239–1249. doi: 10.1111/j.1476-5381.2010.01127.x
- Huo, L., Zhao, X., Acedo, J. Z., Estrada, P., Nair, S. K., and Donk, W. A. (2020). Characterization of a Dehydratase and Methyltransferase in the Biosynthesis of Ribosomally Synthesized and Post-Translationally Modified Peptides in Lachnospiraceae. *ChemBioChem* 21, 190–199. doi: 10.1002/cbic.201900483
- Hu, Y., Stumpfe, D., and Bajorath, J. (2017). Recent Advances in Scaffold Hopping. *J. Med. Chem.* 60, 1238–1246. doi: 10.1021/ACS.JMEDCHEM.6B01437
- Ikeogu, N. M., Akaluka, G. N., Edechi, C. A., Salako, E. S., Onyilagha, C., Barazandeh, A. F., et al. (2020). Leishmania Immunity: Advancing Immunotherapy and Vaccine Development. *Microorganisms* 8, 1201/1–1201/21. doi: 10.3390/MICROORGANISMS8081201
- Islam, M. A., and Pillay, T. S. (2020). Identification of Promising Anti-DNA Gyrase Antibacterial Compounds Using De Novo Design, Molecular Docking and Molecular Dynamics Studies. *J. Biomol. Struct. Dyn.* 38, 1798–1809. doi: 10.1080/07391102.2019.1617785
- Jacquemard, C., and Kellenberger, E. (2019). A Bright Future for Fragment-Based Drug Discovery: What Does It Hold? *Expert Opin. Drug Discov.* 14, 413–416. doi: 10.1080/17460441.2019.1583643
- Jeon, B., Ruszczycky, M. W., Russell, W. K., Lin, G.-M., Kim, N., Choi, S., et al. (2017). Investigation of the Mechanism of the SpnF-Catalyzed [4+2]-Cycloaddition Reaction in the Biosynthesis of Spinosyn A. *Proc. Natl. Acad. Sci.* 114, 10408–10413. doi: 10.1073/pnas.1710496114
- Karplus, M., and Kuriyan, J. (2005). Molecular Dynamics and Protein Function. *Proc. Natl. Acad. Sci.* 102, 6679–6685. doi: 10.1073/PNAS.0408930102
- Kaur, N. (2013). An Insight Into Medicinal and Biological Significance of Privileged Scaffold: 1,4-Benzodiazepine. *Int. J. Pharma. Bio Sci.* 4, 318–337.
- Kidane, M. E., Vanderloop, B. H., Zhou, W., Thomas, C. D., Ramos, E., Singha, U., et al. (2017). Sterol Methyltransferase a Target for Anti-Amoeba Therapy: Towards Transition State Analog and Suicide Substrate Drug Design. *J. Lipid Res.* 58, 2310–2323. doi: 10.1194/JLR.M079418

- Kim, S., Chen, J., Cheng, T., Gindulyte, A., He, J., He, S., et al. (2021). PubChem in 2021: New Data Content and Improved Web Interfaces. *Nucleic Acids Res.* 49, D1388–D1395. doi: 10.1093/NAR/GKAA971
- Kranthi, K. R., Mathi, P., Prasad, M. V. V., Botlagunta, M., Ravi, M., and Ramachandran, D. (2018). *De Novo* Design of Selective Sortase-A Inhibitors: Synthesis, Structural and *In Vitro* Characterization. *Chem. Data Collect.* 15, 126–133. doi: 10.1016/j.cdc.2018.04.007
- Kshirsagar, U. A. (2015). Recent Developments in the Chemistry of Quinazolinone Alkaloids. *Org. Biomol. Chem.* 13, 9336–9352. doi: 10.1039/x0xx00000x
- Kumari, R., Kumar, R., and Lynn, A. (2014). G\_Mmpbsa —A GROMACS Tool for High-Throughput MM-PBSA Calculations. *J. Chem. Inf. Model.* 54, 1951–1962. doi: 10.1021/ci500020m
- Kwofie, S. K., Broni, E., Dankwa, B., Enninful, K. S., Kwarko, G. B., Darko, L., et al. (2020). Outwitting an Old Neglected Nemesis: A Review on Leveraging Integrated Data-Driven Approaches to Aid in Unraveling of Leishmanicides of Therapeutic Potential. *Curr. Top. Med. Chem.* 20, 349–366. doi: 10.2174/1568026620666200128160454
- Kwofie, S., Broni, E., Yunus, F., Nsoh, J., Adoboe, D., Miller, W., et al. (2021). Molecular Docking Simulation Studies Identifies Potential Natural Product Derived-Anti-wolbachial Compounds as Filaricides Against Onchocerciasis. *Biomedicine* 9, 1682/1–1682/33. doi: 10.3390/biomedicine9111682
- Kwofie, S., Dankwa, B., Enninful, K., Adobor, C., Broni, E., Ntiamoah, A., et al. (2019). Molecular Docking and Dynamics Simulation Studies Predict Munc18b as a Target of Mycolactone: A Plausible Mechanism for Granule Exocytosis Impairment in Buruli Ulcer Pathogenesis. *Toxins (Basel)*. 11, 181/1–181/16. doi: 10.3390/toxins11030181
- Lagunin, A., Stepanchikova, A., Filimonov, D., and Poroikov, V. (2000). PASS: Prediction of Activity Spectra for Biologically Active Substances. *Bioinformatics* 16, 747–748. doi: 10.1093/BIOINFORMATICS/16.8.747
- Larsson, P., Wallner, B., Lindahl, E., and Elofsson, A. (2008). Using Multiple Templates to Improve Quality of Homology Models in Automated Homology Modeling. *Protein Sci.* 17, 990–1002. doi: 10.1110/ps.073344908
- Laskowski, R. A., Luscombe, N. M., Swindells, M. B., and Thornton, J. M. (1996). Protein Clefts in Molecular Recognition and Function. *Protein Sci.* 5, 2438–2452. doi: 10.1002/pro.5560051206
- Laskowski, R. A., MacArthur, M. W., and Thornton, J. M. (2012). PROCHECK: Validation of Protein-Structure Coordinates. *International Tables for Crystallography* 21, 684–687. doi: 10.1107/97809553602060000882
- Liang, J., Woodward, C., and Edelsbrunner, H. (1998). Anatomy of Protein Pockets and Cavities: Measurement of Binding Site Geometry and Implications for Ligand Design. *Protein Sci.* 7, 1884–1897. doi: 10.1002/pro.5560070905
- Liao, K. H., Chen, K. B., Lee, W. Y., Sun, M. F., Lee, C. C., and Chen, C. Y. C. (2014). Ligand-Based and Structure-Based Investigation for Alzheimer's Disease From Traditional Chinese Medicine. *Evid. Based Compl. Altern. Med.* 2014, 364819/1–364819/16. doi: 10.1155/2014/364819
- Lighthall, G. K., Parast, L. M., Rapoport, L., and Wagner, T. H. (2010). Introduction of a Rapid Response System at a United States Veterans Affairs Hospital Reduced Cardiac Arrests. *Anesth. Analg.* 111, 679–686. doi: 10.1213/ANE.0B013E3181E9C3F3
- Lima, M. L., Abengózar, M. A., Nacher-Vázquez, M., Martínez-Alcázar, M. P., Barbas, C., Tempone, A. G., et al. (2018). Molecular Basis of the Leishmanicidal Activity of the Antidepressant Sertraline as a Drug Repurposing Candidate. *Antimicrob. Agents Chemother.* 62, e01928–18/1–e01928–18/43. doi: 10.1128/AAC.01928–18
- Lin, X., Li, X., and Lin, X. (2020). A Review on Applications of Computational Methods in Drug Screening and Design. *Molecules* 25, 1375/1–1375/17. doi: 10.3390/molecules25061375
- Lin, J. H., and Yamazaki, M. (2003). Role of P-Glycoprotein in Pharmacokinetics: Clinical Implications. *Clin. Pharmacokinet.* 42, 59–98. doi: 10.2165/00003088-200342010-00003
- Lionta, E., Spyrou, G., Vassiliadis, D., and Cournia, Z. (2014). Structure-Based Virtual Screening for Drug Discovery: Principles, Applications and Recent Advances. *Curr. Top. Med. Chem.* 14, 1923–1938. doi: 10.2174/1568026614666140929124445
- Lipinski, C. A., Lombardo, F., Dominy, B. W., and Feeney, P. J. (2001). Experimental and Computational Approaches to Estimate Solubility and Permeability in Drug Discovery and Development Settings. *Adv. Drug Deliv. Rev.* 46, 3–26. doi: 10.1016/S0169-409X(00)00129-0
- Löbner, R., Amidon, G. L., Ferraz, H. G., and Bou-Chacra, N. (2013). Mechanism of Gastrointestinal Drug Absorption and Application in Therapeutic Drug Delivery. *Ther. Deliv. Methods A. Concise. Overv. Emerg. Areas.* 8–22. doi: 10.4155/EBO.13.349/ASSET/IMAGES/LARGE/FIGURE6.JPEG
- Lorente, S. O., Rodrigues, J. C. F., Jiménez, C. J., Joyce-Menekse, M., Rodrigues, C., Croft, S. L., et al. (2004). Novel Azasterols as Potential Agents for Treatment of Leishmaniasis and Trypanosomiasis. *Antimicrob. Agents Chemother.* 48, 2937–2950. doi: 10.1128/AAC.48.8.2937-2950.2004
- Luer, M. S., and Penzak, S. R. (2016). Pharmacokinetic Properties. *Appl. Clin. Pharmacokinet. Pharmacodyn. Psychopharmacol. Agents.* 3–27. doi: 10.1007/978-3-319-27883-4\_1
- Magaraci, F., Jimenez Jimenez, C., Rodrigues, C., Rodrigues, J. C. F., Vianna Braga, M., Yardley, V., et al. (2003). Azasterols as Inhibitors of Sterol 24-Methyltransferase in Leishmania Species and Trypanosoma Cruzi. *J. Med. Chem.* 46, 4714–4727. doi: 10.1021/jm021114j
- Mak, K. K., and Pichika, M. R. (2019). Artificial Intelligence in Drug Development: Present Status and Future Prospects. *Drug Discov. Today* 24, 773–780. doi: 10.1016/j.DRUDIS.2018.11.014
- Mandal, S., Moudgil, N., and Mandal, S. K. (2009). Rational Drug Design. *Eur. J. Pharmacol.* 625, 90–100. doi: 10.1016/j.ejphar.2009.06.065
- Mavromoustakos, T., Durdagi, S., Koukoulitsa, C., Simic, M., Papadopoulos, M. G., Hodosecek, M., et al. (2011). Strategies in the Rational Drug Design. *Curr. Med. Chem.* 18, 2517–2530. doi: 10.2174/092986711795933731
- Meier, A., and Söding, J. (2015). Automatic Prediction of Protein 3d Structures by Probabilistic Multi-Template Homology Modeling. *PLoS Comput. Biol.* 11, e1004343/1–e1004343/20. doi: 10.1371/JOURNAL.PCBI.1004343
- Mendonça Junior, F. J. B., Scotti, L., Ishiki, H., Botelho, S. P. S., Da Silva, M. S., and Scotti, M. T. (2015). Benzo- and Thienobenzo- Diazepines: Multi-Target Drugs for CNS Disorders. *Med. Chem. (Los. Angeles)*. 15, 630–647. doi: 10.2174/1389557515666150219125030
- Messaoudi, A., Belguith, H., and Ben Hamida, J. (2013). Homology Modeling and Virtual Screening Approaches to Identify Potent Inhibitors of VEB-1  $\beta$ -Lactamase. *Theor. Biol. Med. Model.* 10, 22/1–22/10. doi: 10.1186/1742-4682-10-22
- Mishra, S., Parmar, N., Chandrakar, P., Sharma, C. P., Parveen, S., Vats, R. P., et al. (2021). Design, Synthesis, *In Vitro* and *In Vivo* Biological Evaluation of Pyranone-Piperazine Analogs as Potent Antileishmanial Agents. *Eur. J. Med. Chem.* 221, 113516/1–113516/14. doi: 10.1016/j.ejmech.2021.113516
- Momeni, A. Z., Aminjavaheri, M., and Omidghaemi, M. R. (2003). Treatment of Cutaneous Leishmaniasis With Ketoconazole Cream. *J. Dermatolog. Treat.* 14, 26–29. doi: 10.1080/09546630305552
- Mora Lagares, L., Minovski, N., Caballero Alfonso, A. Y., Benfenati, E., Wellens, S., Culot, M., et al. (2020). Homology Modeling of the Human P-Glycoprotein (ABCB1) and Insights Into Ligand Binding Through Molecular Docking Studies. *Int. J. Mol. Sci.* 21, 4058/1–4058/35. doi: 10.3390/ijms21114058
- Morris, G. M., Ruth, H., Lindstrom, W., Sanner, M. F., Bewle, R. K., Goodsell, D. S., et al. (2009). Software News and Updates AutoDock4 and AutoDockTools4: Automated Docking With Selective Receptor Flexibility. *J. Comput. Chem.* 30, 2785–2791. doi: 10.1002/JCC.21256
- Mouchlis, V. D., Afantitis, A., Serra, A., Fratello, M., Papadiamantis, A. G., Aidinis, V., et al. (2021). Advances in *De Novo* Drug Design: From Conventional to Machine Learning Methods. *Int. J. Mol. Sci.* 22, 1–22. doi: 10.3390/IJMS22041676
- Mukherjee, S., Mukherjee, B., Mukhopadhyay, R., Naskar, K., Sundar, S., Dujardin, J. C., et al. (2012). Imipramine Is an Orally Active Drug Against Both Antimony Sensitive and Resistant Leishmania Donovanii Clinical Isolates in Experimental Infection. *PLoS Negl. Trop. Dis.* 6, e1987/1–e1987/16. doi: 10.1371/JOURNAL.PNTD.0001987
- Mukherjee, S., Xu, W., Hsu, F. F., Patel, J., Huang, J., and Zhang, K. (2019). Sterol Methyltransferase Is Required for Optimal Mitochondrial Function and Virulence in Leishmania Major. *Mol. Microbiol.* 111, 65–81. doi: 10.1111/mmi.14139
- Onakpoya, I. J., Heneghan, C. J., and Aronson, J. K. (2016). Post-Marketing Withdrawal of 462 Medicinal Products Because of Adverse Drug Reactions: A Systematic Review of the World Literature. *BMC Med.* 14, 1–11. doi: 10.1186/S12916-016-0553-2

- Pandey, P., Prasad, K., Prakash, A., and Kumar, V. (2020). Insights Into the Biased Activity of Dextromethorphan and Haloperidol Towards SARS-CoV-2 NSP6: In Silico Binding Mechanistic Analysis. *J. Mol. Med.* 98, 1659–1673. doi: 10.1007/S00109-020-01980-1/FIGURES/10
- Parasuraman, S. (2011). Prediction of Activity Spectra for Substances. *J. Pharmacol. Pharmacother.* 2, 52–53. doi: 10.4103/0976-500X.77119
- Pathania, S., Singh, P. K., Narang, R. K., and Rawal, R. K. (2021). Identifying Novel Putative ERK1/2 Inhibitors via Hybrid Scaffold Hopping –FBDD Approach. *J. Biomol. Struct. Dyn.* 39, 1–16. doi: 10.1080/07391102.2021.1889670
- Pence, H. E., and Williams, A. (2010). Chemspider: An Online Chemical Information Resource. *J. Chem. Educ.* 87, 1123–1124. doi: 10.1021/ED100697W
- Pérez-Moreno, G., Sealey-Cardona, M., Rodrigues-Poveda, C., Gelb, M. H., Ruiz-Pérez, L. M., Castillo-Acosta, V., et al. (2012). Endogenous Sterol Biosynthesis Is Important for Mitochondrial Function and Cell Morphology in Procyclic Forms of Trypanosoma Brucei. *Int. J. Parasitol.* 42, 975–989. doi: 10.1016/j.ijpara.2012.07.012
- Pettersen, E. F., Goddard, T. D., Huang, C. C., Couch, G. S., Greenblatt, D. M., Meng, E. C., et al. (2004). UCSF Chimera - A Visualization System for Exploratory Research and Analysis. *J. Comput. Chem.* 25, 1605–1612. doi: 10.1002/jcc.20084
- Pountain, A. W., Weidt, S. K., Regnault, C., Bates, P. A., Donachie, A. M., Dickens, N. J., et al. (2019). Genomic Instability at the Locus of Sterol C24-Methyltransferase Promotes Amphotericin B Resistance in Leishmania Parasites. *PLoS Negl. Trop. Dis.* 13, e0007052/1–e0007052/16. doi: 10.1371/journal.pntd.0007052
- Prachayasittikul, V., and Prachayasittikul, V. (2016). P-Glycoprotein Transporter in Drug Development. *EXCLI J.* 15, 113–118. doi: 10.17179/EXCLI2015-768
- Rahman, F., Tabrez, S., Ali, R., Akand, S. K., Zahid, M., Alaidarous, M. A., et al. (2021). Virtual Screening of Natural Compounds for Potential Inhibitors of Sterol C-24 Methyltransferase of Leishmania Donovanii to Overcome Leishmaniasis. *J. Cell. Biochem.* 122, 1216–1228. doi: 10.1002/JCB.29944
- Reynolds, C. H., Bembek, S. D., and Tounge, B. A. (2007). The Role of Molecular Size in Ligand Efficiency. *Bioorg. Med. Chem. Lett.* 17, 4258–4261. doi: 10.1016/J.BMCL.2007.05.038
- Reynolds, C. H., and Reynolds, R. C. (2017). Group Additivity in Ligand Binding Affinity: An Alternative Approach to Ligand Efficiency. *J. Chem. Inf. Model.* 57, 3086–3093. doi: 10.1021/ACS.JCIM.7B00381
- Richardson, J. L., Nett, I. R. E., Jones, D. C., Abdille, M. H., Gilbert, I. H., and Fairlamb, A. H. (2009). Improved Tricyclic Inhibitors of Trypanothione Reductase by Screening and Chemical Synthesis. *ChemMedChem* 4, 1333–1340. doi: 10.1002/CMDC.200900097
- Rinschen, M. M., Ivanisevic, J., Giera, M., and Siuzdak, G. (2019). Identification of Bioactive Metabolites Using Activity Metabolomics. *Nat. Rev. Mol. Cell Biol.* 20, 353–367. doi: 10.1038/S41580-019-0108-4
- Sakyi, P. O., Amewu, R. K., Devine, R. N. O. A., Bienibuor, A. K., Miller, W. A., and Kwofie, S. K. (2021a). Unravelling the Myth Surrounding Sterol Biosynthesis as Plausible Target for Drug Design Against Leishmaniasis. *J. Parasitol. Dis.* 45, 1152–1171. doi: 10.1007/S12639-021-01390-1
- Sakyi, P. O., Amewu, R. K., Devine, R. N. O. A., Ismaila, E., Miller, W. A., and Kwofie, S. K. (2021b). The Search for Putative Hits in Combating Leishmaniasis: The Contributions of Natural Products Over the Last Decade. *Nat. Prod. Bioprospect.* 11, 489–544. doi: 10.1007/S13659-021-00311-2
- Sander, T., Frey, J., Von Korff, M., and Rufener, C. (2015). DataWarrior: An Open-Source Program for Chemistry Aware Data Visualization and Analysis. *J. Chem. Inf. Model.* 55, 460–473. doi: 10.1021/CI500588J
- Sasin, J. M., and Bujnicki, J. M. (2004). COLORADO3D, a Web Server for the Visual Analysis of Protein Structures. *Nucleic Acids Res.* 1, 586–589. doi: 10.1093/NAR/GKH440
- Satari, M. H., Primasari, A., Dharsono, H. D. A., Apriyanti, E., Suprijono, M. M., Herdiyati, Y., et al. (2021). Mode Action Prediction of Butein as Antibacterial Oral Pathogen Against Enterococcus Faecalis ATCC 29212 and an Inhibitor of MurA Enzyme: In Vitro and In Silico Study. *Lett. Drug Des. Discov.* 18, 744–753. doi: 10.2174/1570180818666210122163009
- Sawale, R. T., Kalyankar, T. M., George, R., and Deosarkar, S. D. (2016). Molar Refraction and Polarizability of Antiemetic Drug 4-Amino-5-Chloro-N-(2-(Diethylamino)Ethyl)-2-Methoxybenzamide Hydrochloride Monohydrate in {Aqueous-Sodium or Lithium Chloride} Solutions at 30 °C. *J. Appl. Pharm. Sci.* 6, 120–124. doi: 10.7324/JAPS.2016.60321
- Schneider, P., and Schneider, G. (2016). De Novo Design at the Edge of Chaos. *J. Med. Chem.* 59, 4077–4086. doi: 10.1021/ACS.JMEDCHEM.5B01849
- Schultes, S., De Graaf, C., Haaksma, E. E. J., De Esch, I. J. P., Leurs, R., and Krämer, O. (2010). Ligand Efficiency as a Guide in Fragment Hit Selection and Optimization. *Drug Discov. Today Technol.* 7, e157–e162. doi: 10.1016/J.DDTEC.2010.11.003
- Sharma, M., Chauhan, K., Shivahare, R., Vishwakarma, P., Suthar, M. K., Sharma, A., et al. (2013). Discovery of a New Class of Natural Product-Inspired Quinazolinone Hybrid as Potent Antileishmanial Agents. *J. Med. Chem.* 56, 4374–4392. doi: 10.1021/jm400053v
- Shen, M., and Sali, A. (2006). Statistical Potential for Assessment and Prediction of Protein Structures. *Protein Sci.* 15, 2507–2524. doi: 10.1110/PS.062416606
- Singh, S., McCoy, J. G., Zhang, C., Bingman, C. A., Phillips, G. N., and Thorson, J. S. (2008). Structure and Mechanism of the Rebeccamycin Sugar 4'-O-Methyltransferase RebM. *J. Biol. Chem.* 283, 22628–22636. doi: 10.1074/jbc.M800503200
- Sinha, S., and Wang, S. M. (2020). Classification of VUS and Unclassified Variants in BRCA1 BRCT Repeats by Molecular Dynamics Simulation. *Comput. Struct. Biotechnol. J.* 18, 723–736. doi: 10.1016/J.CSB.2020.03.013
- Sippl, M. J. (1993). Recognition of Errors in Three-Dimensional Structures of Proteins. *Proteins Struct. Funct. Genet.* 17, 355–362. doi: 10.1002/prot.340170404
- Sterling, T., and Irwin, J. J. (2015). ZINC 15 - Ligand Discovery for Everyone. *J. Chem. Inf. Model.* 55, 2324–2337. doi: 10.1021/ACS.JCIM.5B00559
- Šudomová, M., Hassan, S. T. S., Khan, H., Rasekhian, M., and Nabavi, S. M. (2019). A Multi-Biochemical and In Silico Study on Anti-Enzymatic Actions of Pyroglutamic Acid Against PDE-5, ACE, and Urease Using Various Analytical Techniques: Unexplored Pharmacological Properties and Cytotoxicity Evaluation. *Biomolecules* 9, 392–405. doi: 10.3390/BIOM9090392
- Sun, H., Tawa, G., and Wallqvist, A. (2012). Classification of Scaffold-Hopping Approaches. *Drug Discov. Today* 17, 310–324. doi: 10.1016/J.DRUDIS.2011.10.024
- Tabrez, S., Rahman, F., Ali, R., Muhammad, F., Alshehri, B. M., Alaidarous, M. A., et al. (2021). Repurposing of FDA-Approved Drugs as Inhibitors of Sterol C-24 Methyltransferase of Leishmania Donovanii to Fight Against Leishmaniasis. *Drug Dev. Res.* 82, 1154–1161. doi: 10.1002/DDR.21820
- Talevi, A., and Bellera, C. L. (2019). Challenges and Opportunities With Drug Repurposing: Finding Strategies to Find Alternative Uses of Therapeutics. *Taylor. Fr.* 15, 397–401. doi: 10.1080/17460441.2020.1704729
- Tian, W., Chen, C., Lei, X., Zhao, J., and Liang, J. (2018). CASTp 3.0: Computed Atlas of Surface Topography of Proteins. *Nucleic Acids Res.* 46, W363–W367. doi: 10.1093/nar/gky473
- Tippmann, S. (2014). Programming Tools: Adventures With R. *Nature* 517, 109–110. doi: 10.1038/517109a
- Torres-Santos, E. C., Andrade-Neto, V. V., Cunha-Júnior, E. F., Do Canto-Cavaleiro, M. M., Atella, G. C., De Almeida Fernandes, T., et al. (2016). Antileishmanial Activity of Ezetimibe: Inhibition of Sterol Biosynthesis, In Vitro Synergy With Azoles, and Efficacy in Experimental Cutaneous Leishmaniasis. *Antimicrob. Agents Chemother.* 60, 6844–6852. doi: 10.1128/AAC.01545-16
- Trott, O., and Olson, A. J. (2010). AutoDock Vina: Improving the Speed and Accuracy of Docking With a New Scoring Function, Efficient Optimization and Multithreading. *J. Comput. Chem.* 31, 455–461. doi: 10.1002/JCC.21334
- Urbina, J. A., Visbal, G., Contreras, L. M., McLaughlin, G., and Docampo, R. (1997). Inhibitors of  $\Delta(24/25)$  Sterol Methyltransferase Block Sterol Synthesis and Cell Proliferation in Pneumocystis Carinii. *Antimicrob. Agents Chemother.* 41, 1428–1432. doi: 10.1128/AAC.41.7.1428
- Urbina, J. A., Vivas, J., Visbal, G., and Contreras, L. M. (1995). Modification of the Sterol Composition of Trypanosoma (Schizotrypanum) Cruzi Epimastigotes by  $\Delta(24/25)$ -Sterol Methyl Transferase Inhibitors and Their Combinations With Ketoconazole. *Mol. Biochem. Parasitol.* 73, 199–210. doi: 10.1016/0166-6851(95)00117-j
- van den Anker, J., Reed, M. D., Allegaert, K., and Kearns, G. L. (2018). Developmental Changes in Pharmacokinetics and Pharmacodynamics. *J. Clin. Pharmacol.* 58, S10–S25. doi: 10.1002/JCPH.1284

- Van Der Spoel, D., Lindahl, E., Hess, B., Groenhof, G., Mark, A. E., and Berendsen, H. J. C. (2005). GROMACS: Fast, Flexible, and Free. *J. Comput. Chem.* 26, 1701–1718. doi: 10.1002/JCC.20291
- Van Norman, G. A. (2019). Phase II Trials in Drug Development and Adaptive Trial Design. *JACC Basic. To. Transl. Sci.* 4, 428–437. doi: 10.1016/J.JACBTS.2019.02.005
- Veber, D. F., Johnson, S. R., Cheng, H. Y., Smith, B. R., Ward, K. W., and Kopple, K. D. (2002). Molecular Properties That Influence the Oral Bioavailability of Drug Candidates. *J. Med. Chem.* 45, 2615–2623. doi: 10.1021/JM020017N
- Waterhouse, A., Bertoni, M., Bienert, S., Studer, G., Tauriello, G., Gumienny, R., et al. (2018). SWISS-MODEL: Homology Modelling of Protein Structures and Complexes. *Nucleic Acids Res.* 46, W296–W303. doi: 10.1093/NAR/GKY427
- Wiederstein, M., and Sippl, M. J. (2007). ProSA-Web: Interactive Web Service for the Recognition of Errors in Three-Dimensional Structures of Proteins. *Nucleic Acids Res.* 35, W407–W410. doi: 10.1093/nar/gkm290
- Wishart, D. S., Feunang, Y. D., Guo, A. C., Lo, E. J., Marcu, A., Grant, J. R., et al. (2018). DrugBank 5.0: A Major Update to the DrugBank Database for 2018. *Nucleic Acids Res.* 46, D1074–D1082. doi: 10.1093/NAR/GKX1037
- Wyllie, S., Thomas, M., Patterson, S., Crouch, S., De Rycker, M., Lowe, R., et al. (2018). Cyclin-Dependent Kinase 12 Is a Drug Target for Visceral Leishmaniasis. *Nature* 560, 192–197. doi: 10.1038/S41586-018-0356-Z
- Xu, D., and Zhang, Y. (2011). Improving the Physical Realism and Structural Accuracy of Protein Models by a Two-Step Atomic-Level Energy Minimization. *Biophys. J.* 101, 2525–2534. doi: 10.1016/j.bpj.2011.10.024
- Zhang, L. L., and Skolnick, J. (1998). What Should the Z-Score of Native Protein Structures Be? *Protein Sci.* 7, 1201–1207. doi: 10.1002/PRO.5560070515

**Conflict of Interest:** The authors declare that the research was conducted in the absence of any commercial or financial relationships that could be construed as a potential conflict of interest.

**Publisher's Note:** All claims expressed in this article are solely those of the authors and do not necessarily represent those of their affiliated organizations, or those of the publisher, the editors and the reviewers. Any product that may be evaluated in this article, or claim that may be made by its manufacturer, is not guaranteed or endorsed by the publisher.

Copyright © 2022 Sakyi, Broni, Amewu, Miller, Wilson and Kwofie. This is an open-access article distributed under the terms of the Creative Commons Attribution License (CC BY). The use, distribution or reproduction in other forums is permitted, provided the original author(s) and the copyright owner(s) are credited and that the original publication in this journal is cited, in accordance with accepted academic practice. No use, distribution or reproduction is permitted which does not comply with these terms.



# Advantages of publishing in Frontiers



## OPEN ACCESS

Articles are free to read  
for greatest visibility  
and readership



## FAST PUBLICATION

Around 90 days  
from submission  
to decision



## HIGH QUALITY PEER-REVIEW

Rigorous, collaborative,  
and constructive  
peer-review



## TRANSPARENT PEER-REVIEW

Editors and reviewers  
acknowledged by name  
on published articles

## Frontiers

Avenue du Tribunal-Fédéral 34  
1005 Lausanne | Switzerland

Visit us: [www.frontiersin.org](http://www.frontiersin.org)

Contact us: [frontiersin.org/about/contact](http://frontiersin.org/about/contact)



## REPRODUCIBILITY OF RESEARCH

Support open data  
and methods to enhance  
research reproducibility



## DIGITAL PUBLISHING

Articles designed  
for optimal readership  
across devices



## FOLLOW US

@frontiersin



## IMPACT METRICS

Advanced article metrics  
track visibility across  
digital media



## EXTENSIVE PROMOTION

Marketing  
and promotion  
of impactful research



## LOOP RESEARCH NETWORK

Our network  
increases your  
article's readership